Renewable Energy Potential of Greenland with emphasis on wind resource assessment

Jakobsen, Kasper Rønnow

Publication date:
2016

Document Version
Publisher's PDF, also known as Version of record

Renewable Energy Potential of Greenland with emphasis on wind resource assessment

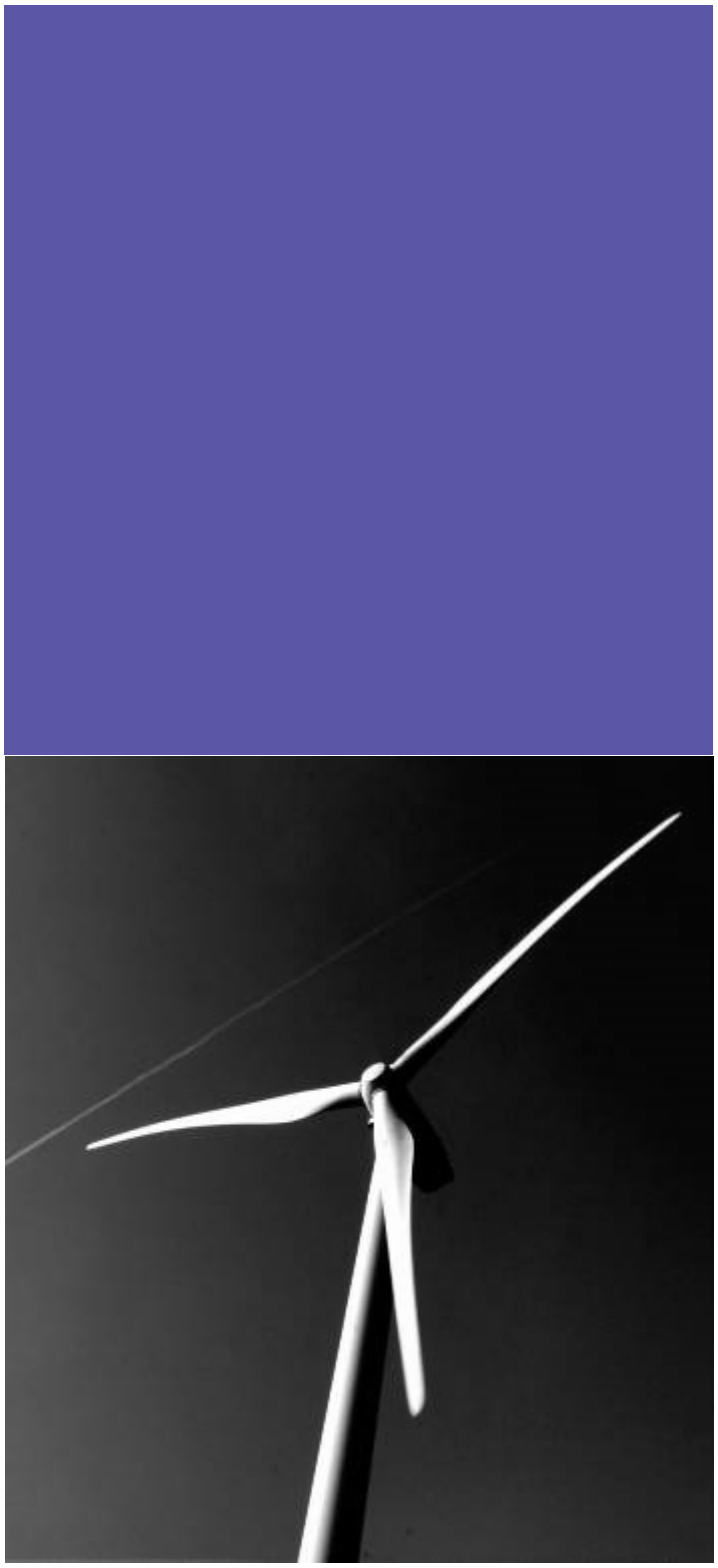

Kasper Rønnow Jakobsen

DTU Wind Energy PhD-0043 (EN)

February 2016

Authors: Kasper Rønnow Jakobsen

Title: Renewable Energy Potential of Greenland with emphasis on wind resource assessment

Department: DTU Wind Energy, Fluid Mechanic

Summary:

This thesis describes the different steps in the investigation of the Greenlandic Renewable potential. In this project varies wind resource assessment methods are tested to validate their performance in the complex Arctic terrain of Greenland. The energy systems are studied to identify the potential use of renewable energy in the systems. Finally, a short historical description of wind power development of Greenland and some recommendations for further development are provided.

The power systems were studied with focus on system efficiency in both the production, distribution and consumption part. The studies were based on; SCADA data and production reports for power plants, individual automatic consumption meter data, and visual inspection of all parts of the system. An energy saving potential of above 20% was found in some of the systems just by optimizing the use of existing installations. By replacing outdated systems with modern and use the heat production efficiently, then many of the diesel-based systems can double their fuel utilization.

The Greenlandic power systems have a high-unused potential for renewable energy. The largest systems, with connected electrical and heating grids is the most flexible and able to handle the highest RE penetration, but even the small electrical systems can handle a considerably RE-share, if the system is modernized. For most of the diesel-based power systems, the study shows that, both large-scale wind power and Photovoltaics is profitable.

For wind resource assessment, various methods of monitoring and modeling of wind resources were studied with focus on their performance in complex Arctic areas. The existing climate station, was found to be less useful due to insufficient design, and some dedicated wind monitoring stations were designed for the project. Micro- and Mesoscale models were tested against measurement stations and satellite-based ocean wind observations. The microscale models were valid in a very narrow (500m) range. The mesoscale models showed good performance in some areas, but imperfect surface data (sea ice and surface elevation) affected the results, especially in the coastal part areas.

DTU Wind Energy PhD-0043 (EN)

Project period:
2010-2014

Key words:
Wind Energy, Greenland, power systems, RE-resources, WRF-validation

Supervisors:
Martin O. L. Hansen
Claire L. Vincent

Remarks:
Project was hosted by Arctic Technology Center, (Artek) DTU

Contacts:
kasj@dtu.dk
Kasper.jakobsen@hotmail.com

Project nr.:
PhD-0043 (EN)

Sponsorship:

Front page:

Pages: 158
Tables: 30
References: 115

Technical University of Denmark
Department of Wind Energy
Frederiksborgvej 399
Building 118
4000 Roskilde
Denmark
Phone 46 77 50 24
bcar@dtu.dk
www.vindenergi.dtu.dk

Preface

This thesis is submitted for the degree Doctor Philosophy (philosophiae) at the Technical University of Denmark. The aim of the thesis is to increase the knowledge about Greenlandic renewable resources and how they can be utilized in power systems. The resource were equally shared between the three main areas; system analysis, resource monitoring and resource modeling.

The project was performed from April 2010 until November 2014 and was funded by Arctic Technology Center DTU, DTU Mechanical Engineering, and DTU Wind Energy. Additional funding was granted by the Renewable Energy and Climate Fund of the Greenlandic government. The report and review process was partly funded by Siemens AG.
The work was conducted at ARTEK, Arctic Technology Center, in the Department of Civil Engineering; the Department of Mechanical Engineering; and the Department of Wind Energy, all at Technical University of Denmark; Tech College Greenland; and Nukissiorfiit, Greenlands national power company. Field experiments and studies were carried out in West Greenland, supported by TELE Greenland, Qeqqata Kommunia, and Kujalleq Kommunia. The supervisors were Associate Professor Martin O. L. Hansen, Postdoc Claire Louise Vincent, Head of Section, Professor Arne Villumsen, and Head of Section, Associate Professor Brian Elmegaard.
Some of the work presented in this thesis was previously disseminated in the following papers, reports and conferences:

- Jakobsen K. R, Vincent C. L. (2016). *Evaluation of WRF Mesoscale Model performance for south Greenland* . (In review)
- Jakobsen K. R, Hansen K. S. (2016). *Experience of exploring wind resources in west Greenland* (In review)
- Jakobsen K. R, Vincent C. L,(2013). *Mesoscale modeling of South Greenland* European Geosciences Union General Assembly 2013, Poster and presentation.
- Dragsted J., Villumsen A., Larsen E., Jakobsen K. R., Hudecz A.(2012). *Fyrtaarnsprojekt VI 2012 : Afsluttende rapport*
- Dragsted J., Villumsen A., Larsen E., Jakobsen K. R., Hudecz A., Kotol M., Villumsen O. (2011). *Fyrtaarnsprojekt V 2011 : Afsluttende rapport.*
- Jakobsen K. R., Villumsen, A., Hudecz A., Andersen P., Hvidthoeft D., Groenvold H. (2010). *Fyrtaarnsprojekt IV 2010 : Afsluttende rapport.*
- Prof. Villumsen A., Jakobsen K. R,(2010). *Baeredygtig energiforsyning - hvad vaelger Groenland* Article in proceedings and presentation.

Abstract

As consumption, of the expensive energy, in the remote Arctic area increases, the demand for alternative energy sources will grow. For Greenland, hydropower is the preferred renewable energy source, but the resource is limited and the investment costs are high, and this moves the focus to other sources, such as wind and solar power. The biggest barriers to implementing these sources are lack of knowledge about the resources and their geographical distribution. In this project, different sources and methods for wind resource assessment are studied, with a focus on their performance in the complex Arctic terrain of Greenland. The energy systems are studied to identify the potential use of renewable energy in the system. Finally, a short description of wind power development in Greenland and some recommendations for further development are provided.

The power systems can be split into three categories, based on the type and existing energy source. Small village systems are supplied with diesel generators with limited heat utilization. These generator units have a relatively low efficiency (0.25 - 0.35) because of obsolete technology and low-load factors. To demonstrate the optimization potential for these village systems, the village Sarfannguaq was selected for a detailed study of consumption, saving potential, and renewable energy potential. The saving potential for nonindustrial use was, with only small adjustments, 20% of total consumption, and depending on the definition of Profitable (required returns of investment), more can economically be saved by replacing outdated equipment. The renewable energy potential for both solar and wind was relatively high, with solar radiation above 1000 $kWh/m^2/year$ and mean wind speeds of 6.1 m/s at 10 MAG. For a 50 kWp PV installation the 25 year average production cost was estimated to be less than 0.83 DKK/kWh and for a 100kW wind turbine, installed at site 2 (South-west of Sarfannguaq), the 20 year average production cost was estimated to be 0.85 DKK/kWh. Compared to the 2013 cost of goods for the diesel generators of 2.29 DKK/kWh, there is room for system updates to obtain a high RE penetration.
In the next category, named diesel cities, a large potential for waste-heat utilization was discovered, and in the city of focus, Nanortalik, updating the diesel generator unit, expanding the district heating grid, and implementing 500-1500 kW wind power were suggested. For the last category, named hydro cities, there is potential for other sources if or when the hydro resources are used up.

For wind resource estimation, various methods of monitoring and modeling of wind resources were studied with a focus on their use in complex Arctic areas. First, the existing ground-based measurements (Climate stations) were studied to determine applicability for wind resource estimation, and for many of the stations, a high local effect, inhomogeneous time series, and deviance from the WMO guidelines were found. The next step was to design a dedicated wind monitoring system usable in the Arctic environment and to

test it at different types of sites. The instrument test showed that even the highest quality of equipment failed in harsh climate. An extended test was planned, but due to delays, the test result is not ready yet. Based on the measurements, 10 sites were evaluated, 4 in the Uumannaq district, 5 in Sisimiut district and 1 in the Nanortalik district. Only two of them have a verified resource above 6m/s, but one more has the potential. One of the sites, Nanortalik Dump 1601, was studied in more detail by estimating the inflow angle, BL stability and turbulence distribution. The site class was found to be IEC class IIIS due to raised turbulence levels in some sectors.

For wind resource modeling, two types of models were evaluated; micro- and mesoscale models. The validation work showed that the microscale models performed relatively well within a 500m range of the reference site, depending on terrain and metrological conditions. The mesoscale models WRF and Polar WRF were validated against 14 measurement points in an 800x800km domain, and a detailed study of the 3D flow field in a complex fjord system was done. Furthermore, the modeled wind speed distribution was compared to satellite based ocean wind observations. The mesoscale work showed that the surface data available, especially the sea ice concentration and the surface elevation, need to be improved to obtain optimal model performance throughout the domain.
In the last part of the thesis, some suggestions for how wind power can be successfully developed in Greenland are given, together with the experiences gained from the test turbine. The main conclusion in this part is that a high-quality preliminary study (level 1) of available data, such as ocean wind, reanalysis data, inferred pictures of katabatic flow pattern, and station observation, together with good models is the key to a good site selection. To estimate project feasibility, detailed studies of infrastructure, raw materials, and wind resources are needed.
Since the unsuccessful introduction of commercial wind turbines in 1983-1986, wind power has not been a part of public systems, but technological development and the fact that verified resources now are available might open the way for Greenlandic wind power. There are still some model problems that need to be solved before a reliable resource map for all Greenland can be made, but with this project, Greenlandic wind power has come one step closer.

Abstract (Danish)

I takt med forbruget af dyr energi i de fjerne Arktis områder stiger, øges efterspørgslen efter vedvarende energi. I Grønland er vandkraft den foretrukne vedvarende energikilde, men resurserne har en begrænset udbredelse og investeringsomkostningerne er høje. Det har flyttet fokus til andre resurser, som vind og solenergi. Den største barriere for at udnytte disse resurser er manglende viden om resurserne og deres geografiske fordeling. I dette projekt er forskellige metoder for vindresurseestimering undersøgt, med fokus på deres anvendelighed i det komplekse Arktiske terræn på Grønland. De grønlandske energisystemer er undersøgt for at identificere potentialet for vedvarende energi i de enkelte systemer. Rapporten er afrundet med en historisk beskrivelse af vindkraftens udvikling på Grønland og nogle anbefalinger til fremtidige tiltag.
De grønlandske forsyningssystemer kan opdeles i tre kategorier, baseret på type og den anvendte energiresurse. De små bygdesystemer som forsynes med dieselgeneratorer, med begrænset udnyttelse af restvarmeproduktionen. Generatorerne har en relativ lav elvirkningsgrad (0.25-0.35) på grund af forældet teknologi og lav lastfaktor. For at demonstrere optimeringspotentialet for disse bygdesystemer, blev bygden Sarfannguit udvalgt til et detaljeret studie af forbruget, sparepotentialet og potentialet for vedvarende energi. Sparepotentialet for de ikke industrieller forbrugere, blev estimeret til 20% af det samlede forbrug, ved mindre justeringer af systemet. Alt efter hvordan rentabiliteten af en investering defineres, kan der spares væsentligt mere, primært ved udskiftning af forældet udstyr. Den vedvarende energi potentiale for både PV og vind er relativ højt, med en solindstråling på over 1000 $kWh/m^2/year$ og en middel vindhastighed på 6,1 m/s i 10 meters højde. For en $50kWp$ PV installation er produktionsomkostningerne estimeret til 0,83 kr./kWh over 25 år. For en 100kW vindmølle, installeret på Site 2 (Sydvest for bygden), er de gennemsnitlige produktionsomkostninger estimeret til 0,73 kr./kWh over 20år. Sammenlignet med vareforbruget for dieselgeneratorerne, 2,29 kr./kWh i , er der gode muligheder for en rentabel omstilling til vedvarende energi. I næste kategori, benævnt diesel byer, blev der fundet et stort potentiale for udnyttelse af restvarmen fra elproduktionen. I fokusbyen, Nanortalik, forslås på baggrund af analysen, opdatering af dieselgeneratorerne, udvidelse af fjernvarmenettet, og introduktion af 500-1500kW vindenergi. For den sidste kategori, benævnt vandkraftbyer, er der et potentiale for andre vedvarende energikilder, hvis vandkraftresursen bliver utilstrækkelig. Forskellige monitorerings- og modelleringsmetoder for vindresurseestimering er undersøgt, med fokus på deres anvendelighed i kompleks arktisk terræn. Først blev de eksisterende klimastationer undersøgt for at fastlægge deres anvendelighed for vindresurseestimering. Målingerne var meget påvirket af det komplekse terræn, inhomogenitet i måleserierne, og afviger fra de gældende WMO retningslinjer. Næste step var udvikling af dedikerede vindmonitoreringsstationer til brug i dette miljø og testning af dem på udvalgte sites. De gennemførte instrumenttests viste, at selv ikke de bedste instrumenter kunne overleve på de mest udsatte steder. En større

testserie er planlagt, men på grund af forsinkelser er testresultaterne endnu ikke tilgængelige. Baseret på målinger, er vindklimaet for 10 sites blevet vurderet, 4 i Uummannaq området, 5 i Sisimiut området og foreløbig 1 i Nanortalik området. Kun to af disse sites havde en verificeret middel vindhastighed på over 6 m/s, men yderligere èt har potentialet. En af disse sites, Nanortalik Dump 1601, blev studeret mere detaljeret ved estimering af indstrømningsvinkel, grænselagsstabilitet og fordeling af turbulensintensiteten. Nanortalik Dump blev klassificeret til IEC IIIS på grund af et forhøjet turbulensniveau.
Til vindresurseestimeringen blev to typer modeller testet, mikro- og mesoskala-modeller. Testene viste at mikroskala modellerne alene kunne give et rimeligt resultat indenfor 500m fra reference sitet, afhængig af terrænet og de meteorologiske forhold. Mesoskala modellerne WRF og Polar WRF blev valideret imod 14 målepunkter i et 800 x 800 km stort domæne, og 3-D strømningerne i de komplekse fjordsystemer blev undersøgt. Endvidere blev modellernes vindfordeling sammenlignet med satellitbaserede vindobservationer. Valideringsarbejdet med mesoskale-modellerne viste at de tilgængelige overflade data, specielt haviskoncentrationer og terrænelevation, skal forbedres for at opnå en optimal modellering i hele domænet. I den sidste del af rapporten er der præsenteret nogle forslag til hvordan grønlandsk vindkraft kan udvikles, baseret på erfaringerne fra testvindmøllen i Sarfannguit. Hovedkonklusionen i denne del er at et godt forstudie af det eksisterende data, som satellit-baseret SAR vind, reanalysis data, infrarøde billeder af katabatiske strømningsmønstre og meteorologiske observationer, sammen med gode modeller er nøglen til en god site identificering. For at vurdere et projekts gennemførlighed og rentabilitet er detaljerede studier af infrastrukturen, råmaterialer og resurser nødvendige. Siden den fejlslagne vindmølle introduktion i 1983-1986, har vindkraft ikke været en del af de grønlandske forsyningssystemer, men den teknologiske udvikling og det at der nu findes verificerede resurser, kan måske åbne for vindkraften igen. Der findes stadig nogle modelleringsudfordringer, som skal løses før et vindresursekort for hele Grønland kan udarbejdes, men med dette projekt er grønlandsk vindkraft kommet et skridt nærmere.

Acknowledgement

Many persons have helped and supported me during these years of study, without whom I would not have managed to complete this thesis. I would like to thank them all for their help and contributions. I would like to give special thanks to the following:

- My supervisor, Martin O. L. Hansen for strong support and always taking the time to talk to me.
- My supervisor, Claire L. Vincent for inspiring discussions, strong support and invaluable input to the project
- My supervisor, Prof. Arne Villumsen for initiating this project and for sharing his network
- Senior researcher, Kurt S. Hansen, for good discussions, guidance and support
- The staff at Nukissiorfiit for sharing data, information and personal experiences with me
- The staff at Kujalleq Kommunia for practical support during the planning and field trips
- The staff at the Danish Meteorological Institute for sharing data and knowledge
- Senior scientist Merete Badger for sharing SAR images and knowledge with me
- Former CTO at TELE Greenland Steen Grossmann for his support and engagement and for sharing priceless knowledge with me -rest in peace.
- The staff at the Climate and Energy office Naalakkersuisut, for appreciation and support
- My colleagues at Artek, MEK and Wind for a very nice and inspiring working environment. Special thanks to Adriana Hudecz for nice cooperation and for surviving many weeks with me in the Greenlandic wilderness.

Contents

Abbreviations

ABL Atmospheric Boundary Layer

AEP Annual Energy Production

AMR Automatic Meter Reading

AMSL Above Mean Sea Level

AO Arctic Oscillation

ASIAQ Greenland Survey

ASR Arctic System Reanalysis

AWS Automatic Weather Station

BC Boundary Conditions

BL Boundary Layer

CFD Computational Fluid Dynamics

CHP Combined Heat and Power

DD Direct Drive

DMI Danish Meteorological Institute

DRR Data Recovery Rate

ECMWF European Centre for Medium-Range Weather Forecasts

ERA-I ERA-Interim

ETJ Easterly Tip Jet

GIS Geographic Information System

GLV Mittarfeqarfiit/Greenlandic airports

GSM Global System for Mobile communication

GTO Greenland Technological Organization

H stab. Hydro static stability method

HYP Hydro Power based systems

IC Internal Combustion

JMA Japan Meteorological Agency

LAM Local Area Model

LD Large Diesel based systems

MAG Meters Above Ground

MCP Measure Correlate Predict methods

METAR METeorological Aerodrome Report

MO Monin Obukhov

MTBF Mean Time Between Failures

MTBV Mean Time Between Visit

NAO North Atlantic Oscillation

NASA National Aeronautics and Space Administration

NCAR National Center for Atmospheric Research

NCEP National Centers for Environmental Prediction

NunaGIS Geographic Information System for Greenland

O&M Operation & Maintenance

OSU Ohio State University

PBL Planetary Boundary Layer

PRP Prime Rated Power

PV Photovoltaics

RANS Reynolds-Averaged Navier-Stokes

RE Renewable Energy

RIX Ruggedness Index [%]

SCADA Supervisory Control And Data Acquisition

SD Small Diesel based systems

SLP Surface Layer Pressure

TBO Time Between Overhaul

Tele Tele Greenland A/S

TKE Turbulent Kinetic Energy

UCL Urban Canopy Layer

WAsP Wind Atlas Analysis and Application Program

WMO World Meteorological Organization

WPD Wind Power Density

WRF Weather Research and Forecasting model

WT Wind Turbine

WTJ Westerly Tip Jet

Nomenclature

α Wind shear exponent (Power law)[-]

ap Atmospheric pressure [Pa]

β Empirical correction parameter [-]

D Displacement height [m]

ΔRIX RIX difference between reference and prediction site [%]

θ Potential temperature [K]

E_{kin} Kinetic energy [J]

E_{pot} Potential energy [J]

g Gravety $[m/s^2]$

k Von karman constant [-]

kWe kilo Watt electric [kW]

kWp kilo Watt peak [kW]

L Monin Obukhow Length scale [m]

N Number of measurements [-]

n Number of steps in the period

P Power [W]

P_{pa} Actual average power [W]

$\psi(z/L)$ Empiral stability correction term [-]

Q Radiation on surface $[W/m^2]$

Q_{tot} Total solar radiation on surface $[W/m^2]$

ρ Air density $[kg/m^3]$

RH Relative humidity [%]

Ri Richardson Number [-]

σ_u Standard deviation of wind speed [m/s]

t Time step length [s]

T Temperature [K]

T' Temperature fluctuations [K]

TI Turbulence Intensity [-] or [%]

u Horizontal wind speed [m/s]

u' Horizontal wind speed fluctuations [m/s]

U_m Horizontal wind speed modified

U_p Horizontal wind speed (predicted)

u_* Friction velocity [m/s]

V_N Norminel system voltage [V]

w' Vertical wind speed fluctuations [m/s]

wd Wind direction [Degree(N)]

ws Wind speed [m/s]

z Height above ground [m]

z_0 Roughness length [m]

Chapter 1

Introduction

This project deals with the estimation and implementation of renewable energy resources in Greenlandic energy systems. The focus area is wind power, but the status and potential of other sources, such as solar and hydropower, will also be described. The Greenland community is in a transition process where fossil fuel is being partly replaced by renewable energy. Hydropower resources have been implemented in several Greenlandic town systems, but growing demands and limited resources have opened for other renewable sources. One of these potential sources is wind power. To develop wind power in an area, knowledge about its wind resources is vital. In this project, different wind resource assessment methods, both direct on site measurements and modeling are tested in the Greenlandic environment. The performance of meso- and microscale modeling for wind resource estimation are evaluated for the southern and western part of Greenland.
Based on the wind resources for selected areas, the wind power potential for different types of Greenlandic energy systems are studied. To implement renewable energy sources in small isolated power systems knowledge about consumption, consumption patterns etc. is crucial. Methods to determine these for the different system types, based on existing data, are developed together with simple methods to identify reduction potentials, flexible consumption and system leaks.

1.1 Greenland

Greenland or Kalaallit Nunaat is an island located $59 - 84^o$ north and $11 - 74^o$ west. Greenland has an area of $2.2 \cdot 10^6 km^2$, and only $4.1 \cdot 10^5 km^2$ of this is ice-free. The ice cap covers the central part and with a height of up to 3.2 km, it has a major influence on the climate and the conditions of life in the area. The ice-free and populated part is located in the coastal area around the large ice cap.

The topography of the main part of the ice sheet is relatively simple with soft curved elevation changes, but on the edge, rivers of melting water and ice transport, have created a more complicated and even dynamic topography. The ice-free coastal areas consist of mountains and many islands, mainly of rock with limited or low vegetation. In most of the ice-free part the mountain peaks are 500-1500m Above Mean Sea Level (AMSL) and are split by valleys and fjords. The complexity of this terrain varies from area to area, but most of it can be characterized as moderate to very complex, with steep slopes and narrow valleys.

With a population of 56,282 in 2014 [Petersen, 2014], it is generally one of the least

populated parts of the world. The population is distributed along the coast within 17 towns and 53 settlements. Over the last decades, the population in the largest towns has increased, while the settlements have been depopulated. The five largest towns have grown in the last 30 years from 44% to 57% of the total population, and in the capital, Nuuk (Godthaab), the population has doubled.
Greenland is an autonomous part of the Danish kingdom, with its own legislature controlling some of its internal policies. Greenland entered the European Economic Community in 1972 as a part of Denmark. After the Home Rule Act in 1979, the Greenlandic home rule government was established, and after some disagreement about commercial fishing regulations, Greenland decided in 1985 to leave the European Common Market. A revision of the Home Rule Act providing greater self-administration came into force in 2008, and as a result, Greenland is not subject to internal Danish or European laws.

Public transport in Greenland is based mainly on small air planes, helicopters, and boats. The mountains and fjords limit the areas where road and rail transport are feasible to small areas around the cities. The large distances make boat transport very time consuming, so it is used mainly for local transport and for tourists. All telecommunication is handled by the monopoly company TELE Greenland, which is owned by the home rule government. This structure has secured a strong communication infrastructure even for the most remote villages. The power infrastructure is very limited, and only two towns, Qaqortoq and Narsaq, are connected with overhead lines. The rest of the overhead lines only connect hydropower plants with the related town. As the overhead lines are possible points of connection for larger RE systems, the potential catchment areas are limited by the distance to the existing infrastructure. All power infrastructures are owned by the home rule government company Nukissiorfiit, which has a monopoly on power production to the grid except from small private RE installations.

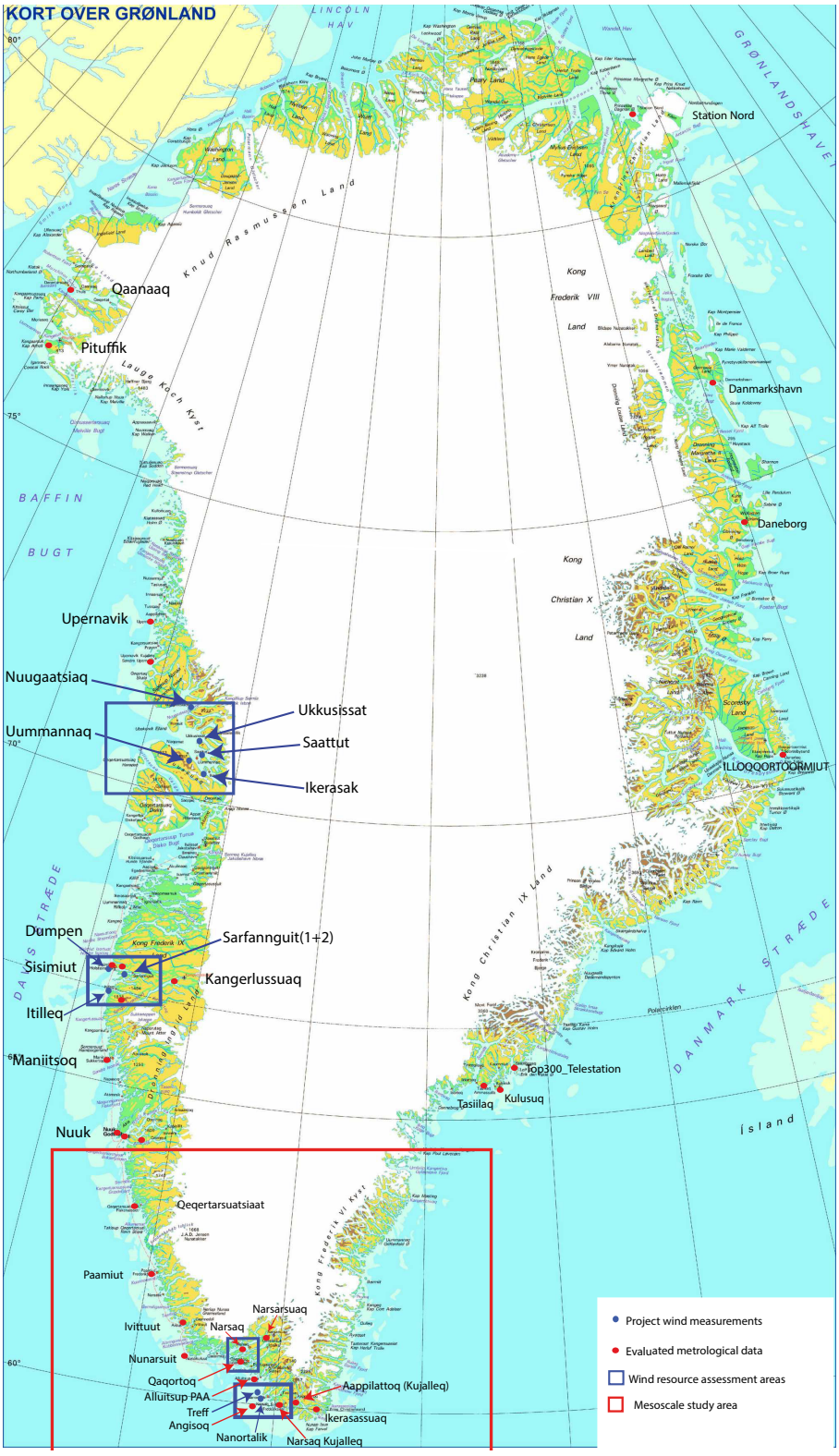

Figure 1.1: *Geographically overview of project activities. Data source: KMS(G250)*

1.2 Greenlandic energy consumption

Greenlandic energy consumption increased during the 1990s to 2700 GWh in 2000. Higher gas oil prices in 2001 and 2002 might have led to lower demand in these years, because when prices increased again, the consumption followed down. The same relation was not seen when energy costs really started to raise from 2004, Fig. 1.2. The gas oil price has grown about 10% per year for the 10 year period 2002-2012, from 2.38 to 6.65DKK/L. If energy for oil & gas exploration activities is excluded, the oil based consumption decreased by 200 GWh from 2009 and on. This can partly be explained by the large hydropower expansion, by which installed capacity was enhanced from 31 MW in 2009 to 91 MW in 2012, Fig. 1.4b. The hydropower plants replaced old diesel generators with relatively low efficiency. The energy supply consists mainly of gas oil, 68%, but renew-

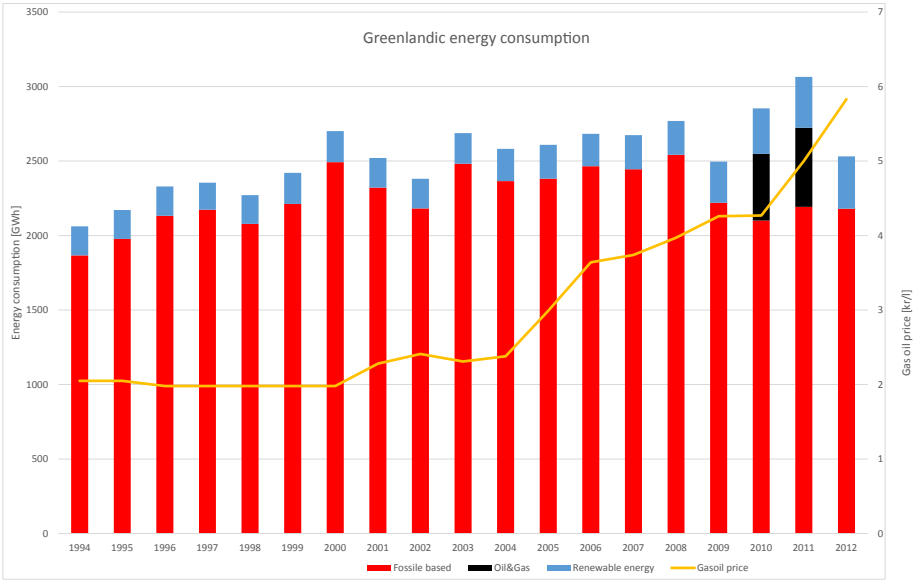

Figure 1.2: *Energy consumption split into fossil and renewable sources. The black market consumption for 2010-11 is related to offshore oil and gas exploration by Cairn Energy. The Greenlandic gas oil price [DKK/L] is shown by the curve. Data source [Baunbaek, 2013]*

ables gradually increased to 14% in 2012, Fig. 1.3. Of the total consumption, 28% is used for industry, mainly the fishing industry, 27% in households for power and heating, 19% for trade and service, and 14% for transport.

Around 85% of energy consumption in Greenlandic households, or 583 GWh, is used for heating, while the remaining 103 GWh is used for light and power [Baunbaek, 2013]. The large heat fraction emphasizes that the heat demand has to be considered whenever a renewable energy supply is introduced. Grid-based energy consumption consists of electrical consumption in the 17 towns and 53 villages on the public electricity grid and parts of heat consumption for the 12 towns with district heating systems. Grid-based

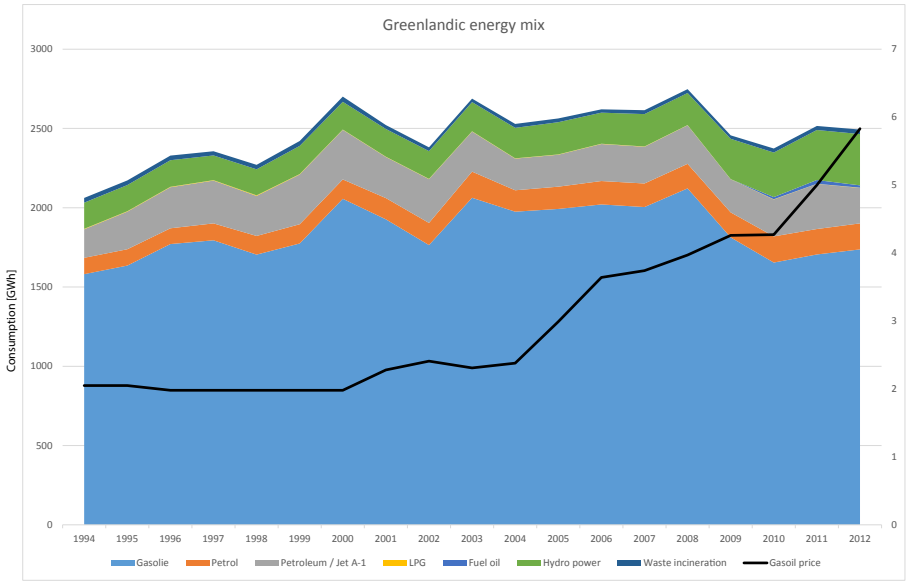

Figure 1.3: *Inland energy consumption in [GWh] distributed by the different sources (without oil and gas activities). The black line shows the Greenlandic gas oil price [kr/l] in the period. Data source [Baunbaek, 2013]*

energy consumption was 20% of total energy consumption in 2013, and 64% of this was based on renewable sources, Fig. 1.4a. Renewable energy consists of 20-30 GWh heat from waste incineration and the rest is hydropower. The first hydropower plant at Bukesfjorden was put into operation in 1993 with a capacity of 30 MW. In 2005 the 1.2 MW Tasilaq plant was built. In 2007 the 7.6 MW Qorlortorsuaq plant was operational, and in 2008 the Buksefjorden plant was expanded with another 15 MW turbine. This was followed by a 15 MW plant in Sisimiut in 2010 and Ilulissat a 22.5 MW plant in 2012 Fig. 1.4b. The total production at the Greenlandic hydropower plants was 325GWh in 2013.

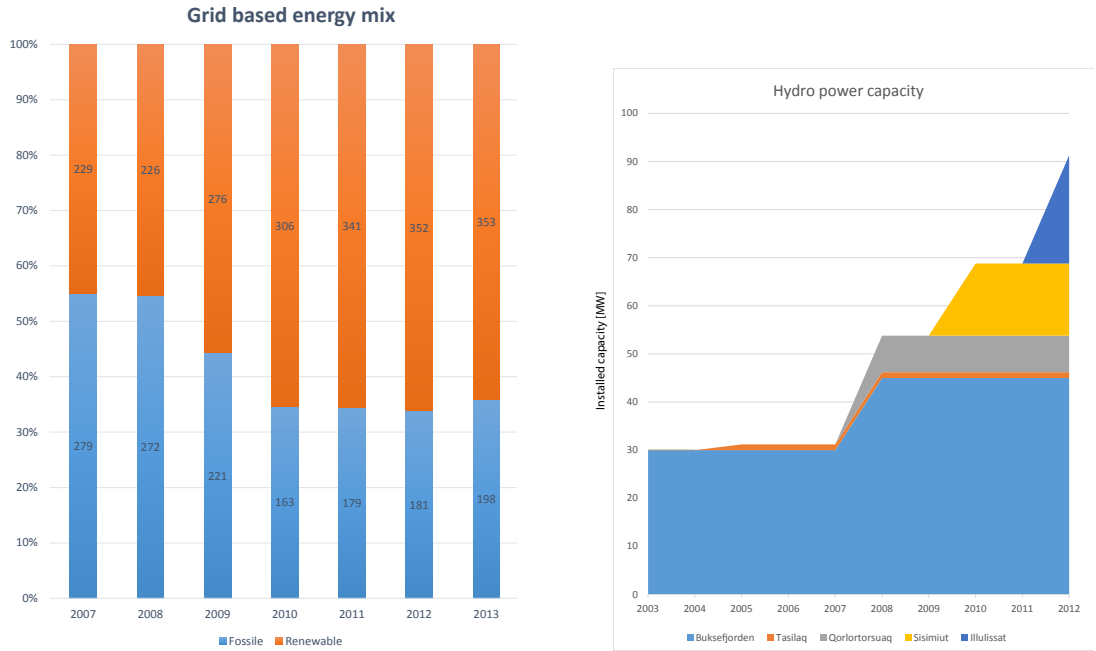

(a) (b)

Figure 1.4: *a) Electrical and heat grid-based power. The renewable energy sources are waste incineration and hydropower. The main fossil source is gas oil converted into heat by boilers or into electricity by generators. b) Development in installed hydropower capacity. Data source Nukissiorfiit and [Baunbaek, 2013]*

1.3 Energy costs in Greenland

Gas oil is the main energy source in Greenland and the price of gas oil controls the main energy cost in the country. In the period 2000-2013, the gas oil price has tripled, and it directly influences the price of central and local heating, and the cost prices of electricity, except for the five hydropower systems. Greenlandic energy prices have historically been controlled by long-term delivery agreements between international oil companies and the home rule company Polaroil. These contracts have kept energy prices very stable compared to the world market, but in the period 2000-2013, the price has increased by 10% each year. The average gas oil-based energy price in 2014 was 0.667 DKK/kWh, and the petrol-based was 0.684 DKK/kWh, Fig. 1.5.
The central heating cost is not directly linked to the gas oil price, but is set by the government, based on the cost of individual heating. From 2006, the electricity prices in Greenland should have been based on the local cost prices for electricity production, but to protect the villages, a cost distribution system was introduced. The system consists of a minimum and maximum price set by the government, based on the total cost of electricity production in the country. The minimum price was 1.62 DKK/kWh on 1. of January 2014 and the maximum price was 3.29 DKK/kWh. In 2013, under this system the 6 towns with access to hydropower paid between the minimum and the maximum price while the remaining 65 paid the maximum price. The production costs in 2013 ranged from 1.11 DKK/kWh in Nuuk (230 GWh/year) to 16.76 DKK/kWh in Naajaat (0.05 GWh/year). The fishing industry pays only 41.5% of cost price, and in this way,

the government uses the energy price as a subsidy, but the fixed fraction encourages the industry to pursue the systems with the lowest costs.

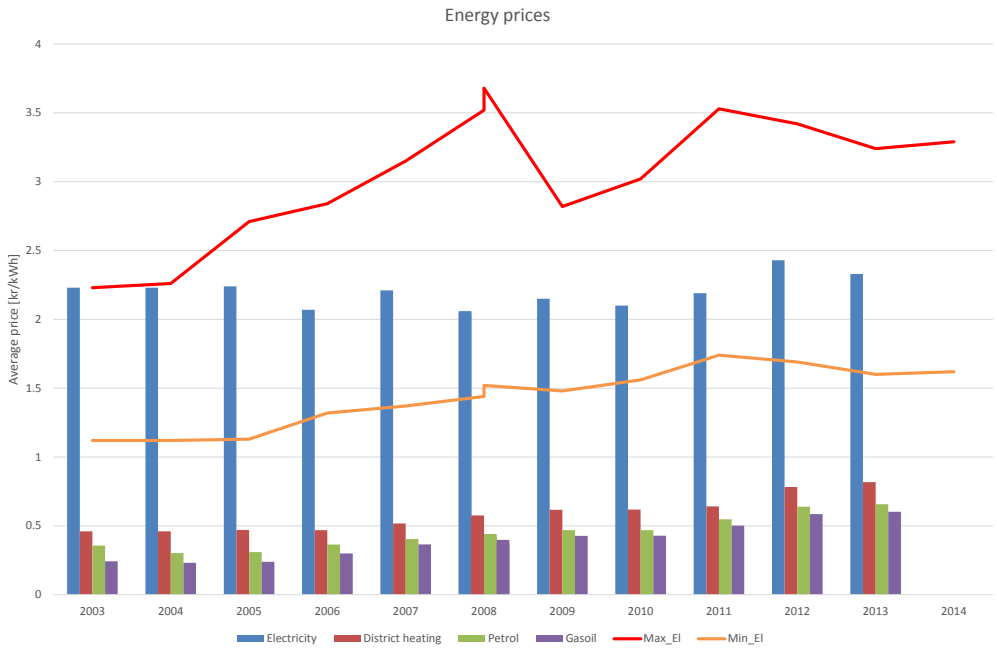

Figure 1.5: *Greenlandic energy costs and the politically set limits for the electricity prices. Data source Nukissiorfiit and [Baunbaek, 2013]*

1.4 Objective

The objective for this work, performed in the period 2010 to 2014, was to add new knowledge about the renewable energy potential and especially resource assessment and implementation in complex Arctic areas. More specific, the aim of the project was to test methods for wind resources assessment and optimization of the Arctic power systems for better planning and development of the renewable energy transition. The objectives can be divided into the following points:

- Test general methods for wind resource assessment in the complex Arctic terrain
- Investigate the potential for implementation of renewable energy in small isolated energy systems
- Examine existing consumption and production data for their applicability in RE implementation studies
- Suggest a general method for wind resource estimation in relation to planning and implementation

This project deals with different methods for wind resource assessment, both locally and for larger areas. Direct measurements via anemometers, indirect measurements through satellite-derived ocean wind, and micro- and mesoscale models have been used to study

the wind in Greenland. A larger validating experiment was designed and installed at a remote location in South Greenland, but the experiment was delayed and was not completed in time for this report. However, the results can be used for coming projects.

The thesis does not deal with system stability analysis as, power quality, or system response in relation to wind power integration in small isolated grids. The PhD project was created in cooperation with two DTU institutes; Mechanical Engineering and the Arctic Technology Center in Civil Engineering, with the Greenlandic energy company Nukissiorfiit as collaborator. Within the frame of this project, three research projects in the lighthouse project line were done and the results published in the lighthouse reports. This report only present the overall results and conclusions. For the full results all the related publications can be examined.

1.5 Structure and reading guide

This thesis consists of 4 main chapters, chapter 1 gives the basic background information about the Greenlandic energy situation and potential, chapter 2 about Greenlandic energy systems, including a presentation of the basic results and detailed examples from the system studies, chapter 3 about wind resource monitoring and modeling, and finally chapter 4 summarize the wind power development and gives recommendations for future projects.
Seven appendixes are included, A-G. In appendix A, all basic information and statistical data for the stations operated in this project are presented. The operation included; design and installation or adaption from other projects, yearly service, data processing, and decommissioning. In appendix B the terrain elevation data used in this project is presented, together with the results of the validation processes. Appendix C includes an example of the standard ice charts from DMI, used in the sea ice data validation process. Appendix D includes a short description of the wind turbine test in Sarfannguit, installed in 2009-2010 and operated in as a part of this project. The experiences gained in the installation and operation is described in this report. Appendix E include the popular science paper populated together with this report. Appendix F present the statistical formulations used to evaluate performance of used model. Appendix G show an example of the used WRF input files with detailed information about the model configurations.

This thesis presents the overall finding of the project together with some basic knowledge, however to achieve the full potential, basic knowledge about; wind power meteorology, wind turbine technology (design, performance, limitations), atmospheric and power system modeling, and arctic infrastructure is required. To help the readers abbreviations and nomenclature is placed in the beginning of the report and hyperlinks to these are placed in the report.

Color print in 600 DPI is recommenced due to detailed color figures

The two papers submitted to international journals, the two conference contributions, and the three reports composed as part of this project are not included in this thesis but are or will be online available.

Chapter 2

Energy systems

This objective for this chapter is to introduce the Greenlandic energy infrastructure, the challenges in, and potentials for system optimization and transition to renewable sources. The public energy grids in Greenland are owned by the home rule company, Nukissiorfiit, and include both electrical and district heating grids. This chapter introduces the basic design methods for fuel-based power plants, and the related cost distribution. In this study the isolated power systems are divided in to three groups based on the overall system types; village systems (Small Diesel, SD), fuel cities (Large Diesel, LD), and hydro cities systems (hydro power systems, HYP).
Site specific case studies were carried out for systems in each group (Sarfannguit (SD), Itilleq(SD), Nanortalik(LD), Qaqortoq(HYP), and Narsaq(HYP)) and the results for two representative systems, Sarfannguit and Nanortalik, are presented in this chapter. The village case study for Sarfannguit is further more used to present examples from; the renewable energy potential studies, the reduction potential studies, and to present the smart meter potential study.

2.1 Introduction

The first public electricity grid in Greenland was established in 1949, and the last town got electricity in 1975. Public electricity in the villages was established by the local municipalities from 1976 to 1998 [Statistik, 1999]. In 1998, Nukissiorfiit acquired the responsibility for 56 electrical systems from the local municipalities, but in 2007 and 2010, the villages Uunarteq and Moriusaq were abandoned.
In addition to the Nukissiorfiit systems, there are electrical systems in the two international civilian airport villages, Narsarsuaq and Kangerlussuaq, operated by Mittarfeqarfiit/Greenlandic airports (GLV). Apart from the civilian systems, there are several military installations where Thule Air Base with its 600 staff members is the biggest.
Electricity production in the 54 villages, 2 airports, 11 towns is based on gas oil, and in the last 6 towns mainly on hydropower.
The Greenlandic systems supply can be grouped by power used/conversion type, Table 2.1. Three towns have medium speed generators, eight towns have Combined Heat and Power (CHP) production units based on single-cycle medium speed generator sets with flue gas boilers, six have hydropower and five have waste incinerators for heat production. The four largest towns, Ilulissat, Sisimiut, Nuuk and Qaqortoq have both hydropower and waste incinerators, while Maniitsoq has CHP and a waste incinerator. The last nine towns have only CHP units supplemented with oil boilers for heating. The 54 village system

consists mainly of standard high speed diesel generator sets, often with a shared cooling water system that is used for local heating. The two airport villages use CHP, like the towns.

	Power	CHP	Hydro	Waste
Towns	3	8	6	5
Villages	54	2	0	0

Table 2.1: *Power production units in the Greenlandic systems. Data source Nukissiorfiit.*

2.2 Design of internal combustion power plants

Most of the Greenlandic power plants are based on Internal Combustion (IC) engines, mechanically coupled to a generator. Optimally designing of Internal Combustion (IC) power plants for isolated systems with high safety of supply is a complicated task. When power plants for isolated systems are designed, there are some standards that can be used as guidelines:

- Unit sizing: ISO 8528, ISO 3046 ...
- Power quality: EN 61000-2-2, EN 50160
- Emission: EU Stage IV, EPA Tier 4 ...
- Noise emission: mst nr. 5 / 1984

The standards, ISO 8528 and 3046, describe test and measurement methods for power generation systems, which make performance comparison possible across brands. The standard also set minimum requirements for the units. The standards state that a prime-rated generator must be able to handle an actual average power (P_{pa}) of 70% of its prime rated power (PRP), unless the manufacturer allows a higher average load factor. In addition, the generator must be able to handle 110% load for 1 hour of every 12 hours.
When the actual average power is calculated according to ISO $8528-1$, based on the expected load profile (2.1), the actual profile is used for all loads above 30% of the (PRP). For loads below 30% of the PRP, 30% of the PRP load is used as the load.

$$P_{pa} = \frac{\sum_{i=1}^{n} P_i t_i}{\sum_{i=1}^{n} t_i} \quad P_i = \begin{cases} P_i, & \text{if } P_i > 0.3PRP \\ 0.3PRP, & \text{if } P_i \leq 0.3PRP \end{cases} \tag{2.1}$$

where:

P_{pa} Actual average power

P_i Load in the time-step i

t_i Time length of the step i

n Number of time-steps in the period

i Actual time-steps

PRP Prime Rated Power

Power quality is another key parameter for isolated power system design. It is necessary to consider both steady-state and transient requirements for voltage and frequency in relation to the actual load characteristic.
For the villages, the standard single used consumption limit is set to 32 amps for 3-phase and 30 amps for single-phase connections. Larger installations need to be approved by the energy company which will take the necessary actions to maintain the power quality in the grid. According to EN50160, the grid limits for non-interconnected systems are $50Hz \pm 15\%$ *and* $V_N \pm 10\%$. Lower voltage levels are accepted for periods up to 60 s a few times a day (voltage drops). If sensitive equipment is connected to the grid, flicker and harmonics also need to be considered.
Unless larger units are approved for a given system, the 32 amps (12.8 kW) limitation can be used as a design criterion. Generally, diesel engines do not allow load steps larger than 33% of rated power, meaning that the minimum running capacity is ≈ 40 kW.

Emission from diesel engines is a focus area in many parts of the world. The United States, India and Europe have restriction programs to force the development of more environmentally friendly engines. The restrictions have driven the development of more efficient engines, but it has also forced the manufactures to implement different flue gas cleaning methods that has a negative impact on both the performance and costs. Greenland has not implemented emission limits in its environmental legislation, but new industries need a pollution permission. The lack of legislation means that the power company has the freedom to optimize the power plant with an economical focus (consumption optimized engines).
Noise emission is in the same way unregulated, however Greenlandic power plants are often centrally located in the villages, limiting the noise emission that the local residents will accept.

The fuel economy of a diesel generator has been more or less constant for many years, but since 1999 the tightening of emission limits has forced the development of more efficient engines. For a typical village generator set, 4 cycle 1500rpm 200kW, this development has cut consumption at the optimal point from 204 to 190g/kWh. On top of this, the consumption is more constant throughout the load span 20-110% PRP. This cuts the fuel cost by > 0.1 DKK/kWh at a fuel cost of 6kr/L. By taking advantage of the lack of emission restrictions, and order fuel optimized versions without cleaning systems (particle filter, exhaust gas recirculation and catalyst), the engine costs will be 5-30% less than the versions in compliance with e.g. Tier 4.

Low load operation is a common problem for diesel generator engines. Long periods of low or extreme low load operation will often result in soot deposits in the cylinders, turbo chargers etc., and unburned fuel accumulation in the turbo charger, caused by low cylinder pressures and temperatures. To prevent larger deposits and consequential damages the load must regularly be increased to $> 50\%$ PRP for some hours to burn the deposits away. The emission optimized engines are more sensitive to low load operation due to lower pressure and temperature operation and exhaustion cleaning systems. The best solution is carefully size the generator engines to the actual load profile, however modern engines controllers has incorporate cleaning programs that is activated if the condition monitoring detect these problems.

% of PRP	Description
0 – 25%	Extreme low load
25 – 40%	Low load
40 – 80%	Regular generator operation load
80 – 90%	High load
90 – 100%	Extreme high load

Table 2.2: *Load definitions for continues operating diesel engines . Data source: [Tufte, 2014].*

An economically optimal design not only depends on fuel economy and capacity costs but also relies on operational and maintenance costs. The service interval for this type of units varies from brand to brand and depends on the actual load profile. In general, periods with very high and low loads shorten service intervals and even the unit lifetime. Some manufacturers deliver dynamic maintenance systems that allow optimal control and service planning (500-1000 hours), other have fixed intervals (typically 400-600 hours), and some design a maintenance plan based on the design load profile (400-800 hours). The labor and transport costs related to maintenance on these remote installations are very high, and if new engines can extend the maintenance from 400 hour today to 800 hours or even more, this will have a considerable effect on production costs.

The power plants are, today, controlled by the power plant master controller and/or a Supervisory Control and Data Acquisition (SCADA) systems. Each generator unit is equipped with an engine speed governor and an automatic voltage regulator.
Modern generator units are equipped with digital unit control and monitoring systems that in addition to basic voltage and speed control, also monitor the generator and engine conditions (temperatures, pressure, vibrations, speed, torque etc.), and communicate with the SCADA system. The master controller takes care of the overall control and monitoring of; generator sets, load management, bus conditions, power quality, and the condition monitoring.
In modern systems, both the master and unit controller are remotely accessible through the Internet. Most manufacturers offer online condition monitoring services, where monitoring data is automatically sent to the manufacturer for processing. Based on the online analysis, the manufacturer delivers remote online error recovery and optimized proactive maintenance plans that minimizes operational costs and unplanned downtime.
Online monitoring services have a high potential for Greenlandic power plants. It offers constant monitoring by the worlds leading experts even for the most remote plants. Proactive maintenance planning can minimize unplanned maintenance, extend service intervals and optimize spare part flow.

2.3 Villages power systems

The 54 village plants are designed with a focus on safety of supply and not cost of energy. The power plants consist of 2 to 4 diesel generator sets, with rated power from 30 to $480kWe$, often with a large excess capacity. The installed capacity depends on the industrial capacity in the villages and the population. Villages with fish factories, which need

a high freezing capacity, need large power capacity, while villages with only light industry and service need much less. The fishing industry uses most power in the freezing processes related to production, but production is often not stable over the year. Some factories are used only in certain periods, and several of the factories have been in unsettled periods with shifting ownership. Total electricity consumption in the 54 villages has increased over the last 10 years from 21 GWh in 2003 to 22GWh in 2013; 5-6GWh of this is used in the fish industry.
Unstable fish production is a challenge for plant design and production planning in the Greenlandic villages. The power plants are often designed based on historical maximum and mean loads and not the full load history. The service intervals are 400 hours per unit, and the time between overhaul (TBO) for the village generators are around 10,000 hours, with a lifetime up to 60,000 hours. With a standard configuration of three units and limited parallel operation hours, this gives up to 20 years lifetime. The lifetime depends on the service and overhaul costs and technological development.

2.3.1 Operational philosophy

The plants are equipped with 2-4 generator units with shared cooling and fuel systems. The shared jacket cooling system is used to heat the standby units and the connected buildings. A few units also have exhaust heat exchangers coupled to the system.
Most of the power plants in this category are designed with equal size generators, where one unit can handle the base load and two in parallel can handle all peak loads. The plant has one SCADA system controlling; the load shear, unit start/stop, cooling, etc. The SCADA system is connected to the internet and can be remote monitored and controlled, however this option is rarely used. The unit controllers are not remote assessable and with no SCADA redundant, the plant control rely on the SCADA unit. A SCADA failure will not necessarily cause a blackout, but the plant cannot react on consumption changes and if an online unit fails a new unit will not automatically take over. To minimize the risk of blackout each plant are regularly inspected (at least once a day on working days) and one local operator has always to be on standby. This service requires no less than 2 skilled operators per plant and this account for the main part of the local staff charges for this category (91 man-years or around 20 mill.DKK/year).

Modern remote power plants are design with minimum two independent communication channels (hardwired+sattelite) connecting both the SCADA system/systems and each generator controller directly to the local (Nukissiorfiit) and the central (supplier) monitoring & diagnostic centers. A failing component will immediately be identified and in most cases backup hardware will take over its functionality automatically. In case of larger failure cascades the local or central monitoring & diagnostic center will take control and in most cases solve the problem.
The condition monitoring systems in modern generator unit is very advanced and includes often dynamic maintenance planning tools. The system constantly estimate the remaining lifetime and maintenance status of the subcomponents (bearings, filters, drains...) and lubricants, enable optimal maintenance processes and minimizing the O&M costs. The service and maintenance performance for these plants is measured in Mean Time Between Visit (MTBV) and ideally this is equivalent to the service interval (6-8 weeks). When or

if the systems are updated, all monitoring and maintenance work on these system can potential be handled by few skilled technicians. The monitoring and diagnostic for all systems are handled central and no local technicians need to be permanently on standby.

2.3.2 Energy costs in village

For all Greenlandic power systems, the production costs are published once a year. The production costs are published as cost per unit sold (DKK/kWh) and are split in five fractions: cost of goods, staff charges, capacity cost, depreciation and interest expenses. It should be noticed that this official statistic presents the total system cost per sold unit. The cost of goods is the variable cost directly related to production and covers;

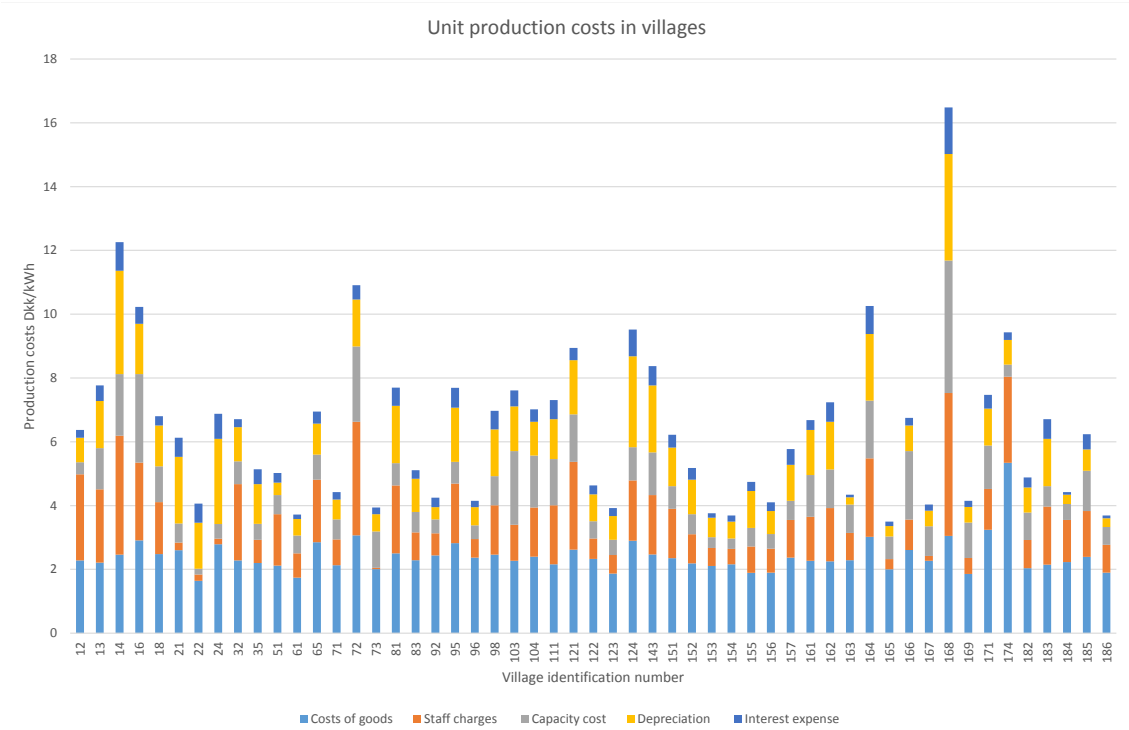

Figure 2.1: *Production costs for the 54 village systems [kr/kWh (sold)], Source: Nukissiorfiit [Nukissiorfiit, 2014]*

gas oil, lubrication oil and filters related to the production. As shown in Fig. 2.1, this cost varies from 1.74 to 5.34 DKK/kWh with a mean of 2.41. Modern generators in this size range have a peak efficiency of $> 44\%$, and with a common load distribution, an average annual efficiency of 38% can be expected. With a mean gas oil price in 2013 at 6 DKK/L, this gives a fuel-related cost of 1.59 DKK/kWh. The costs of the remaining goods will only add for a few percent on top of the fuel costs. The lowest cost of goods is thus close to the expected level for these plants, while the highest is at a very high level.

Staff charges include maintenance work and technical support. The service interval depends on the brand and age of the generator units, while the unscheduled maintenance is highly dependent on the monitoring and service level. With a range from 0.04 to 4.48

and an average of 1.41 DKK/kWh the differences if very large. In general, smaller units require more maintenance per kWh produced because of lower production per operation hour. Staff charges include not only direct generator operation but also system operation and transport. If the staff charges are compared with the generator age or the plant location, there is no clear trend, but it is remarkable that the top 10 highest-cost locations include four out of five villages in the Nanortalik district.

The last three fractions are related to the system costs. The capacity costs are related to the investment. The depreciation ideally scales with operation time or lifetime use, and in this case, where it is per unit, it scales with the capacity factor (average load factor). The interest expenses depend on the interest rate and remaining debt and thus the system age. The interest rate is fixed by the government at 6% per year, so it varies only with remaining debt.

A detailed study of the data behind the official cost statistic showed that the main cause of the large difference is the internal consumption. On average the internal consumption accounts for 14% of the total production, with a variation from 0.4 to 45%, for the 52 villages monitoring this. Based on the internal consumption share for the 52 village systems the total internal consumption is estimated to 1.2 GWh/year.
Inspection of the installations and meters in selected villages showed that the monitoring is not consistent for all plants. The internal consumption covers on top of the direct production related; as pumps, vanes and controllers, also; lightning, heat tracing of sewage and fresh water installations, employer facility heating, hot water production, and various domestic appliances. The inspections and interviews with the local staff exposed a big difference in the knowledge level and focus on internal consumption. Small changes in daily routines and small modification of the installations can have a big impact on the internal consumption. One of the simple and obvious modification is to utilize all "waste" heat before electrical based heating, for facility heating and hot water production.

2.4 Case study, Sarfannguit

In this project some village systems have been studied with a focus on energy savings, system optimization, and renewable energy potential [Jakobsen et al., 2011]. Some results for the case village, 083 Sarfannguit, will be presented here.
Sarfannguit is a small village 40 km east of Sisimiut, West Greenland. The village has 121 inhabitants [1], most employed in the fishing industry. The local fish factory fillets and freezes mainly cod and wolf fish in the simple processing plant. Public service include; school, day care, nursery, shop, post office, telephone and Internet, youth center, administration, a weekly connection boat, water and electricity supply. The village has since 2006 been a part of an innovation project called "Lighthouse village, Sarfannguaq" with a focus on sustainability. The main focus of that project was energy saving and renewable energy supply, and it was further developed in this project.

The key figures for the electrical system are consumption and production costs. The consumption study was conducted, based on AMR data (2007-2014) and manual readings

[1] Statistics Greenland 2014

Figure 2.2: *Local map of the Sisimiut-Sarfannguit-Kangerlussuaq area (Mid-western Greenland), Source: Google Eath*

($<$ 2007), see section 2.4.1. The AMR data include 15 minute or hourly reading for the 71 consumers. To simplify this, the consumers were grouped in 6 main groups Fig. 2.3. The local Pilersuisoq store (KNI), owned by KNI A/S, has implemented some of the identified reduction potentials, for example replacing some of its domestic refrigerators and freezers. This focus on energy savings has led to a 33% reduction for KNI. The industrial consumption is related to the amount of fish landed in Sarfannguit. There is wide variation in yearly industry consumption (63-250MWh) due to the variation in fish, fishing quotas, and operational conditions. The non-industrial consumption was 286MWh in 2013, 100MWh of these were used in private households. Average private household consumption was, based on the detailed building register combined with the AMR data calculated to 2MWh/year, witch is much lower than the 16 GJ (4444 kWh) presented in Baunbaek [2013]. To eliminate the effect of varying occupants, the data was further combined with the population register. A standard households was defined as two adults with 2-3 children and the average consumption of these households in Sarfannguit, for the five years used (2009-2013), was $\approx 2.4 MWh/year$. The deviation from the official average consumption can be explained by the inclusion of electrical heating, in the hydro cities, in the official data.

The net production costs Fig. 2.4 show how the unit production cost developed in the period (2009-2013). The fact that the unit costs are calculated based on electricity sold ($\approx$ net production) means that they do not directly reflect production costs. Production of internal-used power and system O & M costs influences the unit cost level. The cost of goods is related mainly to fuel oil consumption, but a smaller fraction is for lubrication oil, filters, and other related costs. Staff costs include both local maintenance staff and central planning staff. While most of the unit cost varies with consumption because of

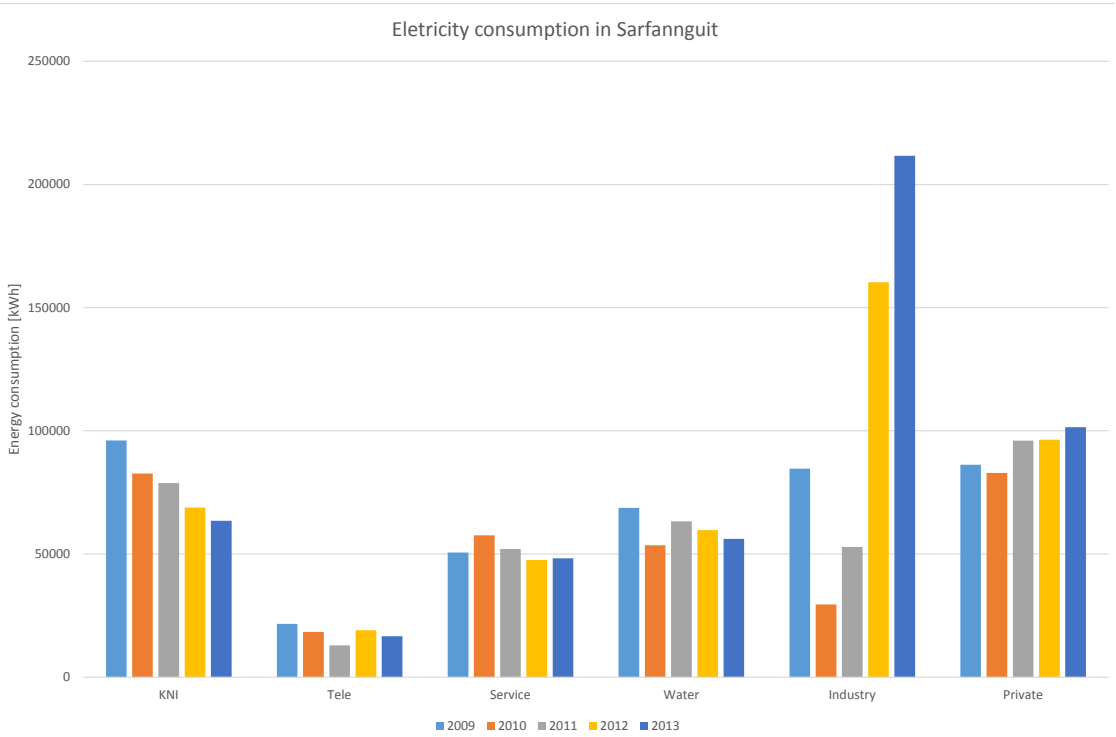

Figure 2.3: *Electrical consumption in Sarfannguit distributed on sectors. KNI is the local store, Tele covers all telecommunication, Service covers school, day care, public house, church, hospital workshop and street light, water distribution, fish factory, private households. Data extracted from the AMR database.*

the high share of fixed costs, the cost of goods just rises owing to increasing fuel costs Fig. 1.5. The internal power plant consumption is in the range 55-75 MWh/year for the period or around 15% of the sold amount and the actual production costs are there by $\approx 87\%$ of the official costs.

As earlier described the relatively high heat demand can be the key to a high renewable energy penetration. To determine all the city/village heat consumption, when all the heat are produced local on individual boilers, can be a complicated task. In Sarfannguit Polaroil/KNI is the only fuel supplier and detailed monthly registrations of their sales (1993-2013) was handed over to this project. Based on a registration of all the fuel consumers in the village it was possible to estimate the amount of fuel used for transport, cooking and heating. The average net heat consumption (assumed average conversion efficiency 85%) in the village (2004-2009) was estimated to 972MWh/year and the monthly distribution as shown Fig. 2.5. The monthly average heat power consumption varies from 33 kW in August to 190 kW in February, and this distribution follows the variation of the wind resources, making it attractive for wind power balancing. The heat consumption cannot, based on the available data, be split into individual user groups. The heat consumption can be distributed of the full building mass, but different heating systems, indoor temperature settings and hot water consumption make this method inaccurate. The total heat consumption can with some uncertainties be transformed to a time series

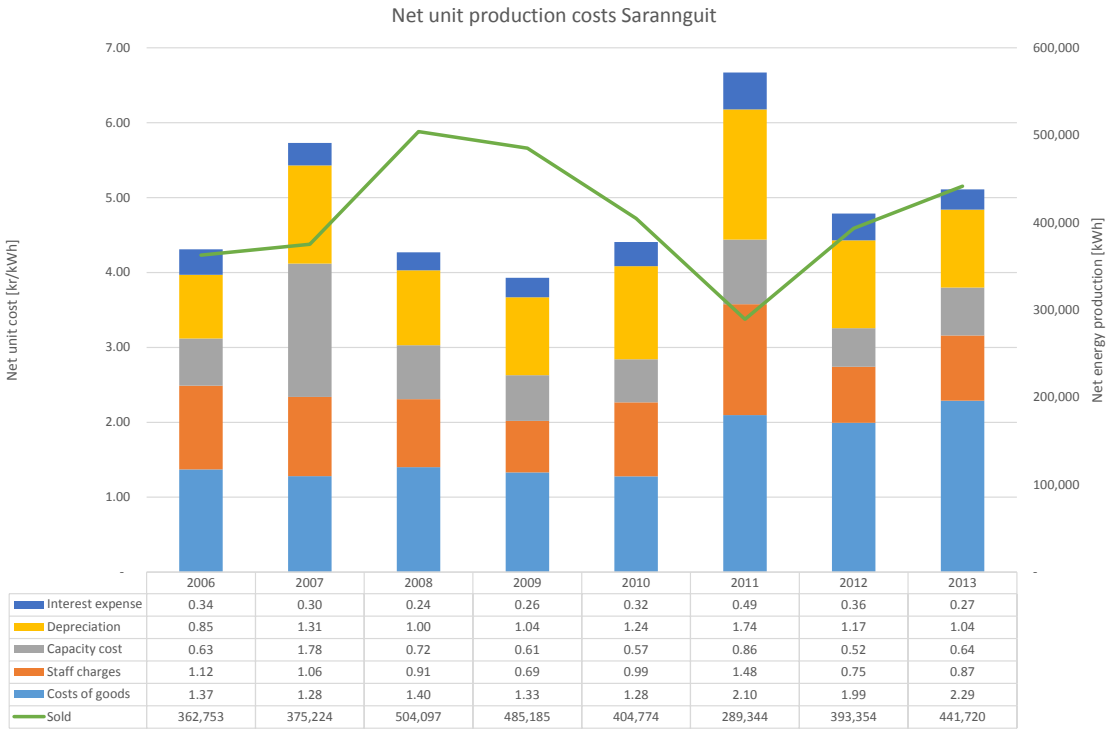

	2006	2007	2008	2009	2010	2011	2012	2013
Interest expense	0.34	0.30	0.24	0.26	0.32	0.49	0.36	0.27
Depreciation	0.85	1.31	1.00	1.04	1.24	1.74	1.17	1.04
Capacity cost	0.63	1.78	0.72	0.61	0.57	0.86	0.52	0.64
Staff charges	1.12	1.06	0.91	0.69	0.99	1.48	0.75	0.87
Costs of goods	1.37	1.28	1.40	1.33	1.28	2.10	1.99	2.29
Sold	362,753	375,224	504,097	485,185	404,774	289,344	393,354	441,720

Figure 2.4: *Net unit cost and net production. Source: Nukissiorfiit*

by using the correlation with outdoor temperature [Jakobsen, 2009].

Based on the measured gross and net heat consumption, the measured net electrical consumption and the power plant oil consumption, the total net consumption and the related losses can be calculated. The average yearly (2004-2009) gross energy consumption for the heat and electrical production in Sarfannguit was 2945MWh/year and the net consumption was 1545MWh/year. The net consumption consisted of 573MWh electricity and 972MWh heat. The monthly average net effect varies from 94 to 251kW.
The Sarfannguit power plant was refurbish in 2006 and the two oldest generators replaced with new 250 kVA New Stamford generators, powered by two Scania 197kW turbo charged engines. The power plant consists of three units based on the same engine:

1. Scania D9 95M 0355 (135kW) with New Stamford UCI274F2 116kW installed in 2002

2. Scania D9-95M 10-40 (197kW) with Newage Stamford HCI 4xxC 184kW installed in 2006

3. Scania D9-95M 10-40 (197kW) with Newage Stamford HCI 4xxC 184kW installed in 2006

The power plant is controlled by a PLC based SCADA system. A second generator is started when the load reach 96 and 150kW for the two generator types respectively. Parallel operation stops when the load for more than 20s has been less than 12/17.7kW of the start criteria. If the startup and synchronization time are neglected this mean that the

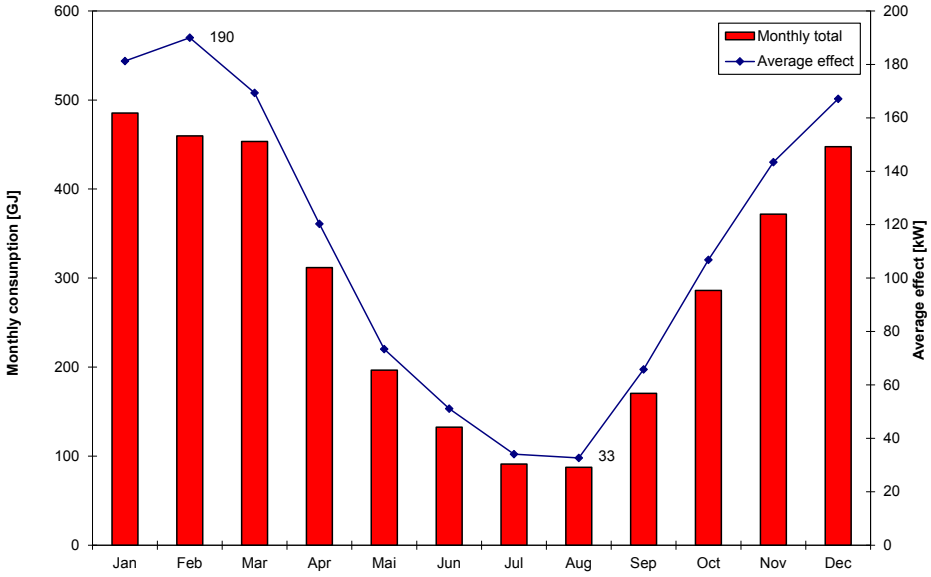

Figure 2.5: *Average heat consumption in Sarfannguit 2004-2009), Source: Polar oil*

engine loads never will exceed 102 and 160kW or 76 and 81 % prime rated power respectively. The maximum consumption (30ms sampling) registered in Sarfannguit 2006-2009 194kW. In the period 2007-2008 the maximum (30ms sampling) was 147kW and the related AMR measured consumption was 134kW (15minute average) or $\approx$ 10% on top of the average value. The generators in Sarfannguit are designed to 110% in up to one hour or 140 and 202kW respectively.

The theoretical efficiency of the generator sets Fig. 2.7a are relatively high from 55kW and up. That the two types of generators use the same engine size, means that the efficiency curves are more or less identical up to the limit of the small set. The load duration curve shows that the load was above the 55kW 5600 hours or 65% of the time in studied period Fig. 2.7b. The curve also shows that the small generator set is able to handle the load 97% of the time and the big units are able to handle all the loads. If the curve is compared with the defined load definitions Table 2.2 the engines operate at extreme low load 12% of the time and at low load 56% of the time. If the theoretical efficiency curve is used to calculate the efficiency directly based on the 15 minute AMR+internal consumption data, then the average efficiency should be 35.9%, however the average efficiency based on the measured oil consumption and production was only 33.4%. A minor part of the difference is parallel operation in relation to the generator shifts, but most likely also lees optimal operational conditions (non-laboratory conditions). The measured efficiency varies from year to year and from month to month depending on the load operation. In the 5 studied years (2004-2008) the measured average efficiency for the power plant was 29.1%.

2.4.1 Smart meter

One of the first initiatives in the lighthouse program was the installation of Automated Meter Reading systems (AMR) or "smart meters" (Kamstrup model 382E). All 71 end-user meters for electricity and 20 water meters were replaced by AMR meters. In the test

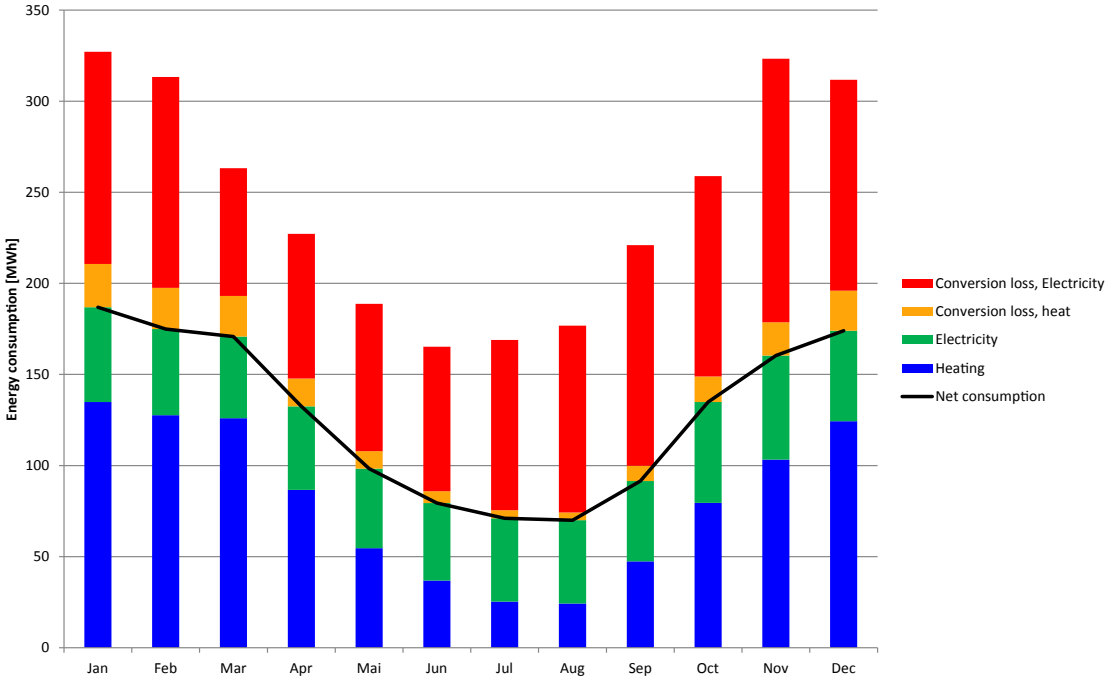

Figure 2.6: *Average heat and power consumption in Sarfannguit 2004-2009, Source: Polar oil, Nukissiorfiit, [Jakobsen, 2009]*

period 2007-2009, the reading interval was 15 minutes, but after 2009 the interval was extended to 1 hour. The meters register the total active and reactive power consumption, peak power and time stamp for peak power in interval, see all documentation at: https://www.kamstrup.com/.
The data is used primarily for automatic invoice generation and accounting, but the power company Nukissiorfiit would like to know other potential uses for the collected data. The study was done as a part of this project, and the main outcome was that the data was useful for:

- Redesign of power plants
- Optimize power plant operation
- Reduce consumption
- Monitor and optimize the grid
- Safe implementation of renewable energy
- Secure water quality by flow control

The SCADA systems installed in the village power plants are often very simple and do not log the full time series, and therefore automatic meters are the only source to derive the full consumption profile of the system. The insufficient setup in Sarfannguit prevents full benefits from being obtained. The main problem is that the power plant output meter, the internal consumption meter, and the production meter have not been upgraded to AMR, and thus total consumption, production, and grid loss cannot be determined with

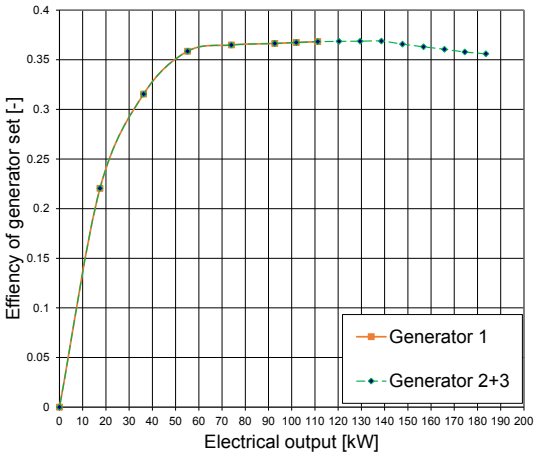

(a) *Theoretical efficiency curve for Sarfannguit generator sets, Source: Scania, Stamford*

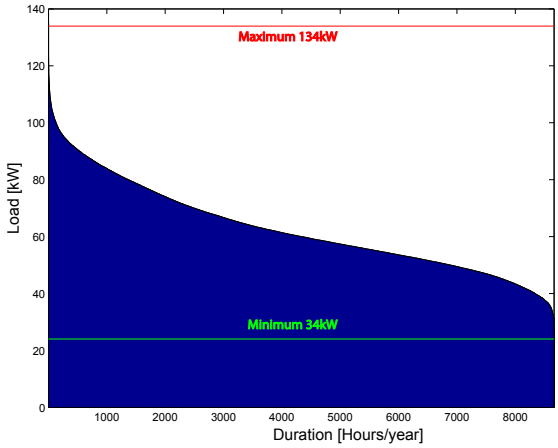

(b) *Electricity load duration curve for Sarfannguit 2007-2008, based on 15 minutes AMR. Source: Nukissiorfiit, [Jakobsen, 2009]*

the full resolution. In the AMR based load profile Fig. 2.7b the average monthly internal consumption was added to the AMR measurement to gain the full load profile, however it adds a bit to the uncertainties.
The system load profile is crucial for correct power plant design/generator unit sizing. The reactive power measurement can also be important for power plant design and optimal operation.
By knowing the load history of each connection point, the load of all parts of the grid can be determined and weak parts strengthened. Reactive power and large reactive power consumers can be monitored to make sure they fulfill the requirements. Point of connection for renewable sources and the effect on the system can be evaluated based on the load history for each connection point.
Similar to the electrical grid, the flow in the water grid can be modeled, segments with low flow can be identified, and problems with bacterial contamination due to long retention time can be minimized. The water plant was equipped with online AMR for output monitoring and by combing this with the consumer AMR system leakages can be detected.
The AMR data are very useful to identify saving potentials at the consumers. Base loads or standby consumption are easy identifiable and there is a large saving potential in this category. Greenland uses a large part of the electricity in thermal unit for frost prevention and backup heating. By correlating the AMR data with climate data, incorrect settings and defect regulation can effectively be identified and corrected. The AMR data can also be used for a complete mapping of the consumption at each consumer.

2.4.2 Reductions

Before renewable source are implemented in an isolated system good practice is to study the actual need. Identification of potential energy savings is a vital part of this process. In Sarfannguit the potential savings for each consumer were analyzed based on the AMR data, weather data, inspection of the main installations and interviews with the consumer. An example of the consumption mapping in Sarfannguit is shown Table 2.3. As the two last lines indicate the estimated consumption did not fully agree with the actual measured

for the particular week. The major part of the consumption in the building is related to the public laundry. Similar consumer mapping was compose for all public and selected private consumers.

Description	Power [W]	Operational [Hours/day]	Consumption [Wh/day]	Operation [days/week]	Consumption [Wh/Week]
Kitchenette	2300	2	4600	5	23000
Coffee machine	600	3	1800	5	9000
Kettle	1200	0.1	120	5	600
Tumble dryer	8500				
T D engine	245	5	1225	5	6125
Heating element T D	8000	3	24000	5	120000
Tumble dryer	2300	3	6900	5	34500
Washing machine	7900	0			
Heating element W M	7500	1.2	27000	5	135000
Engine W M	400	5	6000	5	30000
Electric iron	1200	0.4	480	7	3360
Microwave oven	1600	0	0	0	0
Chest freezer	180	5.5	990	7	6930
Refrigerator	90	3.56	320.4	7	2243
Heating cable	20	12	1200	7	8400
Estimated consumption	42035		74635		379158
Measured consumption					378785

Table 2.3: *Estimated consumption for municipal office in Sarfannguit. Based on AMR, inspections, and interviews*

For KNI new closed refrigerators in the store, with 70% lower energy consumption, were suggested and implemented. Additionally, replacement of circulation pumps in the heating system, service of malfunctioning heat tracing, low energy lightning, and optimization of cold storages and bakery processes are suggested. When the cold-storage room and freezer compartment need to be renovated, free cooling and separation of high and low temperature storage should be considered. The average outdoor air temperature is -2.1^oC and the temperature is below $2^o, C$ 60% of the year. The sea water temperature below the surface layer is relatively constant $1 - 3^oC$ and just outside the building. By using outdoor air or sea water, the energy consumption for cooling can be reduced by at least 50% compared to the present installation, where the heat is transferred to the hot storage $\approx 18^oC$.

The telecommunication installation was not inspected, but for other service installations, the largest reductions can be gained in the laundry, workshop and streetlight. The replacement of all streetlight in Greenland with LED-based light sources is in progress and the municipality has replaced refrigerators and freezers with more efficient versions, but there are more profitable replacements that can be done. The analysis showed that the best investments typically are to replace pumps, thermal and laundry equipment. Some examples of the identified potentials are listed Table 2.4.

In the water supply system, most of the energy is used to prevent freezing of the installations, but the study has shown a high potential for energy conservation.

Current	Current	Replacement	Saving	Saving	Cost
Unit	Type	Unit	kWh/year	kr/year	kr
Accelerator pump	UP20-15	Alpha2 20-40	500	1645	2600
Hot water pump	UPE25-40	Alpha2 25-40	245	806	1280
400l chiller KNI	Vestfrost	Vestfrost M200	1076	3550	5500
Nyborg dryer	T3190	Bosch WTY88890SN	2.7/cycle	8.86/cycle	7000
Tumble dryer	Class C	Heat pump based	3/8kg	9.9/8kg	6400

Table 2.4: *Examples of energy savings by hardware replacement in Sarfannguit. Jakobsen [2009] for further details.*

Modeling of the water flow in the system showed that consumption at tap house 5 (1302), in the depopulated part of the village, is so low that it can create a problem for water quality in the line between tap house 4 and 5(no other consumer on this line). The electricity used to heat trace the pipe from tap house 4 to 5 and heat tap house 5 is around 7MWh/year. Based on this, a reduction of the active water line is suggested.

The water treatment plant is heated by an oil boiler and two electrical heating panels of 1500W each. The heating panels are installed as a backup in case the oil boiler is off. At all inspections, the thermostat of the heating panels were set at or close to max, the indoor temperature was high and the boiler connected radiators was cold. This is an inappropriate setting because of the low oil-electricity-heat efficiency (0.25-0.25) compared to oil-water-heat (0.85-0.95). The suggested solution is; an external temperature control (3 degree set point) for the heat panels together with upgrading the boiler system (new radiator thermostats with remote sensor 5 degree and modern circulation pumps). The potential saving in the water plant building (1316) is 25 MWh/year. Incorrect settings of the heat panels, heat tracing control and defective heat tracing control units use an extra 3-5MWh/year. The result of the inspections and analysis of the water supply showed that 35 of the 60 MWh/year can be saved with very small adjustments.
Industrial consumption reflects that the production of frozen fish is a very energy-intensive process. The facility has ice production, plate freezers for fast freezing, and cold-storage. The refrigeration plant is from 2006 and consists of 9x15kW scroll compressors with R717, mounted in a container. Production, during the observation period was very unstable, and for a longer period, the refrigerating plant was down due to lack of maintenance. The facility was acquired by Royal Greenland in 2014, and more stable production is expected in the future.
The facility can be a key player in system optimization and the implementation of renewable energy sources. If stable production can be established, there are many improvements that can be done to minimize the costs in both the fish factory and the power system. A communication link for ramp up permission between the refrigeration control and the power plant controller is already in place, but it can be used for other purposes as well. Cold storage is ideal for flexible controlled demand (cool down in low load periods and preserve energy for the high load periods) or as dump-load for excess energy from RE-sources. If the energy-intensive quick freezing process can be planned or even be a little flexible, more RE can be implemented in the system and the diesel units can be operated within the optimal efficiency range. It is out of the scope of this project to study this, but it is suggested that Nukissiorfiit and Royal Greenland discuss solutions and planning.

For private households, the common guidance for energy savings can be used, but the high electricity price (3.29 DKK/kWh in 2014), water (0.035 DKK/L) and the low heating cost (0.785 DKK/kWh in 2014) affect profitableness of the investments. Some examples of consumption, costs, and payback time for standard domestic appliances are given Table 2.5. Consumption is calculated according to Directive 2010/30/EU, and cost is based on the energy costs and the online price of standard unit in class A++ or better. As the table shows the best investment is to change accelerator/circulating pumps. The electrical saving varies by model and age, but for the models registered in Sarfannguit, it is 260-550 kWh/year with a mean of 400 kWh/year/unit. With 60-70 pumps installed, the potential saving is over 24 $MWh/year$ or $>$ 79000 $kr/year$, with an average pump cost of 1,550 kr and labour costs of 400 DKK per pump; a full replacement would cost 100,000-120,000 DKK. On top of the electrical savings, heat savings are expected due to less heat loss in the system caused by unnecessary circulation.

Unit(Wash or year)	Old kWh	Old L	New kWh	New L	Saving kr	Payback
Dishwasher	2.0	35	0.7	6.5	4.25	5.0
Washing machine	1.5	100	0.77	37.5	4.02	4.2
Tumble dryer	4.25	0	1.08	0	10.42	3.8
Accelerator pump	569	0	65	0	1658	0.8
Household refrigerator	292	0	97	0	642	3.3
Chest freezer	547	0	215	0	1092	2.2

Table 2.5: *Example of energy and water savings by hardware replacement in Sarfannguit, based on 2014 prices.*

The reduction study has verified the potential of the AMR data, especially for identification of base load units are very efficient. For the water system, the hourly outlet reading combined with 14 days of readings of each consumption meter can be used for quality and flow modeling and to identify when flushing and modification of the net is necessary. Incorrect settings or defect control of electrical heating, including heat tracing, is easy to detect by a simple comparison of ambivalent temperature and power consumption. The full analysis estimated the reduction potential in the water supply system to be 35 MWh/year, or the consumption of 15 Sarfannguit households, just by implementing small adjustments to in the system. In the rest of the system, accelerator pumps and chest freezers has the best potential. For more information on the outcome, see [Jakobsen et al., 2011] or contact the author.

2.4.3 Hydro resources for Sarfannguit

Sarfannguit has access to hydropower, solar and wind power resources. The closest hydropower resource is the water reservoir,(Fig. 2.8, 08.e) 2km northeast of the village. There are some restrictions related to this lake because of its status as a drinking water reservoir. The potentials for this lake were studied by [Atlason and Holm, 2006],[Lerche and Holt, 2008] and [Holm, 2008]. The resource was estimated to be 106MWh/year minus pressure loss and frost protection. Based on the construction costs, the resource was

found uneconomic.

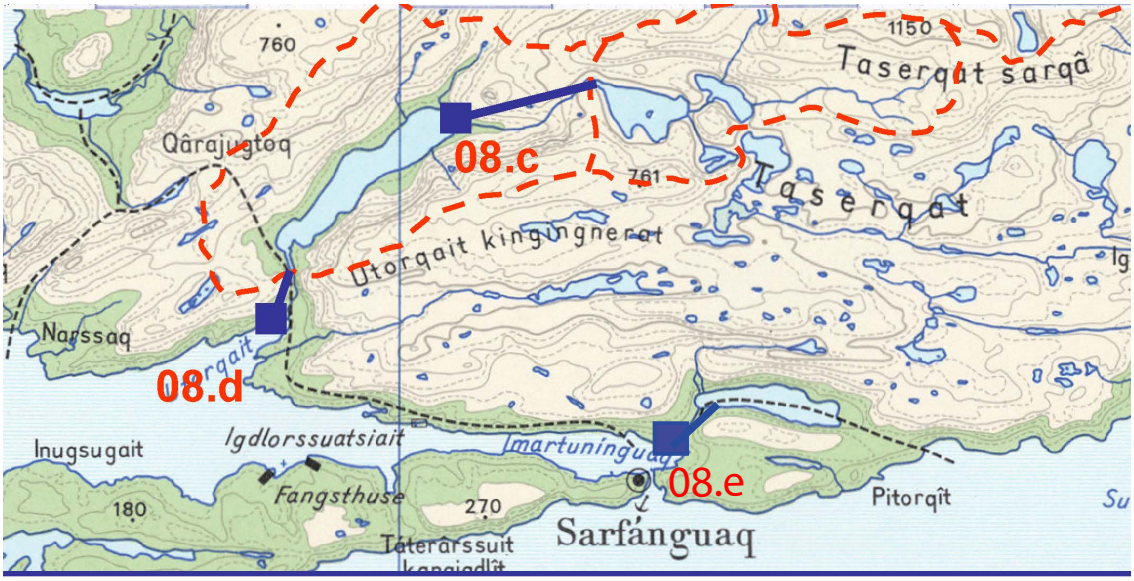

Figure 2.8: *Hydro power resources in the Sarfannguit area, Sources: Grønlands vandkraftresurser, Nukissiorfiit*

The next potential hydropower resource is Lake Utoqqat (Fig. 2.8, 08.d) 10km northwest of Sarfannguit. The lake was studied both by the national screening program in 2004 and further by a student project connected to this project [Lundin, 2010]. The power potential for the Utoqqat catchment area ($32km^2$) is estimated to be 4.4GWh/year. The exploitation cost is unknown, but an simple estimate, based on the cost of other Greenlandic hydropower plants is 35-40 million DKK.

2.4.4 Solar power resources for Sarfannguit

The solar power potential in the area has been analyzed in quite a few project; [Nielsen and Kartic, 1993], [Krag et al., 2002a] and [Dragsted, 2011]. Solar power potential depends on the radiation that reaches the collector and for Photovoltaic (PV) the cell temperature. The total radiation that reaches a surface Q_{tot} can be split into three components; direct beam radiation, ground reflection, and diffuse radiation (2.2). Diffuse radiation can be split into circumsolar radiation, horizontal brightening, and isotropic diffuse radiation from the sky dome.

$$Q_{tot} = Q_{Beam} + Q_{Ground\,reflection} + Q_{Diffuse} \tag{2.2}$$

where:

Q_{Beam} Is the direct beam radiation $[W/m^2]$

$Q_{Ground\,reflection}$ Is the reflection from ground (Albedo) $[W/m^2]$

$Q_{Diffuse}$ Diffuse radiation, see further explanation in text $[W/m^2]$

Q_{tot} Total radiation reaching the surface $[W/m^2]$

The yearly irradiation of a surface parallel to the ground decreases in theory with increased latitude, but the amount of radiation that reaches the surface is highly dependent on atmospheric absorption and scattering, and for tilted surfaces, the ground reflection/albedo effect is important. [Konzelmann, 1994] has parameterized the general radiation model by [Walraven, 1978] for the area east of the Kangerlussuaq and makes estimations more precise.

Site	Lat	Long	Elev	Global rad.	Sun	C cover	C ceilo
			m	kWh/m^2/y.	Hour	$< 20\%$	$< 5000m$
Sisimiut	$66^o55'$	$53^o40'$	15m	830	1550	47.9	15.9%
Tasersuaq 106	$67^o09'$	$53^o16'$	80m	922			
Kangerlussuaq	$67^o00'$	$50^o48'$	50m		1610	50.1	3.6%
Sarfannguit	$66^o53'$	$52^o51'$	$< 120m$				

Table 2.6: *Measurements in the area. Data sources: Asiaq, DMI, ARTEK*

The official climate station records in the area, shown in Table 2.6, indicate more radiation inland (Tasersuaq and Kangerlussuaq) than at the coast (Sisimiut) Fig. 2.2. There are 60 more hours of bright sun in Kangerlussuaq than in Sisimiut, and there is 12.3% more cloudy weather in Sisimiut, as registered by the airport ceilometers. The Tasersuaq 106 is located 30 km from the coastline and Sarfannguit 40 km. Based on this; the radiation in Sarfannguit is expected to be at the same level, or at least the same as in Sisimiut.

The monthly distribution of the solar resource for selected cities are present in Fig. 2.9

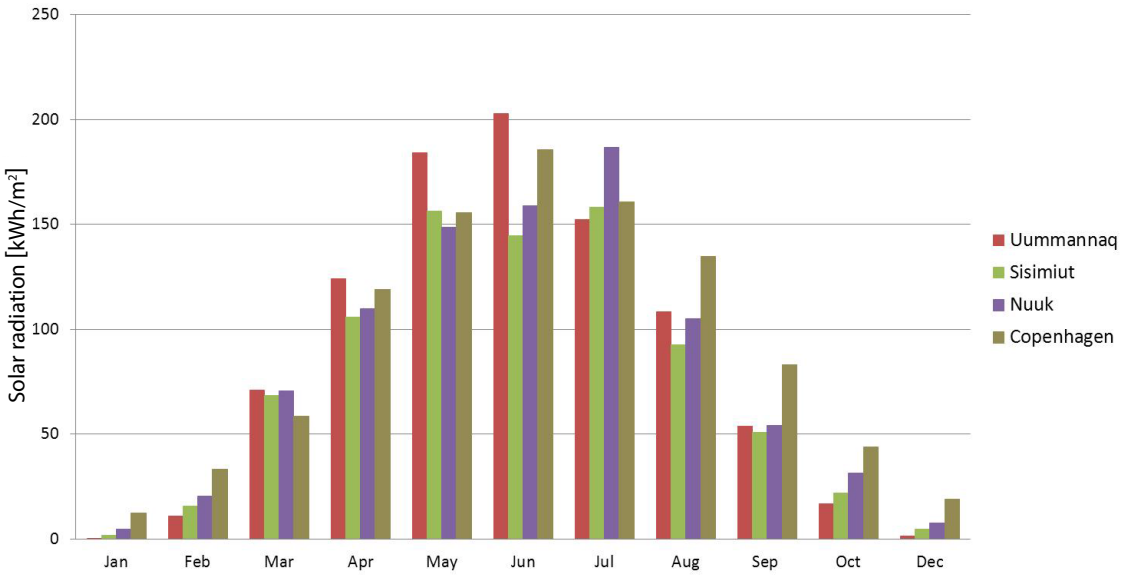

Figure 2.9: *Measured global radiation in reference year, Figure credit: [Dragsted, 2011]*

showing the statistically reference years. The statistically reference year for Sisimiut were developed based on measurements from Asiaq [Krag et al., 2002b]. The radiation reference year is a statistical representation of an average year, based on 10 years observation.

A reference year dataset with a one hour resolution (Global, Beam and diffuse radiation) for Sisimiut was provided by the Solar Energy group, Department of Civil Engineering at Technical University of Denmark. Based on the global, beam and diffuse radiation in the reference year the radiation on a tilted surface can be calculated. The ground reflection/albedo effect varies with the surrounding terrain or more specific the surface reflection and the azimuth difference between the solar and the surface angle. The ground reflection is site specific and is very difficult to model [Dragsted, 2011]. Based on this the observed reflections at the Teleoen climate station was applied to all the solar resource estimation in this project.
The optimal tilt angle for Sisimiut is, based on the reference year, 57^o from horizontal, with an radiation of $1107kWh/m^2/year$.

A $7.05kWp$ roof-mounted test system was installed in Sisimiut in 2012 as part of the Lighthouse project 6. The orientation is 168^o north and at a 45^o tilt. The PV performance was estimated based on Sisimiut reference year and modeled PV cell temperature [Algren, 2012] and [Grabow, 2013].

The first year performance was estimated to be 6900 kWh, or 978 kWh/kWp, based on the reference year(Teleoen), the modeled cell temperature and the expected first year cell performance. The actual first year production was 7405kWh or 1050kWh/kWp, however if the actual observed radiation(Teleoen) for the period is used the modeled radiation is estimated to 1037kWh/kWp. Most of the extra first year production was caused by a higher resource this year and the performance estimation method, described in [Algren, 2012], performed well for this first year.

If the AMR based consumption for Sarfannguit is compared with the PV production, for optimal orientated panels (south facing, 57^o tilt), based on Sisimiut reference year, the maximum allowed autonomous PV size can be estimated. The maximum autonomous PV size for Sarfannguit, if grid stability and reactive power etc. are neglected, is $\approx 70kWp$ with the limiting between 12 and 13 o'clock in June. In reality a $\approx 70kWp$ (12% PV penetration) autonomous PV installation can cause problem for the grid stability due to the fast ramp up an down for this system. The implementable maximum is around 50kWp (8.5% PV penetration) with some restriction on the ramp rates and grid support. Energy storage systems are often used in medium penetration PV systems to smoothen out PV fluctuations and give the other units time to adapt. For large penetration ($> 25\%$) storage systems are needed for daily and weekly distribution of production and consumption patterns. Safe implementation of scale PV involves main SCADA system control of the PV power converter and energy storage.

Most small scale hybrid PV systems involve some kind of energy storage for grid stabilization or even storage based grid operation. The optimal system configuration varies with the price movements of fuel, components, solar resource and labor costs. Generally the fuel costs varies with an increasing trend, labor costs increases and the component costs (PV panels, converters, storage) decreases. This drives the development towards more PV and more storage and less conventional diesel. The development status for hybrid mini-grid systems, as PV/diesel, can be found at the IEA-PVPS website http://www.iea-pvps.org/ and the current status is described in [Grégoire, 2013].

2.4.4.1 Cost of PV energy in Sarfannguit

The Sisimiut test system was acquired in 2011, and its financial profile is shown Table 2.7. Favorable development in the solar panel and inverter market has made new installations much cheaper. For Sarfannguit, a ground based PV plant $> 50kWp$ is expected to be the most feasible; see 2.7 right column. The PV system prices is still in a positive development and from 2013 to 2014 the prices has dropped approximately 15%. The battery storage systems are in the same positive prize movement with yearly reductions of 10-20%.

Sisimiut 7 kW test system 2011				2014 (7)	2014 GL (7)	50kW GL
Cost	Total	Share	[kr/kW]	[kr/kW]	[kr/kW]	[kr/kW]
System	153000	82%	21702	10700	12900	10087
Transport	6640	4%	942	1150	1260	870
Installation	26100	14%	3702	4200	4400	3500
Total	185740	100%	26346	16050	18560	14457
Financial (4%)	64800	35%	9191	5569	6440	5017
Maintenance	37148	0.8%	5269	3210	3712	2891
Total (25 year)	287688	136%	40807	24829	28712	22365
Production[kWh]	180904		25660	25660	26943	26943
Cost [DKK/kWh]	1.59		1.59	0.97	1.07	0.83

Table 2.7: *PV cost estimations for Greenland, based on 4% interest rate paid over 25 years, a first year production of 1050 kWh/kWp, and a decreasing system efficiency of 0.5%/year.(all in 2014 prices)*

With costs of goods of 2.29kr/kWh and staff related costs of 0.87kr/kWh the estimated PV cost of 0.83kr/kWh is inexpensive. With the current cost of battery based, daily-weekly cycle, storage systems (0.66-2.10kr/kWh) even stored energy is competitive with the present system.
The relatively large seasonally variation of the solar resource is a challenge for the PV based hybrid systems Fig. 2.9. Battery based season energy storage is still uncompetitive; however hydropower based season storage may be useful in some villages. With the solar resource variations in the Sisimiut area, PV is only able to cover a major part of the consumption in 3-5 months/year, and the November-January production is negligible. To cover the power requirement for the Sarfannguit system additional sources are need and a obvious candidate is wind power.

2.4.5 Wind resources for Sarfannguit

The Sarfannguit wind resources have been studied [Jakobsen and Hansen, 2016a], and the average wind speed at 10 MAG is estimated to 6.1 m/s for Sarfannguit site 2 Appendix A.3.2 and 5.5m/s for site 1 Appendix A.3.1. Turbulence at site 1 exceeds IEC 61400-1 class A, while site 2 is within the range of class A. The extreme wind speeds measured both at site 1 (7 years) and site 2 (3 years) are relatively low, and even when scaled to 50m hub height, with the power law and 50 year return rate by Gumbel distribution, they will still

stay within wind class 3, Table 2.8. Based on the terrain slopes, the directionally distribution of the resources and the three level measurements at Site 2, the wind resource will increase with the height above ground, however the seasonally distribution will be similar.

Met. site	Mean *ws*	Weibull	Weibull	Max power	WPD	Max *ws*	Turb.
	[m/s]	A	k	12 sectors	[W/m2]	[m/s]	IEC class
Sarf. 1	5.5	6.35	1.81	3 (E)	228	25.8	IIIS
Sarf. 2	6.1	6.69	1.68	2 (NE)	340	28.2	IIIA

Table 2.8: *Wind power key parameters for the two Sarfannguit sites, Appendix AA.3.1+A.3.2.*

The Sarfannguit wind resources has a large seasonally variation with high potential in the winter period and very low in summer, Fig. 2.10. The wind speed is shown in terms of wind power density (WPD) because the potential wind turbine power production for sites with low extreme winds(below turbine cut out speed), like Sarfannguit, will scale with the WPD. The WPD is the average power in the wind for the particular period and is calculated at the actual pressure and temperature corrected air density, rho, multiply with the horizontal wind speed cubed, (2.3).

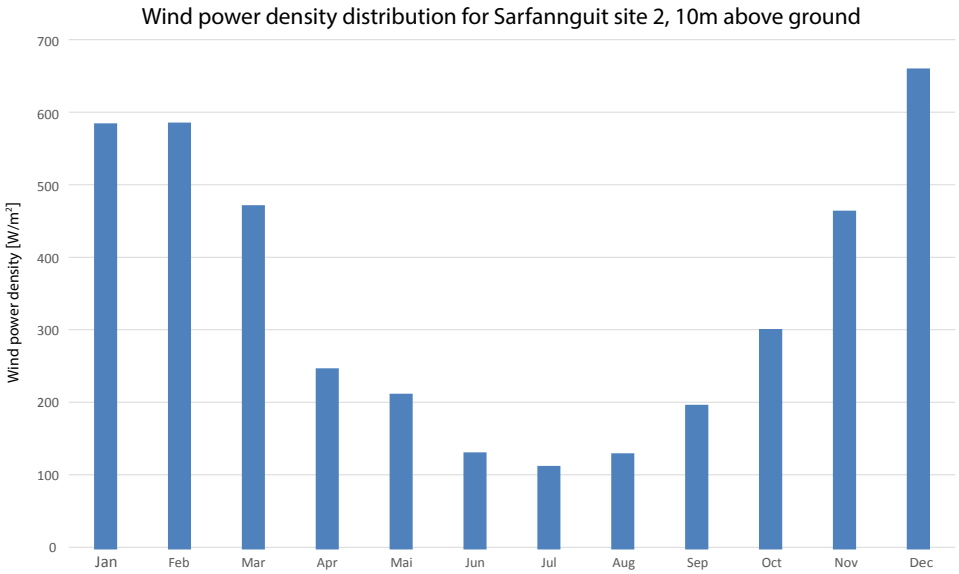

Figure 2.10: *Wind power density for Sarfannguit site 2, 10m above ground, based on 3 years of observations*

$$WPD = \frac{1}{2N} \sum_{i=1}^{N} \rho_i u_i^3 \tag{2.3}$$

where:

u Horizontal wind speed [m/s]

ρ Air density $[kg/m^3]$

N Number of measurement in serie [-]

i Index for actual measurement [-]

The seasonally variation of the Sarfannguit wind resource, Fig. 2.10 fit the variations of the energy consumption Fig. 2.6 and opposite to the seasonally variation of the solar resource, Fig. 2.9. The daily and weekly variations of the wind resource and consumption imply that variable consumption and energy storage systems must be included in the system design. A proper designed energy system for Sarfannguit can include 50-250kW wind power, depending of the design and the amount of grid based heating included.

2.4.5.1 Cost of wind power in Sarfannguit

For a remote site like this a robust, direct drive, variable speed, variable pitch control turbine would, with full cold climate package will probably be the best choice. A wind turbine of this size costs 22-27.000 DKK/kW for a normal installation, but here it would not be a normal installation. A turbine installation at both sites in Sarfannguit would cost much more. Depending on the turbine and the foundation, additional costs for transport, roads, cranes and materials are expected. The potential yearly gross production, based on the measured wind speeds at 10 MAG, is 380MWh for a 100 kW WT. The low air density will add a few percentage points to this; turbine down-time and cold climate consumption will reduce it. If wind speed increases with height, the wind speed at hub height (30-70m) can be considerably higher than the 10 MAG measurements used for this calculation. Before a WT can by selected and the bankable production calculated, measurements at higher altitude (50-80 MAG)is necessary.
An example of the estimated costs related to a 100kW wind power project in Sarfannguit is shown Table 2.9. The estimated costs are subject to very high uncertainties and especially road construction and additional transport can deviate due to multiple unknown factors. On top of the wind power costs, insurance costs, system modification costs etc. must be added to get future the energy cost.
As a part of the lighthouse project, a simple 6 kW test turbine was installed in 2009 close to site 1, see description Appendix D. The turbine is connected to the grid through a 500m cable. The O&M cost after commissioning has been less than 170 DKK/kW/year and covers mainly labor costs and lubrication grease. The inverter setting was not optimal in the beginning, and the specially designed operational monitoring system failed, so only a few data series are available and performance cannot be validated. The turbine was assembled at Sarfannguit harbor and hoisted to the site in one piece, by a Mil Mi-8 helicopter, except for the blades. The helicopter placed the tower bottom directly on the foundation where it was attached. Later, the blades were transported to the site and

Expense	unit cost	100 kW
Turbine installed	25000 kr/kW	2500000 kr
1500m road	1600 kr/m	2300000 kr
Add foundation	850 kr/kW	85000 kr
Add transport WT	1500 kr/kW	150000 kr
Add transport eq.	900 kr/kW	90000 kr
Decommissioning	2000 kr/kW	200000 kr
Total		5425000 kr
Financial cost	4% 10år	1144000 kr
O & M DK	150 kr/kW/year	300000 kr
Add Gl O&M	50 kr/kw/year	100000 kr
Add transport O&M	30000 kr/year	600000 kr
Total cost	20 years	6425000 kr
Production	20 years	7600000 kWh
Production cost		0.85 DKK/kWh

Table 2.9: *Estimated cost of wind power by installing 100kW at Sarfannguit site 2, based direct on the measured 10 MAG wind speed*

installed on the turbine. By using a helicopter, expensive road construction was avoided, and by coordinating the installation with other helicopter dependent activities in the area, the helicopter costs were minimized.
Similar installation method, were used for turbines up to 50kW in the 1980s. If the turbine is hoisted in sections, instead of assembled, larger turbines can be installed without the need for very expensive high-quality roads. The payload of larger commercial helicopters is often limited to (3-5tons), but for larger operations, special heavy-lift helicopters with a capacity of up to 13 tons can be rented, at a cost up to 160,000 DKK/hour. The project cost of a larger wind turbine project in Greenland is therefore highly dependent on the road infrastructure and the sites accessibility.

Proven 6 kw 9 m tower	189000 kr
Foundation	38600 kr
Grid connection	17670 kr
Helicopter lift	22000 kr
Installation 84 hr.	17640 kr
Inland transport	17500 kr
Transport to GL	15900 kr
Total	318310 kr
O&M	4500 kr/year
Production	12100 kWh/year
Unit cost 20 years	1.69 DKK/kWh

Table 2.10: *Actual cost for the 6 kW Proven wind turbine installed in 2009 close to Sarfannguit site 1.*

2.4.6 Conclusions on the village system studies

The Greenlandic villages have with their high electricity costs, relatively good basic consumption data, and good renewable sources a high optimization potential. These small systems can benefit from the technological development within control and remote operation, proactive service, fast dropping prices on PV and battery storage and general more efficient consumer hardware.
Generally the recommended actions for the villages are, in prioritized order:

1. Reduce the consumption, especially in public service and internal
2. Optimize existing power system to reduce O&M and fuel costs
3. Implement as much PV as the system can handle
4. Introduce storage system as the prices drops
5. Large wind power penetration with energy storage

With production costs of in the range 4-15 kr/kWh and a fuel to electricity efficiency often below 30% every kWh saved makes a large impact both on cost and the environment. In the Sarfannguit case 10% of the consumption can be saved just by small modification of the public service system and if the entire village is included, a 20% reduction can be achieved with small adjustments.
The O&M costs can be reduced by remote control and diagnostic, optimized maintenance routines, and material flows. The flexibility and low cost of PV makes it optimal for these small system, and is it implemented together with energy storages a safe high penetration is possible. Battery-based energy storages are together with fly-wheel storages the best solution for serving the grid, without online IC generators. The price reduction on primary lithium-ion batteries drives the storage prices down to a level where off generator operation is attractive for the smaller systems in Greenland. The modern storage technologies are the major key to more renewable energy in the small systems and to drive down the high energy losses.

For villages with larger consumption or where the wind resource and infrastructure is good, wind power will be attractive. For the smaller system, as supplement to PV, and for the larger systems as source for both heat and power. The broad range of modern pitch controlled, low wind DD wind turbines makes them attractive for the small system. A scalable standard system design with; modern SCADA based control, day-week energy storage, ground based PV, backup diesel generators and optional wind power, would be a good solution for the Greenlandic villages.

2.5 Fuel based city systems

Eight Greenlandic cities use diesel generator-based CHP plants and associated heat and power grids, and three cities are use power plants without heat regeneration. The systems typically consist of 3-4 main generators and 2-3 backup generators separated from the main power plant for safety reasons. The main power plant is a CHP plant, but the backup is without heat production systems. The first of these diesel power plants was built

in 1950, and was extended and updated step by step, but it was not until after the first energy crisis in 1973 that the plants was upgraded to CHP (1975-80). Some cities had a district heating grid, but some plants were just connected to the closest larger buildings. Today some plants simply deliver heat to the closest building cluster, often a housing block or public buildings owned by the home rule government. Other cities have several smaller isolated systems; however, most cities have a well-developed district heating system owned and operated by Nukissiorfiit. The electrical grid in these cities consist of a high- and a low-voltage grid, typically 6-10kV and 400V. Historically most of the high-voltage grids were 6kV, but some have been upgraded to 10kV or at least redesigned for it.

Modern IC-based CHP plants are highly optimized systems that provide high efficiency over a larger load range than the older systems. A diesel engine is the main component of the system, and engine development has led to better system performance. Some of the technical improvements that have been implemented are; improved supercharger control, waste gate, and common rail injection. The mechanical maximum efficacy of 4-stroke engines in the range of 200-1500kW is around 44% or a specific fuel consumption of around $190g/kWh$, and they have a relatively flat efficiency curve all the way down to 20% PRP, where efficiency is around 40% ($\approx 212g/kWh$), according to the standardized test (MAN, Scania...). For larger 2-stroke engines mechanical efficiency can reach 48-49%.

In a typical IC CHP system, 35-38% of the inlet energy can be recovered from the oil and coolant typically under 80^oC. The flue gas cooler can usually extract 7-10% of the inlet energy from the exhaust gas, but the engine outlet temperature and flow rate vary with the load. Modern engines on reduced-sulfur fuel produce less particles and less corrosive condensate, and this allows lower outlet temperature ($100 - 110^oC$) and higher efficiency, with a peak above 85% and an average of 70-80%.

Modern fully equipped IC CHP systems are typically designed as shown in Fig. 2.11, where the incoming return water first passes the low-temperature sources (oil, air charger, jacket water and condensing exhaust) and then passes the high-temperature exhaust heat exchanger. By using a condensing exhaust heat exchanger (condensing economizers), the outlet temperature of the flue gas is brought down to $40 - 50^oC$, and the system can reach an efficiency above 90% of the fuel energy contend or a yearly average efficiency above 85% Fig. 2.12.
Heat production relies on the design and control of the heat exchangers, system flow, and the heat consumption. The heat exchangers need to have the capacity to extract the heat at a sufficiently low temperature difference, to maintain the target temperatures for oil, coolant and exhaust flue gas. The control system must, in any given load case and ambivalent conditions, be able to keep the oil, coolant and flue gas at optimal temperatures by regulating the flow and the temperatures. One important design parameters are simple manual or automatic cleaning of the flue gas cooler to obtain a high performance throughout its lifetime and a corrosion-resistant design for extended lifetime.
To obtain high efficiency, the CHP plant depends on a well-controlled district heating network with sufficient demand. The return temperature must stay below 55^oC and the outlet preferably below 85^oC. To minimize losses in the district heating grid, consumer cooling must be as high as possible and typically below 35^oC return, which allows for a lower outlet temperature of $60 - 85^oC$. Losses in a district heating grid are typically in

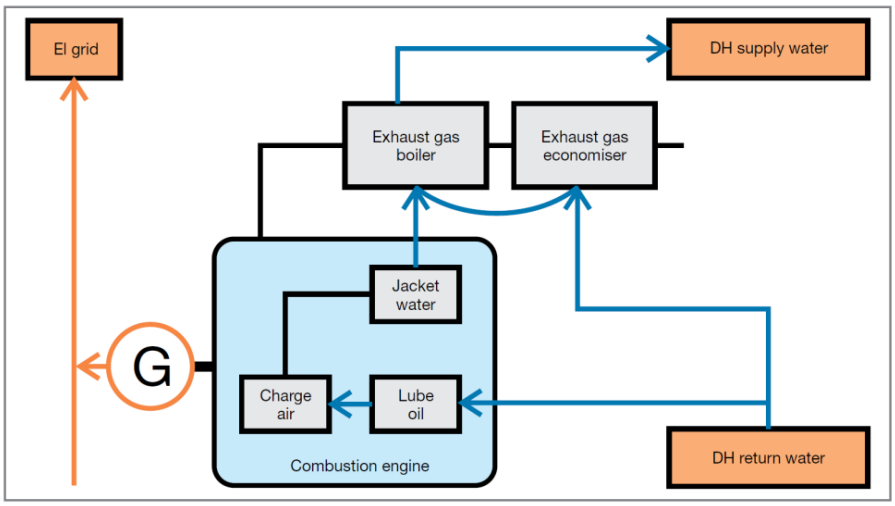

Figure 2.11: *System chart for diesel-powered combustion engine CHP plant (Figure credit:Edward Nagelhout)*

the range of 5-10% and this means a total system efficiency around 75%. This is the interesting parameter for Nukissiorfiit, because the income is based on the energy delivered to the consumer; the same is true for electricity.

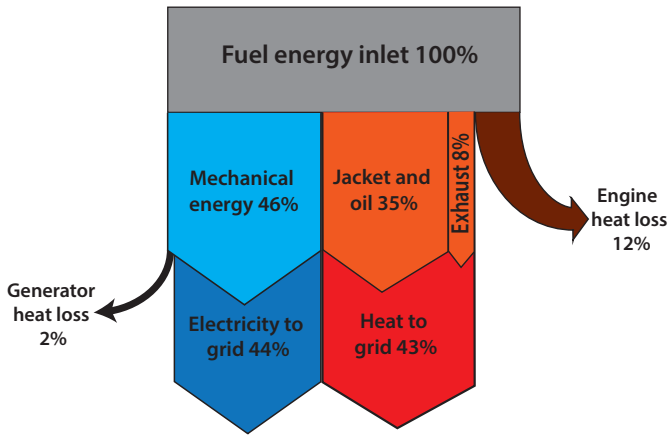

Figure 2.12: *Energy flow for typical diesel-fired CHP plant at* $> 70\%$ *load. Data delivered by MAN Diesel & Turbo.*

Electrical consumption in the eight Greenlandic CHP systems varies from 2.6GWh in Qaanaaq to 15.3GWh in Aasiaat and the three city power plants produce from 1.5GWh in Ittoqqortoormiit to 3.4GWh in Qeqertarsuaq(2013), Table 2.11. Evaluation of the individual Greenlandic CHP plants, based on total heat sold and power used is not possible because some systems supply the grid with heat from oil-fired boilers, and waste incinerators, and various grid losses are included, however the total share in the district heating system is shown Table 2.12. The average heat-to-power ratio for the 8 CHP plants can then be calculated as $34/50.8 \approx 0.67$. The available heat can be estimated by assuming a recoverable

share of the input at 80% and average electric efficiency of 35% Then the possible heat-to-power ratio will be $(80-35)/35 \approx 1.29$. The utilized share of the potential heat is then $0.67/1.29 \approx 0.52$ + grid loss, or the potential extra heat production is 31.4 GWh minus the grid loss (typically 10% in Greenlandic systems). If this can be achieve Nukissiorfiit can gain an extra turnover of $\approx 28.000 \quad MWH * 850 \quad kr/MWh = 23.8 \quad mill.DKK/year$. Two of the parameters that have a direct influence on the official unit production cost are the share of the power used internally and the grid loss, because the official production costs are calculated from the total costs divided by the amount sold. As the column "E int" Table 2.11 shows, this varies from 4% to 14% of production. Part of the explanation for the highest share is the fact that Qaanaaq(170) is located far north (77^oN) and needs power for anti-freezing systems, but the mean yearly consumption of 44.5kW must include something else in addition to heat tracing. In the unit cost, it is surprising that the power plant without heat production is not the most expensive, but this might be due to expenses not related to production. The unit cost for heat has a large range from 0.13 to 0.95; however, this is partly related to investments and to various methods to estimation the costs related to heat and electricity production.

ID	Name	E prod.	E int	E unit	H prod	H unit	H/P
		GWh	%	kr/kWh	GWh	-	
010	NAN	3.396	5	4.24	1.494	0.13	0.44
050	PAA	5.666	6	3.59	12.135	0.80	2.14
070	MAN	8.890	6	3.21	20.161*	0.95	2.27*
090	KAN	1.833	12	3.92	0	-	0
100	AAS	15.308	8	3.14	14.559	0.74	0.95
110	QAS	5.332	6	3.45	6.248	0.72	1.17
140	QEQ	3.415	4	3.90	0	-	0
150	UUM	5.435	11	3.63	2.002	0.45	0.37
160	UPE	4.076	6	4.30	94	0.70	0.02
170	QAA	2.700	14	5.18	4.642	0.67	1.72
190	ITT	1.459	10	4.98	0	-	0

Table 2.11: *Production statistic for city power plants 2013. *Include waste plant production. Source: Nukissiorfiit*

E prod Used electricity [GWh]

E int Internal used electricity fraction [%]

E unit Total production cost per kWh electricity used [kr/kWh]

H prod Sold heat [GWh]

H unit Production cost per kWh heat [kr/kWh]

H/P Sold heat to used power ratio [-]

The electricity cost in the cities is 3.14-5.18DKK/kWh, and only two of the cities are below the max cost limit set by the government. The average oil cost in 2013 was 6.00DKK/L or 0.60DKK/kWh (LHV). In the shared costs Fig. 2.13 the costs of goods is 1.64-1.95DKK/kWh, and this covers mainly oil, but also lubrication oil, oil filters and

Source	Production
	GWh
Hydropower	90
Gas oil	52
CHP plants	34
Waste incinerating	29
Total	205

Table 2.12: *Sources for district heating. Source: Nukissiorfiit*

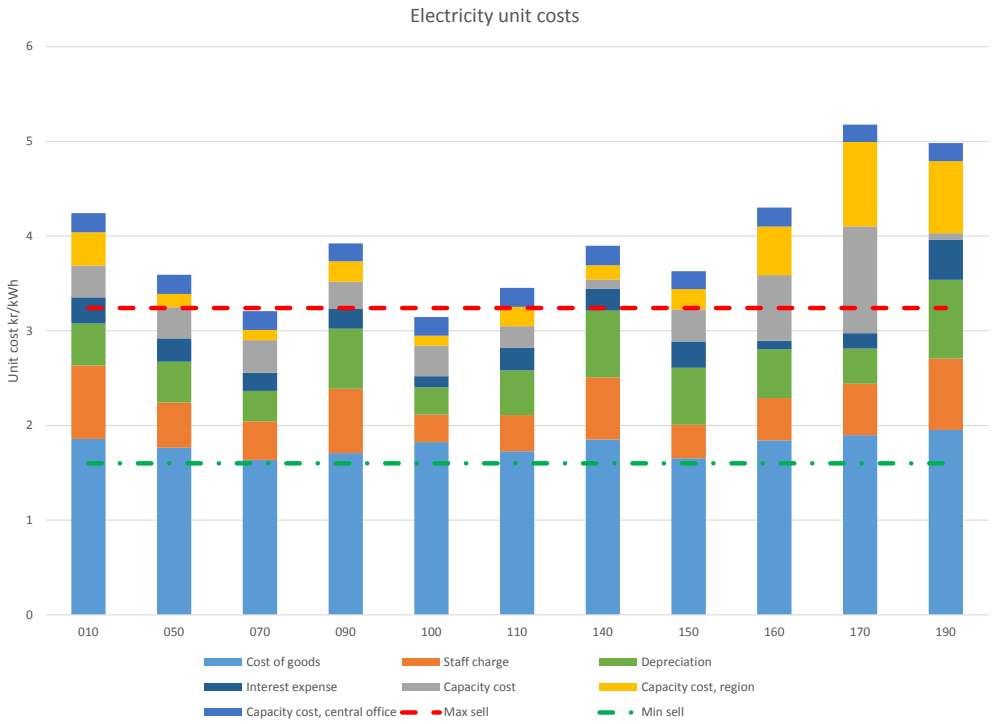

Figure 2.13: *Production costs of electricity in diesel cities and with indication of the minimum and maximum selling price. Source: Nukissiorfiit*

other production related goods. By a rough estimate this means that the efficiency is in the range of 0.3 to 0.36, but if the production units are a mix of old units from the 1960s/1970s and newer units from the 1990s/2000s, with a large excess capacity, this is not unrealistic. It is not the 0.3DKK/kWh that makes the big difference in the cost; it is the local and regional capacity cost, which covers the local fixed cost of the plants. The capacity costs range from 0.25DKK/kWh in Aasiaat to 2.02 in Qaanaaq, but what makes this large difference and how local and region costs are calculated are not clear in the available data. Two of the three city power plants has similar total costs (3.9 & 3.92), and only the interest expenses, local capacity costs, and cost of goods were different.
The last plant is the smallest and the most isolated, on the east coast, which might make it more expensive to run. As shown here, the electrical unit production cost of the CHP plants is not different from the conventional power plants, because of the way the costs are distributed in the CHP plants. The heat production cost include only the costs di-

rectly related to the heat production system, all other costs are included in the electricity cost. This cost method is historical and is based on the idea that, heat is waste from the electricity production, without any value (internal value set to 0.01DKK/kWh). In this way, only oil and incineration based heat have a value or cost. The selling price for heat is fixed by the government and varies only with the official oil price.

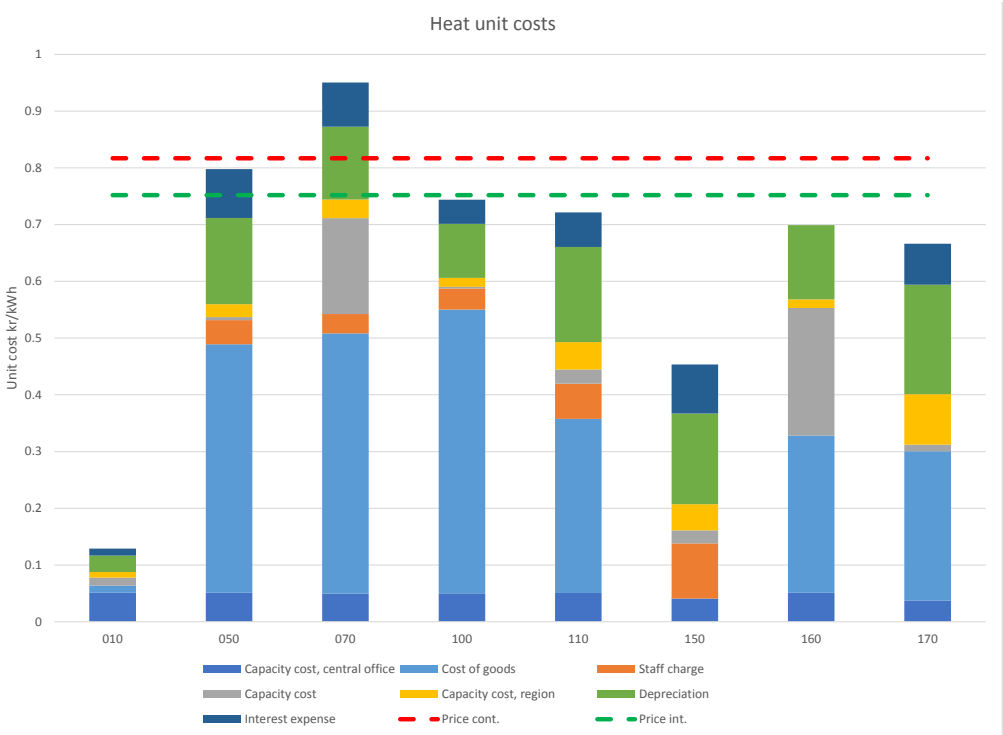

Figure 2.14: *Production costs for heat in different cost fractions and indication of the selling price for continues heat and interruptible. Data source Nukissiorfiit*

The district heating systems are very different and the way cost are calculated and shared with electrical production is different from system to system. The difference is clear when Maniitsoq (070) is compared with Nanortalik (010). In Nanortalik, heat is delivered only to the local INI system, and it is mainly produced by exhaust heat exchangers, because of a small and ineffective regeneration system. In Maniitsoq, Nukissiorfiit operates a traditional district heating grid where only a small fraction of the heat is from the CHP plant, and the main part is from oil boilers and the local waste plant. The calculated costs are based only on the goods and other expenses directly related to heat production, and therefore the official cost can be as low as in Nanortalik and Uummannaq.

The price and cost structure, with fixed selling price, limited heat production value, and high costs loads on electricity, has some negative consequences. The fixed selling prices do not attract new customers more in areas with low heat production costs, than in areas with an expensive heat production, and this is a barrier to the development of heating systems in these areas. Ignoring the heat value, affects both investor engagement and employer commitment, and this has a very negative effect on the production. Removing the costs from the heat production does not official affect anything else than internal account balances at Nukissiorfiit, but these costs are then shifted to electricity, making

the electricity costs artificially high. In a free market, this would not be a problem, but because of the electricity monopoly, the costs are moved from the competitive heat market (District heating competes with individual boilers) to the protected electricity market.

2.5.1 Case study, Nanortalik

Nanortalik is a small town in Southwest Greenland with 1294 inhabitants, (2013) and a minor fishing and tourism industry. The city has been target for wind resource monitoring since 2007 and for major parts of the field activities, related to this project. Two groups of student were connected to the field activities, and much detail is described in the two reports by [Finnby et al., 2011] and [Sæbø et al., 2012].
The electrical transmission grid consists of a high-voltage 6kV main grid and a 400V distribution grid. The power plant is located close to the harbor and consists of a main plant with three units and a backup plant with two units Table 2.13. MG1 and MG2 are the main units, MG3 is used as backup, and the reserves are only used in emergency situations or in case of maintenance work on the power plant. MG1 and MG2 are based on the MAN L16/24 engines, designed in 1995, and the units were installed in 2005. The average specific fuel consumption in the period 2006-2012 was 221g/kWh or an average electrical efficiency of 38%. The consumption is only 10% lower than the engine peak point(199g/kWh) and is good for this type of engine. This level of electrical efficiency is achieved by a simple low (night) and high (day) load operation and is adjusted for workdays and weekends. MG2 is used for night operations when the load is in the range of 100-500kW; for day operations MG1 or MG3 is used; and for peak load periods MG1 and MG2 or MG1 and MG3 are used in parallel.

ID	Brand	Type	Power	Year
M1	MAN	8L16/24	720kW	2005
G1	Alternateur	LSA52.2L55	683kW	2005
M2	MAN	6L16/24	540kW	2005
G2	Alternateur	LSA52.2L45	509kW	2005
M3	MAN	8L23/40	1080kW	1989
G3	AVK	DIP130 k/8	912kW	1989
R1			370kW	
R2			370kW	

Table 2.13: *Nanortalik power plant configuration. Data source: Nukissiorfiit*

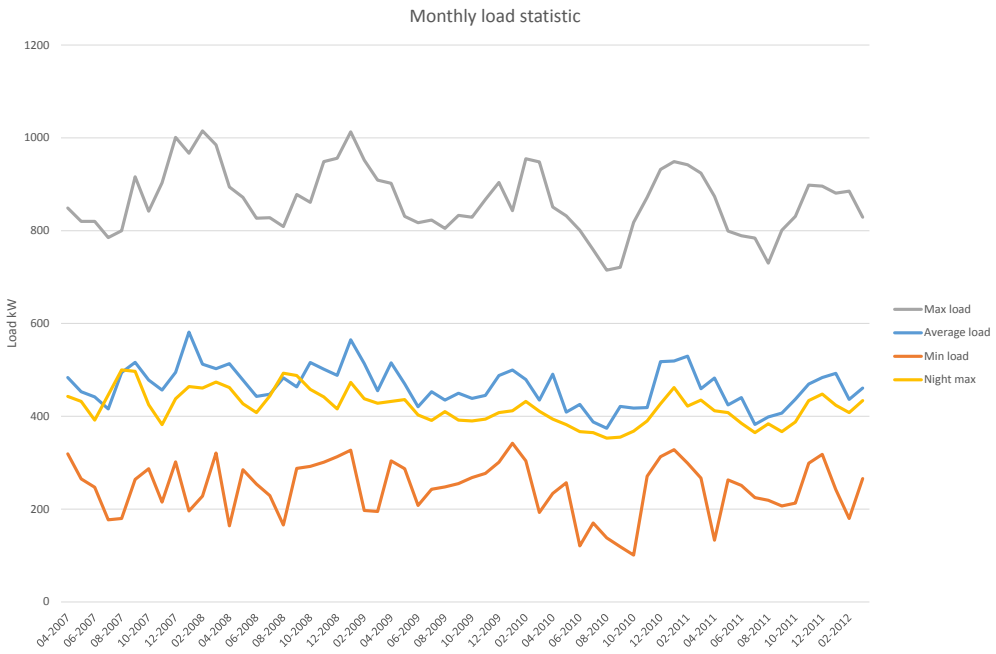

Figure 2.15: *Monthly load statistics for Nanortalik power plant. Data source: Nukissiorfiit*

Heat utilization at the Nanortalik plant is generally low, for several reasons:

- Only MG1 and MG2 are equipped with exhaust boilers.
- The exhaust boiler is poorly designed and poorly controlled.
- The oil and jacket cycles are not optimized for heat production.
- The return temperature is too high due to the small grid.
- There is no monitoring or control of the heat production.

There are several optimization possibilities for the Nanortalik power plant. The two main engines MG1 and MG2, can be updated with the available retrofit package, including new turbochargers, charge air preheating systems, an updated valve train, cams and control. This would improve the efficiency, especially for part loads, increase the max power and extend the TBO Fig. 2.16. This would increase average efficiency from 38% to 41% and save $70m^3$ fuel a year, or 70.000L*6.00DKK/L = 420.000DKK/year (based on the 2013 load profile and oil cost).

The two main engines can be fitted with a full waste heat recovery package to bring heat production to above 44% of the input. The heat production would then be 3644MWh/year, or 2150MWh extra with an oil heat value of $\frac{6.00DKK/L}{9.96kWh/L} * 2,150,000kWh \approx 1.3million.DKK/year$ To utilize extra heat production, a large expansion of the district heating grid is required (15-20,000 m^2 heated area), but there is a large home rule or council-controlled building mass in the area, that can be included. If the heat is sold through a new district heating grid, it will generate an extra income of $810\frac{DKK}{MWh} * 0.9 * 2150MWh \approx 1.57million.DKK/year$ and replace up to $\frac{2150,000kWh}{9.96kWh/l} \approx 216\frac{m^3oil}{year}$. Power production,

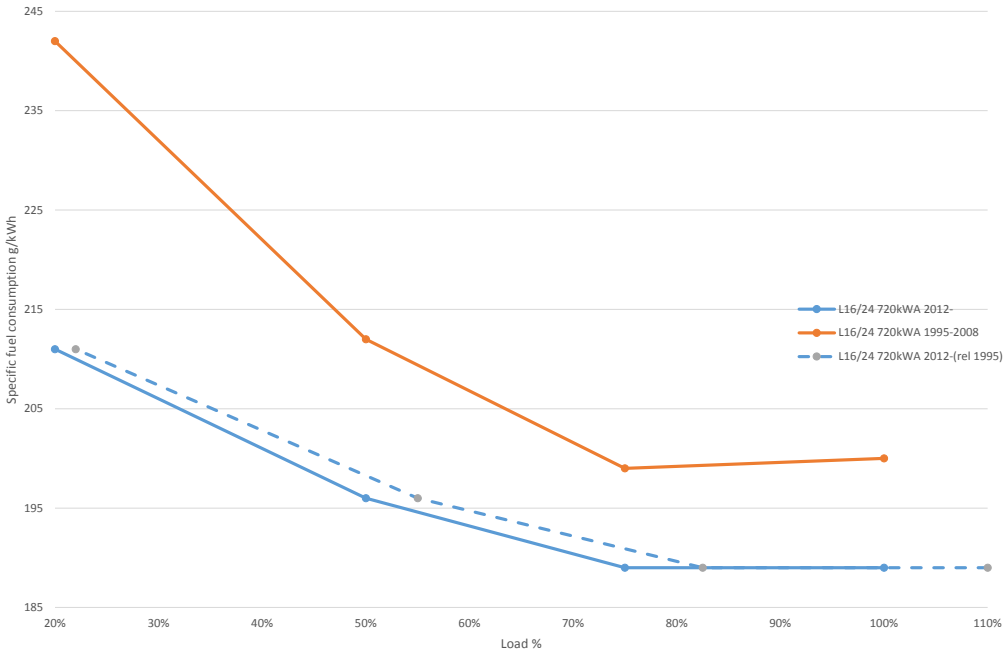

Figure 2.16: *Specific fuel consumption for the existing 1995 version of the L16/24 and the retrofitted version. The dashed line indicates SFOC for the same effects as the old (+10% power for updated version). Data source: MAN Diesel & Turbo.*

heat production, and losses for the last 5 years is distributed as shown in Fig. 2.17, and if the power plant is updated, the distribution will look like the 2015 distribution.
Whether any of these initiatives are profitable is not evaluated, but as the figure shows, the production is decreasing, and if renewable sources, such as wind and solar power are applied to the system, the flat engine efficiency curve of the updated engine version will improve the efficiency even more. The profitability of the extended district heating grid depends on the investment cost and thereby the consumer location.

2.5.1.1 Renewable sources

Nanortalik has access to both promising solar and wind resources, based on its location and hydropower resources have also been identified. There are two identified hydro resources in the Nanortalik area, Narsap Sarqaa (15.2GWh/year) 01.e Fig. 2.18 and Tasiusaarsuk (14GWh/year) 01.f, with investments in the range 150-200mil.DKK [Nukissiorfiit, 2005]. The project was not found attractive enough to receive a higher priority than the consumption level warrants, but the economic situation, industry, and fuel prices can change the priority.

Solar power potential is expected to be high due to the southern location; however the clouds and fog frequencies will affect this. The coastal location allows humid air to be transported in with the sea breeze at night, and this reduces the incoming radiation especially in the morning. Global radiation monitoring is a part of the "Fyrtaarn 6" activities (Nanortalik dump site) and the equipment is installed, but the statistical base is still too small to estimate the resource.

	2009	2010	2011	2012	2013	2015
Loss	4583	4595	4741	4512	4047	1242
Heat	1300	1112	952	1127	1494	3644
Electricity	3606	3498	3489	3456	3396	3396

Figure 2.17: *Yearly energy production for Nanortalik power plant and with the updated scenario for 2015, based on the 2013 consumption and full heat utilization. Data source: Nukissiorfiit*

The wind resources have been estimated at the Dump in Nanortalik, based on measurements from 2007-, Table 3.5. The site is classified as class 3 and turbulence class S, but some manufacturers allow A-class turbines at sites like this. The suitable turbine size depends on the grid and the thermal control loads that can be connected to the grid, but the estimated size is in the range of 500-1500kW. Modern low wind turbines are very good for low-wind sites like this, and a relatively high capacity factor is expected for this site. Sites with larger wind resources are available in the area, but they have not been validated yet, and the installation costs will be higher due to longer distances. More details about installations possibilities and estimated costs can be found in the related student reports [Sæbø et al., 2012] and [Finnby et al., 2011]. The initial measurement campaign is described in [Aakervik et al., 2011] and the main campaign is described in the wind resource chapter 3.3.

2.5.2 Conclusion for fuel based city system studies

In general the city systems have the same reduction potential as the villages. The profitable reduction is estimated to 10-20% of the total consumption and most in the industry and service business. There is a high untapped potential in the old systems that operates with a relatively low total efficiency. The highest potential is in the heat production, however an upgrade to modern CHP systems with modern, SCADA and remote diagnostic will be the optimal solution for most fuel cities. Remote monitored systems, with high efficiency will minimize the costs to staff and goods, but the interest and capacity cost will rise. The cities have a size where a considerable amount of renewable energy can be implemented. As for the village systems PV are the most flexible and with the latest price

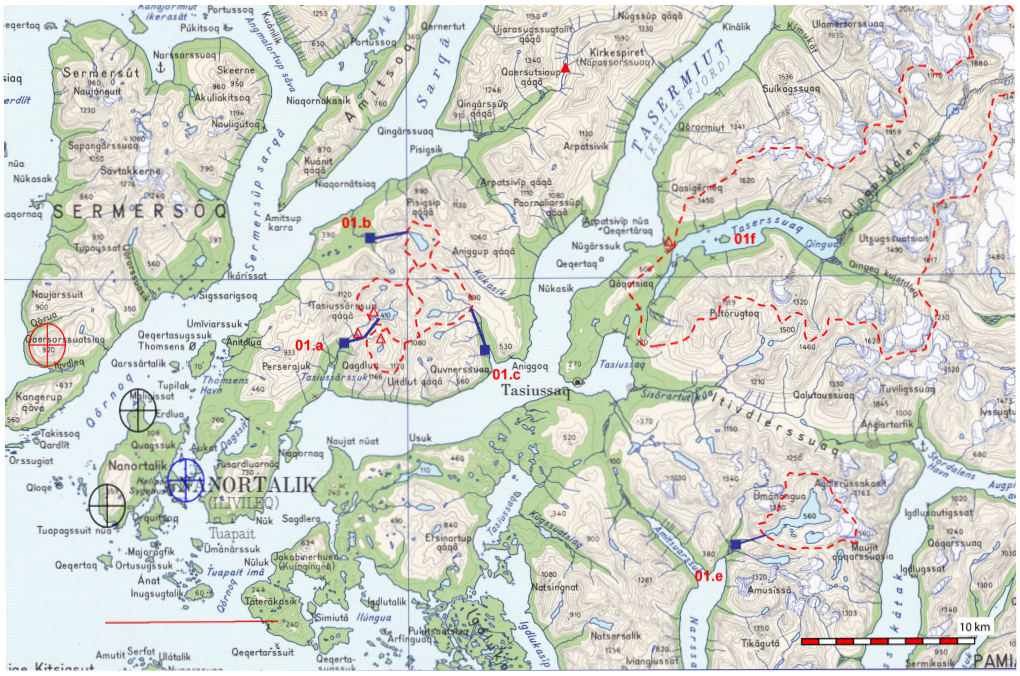

Figure 2.18: *Identified hydropower resources in Nanortalik area(red dotted lines and dark blue stations) Project related wind monitoring stations, Nanortalik dump (Blue), Tref (Red), Station North+south (Black). Data source: Nukissiorfiit*

reductions it is very competitive. With relatively fixed electricity consumption patterns, which fit the solar radiation pattern (high during daytime and low at night) most cities can handle a high PV penetration. The handleable penetration depends of the system design and if the PV is installed central in big units or in small autonomous units. For Nanortalik a 2-300 kWp central system will not be a problem, but autonomous it can challenge the grid.
The wind resources varies often with the seasonal variations of the electricity and heat consumption, but to implement more than a 100 kW wind power will require a full integration with the master controller. A feasible wind power installation will require larger units $> 300kW$ and at least two units. To handle that high penetration heat "dump" loads are needed to utilize the capacity. The same feasibility problem needs to be handled if hydropower is implemented. A large share of the power has to be sold as heat to utilize the capacity and pay the high investment costs. For most cities the consumption is too small for a large hydropower plant, but a development of the district heating system can raise the controllable energy production and stimulate the renewable conversion of these cities.

2.6 Hydro based city systems

The utilized hydro resources are very different and range from a normal yearly capacity of 5 to 230 GWh, Table 2.14. Most of the systems are designed for both heat and power production, but Tasiusaq has only capacity for power production. The heat and power supply are separated in different products: electricity for power, heat and interruptible

heat and water-based heat in continuous and interruptible versions. The electrical grids are mainly controlled at the consumption site, by large electric boilers connected to the district heating grid. When the main power consumption changes, the boilers are adjusted to obtain the set point, and in extreme cases, the interruptible heat can be adjusted. As

City	Capacity	Resource	E cons	H cons
	MW	GWh	GWh	GWh
Nuuk	45	230	76	159
Narsaq	29	14.4	6.1	3.1
Qaqartoq	-	-	10.3	14.5
Tasiusaq	1.2	5	5.5	0
Sisimiut	15	58	21.8	35.6
Illulissat	22.5	65	20.2	22.2

Table 2.14: *Grid-connected consumption in the Greenlandic hydropower cities. Narsaq and Qaqortoq are interconnected with and share the Qorlortorsuaq plant. Data source: Nukissiorfiit*

in most other countries, the population in Greenland concentrate in the cities, and low energy prices attracts more industry that stimulates this movement. This will use up all the excess capacity over time and new sources need to be applied. The extra power can come from more hydro or other conventional or renewable sources. When larger industries, as mining or processing, plan to enter an area, the energy supply and the environment are always an issues. The development in both technology and price means that both large-scale wind and solar power are a good alternative/supplement to the hydropower plants. The flexible hydro-based heat and power system is able to handle even very large wind and solar penetrations, owing to the fast regulation and large controllable loads.

2.7 Discussion

In general, wind and hydropower are easier to incorporate in the larger systems, because the standard unit size is in the MW range, while solar power is more flexible.
To stimulate private investments in renewable energy systems, the home rule government and Nukissiorfiit have made an exception to the electricity monopoly and allowed private persons to produce to the grid. The electricity delivered to the grid is paid at the unit cost of goods for the grid where the renewable source is connected, over (1.64 DKK/kWh in 2013) for the oil based systems. As demonstrated in the Safannguit case, the production cost for a $7kWp$ PV is 1.07 DKK/kWh, and for 2013, the cost of goods in Sarfannguit was 2.29 DKK/kWh. With an estimated production of around 1000 kWh/year/kWp this is a potentially good business case. Although a good business, only a limited capacity has been installed, mainly in the CHP cities. If Nukissiorfiit, the municipalities, or another invested in large-scale PV for diesel systems, for example, by investing in several 50 kWp systems and distributing them in the cities/villages, the cost could be kept down.

Small-scale wind (less than 100 kW) is more complex to estimate production, install, and maintain. In Greenland this requires specialist and long-term planning to minimize the risks and get a good pay off. Medium-scale wind ($100-1000$ kW) also requires specialists

and a large investment and is only feasible for Nukissiorfiit. Large-scale wind($> 1MW$) is feasible only for the large CHP, hydro system or industrial use.
Micro-scale hydropower is installed at several locations, but is used mainly for summer operations by truly dedicated people. Medium-scale hydropower plants ($100 - 1000$ kW) are not used, but some locations have the potential at least for summer river-runoff installations.
Storage systems have not been studied in this project, but with the latest development with in battery storage technologies, it becomes attractive for the diesel based system to include daily to weekly storages. Daily cycle balancing storages can support the grid and minimize the low load operation of the diesel based units and even without renewable source reduce the fuel consumption and the maintenance cost significant. For some systems the low load periods(Night loads) are so low that off generator operation are attractive. The grid balancing service delivered by the modern storage system; above all, enable a safe implementation of a high renewable energy penetration.

2.8 Conclusion drawn from energy system studies

The system analysis found high reduction potential for all systems, by upgrading domestic appliances, system hardware and control systems ($> 20\%$). There is an unutilized potential in the collected smart meter data for system supervision, control and optimization purpose.
The solar resources, the PV system costs, the system size flexibility, and the oil based energy prices, makes PV attractive for all oil based systems. On macroeconomic (National economic) level, only larger PV systems ($> 50kWp$) will be feasible, but the present pricing politics makes even small private systems feasible for local consumers.
The cost and risk related to micro-scale wind power makes these unattractive for the bigger systems, but in small flexible systems it can be a good supplement to PV. Medium-scale can be attractive for small diesel based systems were the consumption flexibility and the system design can handle high wind penetration. Large-scale wind is mainly for bigger systems, and systems with combined heat and power production.
The diesel based system often rely on outdated technology, that need to be upgraded before large RE-penetrations can be handled in a safety way. It is recommended that the total cost is included when systems are updated. This will open for new technology, and not only replacements of worn out components, with cheap outdated material. The electricity costs in the diesel systems are mainly pushed up by; low efficiencies, high labor costs, and high financial costs. The first two can be improved by updating the system design (heat utilization, remote control and diagnostic, few highly skilled service teams).

Battery based energy storages are with the current costs attractive for all diesel based systems for consumption-production balancing and for safety of supply. The storage systems are furthermore the key to safe implementation of variable renewable resources as PV and wind power.
The system studies showed that the optimal system configuration include a high PV penetration in the summer period April- August and for sites with good wind resources furthermore a high wind penetration in the winter period November-Marts. With the current costs of storage systems only daily and up to weekly storage cycles are feasible and thereby some diesel based production is still needed in these systems.

Chapter 3

Wind resource assessment

This chapter describes the greenlandic wind climate, the current monitoring, wind resource assessment, and microscale modeling of wind resources. The current metrological monitoring systems are introduced and specially issue regarding Arctic and complex terrain monitoring is addressed. The requirement for wind resource assessments and local area resource modeling are discussed together with a test of the common used Wind Atlas and Application Program WAsP.

3.1 Introduction

The wind resources in Greenland vary a lot, not only from region to region, but also locally. Knowledge about wind resources and their distribution are very limited. There is a lack of high-quality wind data, and the atmospheric models have a hard time in this terrain. To understand the wind distribution in this very large area, both micro-, meso- and synopticscale systems need to be considered. The 3.2 km high icecap makes a natural barrier in the lower atmosphere, affecting the climate in all the country. The southern part is partly affected by the Westerlies, while the rest of the country experiences more North-South patterns. The flow across and the local systems related to the icecap has a major influence on the climate both East and West of it. The steep easterly slopes generate very extreme weather and the more moderate westerly slope generates more stable weather conditions.
DTU wind energy has a long tradition for wind resource assessment and wind related meteorology. The primary meteorology research covers:

- Boundary layer meteorology
- Meso- and microscale modeling
- Wind resource assessment and wind farm modeling
- Wind loads on structures

DTU Wind Energy has a long range of in-house developed or optimized simulation tools for wind simulation. The main wind model tools are WAsP(Wind Atlas Analysis and Application Program) , WAsPCFD, KAMM(Karlsruhe Atmospheric Mesoscale Model) and WRF(Weather Research and Forecasting model).
Wind resource assessment can be conducted on many levels and on different geographical scales from points evaluation to global mapping. Depending on the task, different

tools can be utilized. For local wind resource assessment direct measurements and/or microscale modeling will often be sufficient. For larger areas meso- and even higher scale tools are needed.
To minimize the required resources, existing large scale atmospheric model results (reanalysis data) is often used as basis for the modeling. The most common setup is to use a mesoscale model to down scale the reanalysis data, both in time and physical resolution. To get further down in resolution a micro scale model can be added on the mesoscale output. More about the option in the modeling sections.
To assess the result, knowledge about the local climate, overall patterns and basic wind conditions is needed. In the following chapter a short introduction to the most relevant processes are presented.

3.2 The Greenland wind climate

Troposphere circulation can be explained theoretically by the Hadley cell Fig. 3.1, where the heat exchange between the pole and the mid-latitudes drives a southern flow close to the ground and a northern flow in the upper part of the troposphere. Similarly the northern Ferrel cell takes care of the exchange between equator and the northern mid-latitudes. The rotation of the earth in relation to the flow make the flow turn against the earth´s rotation, creating westerly winds in the northern Ferrel cell and easterly winds in the Polar region.
At the stratosphere, the so-called Arctic vortex is located with the Polar jet at the southern edge. The strength of this vortex, and thus the temperature, controls the position and the shape of the Arctic front that dominates the weather patterns in the Arctic. The Arctic vortex is often elongated in shape with two centers, one over Baffin Island (Canada) and one over eastern Siberia (Russia).

The Polar vortex has been studied since the 1940s, and the theory was verified by experiments [Palmer, 1959] and [Kellogg, 1951]. The tropopause height is 8-11km in altitude, and varies with the season, low in summer and high in winter [Hall et al., 2011], and is controlled by a complex mix of Brewer-Dobson circulation, solar UV-flux and so on. However, on average, the height reflects the seasonal variations of the Polar vortex strength. The vortex strengthens during fall and winter, resulting in a stationary Polar front at more northern latitude. In spring and summer, the temperature rises and the vortex become weaker, and deformed, and makes the weather situation more unstable.
The Polar front and the Polar jet are located at the southern edge of the Polar vortex, where hot mid-latitude air meets the cold Arctic air. While the fastest jet speeds and coldest air of the Polar vortex are most noticeable at high altitudes, the same temperature, wind, and air pressure patterns can reach all the way down to the surface, especially in winter.
The atmospheric mass exchange between the Arctic and the middle latitudes is often described as the Arctic Oscillation (AO). The Arctic Oscillation is a parameter describing the geographical pattern shifts in multiple features of the Polar vortex (air pressure, temperature, location and strength). When the pressure over the Arctic is lower than average and there is higher than average pressure over the mid-latitudes, the AO index is positive and the jet stream is further north. This situation is related to a strong Polar vortex and pulls the front and the storm track north, minimizing the risk of cold outbreaks from the Polar region. In the opposite situation, the jet is pushed south and the vortex is

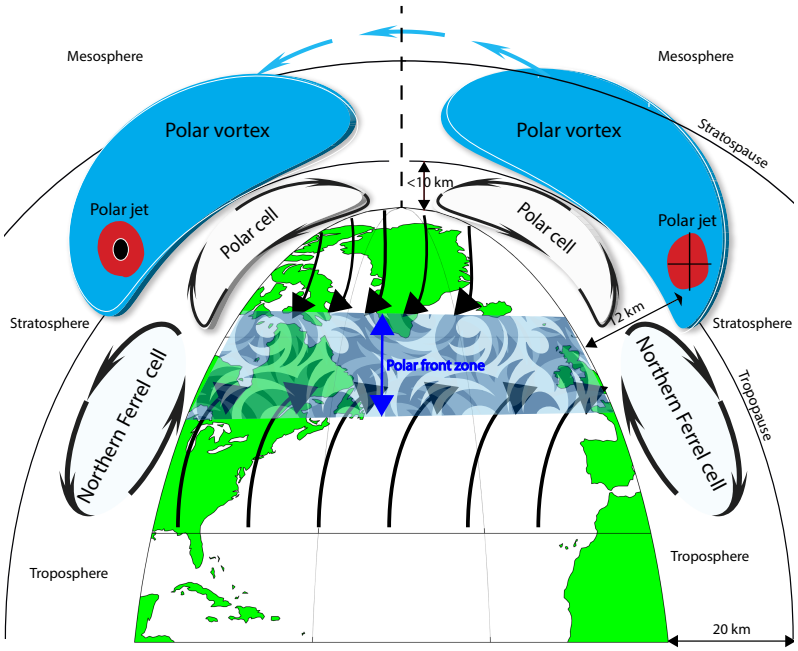

Figure 3.1: *My illustration of the main theories about the overall air circulations in the Arctic region. The illustration include the Polar vortex and cell theory of Ferrel that was based on studies of Hadley Palmer [1959] and others. The position of the polar front based on the theory of Bjerknes and Solberg [1922]. The flow patterns is shown in a standard atmosphere with indications of approximated heights and positions, but it must be noted that this is dynamic and moves with the overall thermal balances.*

weak. The weak vortex/jet stream makes waves at the front and allows cold Polar air to press southward. While the AO describes the whole hemisphere, a more local pattern for the North Atlantic was found by Gilbert Walker in 1932 and named the North Atlantic Oscillation (NAO).

The NAO is defined as the pressure difference between the Azores anticyclone (high) and the Iceland cyclone (low) Fig. 3.2. When the pressure difference is above normal, the NAO is characterized as positive, and in the opposite case it is said to be negative. Studies of Surface Level Pressure (SLP) for the North Atlantic and Europe have shown that the winter (November-March) can be grouped in 4 climate regimes: NAO-, NAO+, NE-high and NE-low [Cassou, 2004]. The last two regimes ware renamed the anticyclonic ridges over Scandinavia ('blocking' regime) and off Western Europe ('Atlantic Ridge'). The frequency of the four regimes is 21,26,28 and 25% of the time, respectively [Hurrell and Deser, 2009]. The variations of the NAO index have a large influenced on, for example the surface winds in the North Atlantic and South Greenland [Greatbatch, 2000], especial in wintertime, when the Polar front is more settled and the two semi-permanent cyclones affect the flow. In summer they get weaker, and together with the weaker Polar vortex, it makes the pattern more scattered.

With a height of up to 3200m AMSL and length of 2600 km, Greenland has a large impact on the flow in the lower part of the troposphere (8-10 km). The land acts as a barrier to the flow and forces the air masses around or above it. The blockage effect

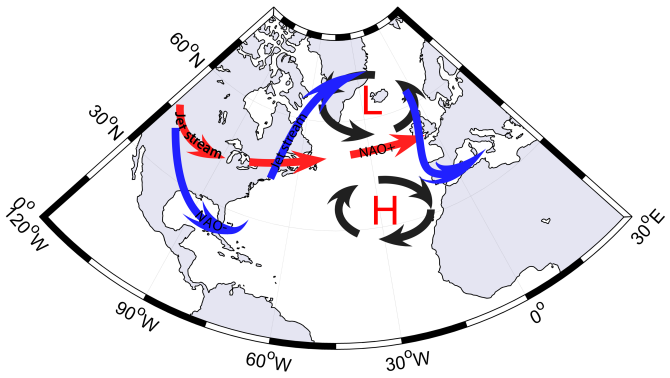

Figure 3.2: *My illustration of the NAO theory [Walker, 1924] and [Walker and Bliss, 1932]. The figure shows the North Atlantic oscillation and the effect of the jet in weak vortex situations. The blue jet represents the negative NAO track and the red jet the positive track.*

and the high frequency of high pressures to the north or west and low pressures at east and south, drives the overall flow. This is mixed with more locally driven flow, such as katabatic winds, and sea and land breezes. The blocking effect of the Greenlandic ice sheet, bends the flow along the coasts, giving mainly northern winds at the west coast and southern at the east coast [Cappelen et al., 2001]. Parts of these flows along the edges of the ice cap are described as the Greenlandic Plateau jets [Moore et al., 2013]. When lows arrive from west or southwest they often pass Cape Farewell and follow the east coast toward Iceland and the Norwegian Sea, bend north at Davis Strait and Baffin Bay, or split and partly continue both ways [Cappelen et al., 2001] Fig. 3.3. In relation to the Arctic front, where cold Arctic air meets warm tropical air over relatively warm water, deep Polar cyclones often appear. The so-called Polar lows have a large impact on the local weather, but their size (often a few hundred km in diameter) and lifetime (1-2 days) are limited [Orr et al., 2005]. Their effect on the general wind climate is therefore very limited, however the local extreme wind speeds is in some regions related to these polar lows.
When the barrier flow reaches the end of the barrier at Cape Farewell, the pressure buildup in front of the barrier is released, and the flow speeds up in a so-called tip jet. These jets make the areas southeast and southwest of Cape Farewell to some of the windiest places on earth. These tip jets and their effects on the winds in South Greenland were studied by [Jakobsen and Vincent, 2016]. The average wind speed in the jet affected area often exceeds 30 m/s [Risien and Chelton, 2006]. The wind speed along the barrier can also be relatively high, especially in the Denmark Strait, and at the first mountain ridge from the coastline [Harden et al., 2011].

3.2.1 Local thermal winds

Local thermal flows, such as katabatic winds, mainly related to the ice cap slope, land and sea breezes, mountain/valley breezes and gravity waves, affects most of Greenland. The frequency and the strength of the katabatic wind are highly depended on the terrain slope and the geographical location. The katabatic flow systems over the Greenlandic ice sheet have a major impact on the climate in most of the country. The near-surface

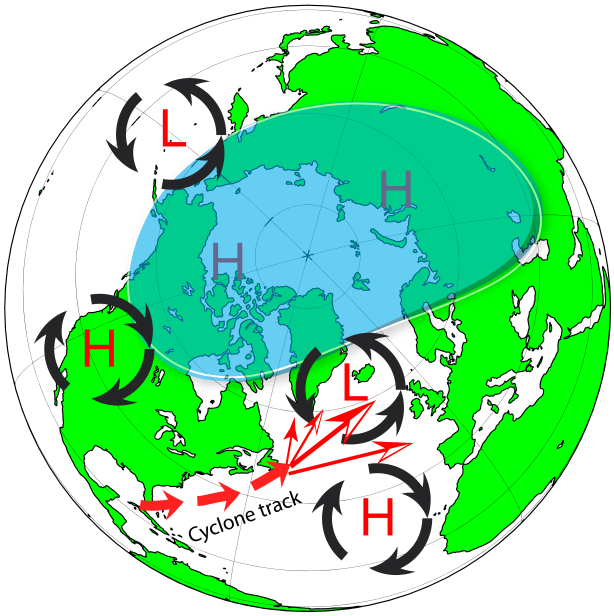

Figure 3.3: *My illustration of the Semipermanent cyclone position and the Polar high based on the studies of Jung and Rhines [2007], [Cappelen et al., 2001], [Orr et al., 2005] and [Moore et al., 2013]. The dominant cyclone track is shown with red arrows.*

climates over the ice are highly affected by the energy exchange between the ice and the air. Periods with stable stratification and low vertical mixing over the ice leads to development of katabatic flow systems as shown by [Heinemann and Klein, 2002]. The air mass temperature and the local slopes affect the strength of the flow. The impact on the local wind climate in the ice-free part of the country varies a lot, both in frequency and in intensity. The highest intensity occurs at the southeastern coast, where the ice cap slope is biggest and some flow channeling occurs. One example of the extreme east Greenlandic katabatic winds, locally called "Piteraq", is described in [Rasmussen, 1989]. The structure of the Greenlandic katabatic winds was studied in the KABEG97 experiment [Heinemann, 1999], where katabatic winds were observed on a daily basis, in both summer and winter. Stable weather at nighttime with strong radiative long-wave cooling forms the katabatic winds; in winter they arrive at the edge of the ice cap in the early morning, while in summer they shift to around noon. The KABEG97 experiment showed classical 2-D katabatic winds at the smooth inner part of the ice cap, although the flow became 3-dimensional at the edge (outer 20-50km), and outside the ice cap, it was channeled in the widely branched valley systems.
In relation to the KABEG97 project, a comparison with the NORLAM mesoscale model was done [Klein, 2002]. The Norwegian Limited Area Model (NORLAM) with a horizontal resolution of 25 km and 18 model levels in the lowest 400 m above ground, were used. The study showed that the model were challenged when modeling the clouds in stable boundary layer situations and especially when the synoptic background analysis used for initial and boundary conditions was wrong. The conclusion of the project was that the mesoscale model was able to capture katabatic winds in the area where the model resolution could resolve the most important terrain features (ice cap except for its complex

edge).
Katabatic winds forms in an isolated case, as shown in Fig. 3.4. When the air mass above the ice cap is cooled down by radiation and the pressure rises. The long-wave radiation over the ice cap is controlled primary by precipitation or cloudiness; in periods with high precipitation, radiation is reduced, and this will reduce the pressure rise.
The theory of the strong katabatic winds was first described by [Ball, 1956] and [Putnins, 1970]. When the surface pressure rises over the ice cap the hydrostatic balance between the ice cap air and the coastal part is disordered, and the pressure drives a flow. The cold ice air mass displaces the warmer air down in the coastal area, but when the air flows down the slope its pressure increases and its temperature rises. When the flow reaches the edge of the ice cap, the temperature is often higher than the coastal air temperature, especially if the coastal area is covered by snow or ice. In cases of very cold and dense air in the coastal area, the katabatic flow will not be able to displace it but will flow aloft. If the katabatic wind flows into mountain regions, like in the KABEG97/Kangerlussuaq case, the flow pattern can become very complex [Heinemann, 1999].

Land and sea breeze are very common in the coastal regions with open water or, in

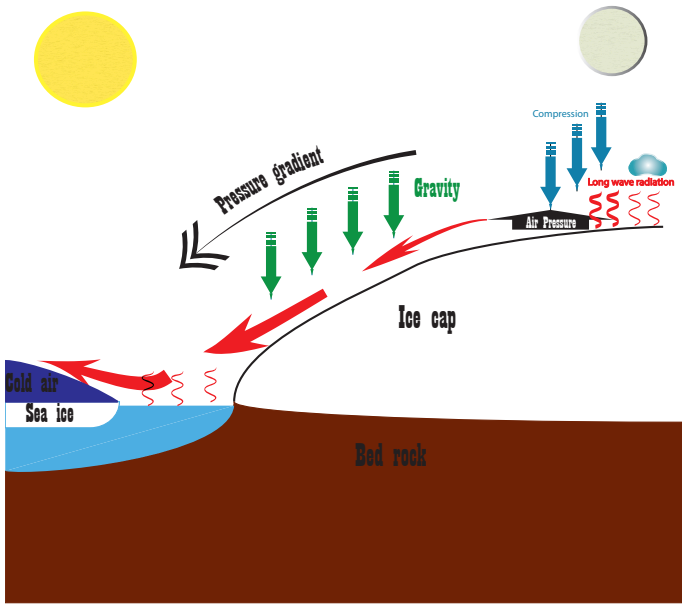

Figure 3.4: *Principle of the katabatic flow, related to the Greenlandic ice cap. My illustration of the physical processes described by [Ball, 1956], [Putnins, 1970] and others.*

smaller scale, in the fjord systems. In wintertime the land is cold and the water is warm, and it can drive land breezes if the overall weather situation allows it. In summer, the often dark land surfaces heat up the air above them and force a sea breeze. In coastal regions, sea breezes transport humidified offshore air inland and form clouds during the day and fog at night, when the temperature drops. In mountainous terrain, sea and land breezes are often a combination of sea-land and mountain-valley breezes.
In wintertime, in areas with open water, the temperature differences between the inland and offshore areas are large, and many land breezes are expected. At the same time, it is the period when the highest frequency of katabatic winds is reported. In large parts

of these areas, the distance from the ice cap edge to the shoreline is so small that these circulations interact and grow in scale.
Mountain, gravity or lee waves are a very common phenomenon in the ice-free part of Greenland. Flow along the coast, perpendicular to the fjords/mountain ridges, is very frequent and related to the plateau jets. When stable air ascends a mountain barrier buoyancy perturbations will develop and propagate away from the mountain as gravity waves. Mountain waves can sometimes be detected through the related cloud formations generated by the temperature drop related to the decreasing pressure at the ridge. The clouds are stationary with shape of a lens (lenticularis) and do not usually move with the wind. The lee vortex, caused by flow separation, also forms clouds but of the cumulus type.
These local micro and mesoscale features interact with the synoptic scale weather systems and form the Greenlandic wind climate. To monitor variability and validate models, monitoring stations are necessary.

3.2.2 The planetary boundary layer

The planetary boundary layer (PBL) or atmospheric boundary layer (ABL) is defined as the part of the atmosphere that is directly affected by its contact with the planetary surface. The PBL is well described by [Stull, 1988], and characterized by high turbulence and strong vertical mixing as opposite to the upper part of the troposphere that is close to the geostrophic wind . The flow in the PBL is affected by surface drag and major terrain features. The wind speed generally increases with height in the surface layer, starting at zero owing to the nonslip condition and to the geostrophic speed at the top of the boundary layer. In simple terms the PBL is split into two sublayers, called the surface layer (mixed layer) and the Ekman layer (mixing layer). The surface layer is additionally split into the Urban Canopy Layer (UCL) and the roughness sublayer [Rotach, 1999].
In cases with homogeneous surface roughness and free turbulent flow, the velocity profile can be derived from the shear stress (3.1), and the profile will look like Fig. 3.5.

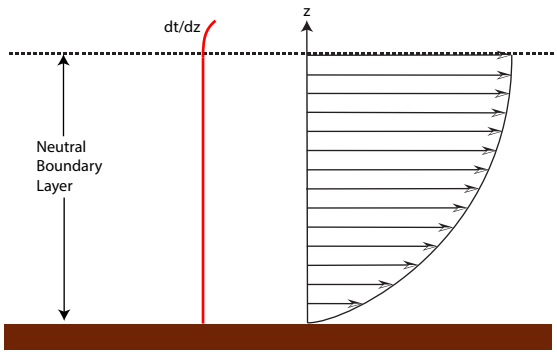

Figure 3.5: *Simple neutral boundary layer profiles as described in e.g. [Santoso and Stull, 1998]*

$$\frac{du}{dz} = \frac{u_*}{kz} \implies u(z) = \frac{u_*}{k} ln\left(\frac{z}{z_0}\right), \qquad u(z_0) = 0 \tag{3.1}$$

Or if the stability correction term is included:

$$u(z) = \frac{u_*}{k}\left[ln\left(\frac{z}{z_0}\right) - \psi(z/L)\right] \tag{3.2}$$

where:

u Horizontal wind speed [m/s]

z Height above ground [m]

u_* Friction velocity[m/s]

z_0 Surface roughness [m]

k Von karman constant ≈ 0.4 [-]

$\psi(z/L)$ Empirical stability correction term [-], se equation (3.8)

The surface is often not homogeneous, and the flow is forced by several external parameters. When the surface is very rough such as in urban, forest or other areas with many objects, the point of zero velocity is elevated above the surface; this distance is described as the displacement height and denoted as D [Stearns, 1970]. This displacement height is used to reduce the height z. The flow displacement in the roughness layer is the (UCL) and is often determent as $\approx 70\%$ of the mean urban or canopy height; however, this is an often rough estimate. The same is the case for the roughness length z_0 for UCL, $\approx 10\%$ of the mean urban or canopy height.

$$u(z) = \frac{u_*}{k} ln\left(\frac{z-D}{z_0}\right), \qquad u(z_0 + D) = 0 \tag{3.3}$$

where:

u Horizontal wind speed [m/s]

z Height above ground [m]

u_* Friction velocity [m/s]

z_0 Surface roughness [m]

k Von karman constant ≈ 0.4 [-]

D Displacement height [m]

I case of one or more known wind speed levels the relation between the wind speeds at different heights can be derived from the relation (3.4), if D and z_0 can be estimated. If multiple levels are known, the two parameters can be estimated directly from data. These equations are valid only for neutral boundary layer stability, but they can be expanded with an empirical stability correction term $\psi(z/L)$, often based on the Monin Obukhov length L like equation (3.2).

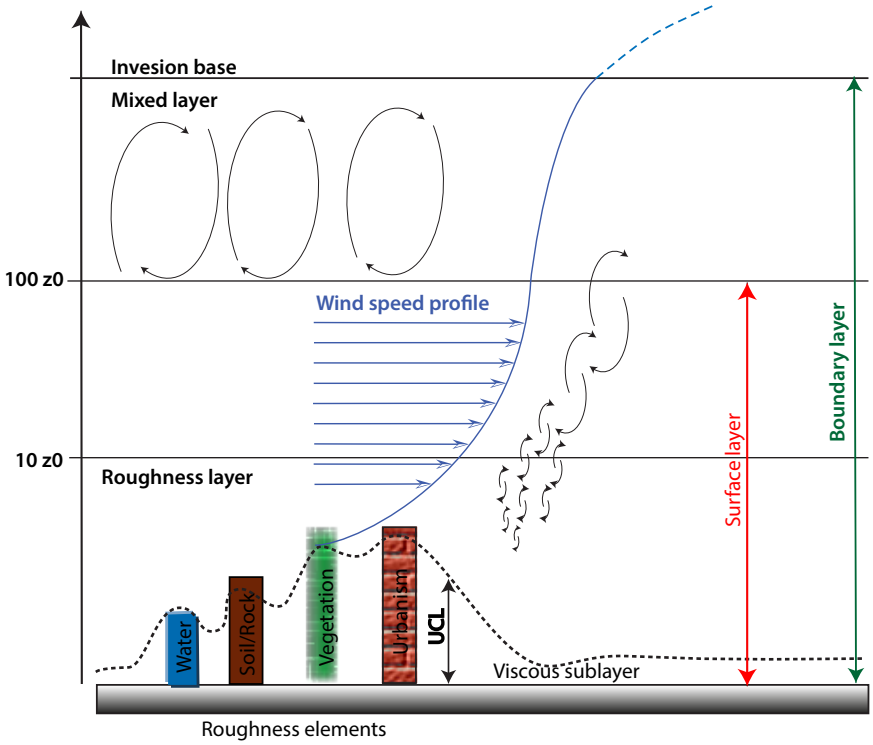

Figure 3.6: *Boundary layer illustration inspired from the description by [Stull, 1988].*

$$\frac{u_1}{u_2} = \frac{(\frac{u_*}{k})ln(\frac{z_1}{z_0})}{(\frac{u_*}{k})ln(\frac{z_2}{z_0})} \implies u_2 = u_1 \frac{ln(z_1)}{ln(z_2)} \tag{3.4}$$

where:

u_1 Horizontal wind speed reference height 1[m/s]

u_2 Horizontal wind speed reference height 2[m/s]

z_1 Height above ground for reference 1 [m]

z_2 Height above ground for reference 2 [m]

u_* Friction velocity[m/s]

z_0 Surface roughness [m]

k Von karman constant ≈ 0.4

The correction is based on the Monin Obukhov similarity theory and the length scale parameter describes the relative contribution of buoyant and mechanical shear production to the turbulent kinetic energy [Obukhov, 1971]. The mechanical part is caused by shear instability and friction and is present in all BL stabilities. The buoyant turbulence is induced by positive buoyancy or, more generally positive turbulent heat flux and is reduced in cases of negative turbulent heat flux. The MO length is defined as (3.5) and normalized with height $\zeta = z/L$ it is called a stability parameter. The stability parameter can be converted to the correction term ψ by the empirical functions (3.7) + (3.8) [Golder, 1972].

$$L \equiv -\frac{u_*^3 T}{k\ g\overline{w'T'}}, \qquad u_* = \sqrt{\overline{u'w'}} \tag{3.5}$$

$$\begin{array}{rcl} \zeta > 0 & \Longrightarrow & \text{Stable} \\ \zeta = 0 & \Longrightarrow & \text{Neutral} \\ \zeta < 0 & \Longrightarrow & \text{Unstable} \end{array} \tag{3.6}$$

$$\varphi(z/L) = \left\{ \begin{array}{ccc} (1-16z/L)^{1/4} & -2 \leq z/L \leq 0 & \text{Unstable} \\ 1+5z/L & 0 \leq z/L \leq 1 & \text{Stable} \end{array} \right\} \tag{3.7}$$

$$\psi(z/L) = \left\{ \begin{array}{ccc} ln\left(\frac{(1+\varphi)^2(1+\varphi^2)}{8} - 2arctan\varphi + \pi/2\right) & -2 \leq z/L \leq 0 & \text{Unstable} \\ -5z/L & 0 \leq z/L \leq 1 & \text{Stable} \end{array} \right\} \tag{3.8}$$

where:

u_* Friction velocity [m/s]

T Temperature [K]

k Von karman constant ≈ 0.4

g Gravity [m/s2]

T' Temperature fluctuations [K]

w' Vertical wind speed fluctuations [m/s]

u' Horizontal wind speed fluctuations [m/s]

z Height above ground for reference 2 [m]

Other measures for stability are the Richardson number, Ri, or the simple hydrostatic/thermal stability, where Ri is based on the ratio between the buoyancy and the flow gradients or the gradients and the flux, and the hydrostatic /thermal is defined by the lapse rate [Panofsky, 1963]. These two stability measures are demonstrated in section 3.4.4.

$$Ri = \frac{E_{pot}}{E_{kin}} = \frac{g}{T}\frac{\frac{d\theta}{dz}}{\frac{du}{dz}} \tag{3.9}$$

where:

E_{pot} Potential energy [J]

E_{kin} Kinetic energy [J]

T Temperature [K]

g Gravity $[m/s^2]$

θ Potential temperature [K]

u Horizontal wind speed [m/s]

To derive the wind profile, the temperature profile, the BL stability measurement, or

model data are needed. However, both modeling and measuring of boundary layer wind is difficult in the complex terrain of Greenland.

3.3 Wind monitoring in complex Arctic terrain

Meteorological monitoring in complex Arctic terrain is a complicated task. In this section the background and the results of the related measurement campaign are discussed. The objectives are to give an introduction to the data sources available for wind resource assessment, the need for additional measurements for wind power projects, and present the experiences gain through the measurement campaigns.

3.3.1 Greenlandic climate stations

Since World War 2, climate data has been recorded in Greenland on a regular basis. The Danish Meteorological Institute (DMI) has data collections back to the 1950s [Cappelen et al., 2001], but there have also been many other actors in Greenland such as the United States Air Force (USAF), Greenlandic airports (GLV), TELE Greenland, and several research organizations, including the Greenland Climate Network (GC-Net) and Promice. Until the 1990s, most data were recorded as a 10 minute average of last part of each 3hour interval, but since then, most of the data have been recorded at hourly intervals or, for some stations even every 10 minutes. The Greenlandic climate stations normally collect the standard parameters of interest for wind power purposes, Table 3.1. Some stations record other parameters, such as visibility, fog, thunder, and sun hours.

Recorded parameters	Met.Int. (Hour)	Height (m)
Mean wind speed (ws)	1/6-3	10
Mean wind direction (wd)	1/6-3	10
Dry bulb temperature (t)	1-3	2
Relative humidity (rh)	1-3	2
Solar radiation	1-3	2
Precipitation (p)	6-24	-
Snow depth (sss)	1-3	-
Air pressure at mean sea level (pppp)	1	-

Table 3.1: *Parameters recorded at standard Greenlandic AWS operated by DMI, GLV, or Asiaq, among others. Codes in bracket are the official parameter title.*

The Greenlandic climate stations are, for historical reasons, often located in relation to telecommunication stations, airports, heliports, military installations or other places where personnel were stationed. When the technological development made it possible, Automatic Weather Stations (AWS) were introduced and remote unmanned stations inaugurated. In this project, the climate stations are grouped by location/use to be able to weight their data quality:

- Airport stations
- Heliport stations
- City/village stations
- Remote stations
- Research stations

The official wind monitoring height is 10 MAG, and for most Greenlandic stations this simply means 10 m from the tower bottom. The height above the general local terrain varies a lot depending on the terrain and the main purpose of the station. The Airport stations are often located next to the runway, with the mast base at the same level as the runway. This position often provides at least 70 m of flat land to the runway side, but outside the landing strip and to the other side, the terrain is unknown. Informations of the Airport stations, including maps of the station position can be found at http://aim.naviair.dk/. Heliport stations are more randomly located close to the helipad or main building and are often not leveled with the pad or the general terrain. Many heliports are located in or on the border of cities, which often results in many surrounding obstacles. If heliport stations are used for any study it is therefore recommendable to inspect the site and carefully control the data. City/village stations have the same problems with obstacles and terrain positioning as the heliport stations, and city development can influence long-term variations. Remote stations include both abandoned manned stations and stations established at remote locations. Some of these stations have been rebuilt several times, and in some cases, this has affected the homogeneity of the observations. The city and remote stations is often shown in the Greenlandic GIS maps and further informations can be ordered at ASIAQ or DMI. Research stations include a wide range of sites designed for a specific purpose or project. Many of these stations are located at or in relation to the ice cap. For stations located in permanent ice- or snow-covered areas the ice accumulation adds extra uncertainty to height-dependent measurements, such as wind speed. The measurement stations height is in the range of 0-50 MAG, but some of the ice cap stations can be covered by snow in periods. For more information see [Jakobsen and Hansen, 2016b]

The location of most Greenlandic climate stations in complex terrain and close to structures means that the measurements are highly influenced by micro- and mesoscale effects. When the data is used in a larger scale, such as for model validation or regional weather classification, this has to be taken into account. Some stations record the standard deviation of the wind speed and/or the wind direction and this can give an indication of the closest microscale effects, but for terrain and obstacle correction, models need to be used. Beside the local terrain and the obstacles, the instrument´s condition and their position

(a) *Wind monitoring tower next to the airstrip in Sisimiut airport (A2 on the map in Fig. 3.8*$(66^o57'07''N, 53^o44'20''W)$*)*

(b) *Wind monitoring tower next to the heliport in Nanortalik (Fig. 3.23* $60^o08'28''N, 45^o14'04''W$*)*

Figure 3.7

on the tower/boom are important for the observations. The instruments are in most cases boom mounted; they are often too close to the boom, and the distance to other installations is too short, causing incorrect measurements [Petter Lindelöw-Marsden, Troels F. Pedersen et al., 2010]. Maintenance is another important issue that needs to be considered when data is used. Most stations are inspected once a year; however, the instruments are not necessarily replaced, and some operators just replace defective components, such as bearings, without recalibrating the instruments (source ASIAQ, climate office). Most stations are unheated or not sufficiently heated to keep them ice-free in harsh weather conditions, and this can be observed in most data sets especially for remote unheated stations.

To study the local effects on wind measurement, four stations with overlapping measurement periods were identified in the area of Sisimiut on the Greenlandic west coast. The four stations are located within a distance of 4 km and are all 10 MAG, Fig. 3.8. The

stations/area are selected because it representanting the typical climate monitoring level in Greenlandic cities. The Teleoen station (T) is the old city station, located next to the old telecommunications facility and the oil depot (tank farm) in the western part of the city, 15m AMSL. The station was in operation from 1961 to 2010 and was highly affected by microscale effects. The airport stations, (A1) and (A2), have been active since 2000, and A1 is the mast used for official measurements. The official airport observations are sent out as hourly METAR reports with hourly 10-minute samples (xx:50-xx:00) [Rzeszotko, 1997]. The data record for both Teleoen and the Dumpen campaign include the full 10-minute mean data series Appendix A.2. The Dumpen campaign was carried out from August 5, 2004, to June 12, 2008, without maintenance.

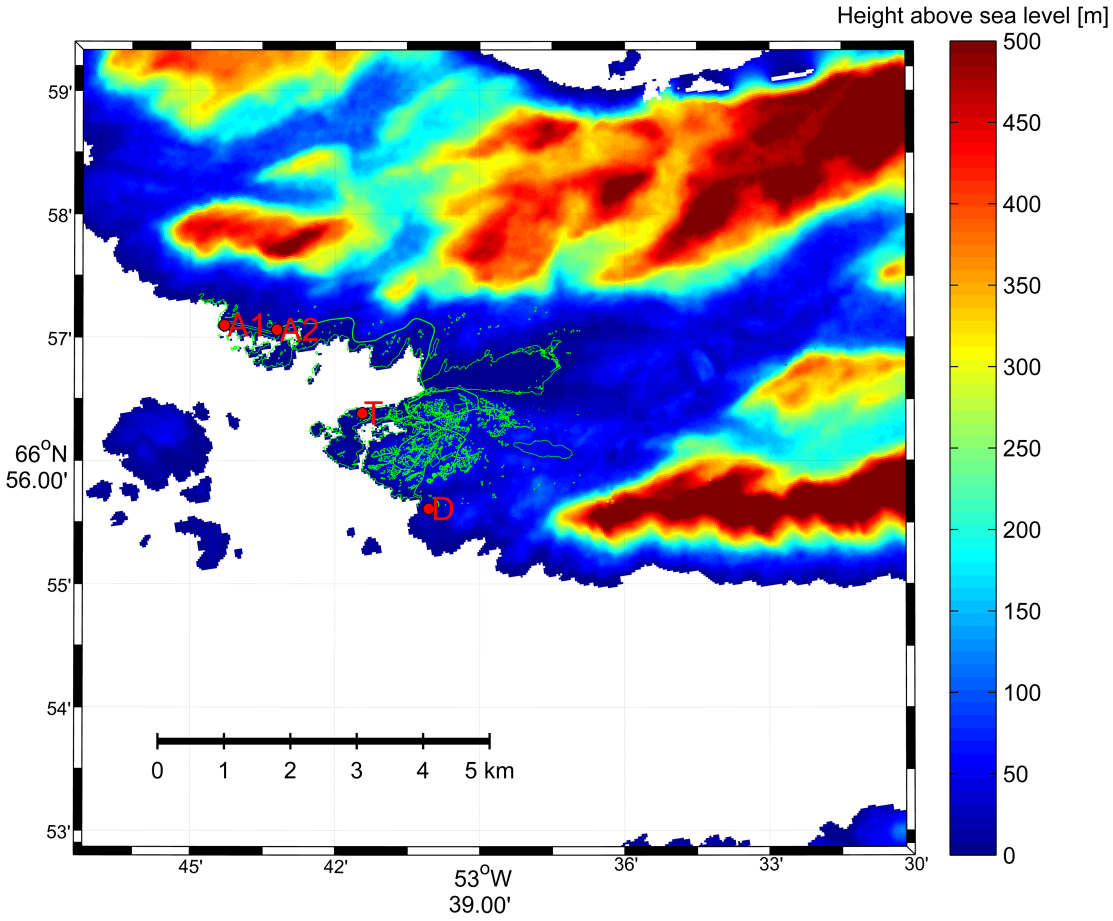

Figure 3.8: *Climate stations in Sisimiut, A1 airport southwest, A2; airport northeast, T; Teleoen, D; Dumpen site.*

There are two overlapping periods available for the four stations August 6, 2004, to May 1, 2005, and October 25, 2006, to June 12, 2008. The period without data was caused by downtime at the Teleoen station in 2005-06. For the Teleoen station, the western and southwestern sectors were blocked by huge oil containers much higher than the mast, and from the eastern to the southern sector, the town itself influenced the flow Fig. 3.9b

& Fig. 3.8. The airport site is also not optimal for wind measurements because all the northern sectors are blocked by a 466m mountain (Praestefjeldet).
To gain extra information about the wind climate in Sisimiut a short measurement campaign was established on a small peak south of the town (Dumpen). A study of the sector-wise wind distribution for the 4 sites showed how difficult it is to get a reasonable picture of the wind climate directly from the measurements even though all the measurements were taken within 4km, and it is confirmed that the flow patterns are very complex in the area.
For this location (Midwest and coastal), two dominant wind directions would be expected, south and eastern [Cappelen, 2004]. Wind from the south, along the coast, is caused by the blocking effect of the land itself (barrier wind). The easterly winds are a combination of; general flow above the ice cap, katabatic winds related to the flow of the ice cap and valley/fjord-to-sea temperature-driven flow systems. As the roses in Fig. 3.9b and Fig. 3.9c show, high wind speeds occur in the southern sectors, but the frequency is relatively low. The easterly wind speed is relatively low for the A1 and Teleoen sites, owing to the blocking effects and the Dumpsite is exposed only to a deflected part of it. The frequency for easterly winds is relatively high for all sites, but the potential of the easterly wind at an unaffected site cannot be estimate directly from these measurements. The lower flow disturbance and better inflow from most directions has a large effect on the mean wind speed for the Dumpsite, that is more than 50% higher than for the other stations Table 3.2. Model based "cleaning" of the observations are necessary if they should be used for wind resource assessment or mesoscale model validation. A WAsP cross-prediction test, based on high resolution GIS data, were conducted, however it was not able to clean/model the wind within the 10% error limit. *The Sisimiut measurements was not a part of this project, however the data collection, quality assurance, statistical processing and site inspections was performed by this project*

The settlement Sarfannguit, 40km east of Sisimiut, has a high easterly wind potential, and parts of this flow will reach the Sisimiut area, but the mountains bend it around the city. To support this theory, a short measurement campaign were launched on Assarqutaq Island (southeast of Sisimiut ($66^o54'52''N, 53^o29'00''W$)) February 24, 2010-August 12, 2010. This campaign underpinned the theory about the predominant east-west flow, but in this period, the westerly wind was the most frequent, with light wind sea breezes mainly causing the high frequency of westerly wind Fig. 3.10a. If the Assargutaq rose is compared with the Teleoen Fig. 3.10b and Airport Fig. 3.10c roses it is clear that only a fraction of the easterly winds reach Sisimiut (Teleoen).

Station	Elev.	06.08.2004-01.05.2005		25.10.2006-12.06.2008	
	[m]	mean	max	mean	max
A1 *ws* [m/s]	5	4.1	28.3	3.4	25.7
T *ws* [m/s]	15	3.9	27.0	3.2	28.8
D *ws* [m/s]	78	6.1	29.1	4.9	31.6

Table 3.2: *Mean and maximum wind speeds for the Sisimiut stations in the overlapping measuring periods August 6, 2004,-May 5, 2005 and October 25, 2006,-June 12, 2008. Data for mast A2 is not available for this periods.*

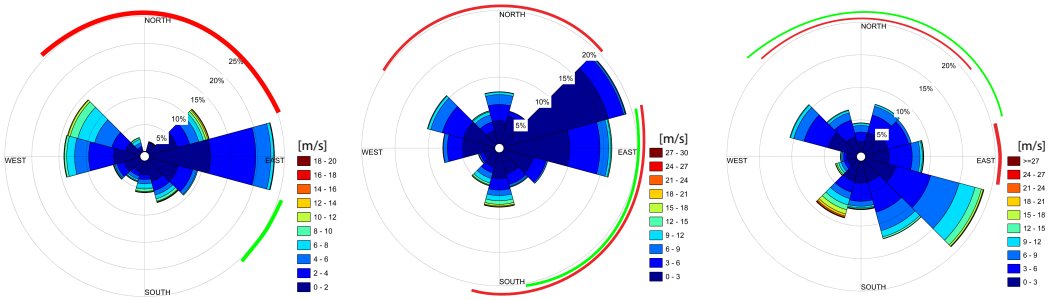

(a) *A1* **(b)** *T* **(c)** *D*

Figure 3.9. *Wind roses for the three Sisimiut site (quality checked, but not terrain filtered). The colored lines indicate sectors where the flow is highly affected by the town, green, and the terrain, red. [Wind speed in m/s and sector distribution in percent of measurement period]*
- Airport 1 site (A1) $(66^o57'01''N, 53^o42'13''W, 5m\ AMSL)$*,*
- Teleoen site (T) $(66^o56'23''N, 53^o41'2''W, 15m\ AMSL)$*,*
- Dumpen site (D)$(66^o55'37''N, 53^o40'03''W, 19m\ AMSL)$*,*

3.3.2 Wind monitoring stations

As shown previously the wind climate can be local, and it can be very difficult to make a reliable wind resource estimations based on one observation point. For small villages far from the nearest climate station, it can be more or less impossible to estimate wind power potential. To get a better picture of the wind power potential for selected settlements on the Greenlandic west coast, the energy company Nukissiorfiit and Technical University of Denmark (DTU) launched the first of several measurement campaigns in 2002. The campaign focused on two areas Sisimiut and Uummannaq. The results of this campaign were presented in main reports [Villumsen et al., 2010b], [Jakobsen et al., 2011], [Dragsted et al., 2011], [Dragsted et al., 2012] and in [Jakobsen and Hansen, 2016a].
These stations was adopted by this project in 2010 and used for local microscale studies. The adoption included; operation, data validation, statistical processing, reporting, station upgrades and field service.

Another wind monitoring campaign, funded by Nordic Energy Research, was launched by Nukissiorfiit in Nanortalik, South Greenland, in 2007. A 50 m meteorological tower was installed and operated until 2011 [Risberg, 2009], [Aakervik et al., 2011]. The tower was incorporated in the "Fyrtaarns projekts" and adopted by this projet in 2011, Appendix A.4. The mast was upgraded with three levels of first class cup anemometers, and a heated 3-D ultrasonic anemometer to estimate instrument icing, inflow angle, turbulence spectrum and boundary layer stability.

An extension of the Nanortalik monitoring, with two new tall tower sites was included in 2013, funded by "Fyrtaarns projekt 6". The design and siting was done based on the gained experiences and the local conditions. The idea was to form a triangle and validate model performances by cross prediction. The final installation was postponed due to harsh weather conditions, management replacements, and finally stopped by the project deadline. More information Fig. 3.23.

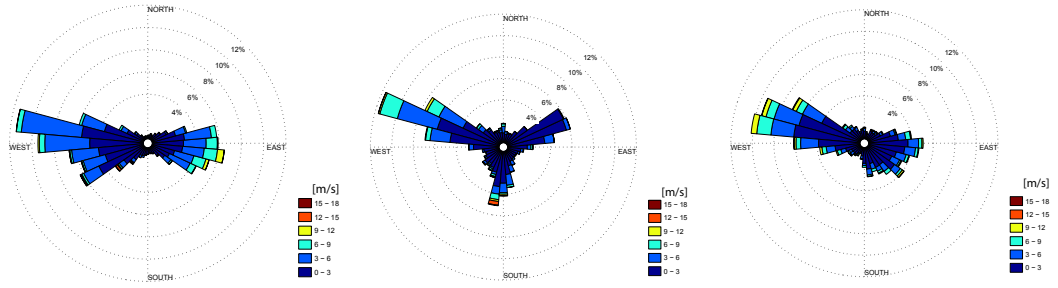

(a) *Ass* **(b)** *T* **(c)** *A1*

Figure 3.10. *Wind roses for the Assargutaq campaign (February 24-August 12, 2010), where the sites is compared, to show how the easterly winds are bended around Sisimiut.[Wind speed in m/s and sector distribution in percent of measurement period]*
- Assargutaq site (Ass)$(66^o54'52''N, 53^o29'00''W, 19m\ AMSL)$,
- Teleoen site (T) $(66^o56'23''N, 53^o41'2''W, 15m\ AMSL)$,
- Airport 1 site (A1) $(66^o57'01''N, 53^o42'13''W, 5m\ AMSL)$

3.3.3 Wind station design

The remote location of sites and the harsh Arctic environment place stringent requirements on the reliability and robustness of the measurement systems. Furthermore, the stations can only be serviced once a year and should otherwise operate unattended [Jakobsen and Hansen, 2016a].
The initial station design was tested in Sarfannguit in 2003-2004. The station were equipped with instruments as listed in Table 3.3 and a Wind Explore data logger from NRG systems, installed on a 10 m tubular tower.

Recorded parameters	**Instrument**	**Brand**	**Height** m
Wind speed ws	#200P	NRG systems	10
Wind direction wd	#40C	NRG systems	10
Relative humidity rh	RH-5x	NRG systems	2
Air temperatureap	110S	NRG systems	2

Table 3.3: *Measurement parameters recorded at the stations for the lighthouse (Fyrtaarn) projects*

The data transfer was manual and carried out by locals. A small SD card was sent by mail and the data later sent by email from Greenland to Denmark for processing. This procedure worked well for the first period but is not recommended for longer campaigns. After some data losses, the loggers were replaced with NRG Symphonie loggers equipped with a GSM modem modules (IPack). The data transfer to DTU Wind Energy has since worked on daily basis with GSM-based Internet. The daily data files includes on top of the collected data, system status such as memory left and battery voltage. The stations are designed to shut down, data transmission and power-consuming instruments when the battery voltage is low. This happened between November and March, depending on the location, for the first design. This low-power mode does not influence the logging of wind speed, wind direction, and temperature, but relative humidity measurements are shut off.

The initial design is continuously updated with new instruments and batteries to obtain higher quality data.

3.3.4 Station positioning

For the settlements, only small wind turbines are implementable in the grid. This often limits the area of interest, to a few kilometers from the existing grid, owing to the cost of cabling and transport. On the other hand, noise limits and restriction zones set the closest boundary for potential sites. The complex terrain itself also limits the number of potential sites in the area because of steep slopes and soft ground.

When stations need to be installed, there are some guidelines that can be used. The most popular is the WMO observation guide [Artz et al., 2010]. The focuses for wind monitoring are surface roughness, obstacles, and measurement height. The basic rules are; no obstacle within 10 times the measurement height (10 m) is allowed, the surface roughness must be 0.03, and the mast should me located at least 30 times the height of surrounding obstacle/terrain features from the obstacle. If the site does not fulfill the standard layout, the guide includes some guidelines for design such as using taller Met. towers and/or data correction. The obstacle related uncertainty for standard observation stations in imperfect environment can according to the guide be estimated by site classification. The WMO defined surface wind is caramelized as; wind blowing at a geometrical height of 10 m with a roughness length of 0.03 m. This is corresponds to a flat surface with low grass. These surface conditions are difficult to find in Greenland, where most land surfaces are irregular bare rocks, gravel or low vegetation (0.05-0.5 m). To obtain the WMO defined surface wind from the Greenlandic stations, detailed information about obstacles and surface roughness is needed, to correct the collected data.
Before the first installation in 2003, a study of climate stations and terrain was carried out [Iversen and Kristensen, 2003] to make sure that the site was suitable as a wind turbine and measurement site. The wind rose and wind speed distribution for the two nearest climate stations (04230 Sisimiut and 04231 Kangerslussuaq), were studied. Topography data, together with orthophotos, was used to identify the most suitable position. After the first successful test in 2003-2004 in Sarfannguit, the station was relocated to Dumpen, close to Sisimiut, in 2004.
When the next measurement campaign was launched in 2006, (Sarfannguit, Uummannaq, Ukkusissat, Saattut and Ikerasak), the local wind and topography were not studied in the same detailed way, but the group relayed information from the local community. This led to the bad positioning of several of the stations installed in the 2006 campaign.

When I was put in charge of the measurement program, as a part of the PhD activities, the program included 6 stations. One of the first activities was a WAsP-based site optimization of the Sarfannguit site, and to verify the result of this optimization a second mast was installed at the selected point 500m west of the existing site in August 2010. The Sisimiut Dump site mast was moved to the village Itilleq 40km south of Sisimiut, in 2010 but was relocated in 2011 due to flow channeling at the first location. In 2012 a 50m tower located in Nanortalik, South Greenland was inherit from the "Vest-Norden" projet and a second station installed on a mountain in the area. The station maintenance and annual reporting of the results was imposed the PhD project until 2013 were a new

structure was incorporated. The activities were used to gain experience with design and operation of remote stations in more or less harsh climate.

3.3.5 Operation of remote stations in Greenland

The first measurement system design was simple and relatively robust except for the (manual) data transfer. Since the Symphonie loggers were installed, both data recording and transfer have been stable. Some stations have experienced unexpected failures, like stolen memory cards, gunfire, and unpaid phone bills, but the data availability in general has been good.

The data transfer and instrument shutdown during winter have caused some frustrations due to lack of humidity data and lack of knowledge about the station conditions. If a failure occurs during this period (November-March), the central data control will first discover it when the data arrive or not arrive in March.
The NRG #40C cup anemometer has been used at both high and low-altitude sites, with maximum wind speeds from 25 to 70 m/s. This cup has failed at both high and low-wind sites without any clear pattern. The most common problems are bearing/shaft defects or cups that break of the spinner.
At some sites, the NRG cups were replaced by P2546A-OPR cups. This cup has survived at the low-altitude site and delivered high-quality data. At higher altitude sites Appendix A.6, where icing is more frequent and the maximum wind speeds higher, the P2546A-OPR also fails. The connection between the spinner and the shaft breaks, and the spinner falls off the instrument, Table 3.4. For the last setup Thies first-class anemometers were used. One of these has failed due to a broken cup-arm, but these instruments have not been in use long enough to evaluate their performance in this climate. The relative humidity and

Brand	Type	Low altitude		High altitude	
		Failed	Total	Failed	Total
NRG Systems	#40C	3	20	3	3
WindSensor	P2546A-OPR	0	4	2	2
Thies	Class 1	0	0	1	5
NRG Systems	IceFree3	1	1	1	1
Metek	uSonic-3 Scientific	0	1	0	0

Table 3.4: *Anemometer failure statistics for the campaign separated by low- and high-altitude sites. This statistics cover only the part of the campaign were I have been in charge of the station maintenance (2009-2014).*

dew point measurement in periods of sub-zero temperatures have led to problems. The first NRG RH-5X was not able to deliver reasonable results and several other instruments seem to have the same problems. At the moment the Heated Vaisala HMP 155 humidity and temperature probe is being tested for this purpose.
One of the most common problems for measurements in the harsh Arctic environment is instrument icing. Heavy instrument icing or fast buildup and melting can be detected directly in the data, but light icing or a long icing period can be more or less impossible to detect without a dedicated system. An ice detection system can be an additional heated anemometer, an ice detector, or a simple camera.

For this project, we have tested the Metek uSonic-3, heated at 100W, as reference for the cup measurements. This instrument is chosen because it also collects information about turbulence, inflow angle, and temperature and it has not the same tendency to drift over time as cup anemometers. The HoloOptics T44 ice rate sensor has also been tested at three sites, but it has not been able to survive more than a few months [Hudecz, 2013].

3.4 Wind resource assessment

To evaluate the site conditions in relation to the IEC standard, basic data is required; wind speed distribution, extreme wind speed, turbulence intensity, wind shear and flow inclination(tilt). The collected data and results of related studies is presented in this section.

The collected data has been quality checked, split into reference years, and statistically processed according to the description in [Jakobsen and Hansen, 2016a]. For each reference year, the statistical parameters were determined and the mean values used to characterize the period. Some of the key parameters are presented in Table 3.5. More detailed information about the sites, setup, and results can be found in [Hansen et al., 2006].

Met. site	Met.	Mean *ws*	Weibull	Weibull	Max power	WPD	Max *ws*
	Days	[m/s]	A	k	12 sectors	$[W/m^2]$	[m/s]
Uummannaq	1587	4.8/6.6[1]	5.82	1.22	5(SE)	277/603	29.4
Saattut	945	4.0*/4.6[2]	5.11	1.61	5 (SE)	-	19.4
Ukkusissat	1077	3.3	3.58	1.34	2 (NE)	64	16.8
Ikerasak	1566	3.4	3.66	1.21	7 (S)	94	20.3
Dumpen, Sisimiut	1208	4.8	5.23	1.32	5 (SE)	230	32.2
Assargutaq	146	2.8*	3.01	1.23	2(NE)	45	16
Sarfannguit 1	2045	5.5	6.35	1.81	3 (E)	228	25.8
Sarfannguit 2	993	6.1	6.69	1.68	2 (NE)	309	28.2
Itelliq	149	5.0*	-	-	7 (SW)	-	-
Nanortalik 10m	1869	5.3	5.82	1.49	2 (E)	268	29.0
Nanortalik 50m	1869	6.0	6.74	1.49	2 (E)	429	31.1

[1] Two different measurement systems
[2] Measure Correlated Predict (MCP) method used
* Missing data basis (Short time series)

Table 3.5. *Site information, for wind resource measurement locations in SW Greenland. More information Appendix A*
- Met(Days): indicate the length of the campaign in days
- Mean ws: Average wind speed of campaign
- Weibull A,k: Weibull probability fit using, maximum likelihood
- Max power: Sector of the 12 with the heights WPD
- WPD: Average wind power density
- Max ws: Maximum 10 minute mean wind speed in campaign

$$\text{WPD} = \frac{1}{2N} \sum_{i=1}^{N} \rho_{(i)} u_{(i)}^3 \tag{3.10}$$

where:

WPD Number of 10 minute average measurements $[W/m^2]$

N Number of 10 minute average measurements [-]

ρ Air density (based on actual temperature & pressure) $[kg/m^3]$

u Horizontal wind speed [m/s]

The highest wind resource 10 MAG was found at Sarfannguit site 2, with $309 W/m^2$ and mean wind speed 6.1 m/s. This is a relatively high resource compared to climate station records in this part of the country. The wind profile above 13m, and thus the wind speed at hub height, is unknown, but the terrain slope and extrapolation from lower 3 measurement levels indicate that the wind speed rises with height. The turbulence level is measured within the limit of IEC 64100-1 class B and is expected to decrease with increased height due to the very rocky surface.
At some sites (marked with * in Table 3.5), only short campaigns have been carried out, and uncertainties related to the results are thus relatively high. Site selection is crucial in this terrain, and for some sites in the Uummannaq area, this has not been handled correctly and has affect the results. The most severe example is the Ukkusissat site that is located close to a cliff, that shelters the mast in the expected main wind direction, see Appendix A. Extreme wind speeds are generally low for all sites, even when they are extrapolated to 50-year extremes, even though wind speed can be high in other regions.
The Nanortalik site Appendix A.2 is the only site equipped with a tall tower and heated instruments. The site has been used to study the wind profile, turbulence variations with height, icing periods, boundary layer stability and inflow angles.
The tower have three instrument levels (10, 30, 50m), all equipped with P2546A-OPR cup anemometers, and wind vanes are installed at levels 1 and 3. The wind speed distribution Fig. 3.11a shows that the highest wind occurs from the northeast and southwest, and the wind speed in these directions is more or less similar at both 30 and 50 MAG. This indicates a low wind shear, as the alpha value in Fig. 3.11b verifies.
The vertical wind profile in the boundary layer is described by a logarithmic profile and expressed by the wind profile power law (3.12). With the three levels, the alpha parameter can be derived from three-level variations, as presented in Fig. 3.11b. If the mean wind profile can be described by the log function, the most accurate estimation of alpha is given by the largest height difference (10/50 MAG), but if the alpha(10/50 MAG) is used to predict the wind profile, it underestimates the level 2 (30m) wind speed and thereby overestimating the profile slope. The same problem is seen when (10/30 MAG) is used to derive the level 3 (50 MAG) wind speed. This means that the log profile will not fit the wind profile in the 10-50 MAG range. This can be caused by non-neutral boundary layer stability and/or high degree of large-scale mixing in the surface layer indicating roughness sublayer behavior. In this case wakes/waves from the surrounding mountains force some mixing, especially in the high frequent eastern sector. Large scale mixing in the surface layer will also affect the vertical Turbulence Intensity

(TI) distribution. TI for level 30 and 50 MAG is more or less identical Fig. 3.12a, while the 10m level, as expected, is higher, indicating high-scale mixing at the upper levels.

$$\mathrm{TI} = \frac{\sigma_u}{\overline{u}} \tag{3.11}$$

where:

TI Turbulence Intensity [-]

σ_u Standard deviation of horizontal wind speed [m/s]

u Horizontal wind speed [m/s]

The mixing above 50 MAG is unknown, but for a conservative estimate, levels 2 and 3 (30/50 mag) can be used to describe the profile and the wind speed interpolated to a given hub height by (3.13) for example 80MAG $\implies 6.14m/s$ and 100MAG $\implies 6.2m/s$. To verify the wind profile a full rotor height (tip top) campaign is recommend for sites like this, because it is fundamental for the turbine performance, load distribution and maintenance costs.

$$\frac{u_2}{u_1} = \left(\frac{z_1}{z_2}\right)^{\alpha} \implies \alpha = \frac{Log_{10}\left(\frac{u_2}{u_1}\right)}{Log_{10}\left(\frac{z_2}{z_1}\right)} \tag{3.12}$$

where:

α Wind shear exponent (Power law) [-]

z_1 Reference height 1 [m]

z_2 Reference height 2 [m]

u_1 Wind speed reference height 1 [m]

u_2 Wind speed reference height 2 [m]

The sector weighted mean α values are 0.0819, 0.0392 and 0.1017 for 10/50 MAG, 30/50 MAG, and 10/30 MAG respectively; this is lower than the neutral $1/7 \approx 0.1429$, indicating that unstable BL dominates the period. To estimate the wind speed at other heights, e.g. turbine hub height, the sector frequency weighted exponents (3.13) are normally used.
The IEC 61400-1 sets the average wind shear limit for the rotor swept area to $0 < \alpha < 0.2$ for standard class turbines. The Nanortalik Dump site is therefore based on the observation within the span, but the rotor plane for small low-wind (class 3) turbines easily reaches the double height of the Nanortalik tower. The consequences of exceeding the IEC design limits can be fatal, causing blade-tower contact for negative shear and destroying the main bearing in high shear cases. Before any turbine siting in the complex Greenlandic terrain, verification measurements for the full rotor plane is therefore recommended.

$$u_{mean(z)} = \sum_{sectors} u_{z50(sector)} \left(\frac{z}{z_{50}}\right)^{\alpha_{(sector)}} \cdot freq_{(sector)} \tag{3.13}$$

where:

$\alpha_{(sector)}$ Sector vise wind shear exponent [-]

$u_{mean(z)}$ Extrapolated wind speed height z [m/s]

z Extrapolation height [m]

z_{50} Reference height (50m) [m]

$u_{z_{50}}$ Sector vise reference wind speed [m/s]

freq Frequency of sector [-]

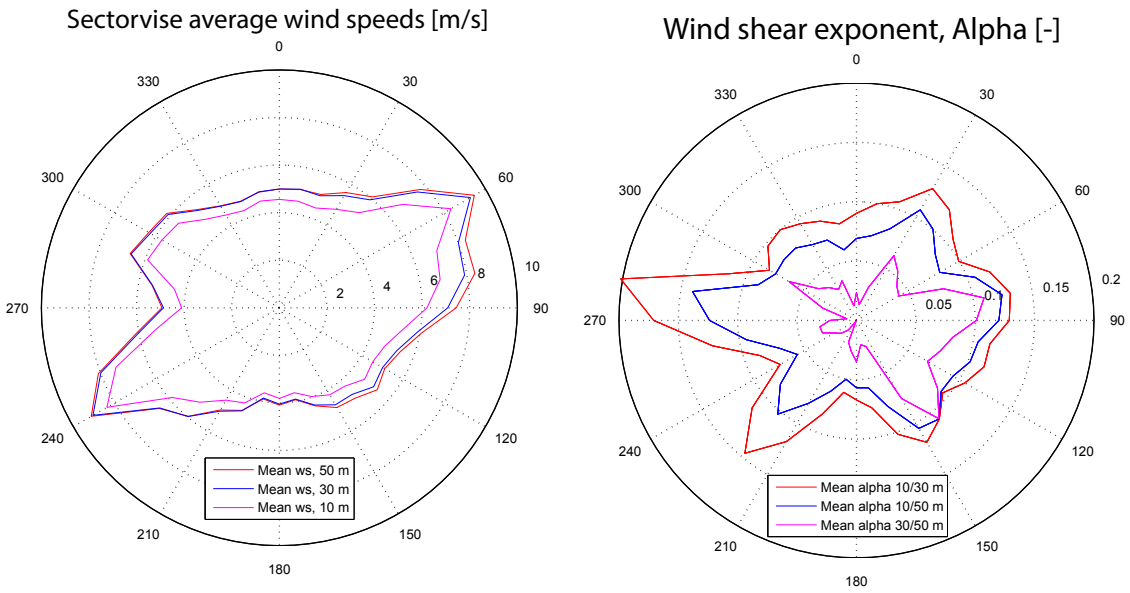

(a) *Sector-wise mean wind speed distribution, magenta 10MAG, blue 30MAG, red 50MAG.*

(b) *Wind shear coefficient alpha, magenta 30/50MAG, blue 10/50 mag, red 10/30MAG, based on wind speed filtered data (ws> 5m/s).*

Figure 3.11. *Sector-wise wind speed and wind shear exponents*

3.4.1 Turbulence in the surface layer

It is preferred that wind speed be measured at hub-height or at least, above the roughness layer Fig. 3.6. Nevertheless the turbulence intensity for some of the sites is so high as to indicate that this is not the case. At the Nanortalik site the turbulence intensity for the three measurement levels was studied to look at the distribution. The results are not general for all sites, but they can give an indication of the height distribution. The turbulence intensity at level 1 (10MAG) is much higher than at the higher levels

Fig. 3.12a, and above 8 m/s, it exceeds IEC 61400-1 class A, while this first happens at 12 m/s for the two other levels. The directional variations of the turbulence intensity Fig. 3.12b show that the highest turbulence levels are related to southeasterly (Tuapait mountain) and westerly (the town) wind directions. The raised turbulence level needs to be considered for turbine selection and AEP estimation for this site. For measurement, this indicates that wind speed measurement close to built-up areas must be carried out at higher levels.

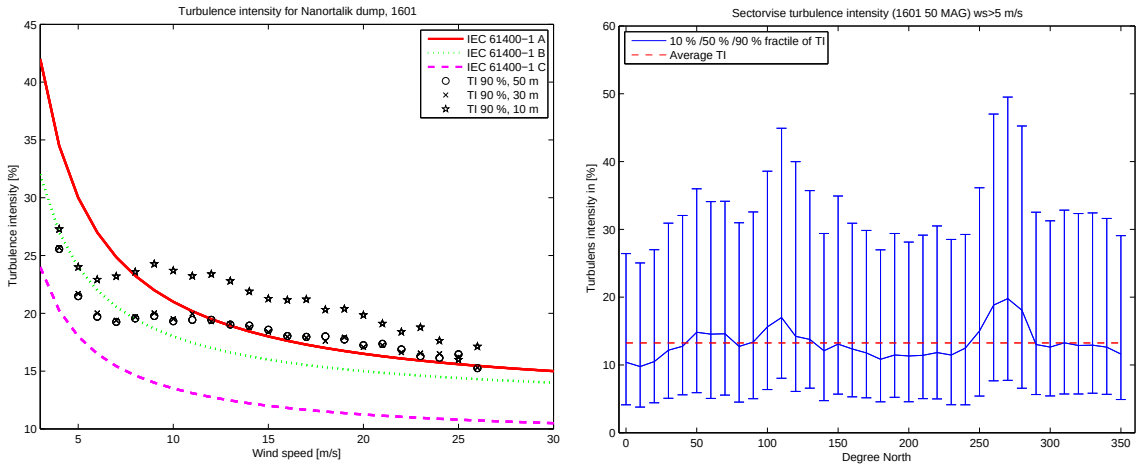

(a) *Turbulence intensity as a function of wind speed, based on IEC61400-1 ED.3 method.*

(b) *Turbulence intensity as a function of direction, based on data with $ws > 5m/s$*

Figure 3.12. *Turbulence data for the Narnortalik Dump site 1601*

Another type of relevant site is the mountain sites. The ground of the ridge at top sites is often bare rocks in different formations but it varies from site to site. Sarfannguit site 2 is a good representative of lower-level mountain ridges. There are no obstacles at the site, but the terrain slope forces the flow to separate for some inflow sectors. The general turbulence level is expected to be moderate to low because of the long distance to terrain objects in the main flow directions and the relatively smooth-curved terrain. The mast was installed with three-level cup anemometers at 4, 8, and 11 MAG to study turbulence level as a function of height. The turbulence intensity at the site is relatively low Fig. 3.13a and stays within the limit of IEC 61400-1 B. As the sector-wise distribution Fig. 3.13b shows, the highest turbulence intensity is in the southern sectors, where the terrain slope is largest. The frequency of these sectors is low, and the effect on the overall turbulence level is thereby limited. From 11 MAG up to turbine hub height, this ridge-induced turbulence will decreases, and in case of a turbine installation, the turbine position can be optimized to minimize turbulence and optimize wind power. For information about turbulence levels and so on, see Appendix A.

3.4.2 Flow inclination

The inflow tilt or flow inclination angle is important for turbines because high tilt causes abnormal load distribution across the rotor, and in the worst case, the blades can hit the tower. The tilt angle can be calculated from relation between horizontal and the

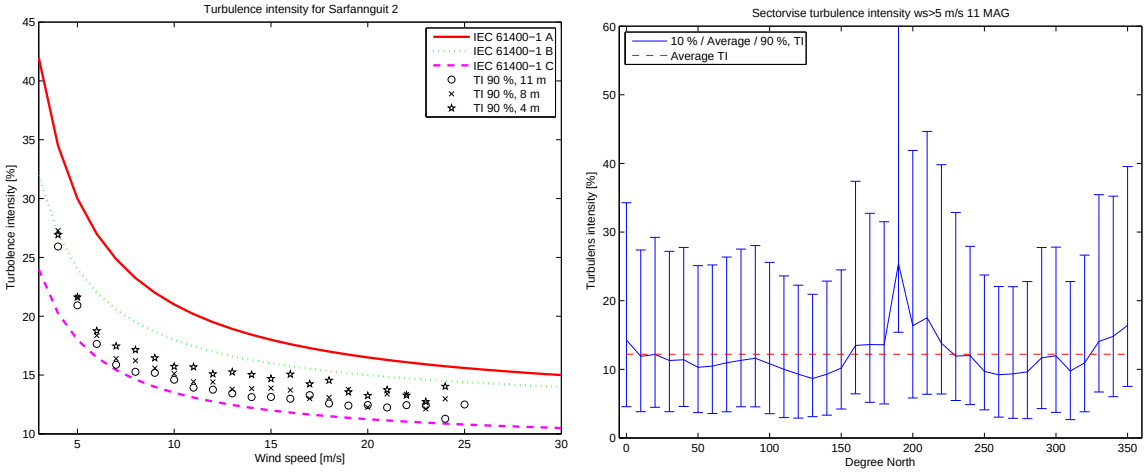

(a) *Turbulence intensity as function of wind speed. (January 1, 2011 to July 1, 2013).*

(b) *Turbulence intensity as function of direction, based on data with $ws > 5m/s$ (January 1, 2011 to July 1, 2013).*

Figure 3.13. *Turbulence data for the Sarfannguit site 2*

vertical wind speed. The two wind components (u and w) can be monitored by individual anemometers or with 3-D anemometers. The IEC 61400-1 has set the limits for standard turbines to $\pm 8°$ from horizontal.
At the Nanortalik Dump site the inflow tilt was monitored by a 3D ultrasonic anemometer, top pole mounted 50MAG. The data is recorded as positive values above horizontal. The sector-wise average distribution is presented Fig. 3.14. The tilt angle is highly dependent on the wind speed and BL. stability. At increasing wind speeds and neutral BL. the tilt angle is around zero. At low wind speeds the stability can be either stable or unstable (convective) and the tilt angle will likewise be more polarized mainly depending on the buoyancy flux. The turbine loads are relatively small at low wind speeds and the tilt angles at lower wind speed ($< 8m/s$) is therefore less relevant for turbine siting. The tilt angels observed in the period for ($u > 8m/s$) range from -2.5 to 6.6° and at 6.5 m/s it reaches the IEC limit. It should be noted that the tilt angle will change with height and for turbine siting it must evaluated at hub height.

3.4.3 Icing

One phenomenon that has the potential to affect measurements is icing. Even light icing of the cup anemometers used for wind speed measurements has a large effect on their performance, and therefore it is important to be able to identify icing periods both for the measurements and later on for the turbine AEP. In the first setup of the Nanortalik tower, the ice estimations were handled by a simple heated anemometer (NRG Systems IceFree3) installed parallel with the main anemometer (2007-2011). At the next setup, a dedicated ice rate sensor was installed (HoloOptics T44)(November 25-30, 2012), and in the last setup, a heated ultrasonic anemometer (Metek uSonic-3 Scientific) was added (May 14, 2013 -). The study of the instrument icing is described in section 5.5

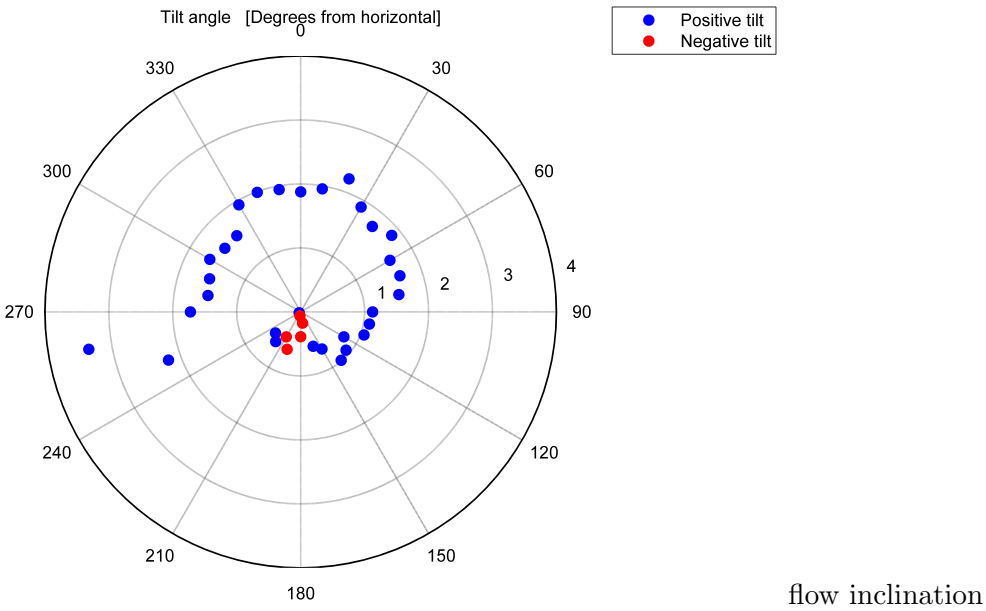

Figure 3.14. *Mean tilt angle as function of inflow direction with positive above horizontal. Nanortalik Dump site 50MAG, period 05/2013-05/2014.*

3.4.4 Stability estimation based on observations

BL stability was studied at the Nanortalik site by measuring the potential-temperature in the form of the temperature difference between 3 MAG and 49 MAG Ri and the MO length based on surface heat flux and friction velocity.
A simple approximation of stability can be found based on the potential temperature and the relation to the lapse rate. If the actual lapse rate is higher than the dry adiabatic lapse rate τ_d, then the BL is absolutely unstable. Similarly, if the actual lapse rate is lower than the saturated lapse rate τ_s, then the BL is absolute stable Fig. 3.15b. The interval in between is called conditionally unstable and is often from $9.8K/km$ to $6.5K/km$. However, the saturated lapse rate varies with temperature, humidity, and pressure, in this case from 3.8 to $7.9K/km$ Fig. 3.15a.

The hydrostatic stability test shows that the absolute stable BL condition is dominant two-thirds of the time, absolutely unstable and conditionally unstable only one-third. A summer and winter example are shown in Fig. 3.16a and Fig. 3.16b. The data are based on 10 minute average potential temperature observations (3-49 MAG), linear scaled to 100m height difference. The complex terrain and the relatively small height difference affect the result because turbulence and mixing affect the two layers differently. Another simple measure of BL stability is the Richardson number (Ri). The Richardson number describes the relation between the potential and the kinetic energy (3.14). When the Ri is evaluated at 50 MAG it gives 60% stable and 40% unstable BL, while the neutral fraction is very small. At rising wind speeds, the Richardson number moves, toward neutral conditions, as expected, while at lower wind speeds it becomes more polarized, Fig. 3.17. Unfortunately, not enough ultrasonic data have been collected yet to perform a study of

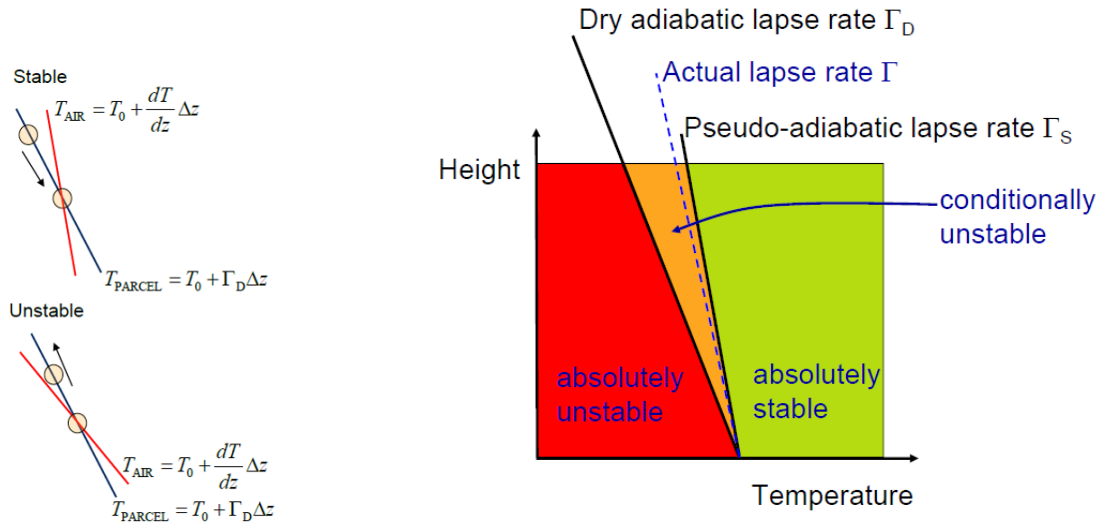

(a) **(b)**

Figure 3.15. *Lapse rate illustrations. (Figure credit: Jacob Mann, DTU Wind Energy).*

the Monin Obukhov stability (3.2). This can be part of the final site evaluation, planned for 2015.

$$Ri = \frac{E_{pot}}{E_{kin}} = \frac{g}{T}\frac{\frac{d\theta}{dz}}{\frac{du}{dz}} \approx \frac{g}{T_{49}}\frac{\frac{\delta T_{49} - T_3}{49-3}}{\frac{u_{50}-u_{10}}{50-10}} \tag{3.14}$$

where:

E_{pot} Potential energy [J]
E_{kin} Kinetic energy [J]
T Temperature [K]
g Gravity $[m/s^2]$
θ Potential temperature [K]
u Horizontal wind speed [m/s]

	Stable	Unstable	C Unstable	Neutral
H stab.	68%	15%	17%	
Ri	60%	40%		0.1%

Table 3.6. *BL stability for Nanortalik test site (1601) in% of time, for the period 05/2013-05/2014.*
- H stab.: Hydrostatic stability
- Ri: Richardson stability

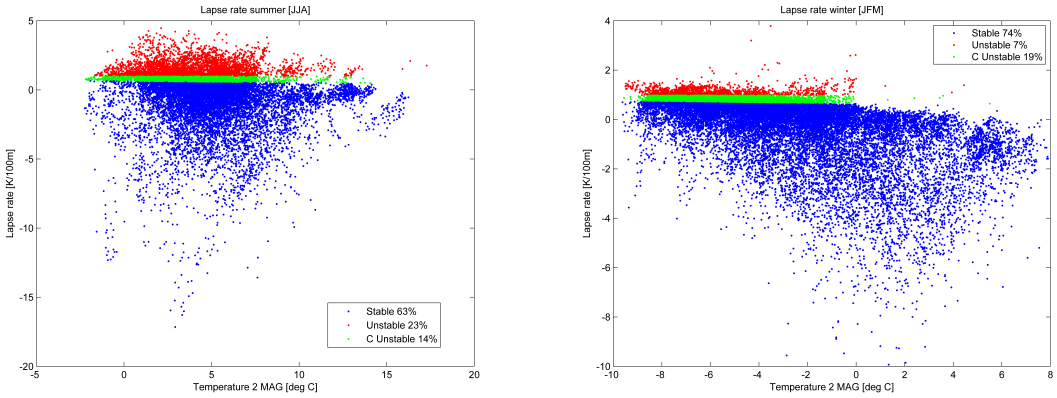

(a) *Lapse rate for summer period June to August.* **(b)** *Lapse rate for winter period January to March.*

Figure 3.16. *Nanortalik Dump site 1601*

3.4.5 Conclusion drawn from wind monitoring

During the measurement campaigns several potential wind turbine sites were investegated, from Uummannaq in North over Sarfannguit to Nanortalik. The measurement campaigns verified that knowledge about the local flows can be used to find potential sites far from the Southern tip were the general potential is highest. The extreme wind speeds measured in the populated western part is not above the design limits for standard wind turbines. Some special events as extreme directional shifts and icing were observed and have to be addressed in site assessments for complex arctic terrain. Mountain wakes and waves is another important feature that has been observed, mainly at the Nanortalik site. These wakes increase the turbulence level and can affect the flow many km downstream depending of the size and shape of the mountain.
The remote locations, harsh weather, limited infrastructure and low budgets has been a challenge for the campaigns. The service was limited to one yearly visit where instruments were replaced and the general conditions checked. Much data was lost until the stations were adopted by this project and upgraded with high quality instruments and modems for online communication. Several data logger systems were tested, but the NRG system was the most robust and reliable. The 3 Ice rate sensors tested was not able to survive more than a few months, only leaving short time series for evaluation. The lack of tall tower and/or LIDAR systems was a major problem for the project, because the complex flow patterns complicate vertical extrapolations and increases the uncertainties. The two new Nanortalik sites (North and South) will together with increased LIDAR availability will have a high potential for model validation and resource estimation in Greenland.

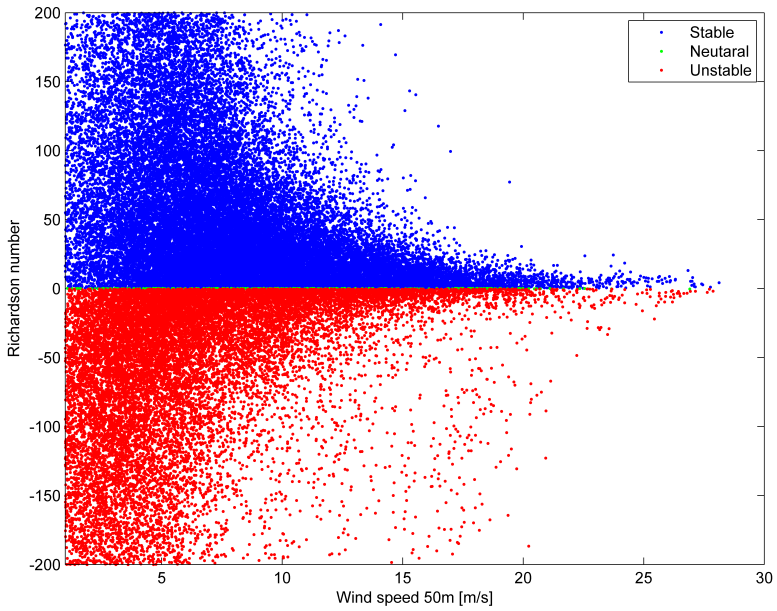

Figure 3.17. *Richardson number as function of wind speed evaluated at 50MAG.*

3.5 Microscale modeling based on local measurements

When the wind speed distribution in an area needs to be estimated, different methods can be applied. Offshore, the wind speed distribution can be estimated directly from the induced waves, but onshore and at higher altitude atmospheric models are needed. Atmospheric models are classified by their temporal and spatial operation area. The microscale models covers the lower part of the spectrum (a few km), the mesoscale models operate typically from a few kilometers to few hundred kilometers, and the synoptic scale is (more than 100km) Fig. 5.6. In the temporal scale, the microscale models handle processes up to 100s, and this covers the turbulence and convective processes. The mesoscale models ($> 10^2 s$ and $< 10^5 s$) handle the range from convection over cyclones to cloud processes. This section deals with local wind resource modeling based on local measurements using microscale models. The objects is to estimate the performance and estimate the valid range of the model (the standard error level for wind resource assessments, $\pm 3\%$ is used).

3.6 WAsP modeling based on local reference measurements

Multiple microscale models and software tools for local wind resource assessment are available on the market. The most common used for wind resource assessments are Meteodyn, Zephy tool, WindSim and WAsP. The most common tool for wind resource assessment WAsP was available for this project and in 2013 the CFD were available. WAsP version 1 was released in 1987 and the latest version is 11.4.

The wind dedicated Wind Atlas Analysis and Application Program, (WAsP) were selected as microscale wind modeling tool. The program is now available with two flow solvers,

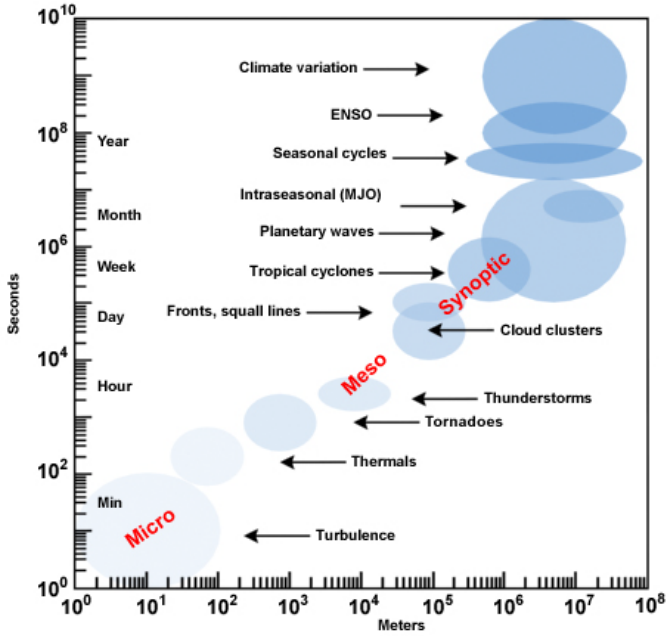

Figure 3.18. *Meteorological classification (Figure credit: COMET)*

one linearized and one CFD based (Reynolds Averaged Navier-Stokes Simulation); however, mainly the linearized version is used in this project because of the late release of the CFD-version in relation to the project deadline (All results in this report is based on the linear version 11.1.0016). The CFD version performs mainly better in areas with high flow separation and thereby in very complex terrain. The main disadvantages of the CFD version in relation to the linear are; longer computation time, limited domain size (2x2km), often lower performance over terrain with slopes $< 20\%$.

The procedure of the wind atlas method is to first clean the observed wind data for microscale effects, based on detailed digital maps of roughness, obstacles, and elevations Fig. 3.19. The cleaned data, called the generalized wind climate, are valid for the area where the higher-scale effects on the flow are similar to the observation site. The model assumes a neutral boundary layer and use the logarithmic wind profile for height extrapolation. The stability study of this project, described section 3.4.4, indicates that this assumption is valid only for very high wind speeds, but the error introduced by this can be minimized by estimation of the wind at the same height as the observations. If higher-level wind speed is needed, stability corrected profiles can be used.

The idea is to use WAsP for local site selection within a few kilometers of the existing climate stations, based on local climate station observations. For the complex Greenlandic terrain, with large separation zones, the linearized flow model is expected to overestimate the wind resource, as thermal effects also add to the uncertainties, but to give a reasonable view of the relative wind speed distribution WAsP can be used.

For WAsP predictions in complex sites outside the valid range of the WAsP flow model, empirical correction of the predicted wind speed can be applied [Mortensen and Bowen, 2004]. The correction procedure, as demonstrated in [Mortensen and Antoniou, 2006], is a demanding process that involves a local correction constant. WAsP operates with

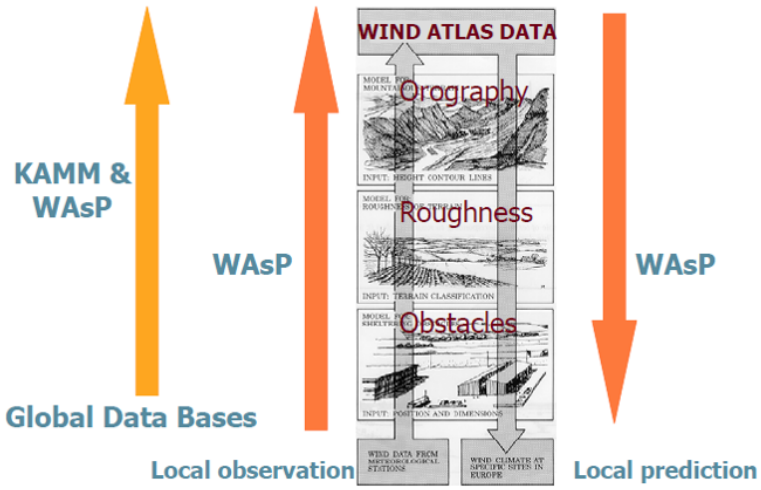

Figure 3.19. *Principle of the wind atlas method,(Figure credit: WAsP-group DTU Wind Energy).*

the ruggedness index (RIX) concept, which indicates how large a fraction of the inflow area exceeds the critical slope (separation $\approx 30\%$), and [Mortensen and Antoniou, 2006] stated that if ΔRIX(RIX difference between reference and prediction site) exceeds a few percentage point, correction is suggested.
The terrain slopes are evaluated in radial lines from the site to a defined radial distance Fig. 3.20. The default values used for the RIX calculations are; calculation radius 3.5 km, critical slope 0.3 and number of radial evaluation lines 72. The number of evaluation lines must correspond to the amount of sectors used for the flow modelling. The RIX value for a particular site is simply the percentage of the terrain in the evaluation lines that exceed the defined critical slope, illustrated with red in Fig. 3.20.

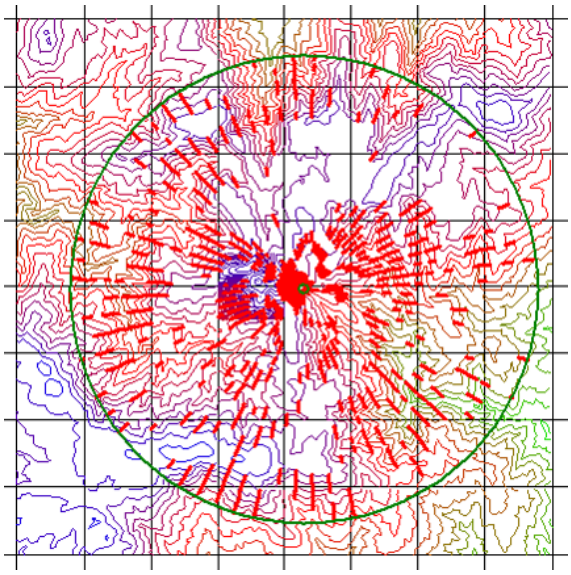

Figure 3.20. *Principle of the RIX estimation for sites,(Figure credit: WAsP-group DTU Wind Energy).*

The difference in RIX between the reference site and the prediction site is called ΔRIX and is used as a performance indicator for WAsP in complex terrain. Studies of prediction errors as a function of ΔRIX [Mortensen and Antoniou, 2006; Mortensen and Bowen, 2004] have found a good description by a log-linear function (3.15), and a critical RIX value in the range of 0.3-0.4 is recommended. According to the description, the correction parameter β in (3.15) is restricted to areas with similar climatological and topographical conditions, but to estimate β several sites with relatively large differences in RIX are needed. A measurement campaign, by which this could be done together with testing the CFD version, was planned and the installation began in the Fyrtaarn 6 project, but different unforeseen challenges delayed the project, and we will have to stick to the β values obtained at other locations. For this project, the value of 1.5 found in [Mortensen and Antoniou, 2006] is applied with some caution; on the other hand, higher-scale meteorological effect often minimized the valid area of WAsP to less than a kilometer, and then ΔRIX is often low, so the correction will be small.

$$U_m = \frac{1}{exp(\beta \cdot \Delta RIX)} U_p \tag{3.15}$$

where:

U_m Horizontal wind speed, modified [m/s]

U_p WAsP predicted wind speed[m/s]

ΔRIX RIX difference between referance and prediction site [%]

β Empirical correction parameter [-]

3.6.1 WAsP test

The model performance was tested at several sites where multiple masts were available for cross-prediction, Uummanaq-Sattut, Sisimiut, Sarfannguit, Qaqortoq, and Nanortalik. The model tests performed in Sarfannguit and Nanortalik is described here.
Close to the village Sarfannguit, a 10 m tower has been in operation since 2006, and the area was selected for a WAsP performance test.

The test is split into the following steps:

1. Run initial WAsP run for validation of site selection
2. Install validation mast and measure
3. Extract data for the overlapping period and re-run WAsP
4. RIX-correct the modelled wind speed and validate

Based on the wind resource estimated by the initial WAsP run a site 500m southwest of the existing Sarfannguit 1 was selected. Site 2 (109 m AMSL) is located more or less downstream of site 1 (80 m AMSL) in the predominant wind direction. The well-defined

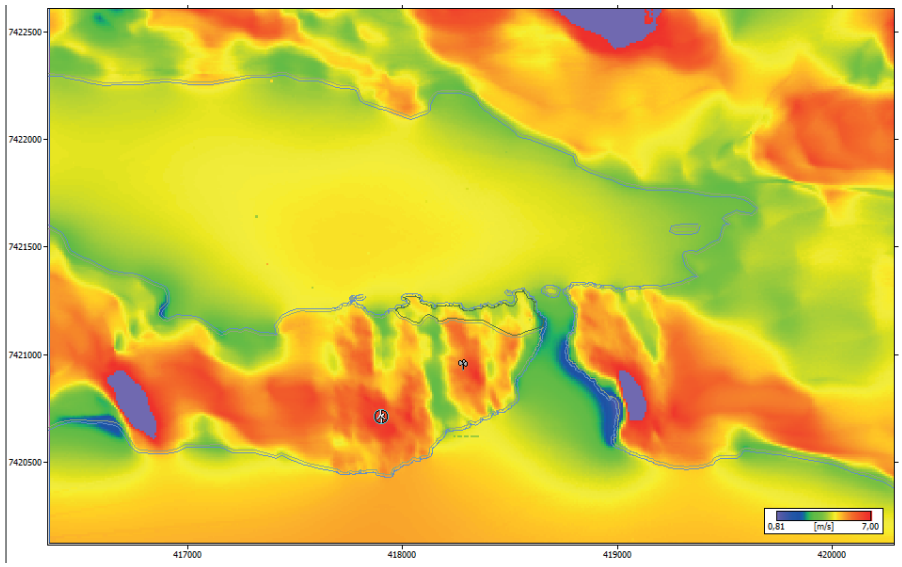

Figure 3.21. *Result of the initial WAsP run, shown as the predicted average wind speed 13 MAG. The turbine indicate location of the validation station, Sarfannguaq site 1 and cup indicate reference site. (Coordinates in UTM zone 23*

flow pattern in the fjord system makes the flow go easterly or westerly more than 80% of the time, and the validation site, west of the reference site, is downstream more than 50% of the time. The selection of a site relatively close to the reference site and in the dominant flow patch minimizes the prediction errors induced by higher-scale processes and flow channeling. The validation station, Sarfannguit 2, was installed in 2010 and has been operating since, except from one down period. The overlapping data series January 1, 2011 to July 1, 2013, with average wind speeds of 5.7 and 6.4 m/s for sites 1 and 2 respectively, was used for the test. The results of the cross- prediction show that the RIX corrected predicted wind speed is 3.5% and 7.8% off, respectively, but the uncorrected speed is only 1.8% and 6.3% off.

In Nanortalik the terrain is relatively simple, both stations are close to sea level, and they have an internal distance of only 520m. Three years of data (July 1, 2007-2010) for the Heliport site (10 m), and Dumpen (10 and 48 m) were included. The 48 MAG level was included because the 10 MAG level at Dumpen showed unreadable behaviour in this period. Prediction of the 48 MAG level from the 10 MAG Heliport site induced profile errors because the neutral BL constraint in WAsP is not valid for this site; section 3.4.4. This is expected to have a negative influence on performance and, in scaling from 48 MAG to higher- levels WAsP, is expected to underestimate wind speed. As the test results in Table 3.8 show, the model was able to predict wind speed at the Heliport site from the Dumpsite 10 MAG, but in the opposite direction it overestimated wind speed and, as expected, highly underestimated the 48 MAG level.
The test system planned for the Fyrtaarn 6 project included higher RIX values sites and higher masts Appendix A.5. The RIX was 7.5 and 16.3 for the planned North and South site, respectively. The predicted wind speed for the two sites were 8.1 m/s for the South and 10.2 for the North site, and the β=1.5 corrected speed were 7.4 and 10.2. The two sites were carefully selected based on flow pattern studies and terrain features. The North

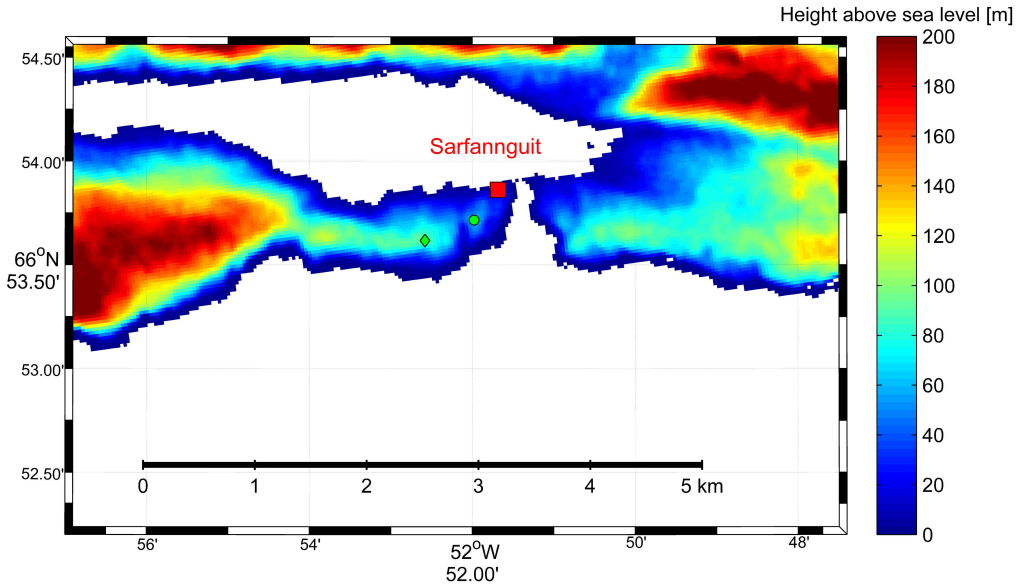

Figure 3.22. *Position of the Sarfannguit sites. Green circle site 1, green diamond site 2, red box village.*

site is exposed to the channeled flow in the Sarqa/Sermersup Sarqa fjord, and the South site is exposed to the flow bending around Cape Farewell and following the coast and above the mountain ridges. Both sites have sectors of simple smooth terrain, and the South site especially has sectors with very steep terrain with an average slope of up to 45%. As described, the equipment is on the sites, but the campaign has been delayed, first by harsh weather and then by some organizationally challenges.

3.6.2 WAsP/microscale test conclusion

Based on the tests, a small improvement of the predictions for similar heights were found in most cases, but a general trend like [Mortensen and Bowen, 2004] and [Mortensen and Antoniou, 2006] were not found. Whether the relatively low ΔRIX values (1.3 and 0.9%), the low validation heights, or atmospheric conditions caused this is unknown, but no clear improvement in predictions were found by implementing the ΔRIX correction. The model performance was generally found acceptable (allowed prediction error on annual average wind speed $< \pm 3\%$) within 500m of the reference site for sites with low mesoscale effects on the flow.
For projects where higher error levels are accepted and for areas with less complex terrain environments, the modelling area/distance will increase. The modeling results are affected by serval parameters both model setup and external like data quality and resolution. The RIX and ΔRIX calculations are for instance highly dependent on the terrain data resolution and homogeneity. The results were not very sensitive to the parameter setting in the WAsP calculation as; calculation radius, critical slope and number of sectors. The external effects cover monitoring errors, errors in terrain representation and surface cover data. To minimize the potential external errors, the terrain data was validated against local fix points and alternative sources, the monitoring systems and surface cover was physical inspected.

WAsP Sarfannguit

	ws	RIX	ΔRIX	P ws	C ws	Bias	β
Site 1	5.7	6.0	-1.3	5.8	5.9	0.2	-1.3
Site 2	6.4	7.3	1.3	6.0	5.9	-0.5	-5

Table 3.7. *WAsP validation for Sarfannguit sites*

ws Wind speed measured [m/s]

RIX Ruggedness Index [%]

ΔRIX Difference in RIX for the sites [%]

P ws WAsP predicted wind speed [m/s]

C ws ΔRIX corrected wind speed [m/s]

Bias Predicted - measured ws [m/s]

β Empirical correction parameter [-]

WAsP Nanortalik

	ws	RIX	ΔRIX	P ws	C ws	Bias	β
Heliport Site 1	4.31	5.3	-0.9	4.25	4.31	0	1.5
Dump 10m	5.18	6.2	0.9	5.39	5.32	0.14	4.4
Dump 48m	5.99	6.2	0.9	5.86	5.78	0.21	-2.5

Table 3.8. *WAsP validation for Nanortalik sites.*

ws Wind speed measured [m/s]

RIX Ruggedness Index [%]

ΔRIX Difference in RIX for the sites [%]

P ws WAsP predicted wind speed [m/s]

C ws ΔRIX corrected wind speed [m/s]

Bias Predicted - measured ws [m/s]

β Empirical correction parameter [-]

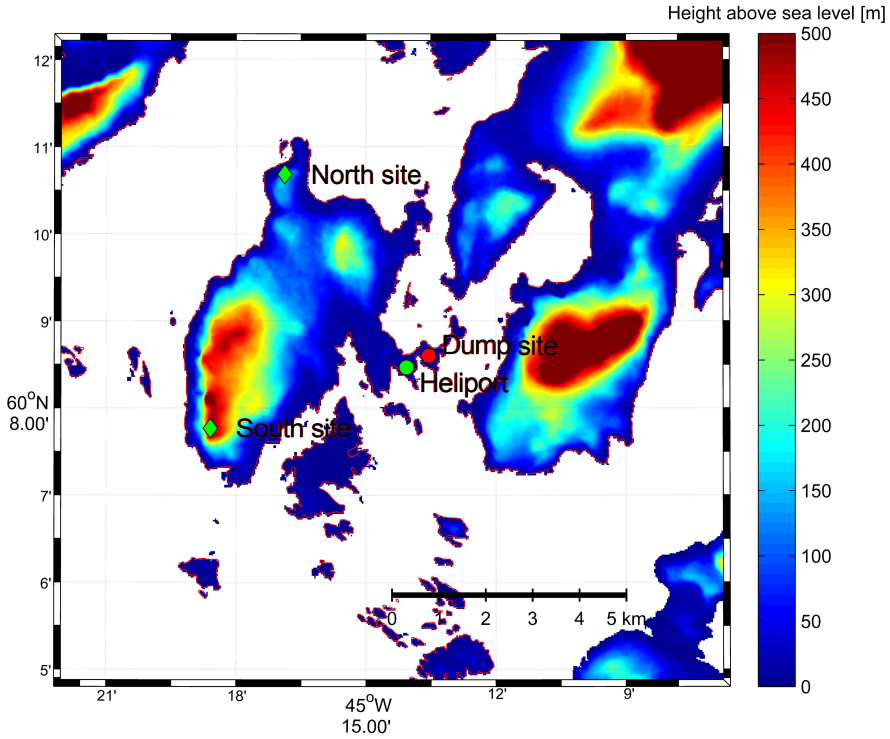

Figure 3.23. *Position of the Nanortalik sites. Green circle Heliport, green diamonds new South site 30 MAG and North site 40 MAG, red circle is the Dumpen site 50 MAG, Topography data source [Howat et al., 2014].*

Chapter 4

Mesoscale modeling of wind resources

In this chapter, the challenges of using mesoscale modelling to characterize the wind resource in Greenland are investigated using two different versions of the Weather Research and Forecast model WRF. First, an general overview of the model will be given, followed by a description of the differences between the standard WRF model and a version of the WRF model customized for the polar regions. Finally, results from a one-month modelling study in southern Greenland will be presented, together with recommendations and unsolved challenges for modelling the wind resource of the region. To demonstrate some of the findings and improvements done in the project, the results from the last two versions of the simulations are presented in this chapter.

4.1 Introduction

As described in the previous chapter the microscale models are only valid within a limited area, due to the lack of atmospheric process modeling. In the mesoscale models the atmospheric process are parameterized based on physical models, in a broad range of sub-models. While the microscale models were limited to domains of a few kilometers, the mesoscale models are design for thousands of kilometers.
In wind power applications the mesoscale models are used for wind resource assessment on wind farm level, based on models in reanalysis setup and for power production forecast, and service schedule, based on models in prediction setup (Operational forecast models).

A wide range of mesoscale models are available word wide. Based on in-house knowledge and experience, from several worldwide wind mapping projects, the NCAR Weather Research and Forecasting model WRF was chosen for this project. The European Centre for Medium-Range Weather Forecasts (ECMWF) provide free access to their ERA-Interim reanalysis data and these data was successfully used in multiple wind related studies at DTU. Based on this initial tests with the ERA-Interim-WRF setup was initiated.
The Polar meteorology group at Ohio State University (OSU) has developed a modified polar version of the WRF model, with a special surface energy balance and heat transfer model using continuously updating sea ice quantities and land mask properties. A Polar optimized reanalysis dataset, based on the Polar WRF version, called Arctic System Reanalysis (ASR) was also published by the Polar meteorology group. The ASR provide

together with the Polar WRF a fully Polar optimize model setup named WRF(ASR). The WRF(ASR) setup was included in this study and evaluated parallel with the WRF(ERA-I) setup.
The model resolution was set to 2 km and was linearly interpolated to the observation (AWS) positions. January 2009 were simulated with both models. In the chosen setup it is the model performance in combination with the associated input data, as for example the reanalysis data, that is evaluated and not only the model. The modelled and measured wind speed and wind direction were evaluated, with focus on mean, bias, and correlation.

The mesoscale modeling part of this project faced unexpected challenges. The first simulation setup, version 1, showed an unexpected poor wind speed modeling performance. Studies of the results and inputs identified large errors in the terrain elevation data (GTOPO30) [Gesch and Greenlee, 2004] used. Furthermore, the study showed that the erroneous terrain data (GTOPO30) was used for the Arctic System Reanalysis simulations. The second version simulations (version 2), with updated terrain elevation data (GMTED2010) [Danielson et al., 2011] performed far better.
A detailed study of the modeled wind fields found incorrect stability effects in both models (version 1+2), caused by incorrect sea ice inputs. Furthermore, ocean wind comparisons indicate problems with the modeled terrain effects around Cape Farewell. It is clear in the ocean wind comparison, that the 2 km horizontal resolution not was sufficient to represent the terrain features and model the wind distribution around the fjord outlets. Based on the experience gained in this project at least new valid terrain elevation and sea ice data are need together with updated ASR data to get the best result. Long-term modeling and coupling to microscale models was outside the scope of this study, but are important areas for further study.
All mesoscale model simulations, in this project, were run by Claire Vincent, formerly of DTU Wind Energy.

4.2 Mesoscale models

DTU Wind Energy has a long tradition in atmospheric mesoscale modeling, mainly for wind resource and pollution purpose. Many different model has been used but the preferred has since its introduction in the late eighties, been the Karlsruhe Atmospheric Mesoscale Model (KAMM) also known as MEMO (MEsoscale meteorological MOdel). For the latest decade the Weather Research and Forecasting (WRF) model has gained ground, due to it high flexibility and the fact that it is freeware.
WRF is a modern mesoscale forecast model and data assimilation system build in a wide multi organizational corporation with National Center for Atmospheric Research (NCAR) as the main coordinator. The source code and documentation can be accessed at the WRF user page http://www2.mmm.ucar.edu/wrf/users/. In this projet the Advanced Research WRF Version 3.4 was used [NCAR, 2012]. The model is very flexible, full parallelized, and anybody has the opportunity to develop their specific WRF based model setup. One of the groups that developed their own version is the Polar Meteorology Group of the Byrd Polar and Climate Research Center at The Ohio State University, OSU. The group developed and continues improve the Polar WRF, specially modified for simulation in the Polar regions.

4.2.0.1 Polar WRF

The polar WRF was developed specific to take account of the particular atmospheric and surface conditions in the Polar regions. The modifications are implemented through changes to the WRF physics packages as well at recommendation for the name-list options [Hines and Bromwich, 2008a; Hines et al., 2011]. The modifications include:

- Arctic optimized surface energy balance and heat transfer model for the Noah LSM.
- Modifications allowing cell sea ice quantities, thickness and snow depth updates during the simulation.
- Modeling of the seasonal variations of the sea ice albedo.
- Optimized latent heat and sensible heat calculations based on snow fractions
- Modified microphysics models for arctic cloud modeling (reduced droplet concentration etc.).

The polar WRF runs were setup with variable sea ice, snow depth and sea ice albedo input from observational data, extreme value checking surface temperature, surface pressure and soil temperature. The [Hines and Bromwich, 2008a; Hines et al., 2011] recommended changes of; base sub-surface temperature for sea ice (271.16 to 276.36) and snow emissivity (0.98), a maximum limit on the snow thickness for ground heat flux calculations and surface temperature based on direction calculation of the surface energy balance included. The sea ice concentration and thickness data were provided by NCEP and downloaded from http://igloo.atmos.uiuc.edu/ASR/. The daily sea ice concentrations are based on the Special Sensor Microwave/Imager (SSM/I) of National Snow and Ice Data Center http://nsidc.org/ were used in time interpolated form. For the WRF(ERA-I) the standard sea-ice cover data in ERA-Interim were used.

The Polar WRF documentation and software are available at: http://polarmet.osu.edu/PWRF/.

4.2.0.2 WRF input data

The model input data are loaded through the WRF Preprocessing System (WPS). WPS include functions for:

- Defining simulation domains and settings.
- Interpolating terrestrial data (terrain elevation, land use and soil data).
- De-gridding and interpolating meteorological data to the simulation domain.

For easy data loading the WPS module include, GRIB variable tables for Meteorological data from various centers; NCEP(R1+2+RUC), ECMWF, etc. Terrestrial data; USGS 24 category and MODIS 20 category land datasets as; USGS GTOPO30 elevation dataset, Global 5-minutes United Nation FAO, and North-America STATSGO 30 sec soil category dataset, 10-min greenness fraction data based on AVHRR and 30-sec greenness fraction data based on 10 years MODIS; MODIS-based leaf-area index, 0.15 degree monthly albedo and snow albedo data, and 1-degree deep soil temperature data; plus a few specialized

datasets.

For data outside the standard variable table the relevant parameter must be setup manually.

4.2.1 Governing Equations

The modern atmospheric models are based on a numerical solution of the basic system of nonlinear differential equations (3D momentum, continuity, thermal, moisture equations), known as the primitive equation system (can be found in e.g. [Stull, 1988]). These equations were the basis for the first numerical weather forecast by Richardson in 1922 and are still a fundamental part of the models. The formulation used in WRF is a compressible, non-hydrostatic, flux-form version and can be found on page 8 in the documentation [NCAR, 2012].
The primitive equation system lead to a "closure problem" due to the fact that the turbulence momentum, moisture and heat flux term are unknown. The unknown turbulence fluxes are approximated by parametrization in the Planetary Boundary Layer PBL scheme. Similar physical parameterization schemes are used to account for other aspects of the unsolved model physics.

4.2.2 Parameterization of processes

Complex or small-scale processes that are too computational expensive to simulate directly are, together with processes where insufficient knowledge make an explicit representation impossible, are parameterized, Fig. 4.1. Most of the parameterizations are based on physical models, with tuning or observational studies. Most models parameterize:

- Land-surface processes (surface fluxes, radiation, and hydrology).
- Turbulent fluxes (momentum, heat and moisture).
- Radiative transfer through the atmosphere.
- Cloud micro physics.
- Cumulus convection (moist convection).

One of the drawbacks with the parametrization compared to the full physical modeling is the limited valid range of the parametrization. A long range of parametrization schemes are available for each physical process. The different schemes are optimized for different climate conditions and model resolutions.
The WRF model includes five physics model categories: microphysics, cumulus parameterization, planetary boundary layer (PBL), land-surface model, and radiation, with multiple schemes available in each category,[NCAR, 2012].

4.2.3 Boundary layer parametrization

To represent the turbulent mixing in the lover part of the atmosphere, Planetary Boundary Layer PBL, accurate models for the thermodynamic and kinematic processes are needed

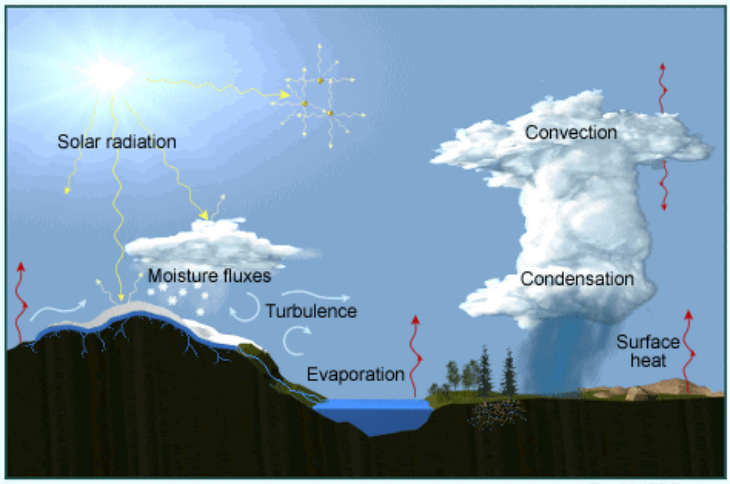

Figure 4.1. *Illustration of the lower scale processes that normally are parameterized, Figure credit: Comet-UCAR*

in the mesoscale model. The models (PBL schemes) have to represent the sub-grid scale mixing of moisture, heat and momentum between the surface and the free atmosphere.

Describing the turbulence mixing of the boundary layer involve more unknowns than the number of available equations, known as the closure problem. The unknown fluctuation and covariance terms are approximated using various order closure of known variables. The closure assumptions are categorized by their statistical order and how mixing between layers is simulated; local means between neighbor layer, non-local means between all layers. More advanced hybrid models are available as ACM2 model by [Pleim, 2007].
The simplest closure type is the first-order closure, where the relation between the average values and the fluctuations are described by a simple turbulent diffusion coefficient. This means that the covariance terms, for example momentum; $\overline{u_i' u_j'}$, are described in terms of $\overline{u}$, $\overline{v}$ and $\overline{w}$ by for example (4.1).
First-order:

$$\overline{C_i' u_i'} = -K_{iC} \frac{\delta \overline{C'}}{\delta x_i} \tag{4.1}$$

Second-order:

$$\overline{C_i' u_i' u_j'} = -K_{iC} \left(\frac{\delta \overline{u_i' C}}{\delta x_i} + \frac{\delta \overline{u_i' C}}{\delta x_i} \right) \tag{4.2}$$

where:

K_{iC} parameterization term

u_i' Velocity flux term

C_i' Varies flux term

x_i Distance in "i" direction

After the same principles as first- and second-order the closure can be expanded to even higher order [Stull, 1988]. A combination of the two methods, parameterization and

prediction, are characterized as half order for example 1.5 order. The most important flow features are described by the average flow and the lower order moments, however the solution should be closer to the exact solution while the closure is pushed to higher order moments.

Alternative closure/representation methods as; Spectral diffusivity, Transilient turbulence, Large Eddy Simulation (LES) and finally Direct Numerical Simulation (DNS) are available.
In this project two PBL schemes were used; Mellor-Yamada-Janjic (MYJ) 1.5 order turbulence closure model [Janjić, 1994] and Yonsei University (YSU) [Hong et al., 2006] first-order non-local closure model, see the WRF model documentation [NCAR, 2012]. The PBL schemes are highly dependent on the stability prediction, which is hard to determine in these areas because of the uncertainties related to the snow and ice cover. The snow and ice cover dramatically alter the surface fluxes and thereby the PBL stability. The actual used PBL scheme is shown in the configuration table for the particular WRF run/version.

4.2.4 Space derivatives

The space derivatives are for most mesoscale models handled by grid point methods, where the equations are solved for each point of a 3D spatial grid. The coordinate system can be cartesian or spherical and the spatial derivatives are solved by finite difference methods.
The grid increment are chosen so that there is a sufficient number of grid point to represent the smallest features of interest in the modeling, however there will always be representations or truncation errors. To understand the effect of the resolution on the results, the kinetic energy spectrum dissipation for the modelled and the correct/theoretical spectrum can be studied. The numerical convergence, as determined by an invariance of the kinetic energy spectrum as a function of the resolution, has been studied by [Marchesiello et al., 2011; Skamarock, 2004], among others. They found, that the WRF standard filter are able of resolve the kinetic energy spectrum of wave lengths down to ≈ 7 times the spatial model resolution, depending on the latitude (Coriolis force). Higher order closure and higher spatial resolution will thereby lead to better representation for normal resolutions. For very high resolutions < 200 m LES or even DNS is needed.

The used WRF model uses an Arakawa-C grid staggering with a 2km horizontal model resolution. Due to the aliasing and finite resolution, and the diffusive processes in the model, the processes resolved by the model are ≈ 7 times the horizontal grid spacing. For the 2km resolution used in this project we do not expect the model to resolve features smaller than about 14km.

4.2.5 Vertical coordinate system

An important difference between the available models is the used vertical coordinate system. The simplest coordinate systems are:

- Height above mean sea level
- Potential temperature of isentropic coordinates
- σ pressure coordinate (Surface reference)
- η pressure coordinates (Surface reference)

The height above mean sea level is not very common, mainly because it involve some extra transformations for the primitive equations. The isentropic coordinates is mainly used in stable stratified parts of the atmosphere, as the stratosphere. Different variation of the terrain-following vertical-pressure coordinate systems are the most common, but more advanced hybrid coordinate systems can be used to optimize the model [Davies, 2002]. The WRF models used in this project uses terrain-following hydrostatic-pressure vertical coordinate η Fig. 4.2.

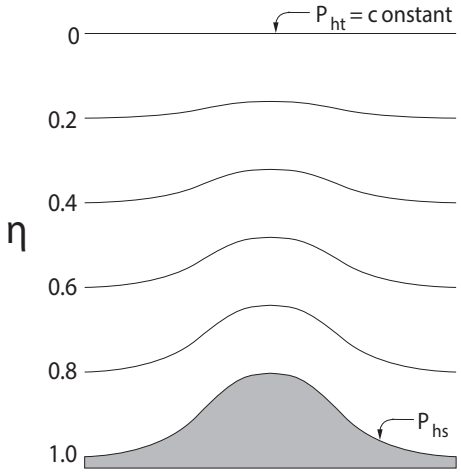

Figure 4.2. *Illustration of eta coordinate system, Figure credit: [NCAR, 2012]*

4.2.6 Initial & boundary conditions

The initial conditions are the atmospheric state at the beginning of the simulation. The initial state is obtained from large scale models or reanalysis data.
Local area models LAM need boundary condition BC on all sides of the domain; upper, lower and lateral. The finite difference equations cannot be solved at the edge points, because there are no points beyond the boundary to use in the derivative calculation. The models therefore need external defined lateral BC and for operational LAM´s the BC are defined from previous large scale simulations. Research simulations usually define the BC from global reanalysis or similar data, including assimilation of observations. For models with multiple nested domains the lateral boundaries can have both one and two-way interaction. In one way interaction the information flows from the coarse-mesh-large

to the fine-mesh-small domain. In the two ways setup the fine-mesh feedback information for the next time-step of the large-coarse domain.

The model atmosphere cannot extent to infinity height, so an artificial upper bound needs to be defined. The upper bound need to avoid unnatural reflection of vertical movements as waves. Most models include different damping/reflection models as: implicit gravity-wave damping, Rayleigh relaxation layer or increased diffusion layer.
The lower BC includes specification of heat moisture and momentum fluxes at the surface. Land and ocean models determine the atmosphere-surface inter action, both in the atmospheric BL and below the surface [NCAR, 2012].
For the simulation in this project, both the initial and boundary conditions are provided by Reanalysis dataset. The initial and boundary conditions for the standard WRF were provided by the ERA-Interim (ERA-I), a global reanalysis product with a spectral resolution of T255 ($\approx$ 80km) Table 4.1 [Dee et al., 2011]. The Polar WRF, initial and boundary conditions were from the Arctic System Reanalysis, a product which combine Arctic observations with data assimilation and modeling with a 30km grid resolution. Some of the lower BC data was provided by other sources, see section 4.2.0.1.

4.2.6.1 Reanalysis data

Reanalysis data is a retrospective analysis using a consistent physical approach on the same analysis system to produce a homogeneous dataset. The reanalysis dataset provide consistent data series produced on state of the art analysis systems, tuning the meteorological parameters to fit the historical observations, with resolutions similar to the forecast analysis. Large metrological organizations, such as European Centre for Medium-Range Weather Forecasts (ECMWF), the National Centers for Environmental Prediction (NCEP), the National Center for Atmospheric Research (NCAR), Ohio State University, Byrd Polar Research Center, the Polar Meteorology Group (OSU), the Japan Meteorological Agency (JMA), and National Aeronautics and Space Administration (NASA), provide historical reanalysis data for different periods and in different resolutions Table 4.1.

Reanalysis data

Name	Provider	Spatial res.	Time res.	Start	End
ERA-Interim	ECMWF	0.7^o	6 hr.	1979	pre.-3mdr.
NCEP-DOE 2	NCAR	2.5^o	6 hr.	1979	2014
JRA-25	JMA	1.125^o	6 hr.	1979	2014
ASR	OSU	30 km	3 hr.	2000	2011
ERA-40	ECMWF	0.75^o	6 hr.	1957	2002
MERRA	NASA	0.5^o	6 hr.	1979	pre.

Table 4.1. *Reanalysis data available*

In this project the ERA-Interim (ERA-I) based on the "IFS Cy31r1" model from European Centre for Medium-Range Weather Forecasts (ECMWF) and Arctic System Reanalysis (ASR) based on Polar WRF from Ohio State University, Byrd Polar Research Center, the Polar Meteorology Group (OSU) was used.

4.3 Mesoscale simulation, version 1

The objective for this simulation is to study the performance of state-of-the-art mesoscale models for wind resource estimation in Greenland. In this setup it is the model performance in combination with the associated input data, as the reanalysis data, that will be evaluated. Moreover, the performance in various terrains and weather situations will be explored.

The method chosen for this study was mesoscale modeling validation based on Automatic Weather Station (AWS). The model output was set to 2 km horizontal resolution and was bilinear interpolated to the AWS positions. Modeled and the measured wind speed and wind direction were then compared with focus on mean, bias, and correlation.
The aim is not to fully validate and compare physics options and input data for the two models, but to examine the differences between the standard WRF configuration and the Polar optimized, and to explore the possibilities and challenges of using mesoscale modelling for near-surface wind studies in the complex Arctic area.

4.3.1 Model 1 setup

Based on the available resources the simulation was limited to one month. Based on the AWS time-series and sea ice data available January 2009 were selected as simulation period. The first model was the standard WRF nested in the ERA-Interim Reanalysis (ECMWF) [Dee et al., 2011], which we label WRF(ERA-I), and the second was the Polar WRF model nested in the Arctic System Reanalysis (OSU) [Wilson et al., 2011], which was labeled WRF(ASR), more information on available reanalysis data Table 4.1. In both cases, the simulations were running with three one-way nests, with horizontal grid spacing of 18 km, 6 km, and 2 km, Fig. 4.3a.

The simulations were reinitialized each day at 18:00 UTC and run for 30 hours. Discarding the first 6 hours as spin-up provided a continuous time series of 24-hour simulations running from 00:00-24:00 UTC each day. The setup was done according to the ARW user's guide [NCAR, 2012]. The main settings are shown Table 4.2 and further information ´s are available in [Jakobsen and Vincent, 2016]. The WRF(ASR) model settings are aligned with the recommendation for polar region simulation by [Hines and Bromwich, 2008b] and [Hines et al., 2011], see section 4.2.0.1. The WRF(ERA-I) settings follow the internal DTU experience based recommendation for WRF simulations.

The both models run as convection-permitting model, (run without convection parametrization) due to the high resolution $\Delta x < 5$ km, [NCAR, 2012].

The calculation grid used in WRF follows the terrain, with hydrostatic-pressure vertical coordinates and a constant top-level pressure. The terrain elevation is based on bilinear interpolated 30-arc second GTOPO30 data, Section 4.4. The model uses 40 vertical levels from 13m to 20km distributed as log-pressure height, based on the surface and the top-level pressure. The 2km inner domain includes $\approx 500x450$ km or 2.3 million grid points in total.

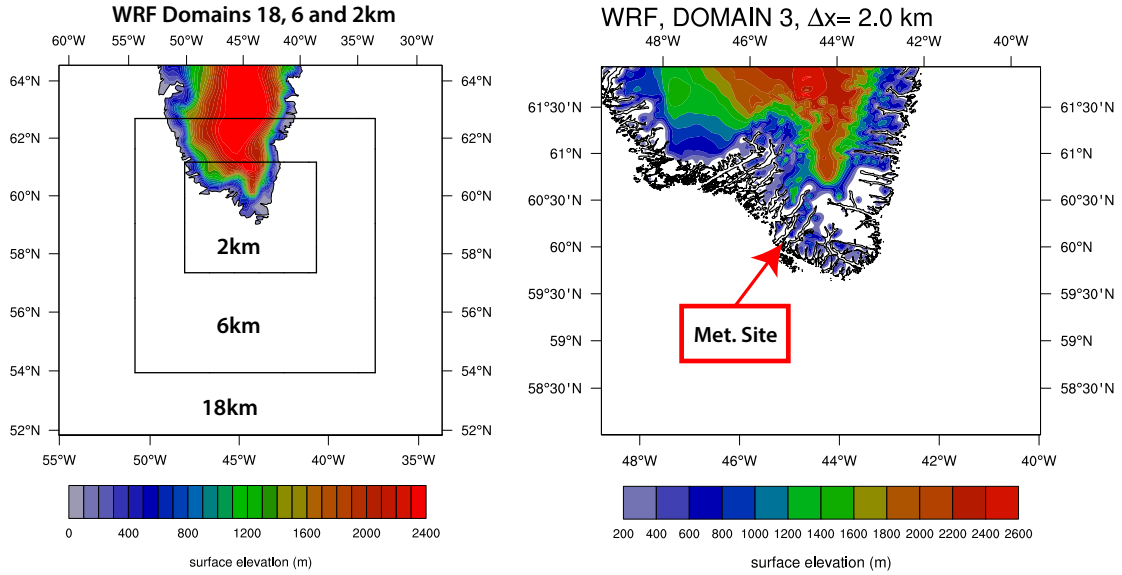

(a) *Location of WRF domains with 18, 6, 2km horizontal resolution*

(b) *Location of AWS station 1601 in the 2km WRF domain*

Figure 4.3. *Model nests and evaluations station*

4.3.2 Results, version 1

The modeled wind fields are first compared to the only tall tower observations available in the domain, Fig. 4.4. The station named "1601" are located in the south-western part of Greenland, close to the city Nanortalik, and is 50 m tall. The modeled wind fields at the 40 and 67 m levels were quadratic interpolated to the 50m observation point and the one hertz observations were averaged to one hour, as the modeling interval.
The modeled horizontal wind speed do not fit the observed very well, Fig. 4.4. The modeled wind speeds are not only deviates from the observations, it is also out of phase with the observations, with many mispredicted high wind events. For some of the high wind events the start and the end of the event are captured, but in most cases both the wind speed level and event durations are off.

To investigate the phenomenon´s behind the model deviations the spatial distribution of the wind field for a selected event was examined, Fig. 4.5a. January 4 00:00 were selected and the wind at 1601 was 23 m/s, 13 m/s and 11 m/s in the WRF(ASR), WRF(ERA-I), and observed respectively. The spatial distributions for the two models were compared and there are obviously some differences in the modeled wind fields. The flow entering the domain from the Denmark Strait (North East) is very different and the same for the barrier flow and tip jet behavior. The tip wake is a bit more to the north in the WRF(ARS) model compared to the WRF(ERA-I). The flow above the Southern part of the island is not that different, however the modeled wind speed seams high especially for the WRF(ERA-I).
To evaluate the spacial distributions of the wind fields, the closest available Synthetic Aperture Radar (SAR) observations were used to produce a high resolution wind field (Ocean wind). The data was process as described by [Hasager et al., 2008] and delivered

Model configuration		
Selected parameters	WRF(ERA-I)	WRF(ASR)
Horizontal res.	18km, 6km, 2km	18km, 6km 2km
Lowest 3 levels	13m, 40m, 67m	13m, 40m, 67m
Initial and BC conditions	ERA-I	ASR
Land cover	MODIS	MODIS
Terrain elevation	USGS GTOPO30	USGS GTOPO30
Sea surface T	Real time(NCEP) (1/12deg.)	Real time(NCEP) (1/12 deg.)
Sea ice	From ERA Interim	Chapman sea ice (T+C)
Cumulus Physics	New Grell Scheme	New Grell Scheme
PBL Physics	MYJ	YSU
Microphysics	Morrison 2 moment	Morrison 2 moment
Shortwave radiation	RRTM	RRTM
Longwave radiation	Dudhia	Dudhia
Surface physics	Unified Noah land-surface	Unified Noah land-surface
Surface layer physics	MYNN	MO Scheme

Table 4.2. *Main parameter for the version 1 model setup.*

to the project by the OMET group DTU Wind Energy.
The ocean wind pattern observed in the Denmark Strait is very close to the pattern modeled by the WRF(ERA-I) model. The deviation in the WRF(ASR) wind field can originate from the reanalysis data or the surface data and not necessarily from modeling errors. The modeled tip jet and especially the wake part of it deviate quite a lot from the ocean wind observations. In the model, the flow penetrates the southern part of the land and cause a too northern location of the tip jet. To study how the models have modified the reanalysis data, used as initial condition and boundary, the lowest level of these 10 MAG are compared to the lowest model level 13 MAG. The height difference will of cause affect the wind speed magnitude, however it has only a minor effect on the overall distribution/pattern.
The wind fields of the two models Fig. 4.7a and Fig. 4.7b agree on the overall flow pattern at this point of time. A closer look at the tip jet Fig. 4.7c and Fig. 4.7d show a clear difference between the two datasets. On this scale the three times higher resolution of the ASR data affect the wind speeds, however the difference in the patterns are clear. The ASR has a high wind field above the southern part of the island with high flows from both the icecap and the Denmark Strait. The ERA-Interim has the highest winds off-shore in the Denmark Strait and west of the tip, with only a limited land penetration.
If the reanalysis wind fields are compared with the observed Ocean wind, the ERA-Interim is very close to the observed pattern although the coarse resolution does not give the same sharp limitation of the tip jet. The ASR wind field is very similar to the modeled Fig. 4.5a and Fig. 4.5b, even though different planetary boundary layer and surface layer physics was used in the two models. That the WRF(ASR) gives similar results as the ASR is obvious, because the model setup is similar. That the WRF(ERA-I), using the preferred DTU setup, and other lateral boundary, and initial conditions, gives nearly the same unlikely results in the southern part indicate problems with the surface data and most likely the terrain elevation.
The WRF model use USGS GTOPO30 as the Arctic System Reanalysis and the ERA-

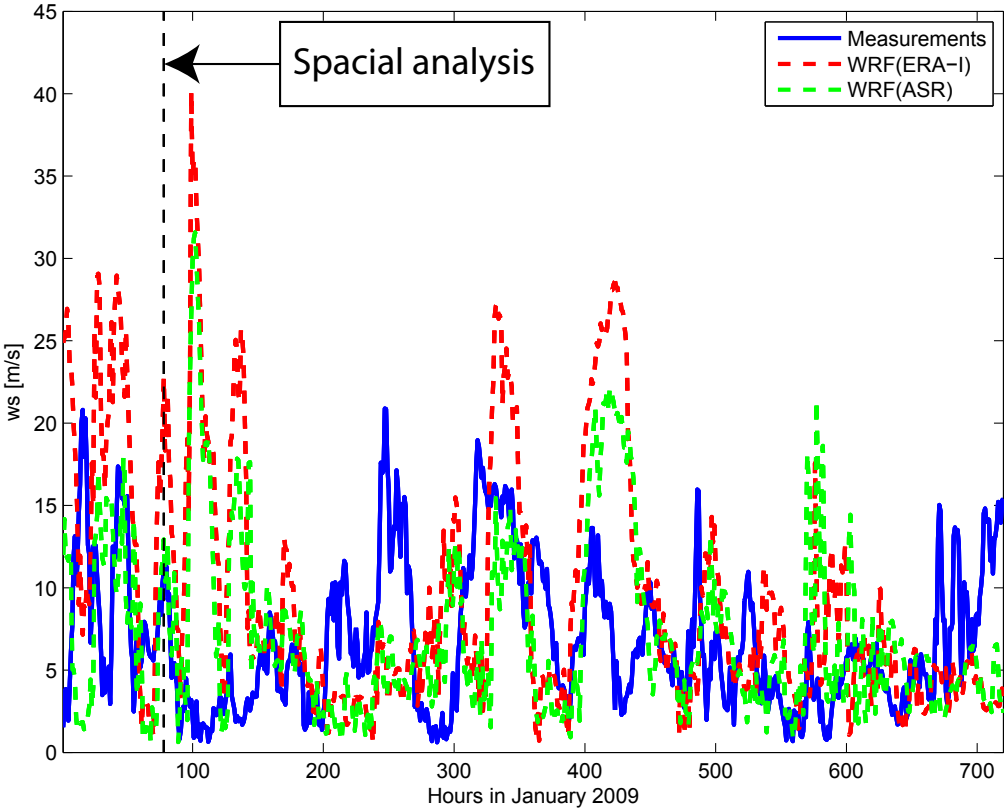

Figure 4.4. *Modeled and measured wind speeds for Nanaortlik Dumpsite 50 MAG (02-31.01.2009)*

Interim use USGS GMTED2010. In section 4.4 the differences between the two dataset in this particular area will be presented.

4.3.3 Sub-conclusion

The first longer WRF simulation was accomplished without notable problems, as stability that can be a problem when the model operates in extreme climate.
The modeled wind speed at the tall tower evaluations site did not agree very well with the observation, nevertheless the two models are in phase for most of the period. Comparisons between the two model result and observed ocean winds showed that the tip jet is modeled too far north and low land friction cause over prediction of the fjord outlets on the downwind side.
The Arctic System Reanalysis data shows the same wind patterns as the WRF modeled, while the ERA-Interim seams closer to the ocean wind observations. This combined with the fact that both the WRF simulations and the ASR uses GTOPO30 terrain elevation data, while the ERA-Interim uses GMTED2010 could indicate a problem with the GTOPO30 for the southern part of Greenland.
The results for the first part of the project, including the simulation results, were presented at the European Geosciences Union, General assembly 2013.
To verify the problems with the GTOPO30 terrain elevation a study were implemented.

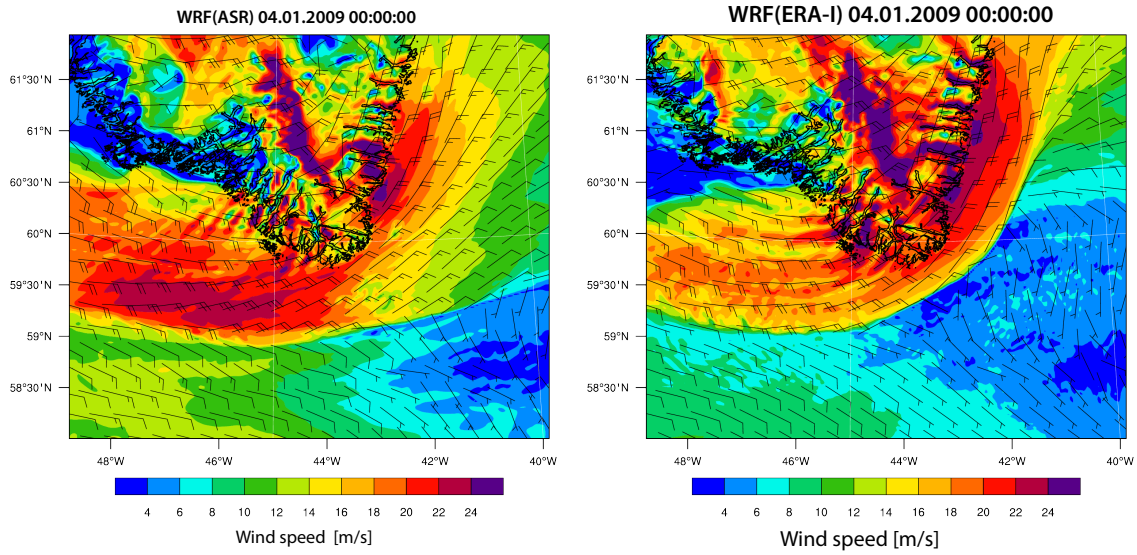

(a) *13 MAG, WRF(ASR)* **(b)** *13 MAG, WRF(ERA))*

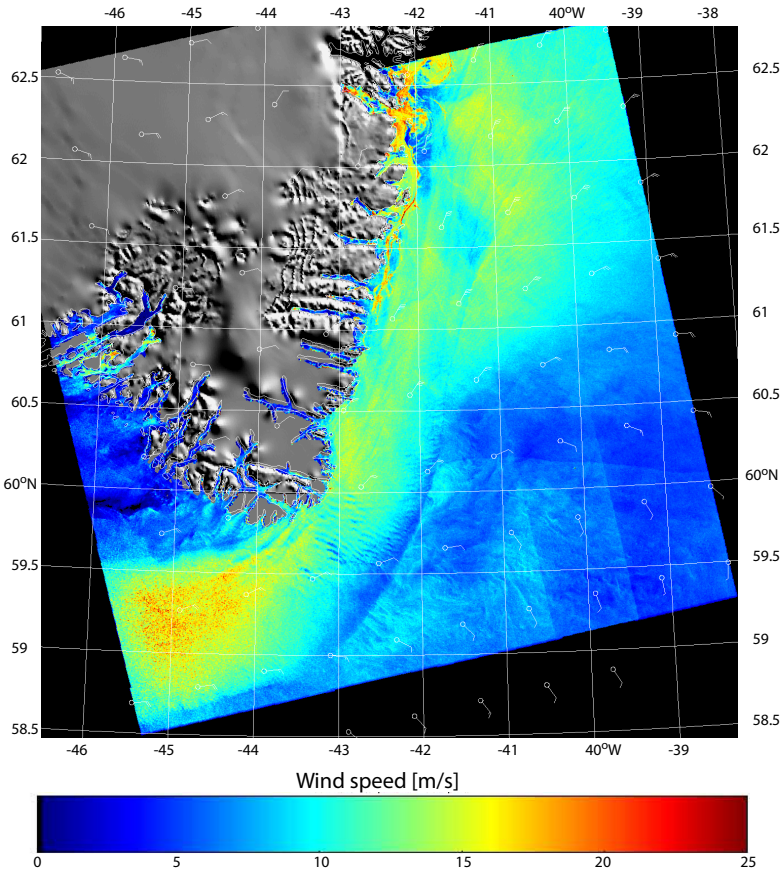

Figure 4.6. *Envisat SAR based wind field 10m AMSL (January 4, 2009 00:20). Figure credit: Merete Badger*

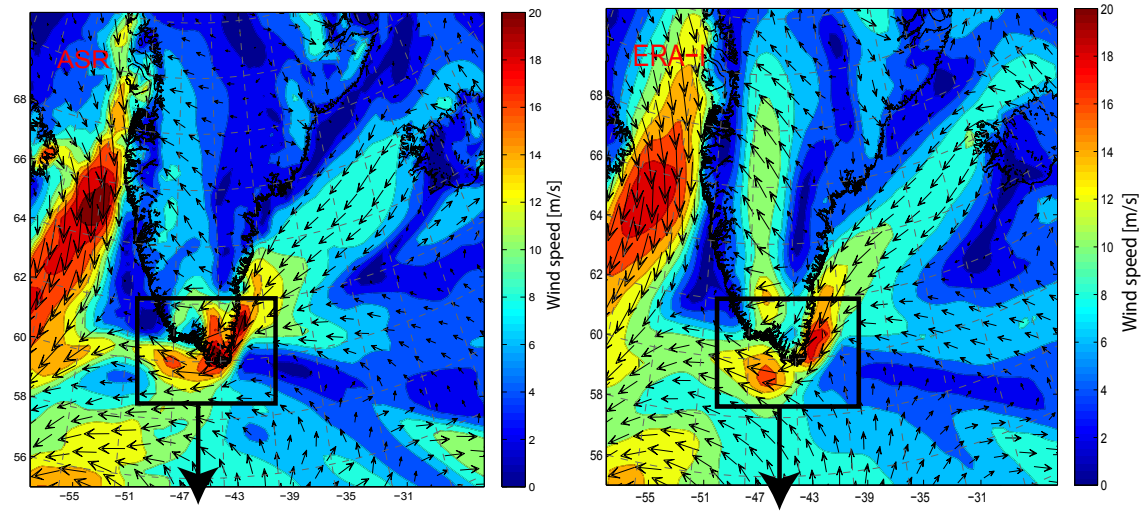

(a) *10 MAG,(ASR)* **(b)** *10 MAG,(ERA-I)*

(c) *Zoom of Fig. 4.7a* **(d)** *Zoom of Fig. 4.7b*

Figure 4.7. *Arctic System Reanalysis (30 km) and ERA Interim (≈ 80 km) wind speed distribution 10 MAG (January 4, 2009 00:00)*

4.4 Elevation data study

The elevation data in the WRF models is based on the GTOPO30, 30-arc second ≈ 1 km resolution interpolated with a 4-point bilinear interpolation scheme to the x km domain grid. The vertical accuracy of the GTOPO30 varies a lot depending on which data source used. The overall RMSE is found to be around 70 m [Gesch et al., 1999], but for Greenland, mainly the Digital Chart of the World (DCW) data is used. The DCW data haves a linear error of $\pm 650m$, at a 90% confidence level [James and Agency, 1990]. This information indicates, that the accuracy of the DEM used is probably very poor for this area. Newer elevation data are available for the area, such as GMTED2010 [Danielson et al., 2011]. The GMTED2010 data set is an updated version of GTOPO30, both developed by the United States Geological Service (USGS). Greenlandic accuracy in the GMTED2010, based on 807 control points, is $\pm 182m$ and the RMSE is 76 m. The Greenlandic part of the GMTED2010 is based mainly on the Bamber model [Bamber et al., 2001]. For the inner domain area, the Bamber model is based on KMS photogrammetry, KMS map digitization, and some unclassified $DTED-0$ data. These data have an estimated accuracy of 20 m RMSE for the KMS and 75 m for the $DTED-0$.

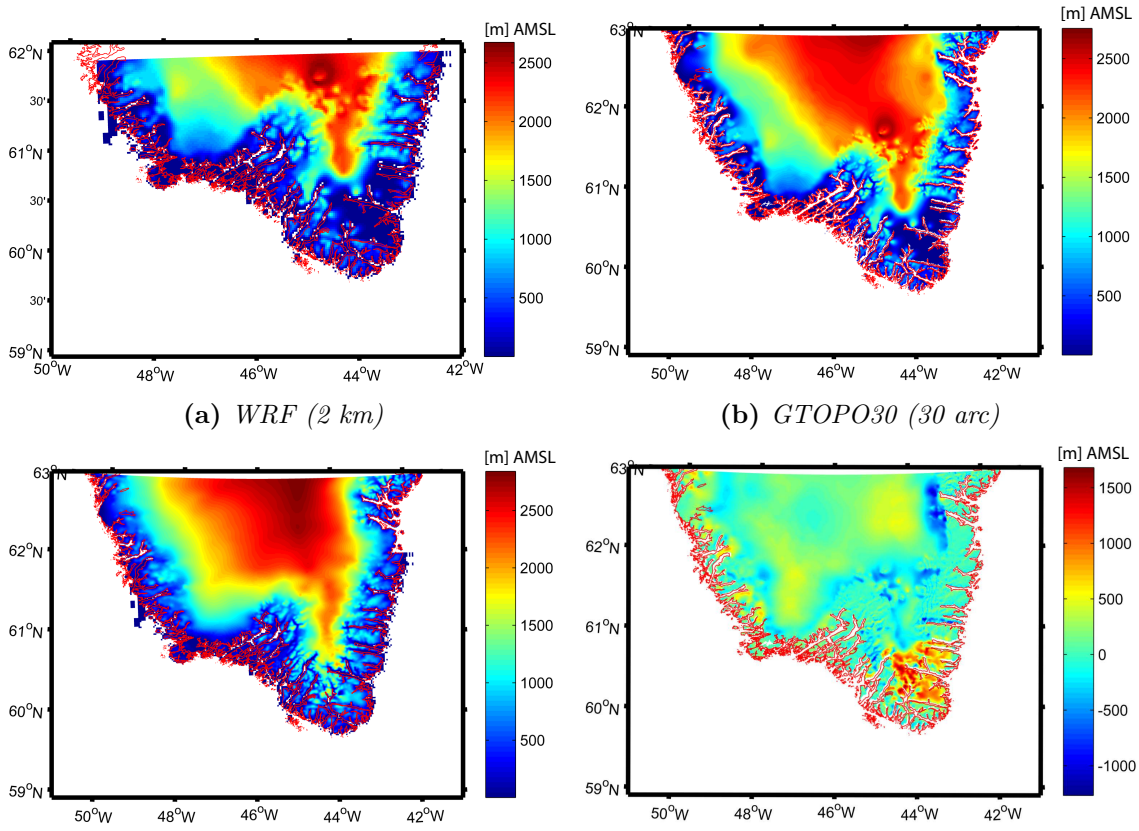

(a) *WRF (2 km)* **(b)** *GTOPO30 (30 arc)*

(c) *GMTED2010 (30 arc)* **(d)** *GMTED2010-GTOPO30*

Figure 4.8. *a) Standard height model for WRF simulation, 2 km resolution, height AMSL plotted with high-resolution shore-line [Dudhia, 1989]; b) Raw GTOPO30 data for the domain, 30 arc sec.; c) GMTED2010 data, 30 arc sec.; d) Bias plot GMTED2010 - GTOPO30 in m.*

The 2km WRF terrain model used in the initial study, Fig. 4.8a is off on some of the

shorelines compared with the raw GTOPO30 Fig. 4.8b. The cell size is 4 times bigger for the WRF model, but the general topography representation seems to be acceptable. When the GMTED2010 data, Fig. 4.8c were introduced, some of the problems with the DCW-based GTOPO30 data become clear. The big dark-blue area in the southeastern part of the domain is now light-blue to green, and the variations in the ice cape topography are smoothed out. In the bias-plot Fig. 4.8d, the big red-to-yellow area in the southwest, represents areas of over $10,000 km^2$, where the GTOPO30 data are more than 500 m lower than the GMTED2010. Most of the areas with negative bias are glaciers which can be hard to process for common elevation models. Some of the minor differences in the glacier topography might also be due to different ages of the data and the dynamic ice mass. The mean bias for the onshore part of the domain is $-37.8m$.
Bilinear interpolated GMTED2010 was used for the second round of WRF simulations (version 2). However, there are still some areas with erroneous terrain elevation. Both the iced and coastal areas move, and the glacier in particular can be very dynamic, with several kilometer of movement per year; this needs to be considered when elevation data is selected. The GMTED2010 includes data from 1996 in the inner domain, and even older data in the outer domain. Based on this, a newer data set, such as OSU/ASTER GIMP [Howat et al., 2014] is recommended as basis for future projects. Another big issue that needs to be studied further is how the raw data are combined and corrected from the source resolution, typically $15 - 100$ m, to the 0.2-5 km that is needed for the models. A common method to process DEM data is a combined method of averaging and Kriging, but before this is done, the data need to be validated with true fix-points and shorelines, and if any areas are missing, these need to be filled with other data.

The finest resolution used in this study is 2 x 2 km, but some studies use WRF at even higher resolutions [Rögnvaldsson et al., 2011]. The 2 km resolution was chosen based on the available computational power, experience from previous projects and the validity of the model parameterization schemes. To investigate the effect of resolution on terrain representation, the terrain was plotted in different resolutions, starting with 100 x 100 m Fig. 4.9a, followed by 1 km Fig. 4.9b, and finally 2 km Fig. 4.9c. A pixelation of the terrain can be seen when the resolution goes from 0.1 km to 1 km, but the main fjords and mountains can still be identified. When the resolution goes down to 2 km, only the biggest fjords and mountains are represented, and the terrain contours are more or less smoothed out. The highest elevation of the 100 x 100 m data is in this case 1834 m. For the 1 km and the 2 km resolutions, the highest elevation is 1687 m and 1471 m respectively. A frequently used parameter for terrain complexity is slope. This parameter can also be used to compare terrain representations. In this case, the mean slope for the onshore part of the terrain is 0.1848, 0.1024, and 0.0681 for the 100, 1000 and 2000 m resolution. The 2km terrain model used for WRF in this study is shown in the red boxes, Fig. 4.9d. The terrain representation in cells that include high variations is, as expected, poor. This affected mainly the coastal area, where small islands are smoothed out. For several coastal areas the elevation error is above 500 m and if validation AWS are located in such areas, it has a major influence on the validation results.

For the microscale models, G50 GIS city maps and k1 maps are used together with ASTER-based GIMP data see Appendix B.

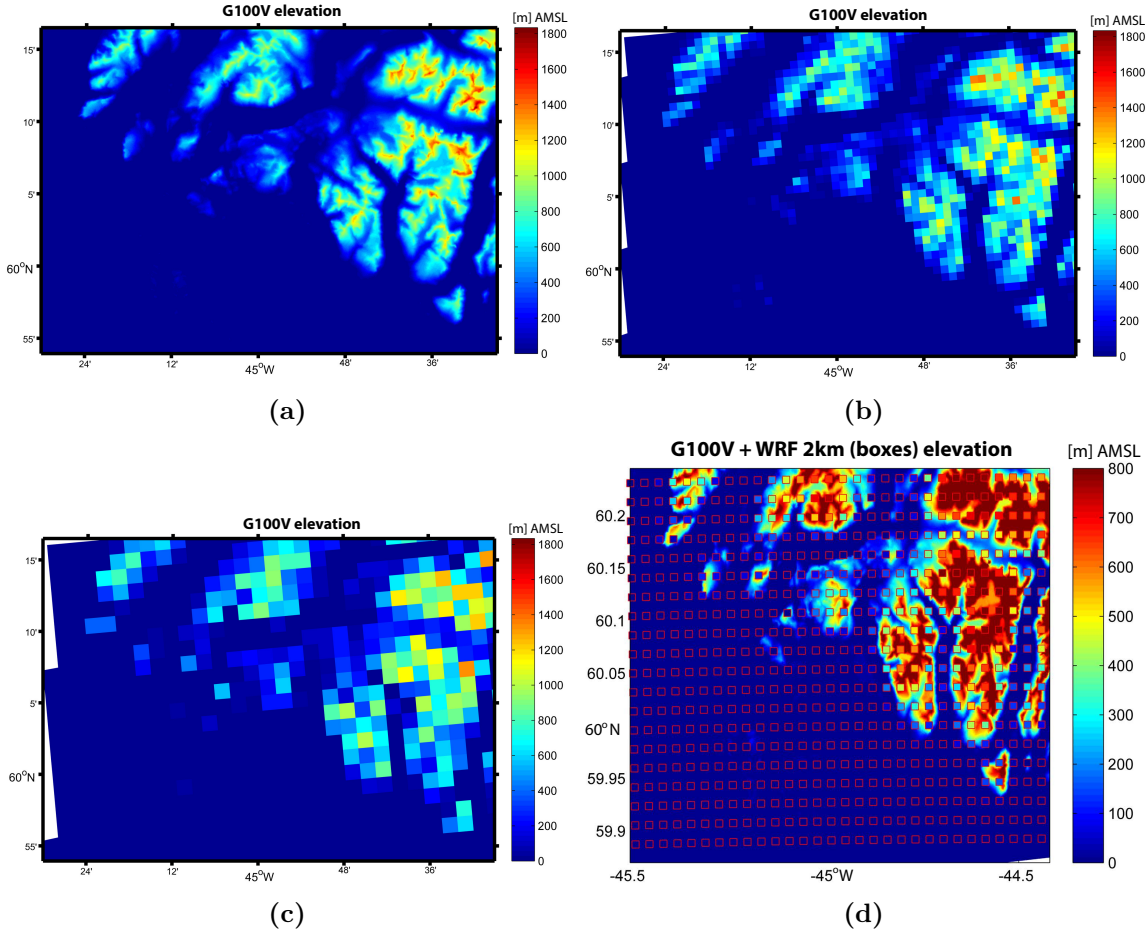

Figure 4.9. *a) Region elevation at 100 x 100 m resolution, aerial-photography-based DEM data; b) Same area at 1 x 1 km resolution; c) Same area at 2 x 2 km resolution; d) Base elevation data at 100 x 100 m resolution, surface color of the boxes indicates elevation of the 2 km WRF terrain model. Based on G100V* ($RMSE < 10m$).

4.5 Mesoscale model, version 2

Based on the experiences gained with first simulations including version 1, presented in section 4.3 a new model were setup. The main update is the updated terrain elevation data, based on GMTED2010, but on top of this the physical parametrization schemes were aligned to enable a clear comparison between the WRF(ASR) and the WRF(ERA-I).

4.5.1 Model setup, version 2

The model setup for both models in version 2 are aligned with the recommendations for Polar region simulations [Hines and Bromwich, 2008b] and [Hines et al., 2011], see section 4.2.0.1. The main model settings are listed Table 4.3, further information can be found; section 4.3.1, Appendix G and [Jakobsen and Vincent, 2016].

Model configuration		
	WRF(ERA-I)	WRF(ASR)
Horizontal res.	18km, 6km, 2km	18km, 6km 2km
Lowest 3 levels	13m, 40m, 67m	13m, 40m, 67m
Initial and BC conditions	ERA-I	ASR
Terrain elevation	USGS GMTED2010	USGS GMTED2010
Sea surface T	Real time(NCEP) (1/12deg.)	Real time(NCEP) (1/12 deg.)
Sea ice	From ERA Interim	Chapman sea ice (T+C)
Cumulus Physics	New Grell Scheme	New Grell Scheme
PBL Physics	MYJ	MYJ
Microphysics	Morrison 2 moment	Morrison 2 moment
Shortwave radiation	RRTM	RRTM
Longwave radiation	Dudhia	Dudhia
Surface physics	Unified Noah land-surface	Unified Noah land-surface
Surface layer physics	MO Scheme	MO Scheme

Table 4.3. *Main parameter for the version 2 model setup.*

4.5.2 Results, version 2

The validation of WRF was carried out in winter to obtain both high and low wind periods, tip jets, with a low influence of local thermal-driven winds. The possibility of local winds, such as sea breezes, is lower in winter because of low solar radiation, however land breezes still occur as the temperature difference between open sea and land is big enough. The larger katabatic flows related to the ice cap is an important feature of the Greenlandic wind climate and occur in the winter season and affect the results. The model output was obtained horizontally at the validation sites through bilinear interpolation from the four neighboring grid points. For the 10 m AWS sites, the lowest model level, 13 m, was used directly even though it induced a minor overestimation of wind speed. The lowest model level is preferred in from of the build-in 10 m estimate, based on Monin–Obukhov theory. Both methods will include minor deviations from the actual 10 m wind speed, however the accuracy will vary from place to place depending on the surface and PBL stability. For the 50 m point, linear interpolation between model level 2 and 3 was used.

4.5.2.1 Observation sites for evaluation

To evaluate the model performance, 13 stations distributed in the high-resolution 2 km domain were selected, Table 4.4. Seventeen stations are located in the inner domain, but only 13 passed the quality test or had data available for the simulation period (Black colored stations, Fig. 4.10 failed the quality test). The stations are not well distributed within the domain but are concentrated in the ice-free western part of the domain. There is only one station available on the east coast and two off the coastline, Fig. 4.10. The stations were chosen based on location, measurement height, availability, and inflow. The airport stations (green) and heliport stations (yellow) belong to the Greenland Airport Authority (GLV), 1601 is a tall tower station operated by DTU, and the rest belong to the Danish Meteorological Institute (DMI). The last three stations, marked with black, are ice surface stations, but the data quality and the availability were found too poor for our purpose. The same was the case for the upper east coast station 04382. Generally, the

DMI stations and the airport station have the highest quality (right height, reasonable instrumentation, yearly maintenance...) and the best location while the heliport stations are often incorrectly designed and unfavorable positioned.

All the sites except for the Nanortalik Dumpsite (1601) are equipped with wind measure-

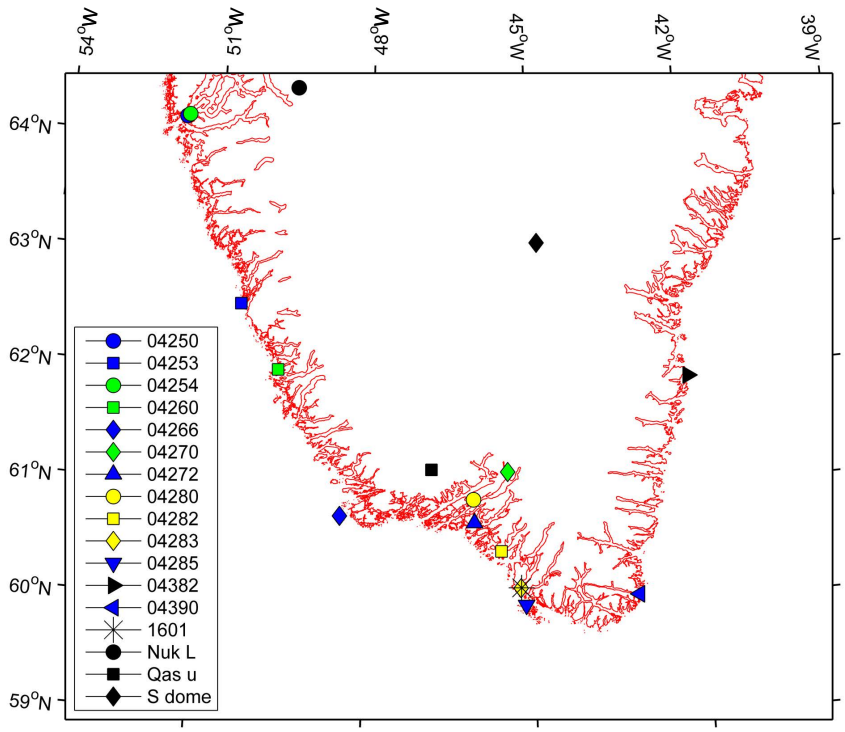

Figure 4.10. *Location of identified AWS in the inner domain, with color classification of site type. See the further description of the color code in the text.*

ments at 10 MAG only. For all stations cup anemometers and wind vanes are used, but of different types and brands. The instrumentation and positioning of the climate stations do not meet the WMO standards [Artz et al., 2010] or requirements for wind resource evaluation as the 1601 site do [Jakobsen and Hansen, 2016a], but for this purpose, the quality was considered to be sufficient (expected model uncertainties $> 10\%$ on horizontal wind speed). Although it is preferable to use tall tower meteorological observations for mesoscale model verification especially in complex terrain. The climate and terrain of Greenland make tall tower installation and operation expensive, and tall meteorological towers are therefore uncommon in Greenland. The observation data used here have been subjected to quality checks, resulting in periods without data, as observed in Fig. 4.13. Periods of missing data covers a wide range of errors, from instrument icing to data transfer errors. For some stations, the total error period corresponds to up to 9% of the test period. This might have had a minor effect on the model evaluation for each station, but did not affect the overall result.

Station	WMO	Name	Latitude	Longitude	Elevation
1	04250	Nuuk	$64^o10'46''$	$51^o43'33''$	80 m
2	04253	Ukiivik	$62^o34'42''$	$50^o25'55''$	22 m
3	04254	Nuuk Airport	$64^o11'48''$	$51^o40'22''$	86 m
4	04260	Paamiut Airport	$62^o01'06''$	$49^o40'34''$	36 m
5	04266	Nunarsuit	$60^o45'49''$	$48^o27'17''$	33 m
6	04270	Narsarsuaq Airport	$61^o09'20''$	$45^o26'20''$	27 m
7	04272	Qaqortoq	$60^o42'54''$	$46^o02'38''$	57 m
8	04280	Narsaq Heliport	$60^o55'01''$	$46^o03'33''$	25 m
9	04282	Alluitsup PAA Heliport	$60^o27'53''$	$45^o34'09''$	46 m
10	04283	Nanortalik Heliport	$60^o08'28''$	$45^o14'04''$	6 m
11	04285	Angisoq	$59^o59'28''$	$45^o08'46''$	20 m
12	04390	Ikerasassuaq	$60^o03'19''$	$43^o09'55''$	70 m
13	1601_10	Nanortalik Dump 10 m	$60^o08'36''$	$45^o13'33''$	19 m
14	1601_50	Nanortalik Dump 50 m	$60^o08'36''$	$45^o13'33''$	19 m

Table 4.4. *Position and elevation of the available validation sites within the 2 km inner domain. Latitude is degree North, longitude degree West and the elevations is meters above mean sea level.*

4.5.2.2 Validation of results

The modeled and measured wind speeds at Nanortalik (west coast), 50 m, are shown in Fig. 4.11. Both models had a tendency to overestimate the wind speed at this site especially the WRF (ERA-I) model. There is a correlation between the estimated and measured high- wind periods, but the wind speeds in these periods are greatly overestimated. The results are direct comparable with the version 1 results presented Fig. 4.4. Compared with version 1 both the correlation and magnitude, between the modeled and observed high wind event, is highly improved.
In the first week of the data series, the synoptic situation was east to north-easterly barrier wind regime. In this situation the strong winds of the tip jet are modulated by flow over land before reaching the measurement site and the effect of this seems to be under estimated in the models. This might indicate that the terrain representation, in the 2 km DEM used for the model, does not reflect the actual terrain topography or that the total drag rising from surface roughness and small-scale terrain is too low in the models. In the WTJ situation, the flow reaches the site from the north, where moderate terrain effect is expected based on the mix of open fjord water and mountain. In this situation both models overestimated the wind speed, especially the WRF(ASR), but the models did a good job in the speed-up and -down part of the event. To study model performance more closely in the WTJ situation, the performance at the off-coast station 04285 Angisoq was examined Fig. 4.12. Unfortunately, the DMI quality filter excluded large parts of the period, but the WTJ was represented, and model performance was clearly better for this site, notably for the WRF(ASR) model. The (East) station 04390 is located on the opposite coast. The measured wind directions verified that the synoptic situation in the first week, was easterly barrier wind regime, and both models did a very good job in easterly wind situations. In high-wind situations with easterly wind, or easterly tip jet ETJ, direct inflow from the Denmark Strait means that the flow is dominated by the synoptic scale flow with little influence from mesoscale effects. In the opposite case, the WTJ on day

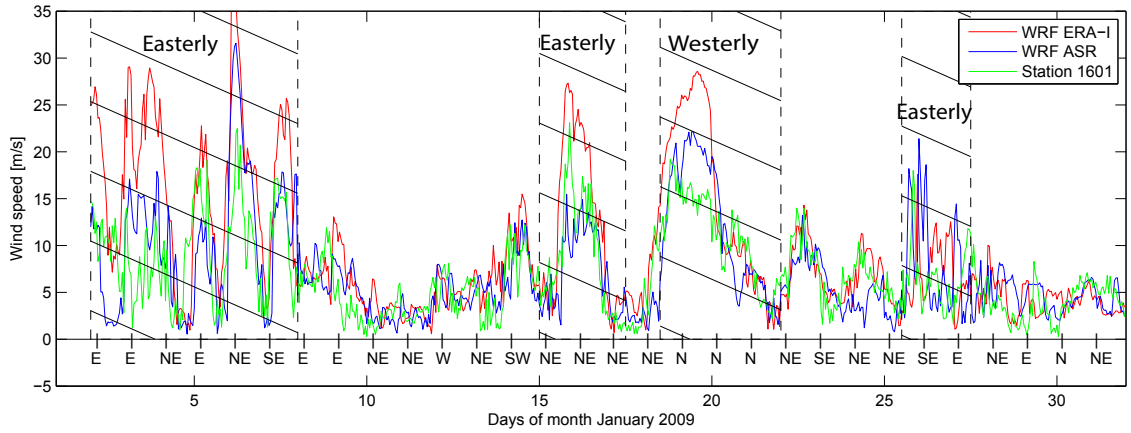

Figure 4.11. *Wind speed (ms^{-1}) 50MAG for AWS site 1601, Nanortalik, WRF (ERA-I) 1601, and WRF(ASR) 1601(January 2-31 2009). Below, wind direction (8 sector) at AWS site 1601 (12-hour intervals).*

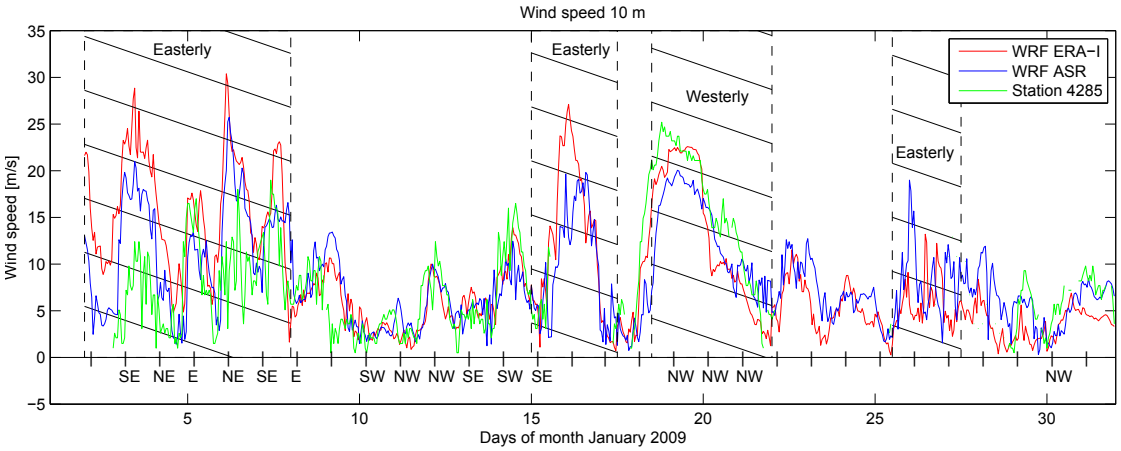

Figure 4.12. *Wind speed (ms^{-1}) 10MAG for AWS site 04285, Angisoq, WRF (ERA-I) 04285, and WRF(ASR) (January 2-31, 2009). Below wind direction (8 sector) at AWS site 04285 (12-hour intervals).*

19, the ERA-I based model performed better than the WRF(ASR) on the lee side(east coast), and vice versa on the west coast.
In between the ETJ and WTJ situations, the stations experienced generally weaker wind, but with a great contribution of hour-to-hour variability. Although neither WRF simulations captured the precise timing of these high frequency fluctuations, the WRF model does appear to have produced a statistically realistic level of wind speed variability. The phase errors in these fluctuations have a negative impact on the verification score, despite the fact that they are representative of well-modeled mesoscale physics such as open cellular convection.

4.5.2.3 Model performance statistic

To evaluate the wind simulation performance of the two model a statistical validation is included. The validation include, mean values of the time series (stations and models),

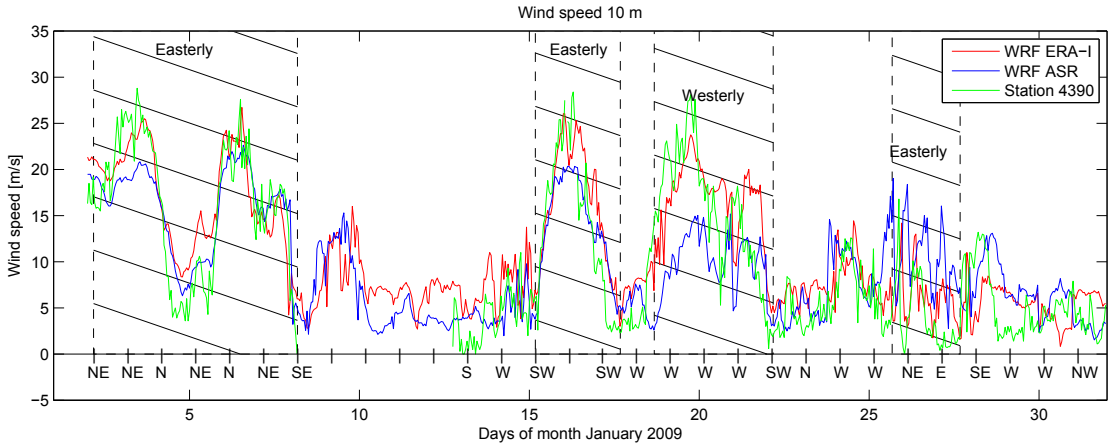

Figure 4.13. *Wind speed (ms^{-1}) 10MAG AWS site 04390, Ikerasassuaq. WRF (ERA-I) 04390, and WRF (ASR) 04390 (January 2-31, 2009). Below, wind direction of AWS site 04390 (12-hour intervals). Some observation data have been excluded by the validation routine and transmission errors, but there are still enough data to do a reasonable test of the models.*

mean absolute error (MAE), Bias, correlation, and Root Mean Square Error (RMSE) for the model results versus the measured level. The average level across the 10MAG is presets in the column "Total" and the 50 MAG level results are shown in the last column, Table 4.6. The mathematical formulation for the statistics is presented in Appendix F.

To evaluate the model performance it is important to define what is good and poor performance and what error level can be expected. For simulations in medium complex terrain MAE and RMSE < 2.0 are characterized as good and > 3.0 poor. For the average correlation coefficient > 0.75 is good and < 0.5 poor [Reid, 2001]. To gain information about the expected error level, the performance of other Greenlandic mesoscale simulations was collected, Table 4.5. The three studies listed in the table used mainly icecap stations for the performance evaluation, however there horizontal grid resolution are also much larger than for this study. The station used for this performance evaluation are located in very different terrains ranging from complex to very complex and therefore it is difficult to set a limit for good and poor performance. The monitoring error levels for the stations are unknown, but station 1601 is design to fulfill the $\pm 3\%$ wind resource limit. A rough estimate for the other stations are $\pm 10 - 15\%$, but most likely negative due to e.g. wear and instrument icing.

The performance statistics for the Polar WRF(ASR) and WRF(ERA-I), Table 4.6, suggest that the Polar WRF(ASR) in most cases performed better than the standard version, but the WRF (ERA-I) combination performed slightly better on correlation. When the means for the two models and the AWS are examined, the total error is not large, +0.5 m/s for WRF(ERA-I) and -0.1 m/s for WRF(ASR). The errors varies from station to station depending on e.g. the complexity of the terrain. If the scores are compared with the predefined error limits only WRF(ASR) wind speed MAE and all the correlations are within the acceptable limits.
Both setups modeled the wind speed for the three heliport stations 4280-4283 higher than the measurements. This was expected because the stations are located in small ravines

	Bias (min/max)	RMSE (min/max)	Corr (min/max)
Bromwich WS	-0.5/1.6	2/3.1	0.65/0.84
Box WS	0.51/4.57	3.35/6.12	0.23/0.68
Cassano WS	-1.55/2.37	1.66/5.49	0.55/0.75
ALL WS	-0.5/4.57	1.66/5.49	0.23/0.84
	Bias (min/max)	RMSE (min/max)	Corr (min/max)
Bromwich WD	-12/1	N.A.	N.A.
Box WD	N.A.	N.A.	N.A.
Cassano WD	-14.2/13	2.7/96	0.86/0.96
ALL WD	-14.2/13	2.7/96	0.86/0.96

Table 4.5. *Mesoscale model performance from: Bromwich [Bromwich et al., 2001], Box [Box, 2004], Cassano [Cassano, 2001]. The minimum and maximum values covers lowest and highest station average in the study. Mainly icecap stations are included.*

and therefore not fully exposed to incoming wind. Based on the location of the stations, the best agreements would be expected at the off-shore sites, 4266 and 4285, but this was not the case, probably because they are on the western side of the land and therefore in the lee of the topography during the ETJ events that occurred during a large part of the test period. For sites in more complex terrain, such as 4250, 4254, 4270, 4272, 4282, 4283, and 1601 the model performance was lower. For 1601, it is remarkable that the model performance was slightly better at 10MAG than at 50MAG, especially because the observation data study showed a high roughness effect at 10MAG, Appendix A.4. One explanation for the mispredicted wind shear can be that local turbulence mixing caused by the surrounding mountain ridges challenge the model. Alternatively it could be a BL stability problem.

Some of the errors were caused by poor terrain representation due to low model resolution and big variations in the terrain elevation. This is clear when the AWS elevation and the elevation in the terrain model are compared, in the last two rows of Table 4.6. For stations 4250, 4253, 4254, and 4266, the low model elevation might have influenced the results. In particular, the model elevation of 0 MAG for stations 4253 and 4266 indicates that they are over the sea in the model, which means that water or sea ice surface roughness would have contributed to the model errors. Generally the sub-grid parametrization schemes are challenged in very complex terrain like this.

The MAE and Bias levels indicate that the data series include both large positive and negative errors. Some of these errors are caused by timing error; where the model-timing of e.g. high wind events is off, see Fig. 4.11-Fig. 4.12. These timing errors effect the correlation score, where both models score a moderate correlation with a slightly better score to the WRF(ERA-I) model.
The main errors, as shown in Fig. 4.11, are related mainly to Easterly Tip Jets (ETJs), as these sites are in the lee of the land. In general, the model results were expected to be slightly higher than the measurements because model results at 13 m were compared to measurements at 10 m and terrain smoothing was caused by the 2 km horizontal model resolution. This is not a general trend in the results, where both large negative and positive bias are represented. Nevertheless the total bias is positive for both models.

The direction performance statistic in Table 4.6, shows that the standard WRF(ERA-I) did a marginally better job than the Polar version. The direction bias and RMSE might be caused by instrument misalignment, and therefore validation based on direction bias is not that useful. The correlation gives a good indication of the model performance for a given site and verifies that both models performed best at the less complex and coastal sites, 4285 and 4266, and the east coast site, 4390. Turning winds due to flow around complex terrain and funneling along fjords makes wind direction difficult to model, not least because the degree of turning is stability dependent and therefore relies on good estimation of stability.

Performance statistics of Polar WRF (ASR) on wind speed for south Greenland															
Station NO.	4250	4253	4254	4260	4266	4270	4272	4280	4282	4283	4285	4390	1610	Total	1650
Station mean	6.3	5.5	5.3	3.3	9.2	5.7	6.0	3.3	4.6	4.7	8.2	10.0	6.0	6.1	7.0
Model mean	4.5	5.7	4.4	5.1	7.7	4.8	4.2	5.3	5.1	5.9	8.6	10.1	5.9	6.0	7.3
MAE	3.1	2.9	2.5	2.9	3.5	2.9	3.1	3.6	2.5	2.9	3.6	3.8	2.8	3.0	3.2
Bias	-1.8	0.2	-0.9	1.8	-1.5	-0.9	-1.8	1.9	0.5	1.2	0.4	0.1	-0.1	0.0	0.3
Correlation	0.35	0.46	0.28	0.43	0.58	0.75	0.64	0.59	0.50	0.61	0.61	0.75	0.62	0.55	0.63
RMSE	4.0	3.9	3.3	3.5	4.3	4.1	4.8	4.6	3.5	3.8	5.0	5.1	3.7	4.1	4.4
Performance statistics of WRF (ERA-I) on wind speed for south Greenland															
Station mean	6.3	5.5	5.3	3.3	9.2	5.7	6.0	3.3	4.6	4.7	8.2	10.0	6.0	6.0	7.0
Model mean	4.1	4.3	4.4	4.8	7.7	5.3	4.7	6.4	6.4	7.7	9.3	11.5	7.8	6.5	9.7
MAE	3.8	3.5	2.5	2.5	3.4	2.3	2.6	4.1	2.9	3.8	4.0	3.4	3.4	3.3	4.1
Bias	-2.2	-1.2	-0.9	1.5	-1.5	-0.4	-1.3	3.1	1.8	3.0	1.1	1.5	1.8	0.5	2.7
Correlation	0.16	0.13	0.48	0.53	0.67	0.85	0.76	0.66	0.71	0.73	0.62	0.86	0.73	0.61	0.73
RMSE	4.7	5.0	4.0	3.3	4.3	3.4	3.9	5.9	4.1	5.4	5.8	4.2	4.8	4.5	6.0
Performance statistics of Polar WRF (ASR) on wind direction for south Greenland															
	4250	4253	4254	4260	4266	4270	4272	4280	4282	4283	4285	4390	1610	Total	1650
Station mean	132	160	134	157	192	116	198	102		110	218	179	108	137	108
Model mean	130	114	140	110	172	154	140	106		145	191	168	144	151	142
MAE	59	52	58	62	40	58	53	53		56	41	37	54	48	53
Bias	8	-19	18	-25	-8	21	-28	4		12	-19	2	11	-1	11
Correlation	0.29	0.27	0.38	0.18	0.57	0.20	0.41	0.21		0.25	-0.21	0.66	0.24	0.32	0.27
RMSE	74	69	70	76	58	75	71	68		72	59	54	69	63	69
Performance statistics of WRF (ERA-I) on wind direction for south Greenland															
Station mean	132	160	134	157	192	116	198	102		110	218	179	108	151	108
Model mean	130	153	139	141	167	135	123	111		133	192	199	132	145	133
MAE	73	65	59	60	41	59	56	58		48	35	34	45	54	46
Bias	3	-2	19	-8	-7	17	-37	13		9	-12	15	9	-2	10
Correlation	0.15	0.06	0.48	0.16	0.57	0.28	0.39	0.26		0.40	0.6	0.67	0.46	0.35	0.45
RMSE	86	82	70	78	58	79	75	74		64	53	53	60	68	61
Station elevation in meter above mean sea level															
Station elev	80	22	86	15	33	27	57	25	46	6	20	70	19		
Model elev	38	0	53	52	0	85	59	63	32	14	2	46	25		

Table 4.6. *Performance statistics of WRF, January 2009. Missing direction statistic for station 4282 is due to missing measurement data. MAE is the mean absolute error, and Bias is the mean bias, see formulation Appendix F. Station 1601 is renamed to 1610 for the 10 m measurements and 1650 for the 50 m. The statistics are based only on the 10 m measurements compared to the modeled 13 m results.*

For wind resource assessment, the average wind speed do not include enough information about the wind resource, and the absolute error is affected by time shift in the model results compared to the observations (Uncorrelated), which is of no relevance for wind resource assessment. What is relevant for wind resource assessment is the total wind speed distribution, or the power available at the site. Two examples of wind speed distribution for the WRF(ERA-I), WRF(ASR), and observed distribution are shown in Fig. 4.14. For station 1601, the models overestimated the high-winds ($> 20m/s$), especially the WRF(ERA-I), and can be seen in the time series plot in Fig. 4.11, these are related to the tip-jet situations. At the off-coast station 04285, the WRF(ASR) underestimated the high-wind speed frequency, and the WRF(ERA-I) again overestimated the high winds.
The power available in the wind scales approximately with the wind speed cubed (4.3). This underline the importance of correct wind speed modeling in wind resource modeling. For the two stations 1601 and 04285 the prediction errors, for example, cause a wind power density error between 4 and 400%, while the expected error level was set to ±30%.

$$Power = \frac{1}{2N}\sum_{i=1}^{N}\rho_i U_i^3 \approx \frac{1}{2N}\sum_{i=1}^{N}1.225U_i^3 \tag{4.3}$$

where:

U_i Horizontal wind speed [m/s]

ρ Air density $[kg/m^3]$

N Number of measurement in serie [-]

i Index for actual measurement [-]

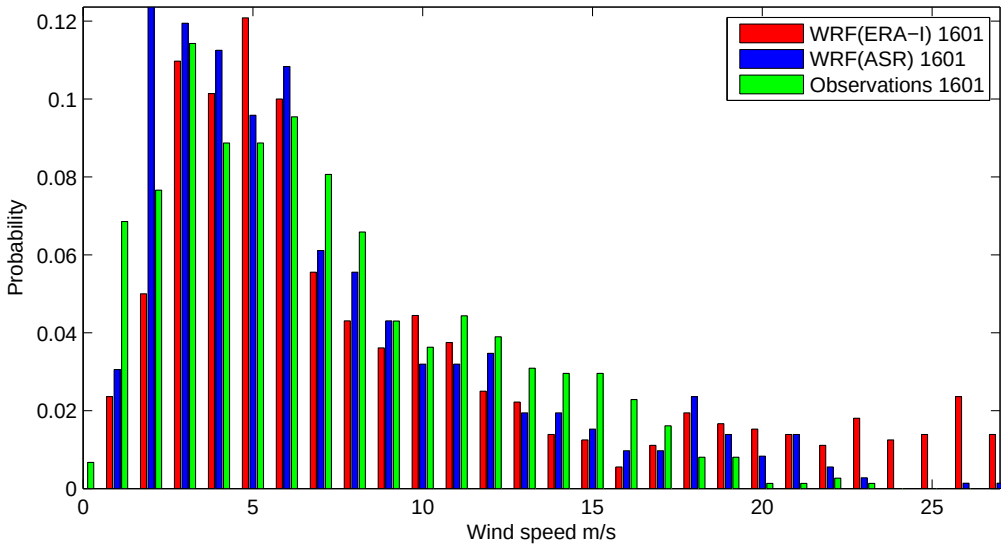

(a) *Station 1601, 50 MAG*

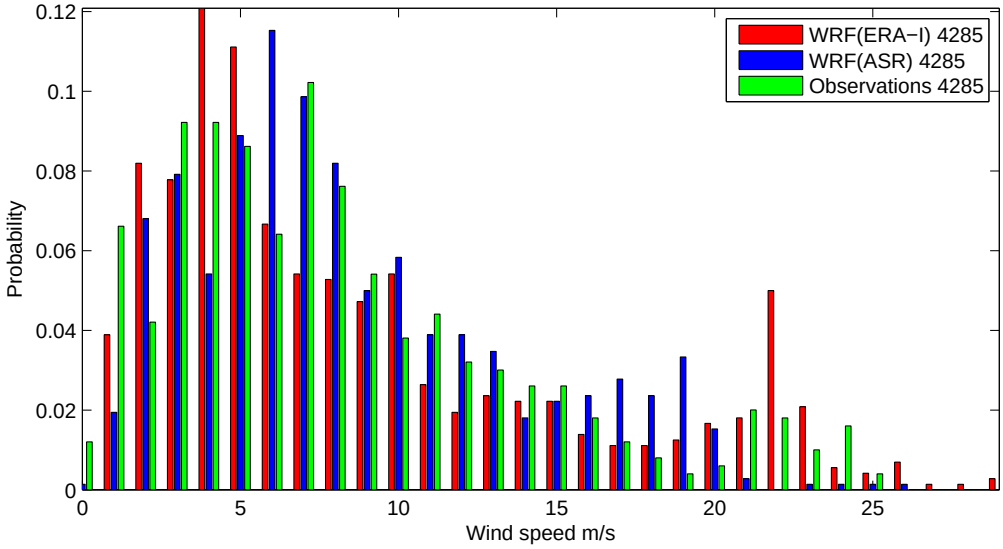

(b) *Station 04285, 10 MAG*

Figure 4.14. *Wind speed distribution for the two Southwest Greenlandic station for January 2009. The WRF(ERA-I) is presented in red, WRF(ASR) in blue and the observations in green.*

4.6 Tip jet study, version 2

The models are challenged in the high-wind barrier flow situations forming the tip jets. In the following, two of these flow cases are studied to examine the model performances. The first case deals with an Easterly Tip Jet (ETJ) situation, on January 16, 2009. A similar ETJ on February 21, 2007 was studied in detail by [Moore, 2003; Renfrew et al., 2009]. The focus of the 2007 study and experiments was offshore wind and wind-ocean interactions. In this study, onshore flow modeling is explored by comparing model results with AWS measurements. In case two, the opposite barrier flow situation, Westerly Tip Jet (WTJ), is examined. For the southern part of Greenland these two cases represent many high-wind situations, and the performance of the models in these cases gives an idea of their general high-wind performance.

4.6.1 Case study: Easterly tip jets

Easterly Tip Jets ETJ is established at the southern tip of Greenland and turn west into the Labrador Sea [Harden et al., 2011; Moore, 2005; Renfrew et al., 2009]. They form when an easterly barrier flow reaches the end of the barrier. When the barrier ends, the pressure buildup in front of it is released so rapidly that the flow accelerates due to the pressure gradient. The collapse of the barrier and the Coriolis force make the flow turn west until the flow far downstream is reduced to the geostrophic level [Outten et al., 2009].

The synoptic situation is dominated by a mesoscale cyclone forcing a pressure gradient between north and south. The overall pressure distribution for the ASR and the ERA-I, shown in Fig. 4.15a and Fig. 4.15c respectively, is different. The high-pressure areas are isolated in the northwestern part of the domain for the ASR, with the biggest pressure gradients in the Davis Strait and the west coast. In the ERA-I, the high-pressure areas extend across the north of the domain, causing higher pressure above the ice cap and bigger pressure gradients in the Denmark Strait region. The higher spatial resolution in the ASR gives a more detailed distribution and bigger local pressure gradients. The wind field shown in Fig. 4.15b and Fig. 4.15d is a product of the pressure, and it is clear that the high wind speed areas in the Denmark Strait, around Cape Farewell and in the Arctic Ocean are caused by pressure distribution. The ASR winds in the Davis Strait are much weaker than the ERA-I winds and vice versa for the Arctic Ocean. The high winds around Cape Farewell, which is in the inner domain of this study, are very different in both intensity and size. The ERA-I jets are located offshore with a maximum intensity of 20 m/s, while the ASR shows a high-wind penetration of the southern part of the island and an intensity above 25 m/s.
Fig. 4.15b and Fig. 4.16b, show the simulated wind field for the 2 km simulations, WRF(ASR) and WRF(ERA-I). The modeled tip jet deviates both in size and intensity between the two in Fig. 4.15b. In particular, the effect of the terrain seems to be modeled differently. In the southwestern area the WRF(ASR) shows a much lower wind speed than the standard version, and the tip jet is more to the north. The two AWS sites in the southern area, 04283 and 04390 (13.4 and 16.4 m/s) agree with the result of the Polar WRF (14 and 18 m/s). The standard WRF(ERA-I) gives too high a wind speed at the two coastal sites (20 and 24+ m/s). Station 04283 is on the edge of the jet in the WRF(ASR), resulting in a modeled wind speed of 15 m/s, and in the WRF(ERA-I) it

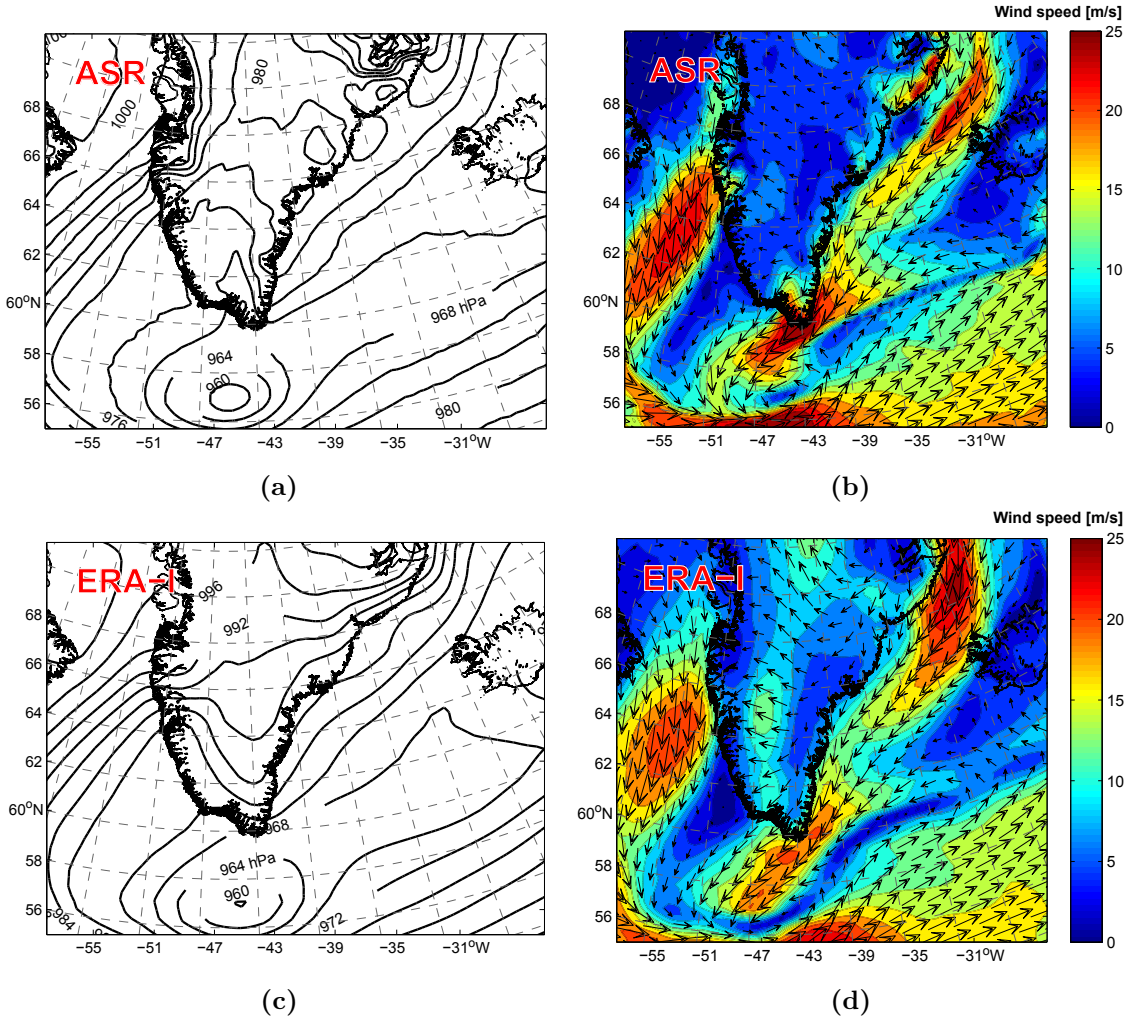

Figure 4.15. *a) Mean sea level pressure [hPa] distribution for 16 January 2009. 12:00, based on the ASR data b) Wind field [m/s], 10m above sea level, for the same situation, based on the ASR data c) Mean sea level pressure distribution for same time based on the ERA-interim d) Wind field, 10m above sea level, for the same case based on the ERA-interim data*

is in the lee with less than 4 m/s and the station measured 8.3 m/s. This demonstrates one of the challenges of accurate modeling for stations that are positioned on the edge of the normal tip-jet location. At the off-coast site 04266 (4.1 m/s) and inland site 04270 (16.4 m/s) both models did a relatively good job, but for the rest of the lee stations, the results are more scattered. The modeled wind directions agree for most of the stations except for 04390, which does not fit any of the model results, and 04266, which fits only the WRF(ERA-I) result. Please note that the ASR (GTOPO30) and the ERA-I (GMTED2010) uses two different elevation models, while the bot WRF simulations uses (GMTED2010).

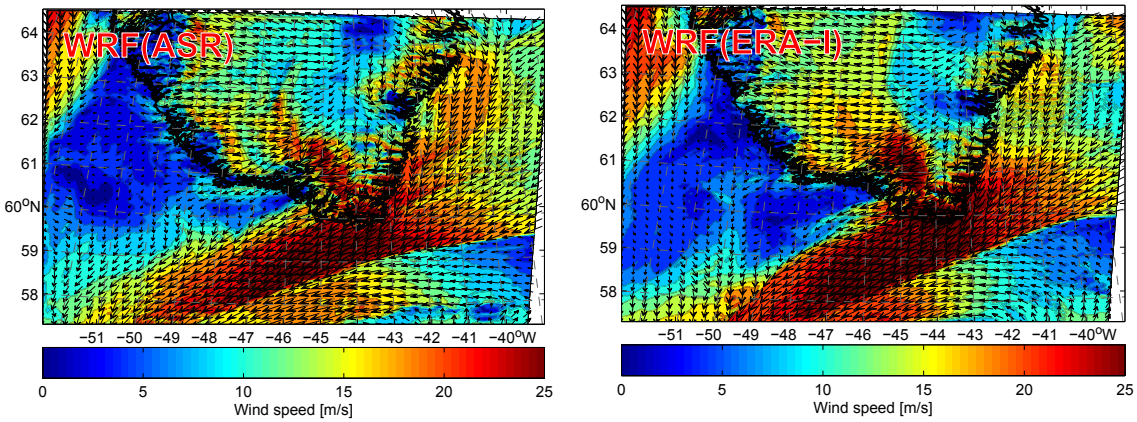

(a) *ETJ results for the WRF (ASR) model. January 16, 2009 12:00*

(b) *ETJ results for the WRF (ERA-I) model. January 16, 2009 12:00*

Figure 4.16

4.6.2 Case study: Westerly tip jet

The synoptic situation is in this case dominated by a mesoscale cyclone southeast of Iceland (the semi-stationary Icelandic low) and the Polar vortex (Baffin Island), a pressure gradient in the Denmark Strait forcing the flow across the Greenland and around Cape Farewell.

The depth controls the strength of the flow in this barrier flow situation and the position of the Icelandic low [Bakalian et al., 2007]. This situation is therefore strongly linked to the NAO index of Hurrell [Hurrell, 1995], [Harden, 2012]. The pressure distribution in Fig. 4.17a and Fig. 4.17c shows only small differences between the ASR and the ERA-I. The biggest pressure gradients are located in the coastal area along the edge of the ice cap in the ASR but are more in the central part of the island for the ERA-I. This has a minor influence on the size and the intensity of the WTJ but it affects the modeled barrier winds across the ice cap. The difference in the modeled barrier flow affects the modeled wind field in the east coast region and over the Denmark Strait. The biggest difference seems to be in areas, where the flow has been modulated by flow over land, as in the lee of the south tip.

A similar situation on March 2, 2007, was studied by [DuVivier and Cassano, 2013]. They compared WRF simulations at 10,25,50, and 100 km resolution, ERA-I 42 km, and QuikSCAT data 25 km for an area similar to the one shown in Fig. 4.17a to Fig. 4.17d. On average, the WRF 25 km wind speed agreed with the QuickSCAT 25 km, while the ERA-I 42 km was 20% lower than the WRF 50 km. In the high-wind field off the tip, the ERA-I wind speed was also lower than both the WRF and the QuikSCAT.

When the ASR tip-jet in Fig. 4.17b is compared to the ERA-I in Fig. 4.17d, the intensity of the tip jet is lower in the ERA-I. The land penetration of the jet at the south tip is different, but it can to some extent be related to the use of GTOPO30 (lower terrain elevation) data in the ASR simulations.

The modeled wind fields for the two models Polar WRF(ASR), Fig. 4.18a and WRF(ERA-I), Fig. 4.18b differ in multiple parts of the domain. Over the central part of the ice cap

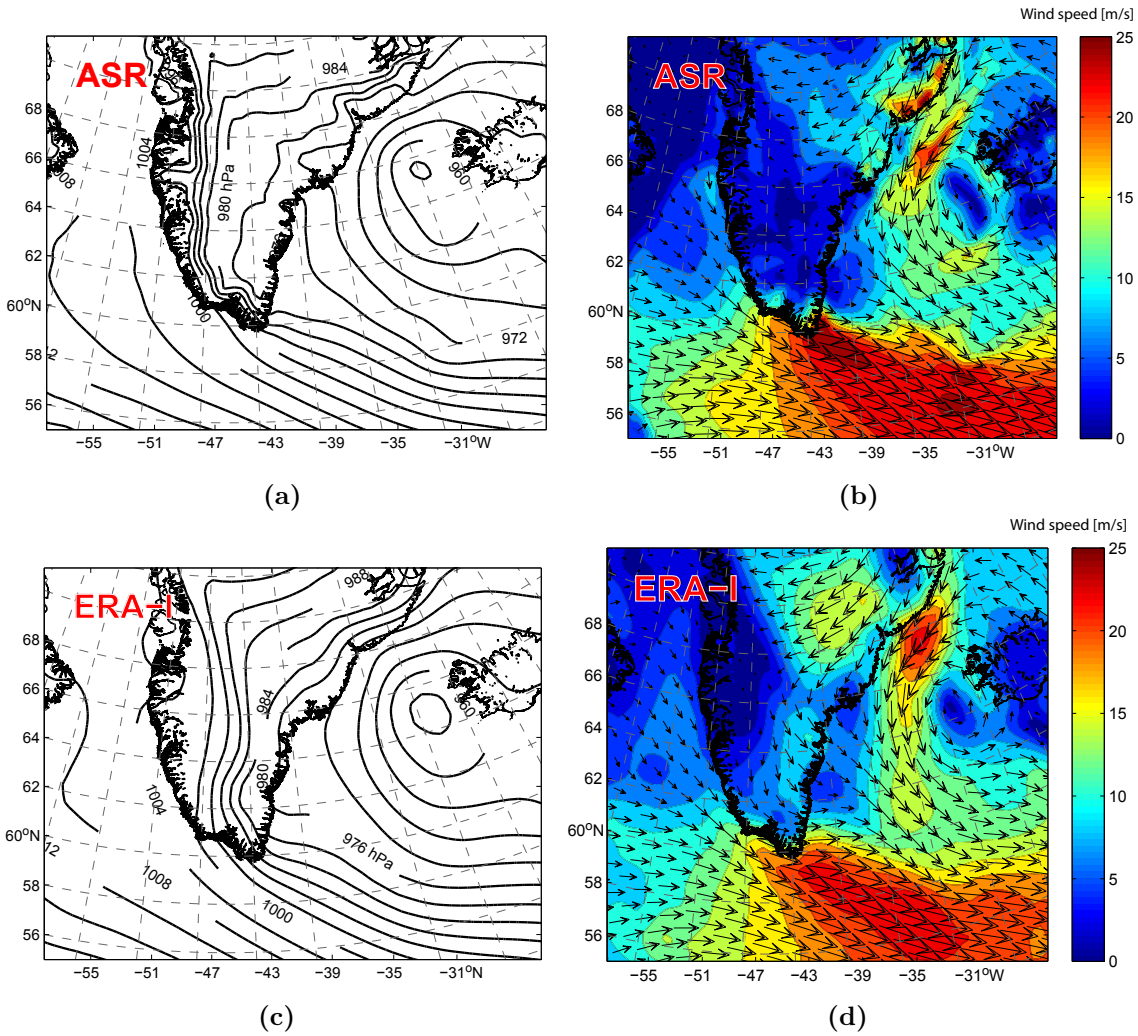

Figure 4.17. *a) Mean sea level pressure [hPa] distribution for January 19, 2009, 12:00, based on the ASR data. b) Wind field [m/s], 10m above sea level for the same case based on the ASR data. c) Mean sea level pressure distribution for same case based on the ERA-interim data. d) Wind field, 10 m above sea level, for the same case based on the ERA-interim data.*

there is a clear difference in the results of the two model. The Polar WRF(ASR) shows wind speed in the range 7-11 m/s, while the WRF(ERA-I) shows barely any flow. At the steep northeastern edges of the ice cap, the Polar WRF(ASR) model gives the highest wind speed and vice versa for the southern part. The Polar WRF(ASR) has some outlet from the ice cap in the north western part of the domain, although the WRF(ERA-I) has only a weak outlet in the northwestern part.

The low-wind, dark-blue area off the northwestern coast, starting around 61^o latitude, and to the north in the WRF(ERA-I) is a result of sea ice affecting the flow. ERA-I has a very large sea ice area along the coast; see Fig. 4.29b, and the temperature over the ice is much lower than over open water. Over the ice, the boundary layer is very stable, the surface wind is decoupled from the flow higher in the atmosphere, and the lower air mass becomes stationary. The large effect of the sea ice can be observed in

the wake of the ice. This large concentration of sea ice is not represented in the ASR data or in the official ice charts for the area, and it is unlikely that this amount of sea ice was present in this area. The large cold air mass in the coastal area can explain the lower flow off the ice cap in this area. This is a concrete demonstration of the importance of good sea ice representation in the Polar region. A snapshot of the flow for the two models, such as in Fig. 4.18a and Fig. 4.18b, does not always give the best picture of the differences. To study the effect of the two tip jet situations in different areas, time series for selected stations are presented, Fig. 4.19a - Fig. 4.19j. The selected stations are presented from north to south on the west coast, and the last station is the east coast station. Stations 1601 and 04285 are more or less at the same latitude but inland and off the coast, respectively. Station 04390 is also at the same latitude but on the east coast.

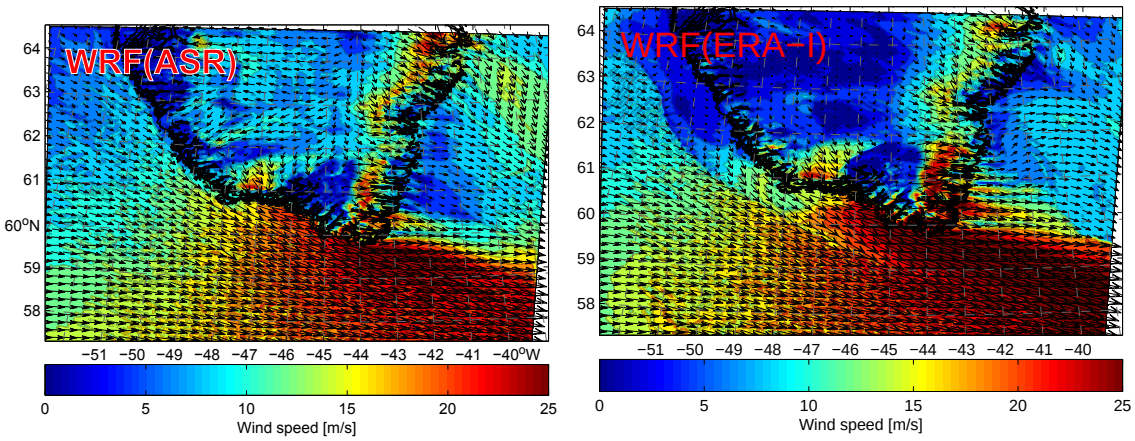

(a) *WTJ results for the WRF (ASR) model January 19, 2009, 12:00*

(b) *WTJ results for the WRF (ERA-I) model January 19, 2009, 12:00*

Figure 4.18

In the easterly barrier flow regime only the east coast, here represented by station 04390 Fig. 4.19i, is fully exposed to the flow from the sea. The shown event lasts two days, maximum hourly mean wind speed reached 28 m/s, and both models caught the duration of the event. On the west coast, the harsh weather conditions unfortunately caused errors at automatic weather station 04285 Fig. 4.19g. In the coastal area, at station 1601 Fig. 4.19e, the wind fluctuated a lot, and the measurements are generally closest to the WRF(ASR) result. Further north, the slope of the ice cap caused speedup and gave high wind speeds in the area of station 04270 and 04266 (Fig. 4.19c and Fig. 4.16b).

For the westerly barrier flow, the wind followed the coast, and stations 4266 and 4285 were exposed for parts of the main flow. Both the measurements and the models show high and sustained flow for a long period. Inland at station 1601 Fig. 4.19f, the WRF(ERA-I) model in particular over predicted the speed and underestimated the variations in wind speed. The missing terrain features in the model topography might have caused this. At the southeastern coast, the WRF(ERA-I) gave a higher outlet speed from the ice cap than the Polar WRF(ASR) model Fig. 4.18b and Fig. 4.18a. The measurements at station 04390 confirm that the high speed modeled by the WRF(ERA-I) is closest to the observed speed and that the measured speed was even higher Fig. 4.19j. For the

two gravity-induced speedup events, caught by the stations and shown in Fig. 4.19c and Fig. 4.19j, the WRF(ERA-I) showed the best performance. In general, the WRF(ERA-I) gave the best results for the barrier flow situation, where the flow was modulated by the land.

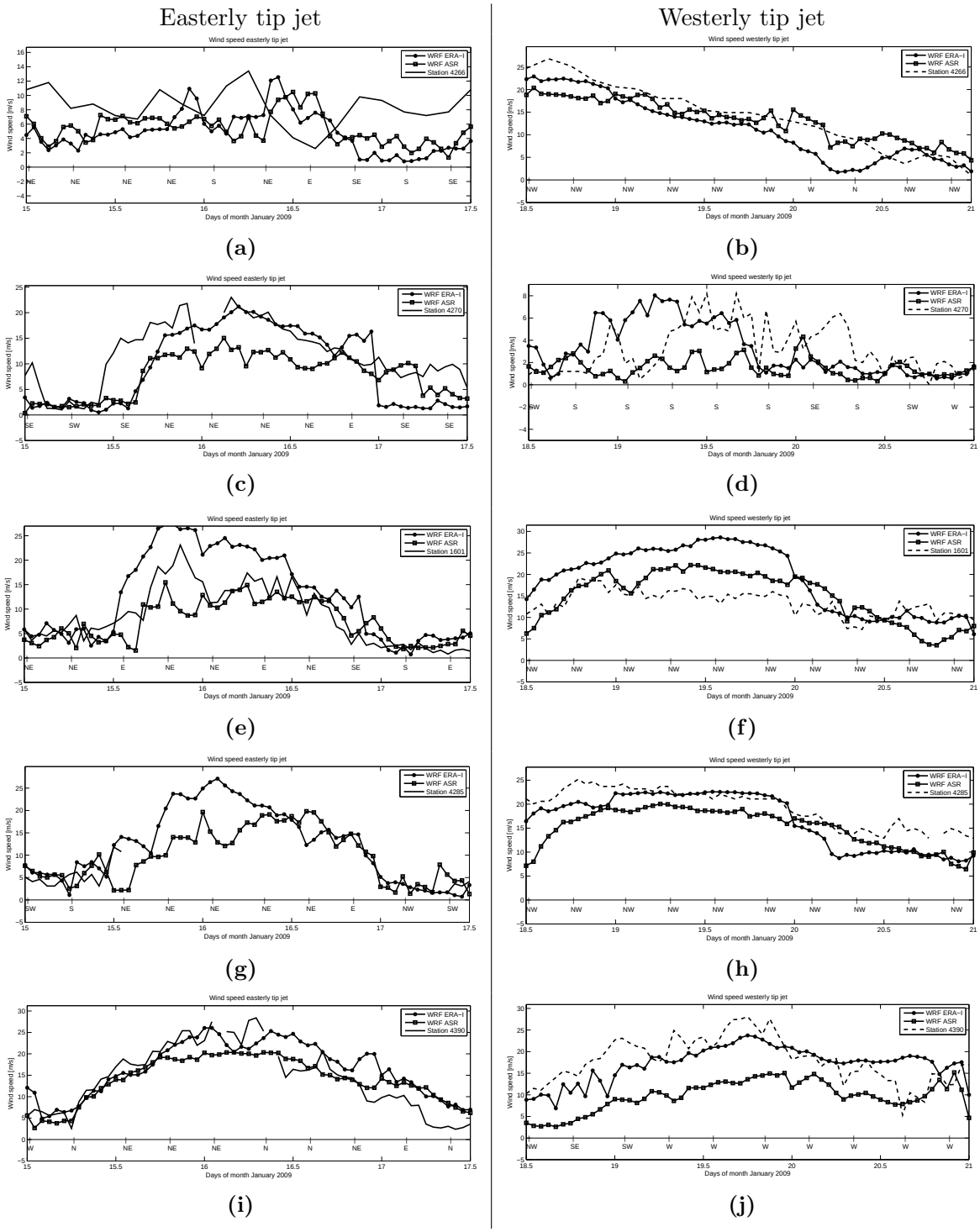

Figure 4.19. *Left column shows the results for selected stations for at the ETJ on January 16, and right column show the results for the WTJ January 19. The upper row (a and b) shows station 04266 on the Greenlandic west coast. The next row (c and d) is a station southeast of this, and on the next rows, the more southern stations are shown. The last row (i and j) is the east coast station*

4.6.3 Vertical wind distribution at ETJ

To take a closer look at vertical wind speed distribution, cross-sections of the modeled wind field are presented in Fig. 4.20a to Fig. 4.20f. Two sections in the easterly barrier wind regime are selected, one along the flow passing station 1601 at the west coast and one across the flow passing station 04390 on the east coast. The flow situation is described in section 4.6.1 and the time corresponds to day 16.5 in the time series plot in Fig. 4.19e. Note that there is a small difference in the modeled wind direction that has a minor influence on the wind speed distribution in the plane.

The modeled wind speed differs significantly for the two models in the ETJ situation. To study the reason for this, the upstream wind speed distribution was extracted in an 80 km long vertical plane. The plane is located from 12 km downstream to 70 km upstream of station 1601 and in the direction 46^o north (flow from right to left). The maximum wind speed on the plane is similar for the two models, but the wind speed distribution, especially the terrain influence on the flow, seems to be very different Fig. 4.20c and Fig. 4.20e. At site 1601, Fig. 4.19e shows that the Polar WRF(ASR) underestimated the wind speed in this situation, while the WRF(ERA) overestimated it. At this specific time step, the WRF(ERA-I) is closest to the measured wind speed, but the Polar WRF(ASR) shows the best overall performance for the whole event. At the validation height 50 MAG the difference is not that big, but higher and offshore, the model results differ more.
The stratification of the flow in offshore part of the plane is also very different. The Polar WRF(ASR) indicates a stratified boundary layer, while the flow in the WRF(ERA-I) is mixed.
The modeled mountain effects are very different. In the Polar WRF(ASR), the high wind areas associated with the mountains are located mainly at high altitudes, while the wave has a smaller height and continues down in the WRF(ERA-I) results. In the Polar WRF(ASR), the lower altitude air mass is affected by the surface heat flux from the open water fjord. In the WRF(ERA-I), the inner part of the fjord is covered by sea ice and the heat flux is negative. The plane touches the fjord again around 50 km, and at this point, the Polar WRF(ASR) has a sea ice fraction of 0.3, while the WRF(ERA-I) has 1. The effect on the flow, at this point is small compared to the inner part, due to the smaller sea surface fraction in these cells.

The other plane is located from approximately 90 km SW of station 4390, perpendicular to the barrier flow Fig. 4.20b. The flow at this point starts to turn from the north-south direction along the coast to a more easterly direction, and the difference in this turn results in a different wind speed distribution. The East Greenlandic tip jet has been studied by [Outten et al., 2009]. The position of the jet in relation to the barrier is closely related to the flow angle at which the flow meets the barrier. In this situation, both models indicate a high-speed area at the first mountain ridge, 15-25 km wide, more than 600 m high, with wind speeds above 30 m/s. This high-wind area is associated with both mountain waves and the tip jet effects [Harden et al., 2011].
The width and the intensity of the ETJ are bigger in the WRF(ERA-I) at level 1 Fig. 4.16a and Fig. 4.16b. The higher intensity is seen in all the jet areas at least up to 1.6 km altitude Fig. 4.20f and Fig. 4.20d. Both models were close to measured wind speeds for the whole event Fig. 4.19i, but the Polar WRF(ASR) was closest to the measured speed

at this time step (16.5). The station is located 70 m above mean sea level, but the model terrain elevation, which is based on interpolated GMTED2010 data, show it less than 46 m AMSL. This might have had a minor impact on model performance.
In the Polar WRF(ASR), there is only one area, 60-70 km, with sea ice concentration of 0.15(15%). In the WRF(ERA-I), there is no ice off the coast, but there are three areas with ice at 130-160 km where the plane crosses water. This makes the surface heat flux much larger for the Polar WRF(ASR) since the water temperature cannot go below the freezing point and displace the wind above the valleys. This plane study demonstrates the impotence of correct sea ice concentration data for mesoscale wind modeling in the Arctic area.
The plane study illustrates how complex the flow is in these valley systems and how difficult it is to follow the flow just by plane extractions of the wind field. To get a clear view of the flow patterns, the full 3- or 4-D (u, v, w, time) flow field need to be studied.

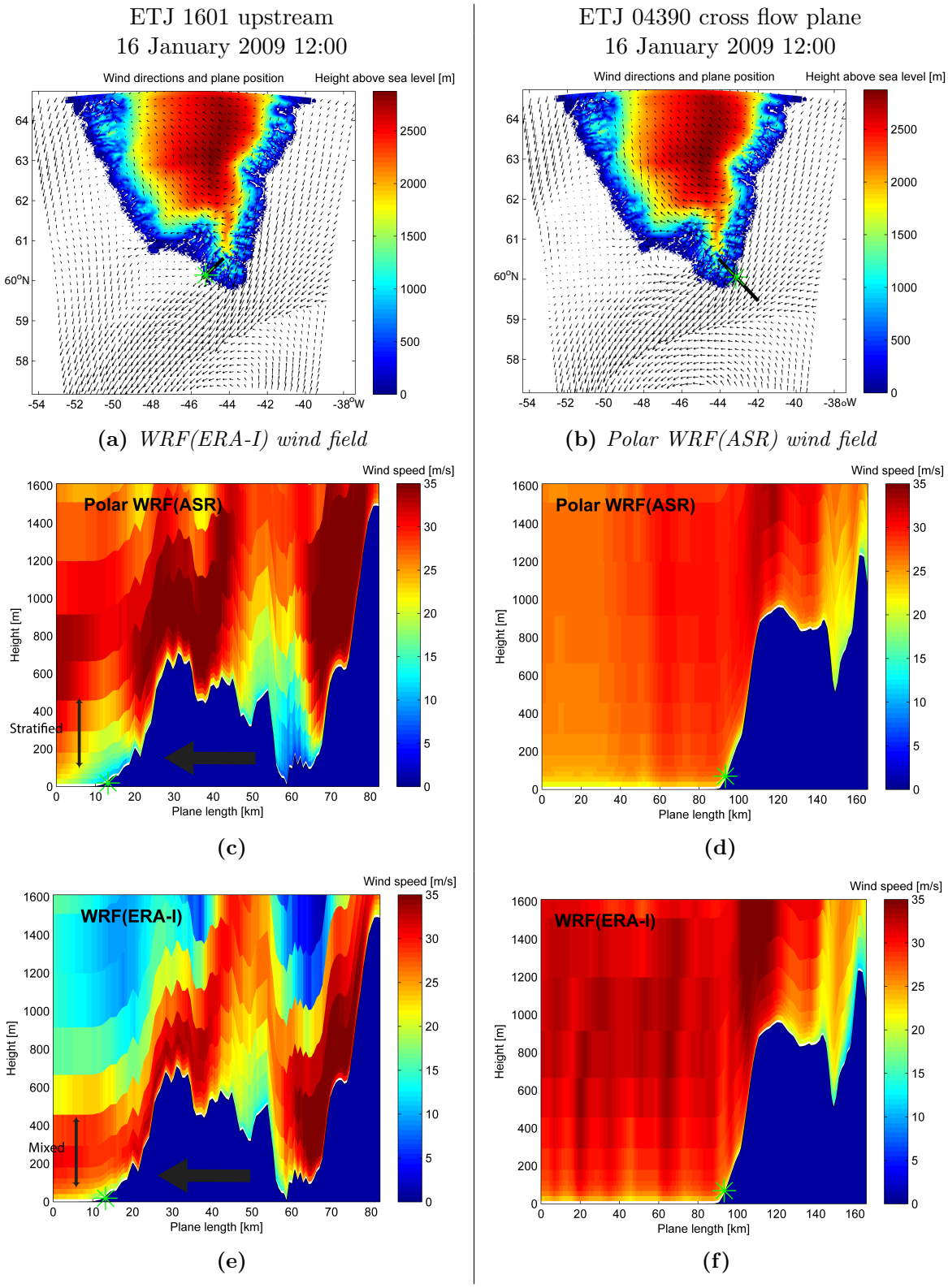

Figure 4.20. *Upstream vertical plane of the total wind speed distribution in ETJ on January 16, 2009, 12:00. a) Terrain elevation, wind speed vectors Polar WRF (ASR), vertical plan position and station position, west. c) Wind speed distribution for 0-1600 m above mean sea level, Polar WRF (ASR), west. e) Wind speed distribution WRF (ERA-I), west. b) Position of plane perpendicular to the ETJ crossing station 4390. Wind vectors based on the WRF (ERA-I) data, east. d) Wind speed distribution in plane WRF (ASR), east. f) Wind speed distributions in plane WRF (ERA-I), east*

4.6.4 Fjord channeling study at ETJ, based on 4D flow field

In the last section, 4.6.3, plane extraction of the modeled flow field was studied to understand the flow in and above the Tasermiut fjord south of Nanortalik. In this section, the 3-D flow in the same area will be studied. The position of the studied subdomain is shown in Fig. 4.21a and a high-resolution view of the subdomain and the plane position used in 4.6.3. The study is based on an off-line calculation and the flow is treated as a static flow field. It is clear in Fig. 4.21b why the plane study had difficulties in keeping track of the high-wind field; the shape of the fjord makes the channeled high-wind field over the fjord pass in and out of the plane, and in the outer part, it bends away from the plane.

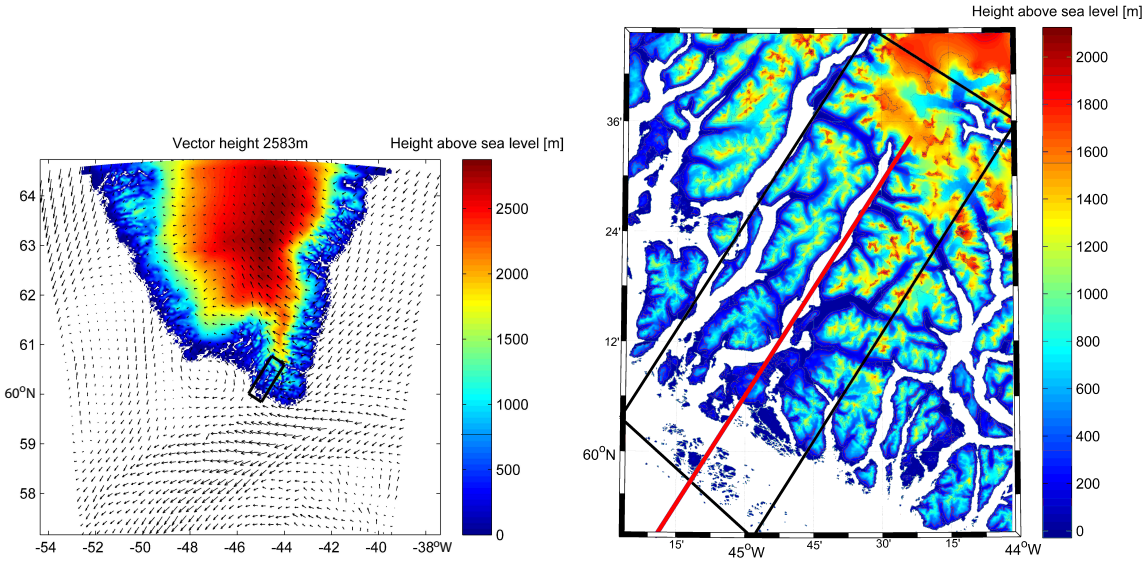

Figure 4.21. ***a)*** *Position of the subdomain in the inner 800x800 km domain. Topography based on [Danielson et al., 2011]*
b) *Position of the plane used in section 4.6.3 and the subdomain for the 3-D study. Terrain resolution 30 m from [Howat et al., 2014]*

The subdomain used for this study is 40 x 100 km and covers both the Sarqa and the Tasermiut fjords beside the three validation stations 04283, 04285, and 1601. The subdomain is aligned with the mean wind direction of the surface wind at the eastern edge of the subdomain. At the first visualization, the focus is on the surface flow, and the method chosen is streamlines of injected particles. In Fig. 4.22, particles are injected in a grid at the edge of the subdomain separated 500 m horizontally and from 20 MAG to 100 MAG with 20 m spacing. The flow patterns of the injected particles are highly affected by the terrain, and as the particles reach the coast, they are concentrated in two streams that more or less follow the two fjords. This is a very simplified illustration because it does not account for interaction with the flow next to and above the studied area, however it gives a good indication of where the surface wind speed is highest (highest line concentration). In the southwestern part of the domain, where all the injected particles merge into two main streams, the flow in the rest of the domain is not visible. By regularly injecting particles into the flow, more patterns will be visible, but it requires a balance because too

many streamlines obscure the picture. In Fig. 4.23, new particles are injected every 10 km throughout the domain. The tendency to follow the slopes down to the fjords/valleys is also seen in this case, but the particles injected in the last smoother part of the domain flow more parallel. At the 1000 MAG level the flow starts to bend toward the geostrophic wind direction that is more along the coast (southeast).

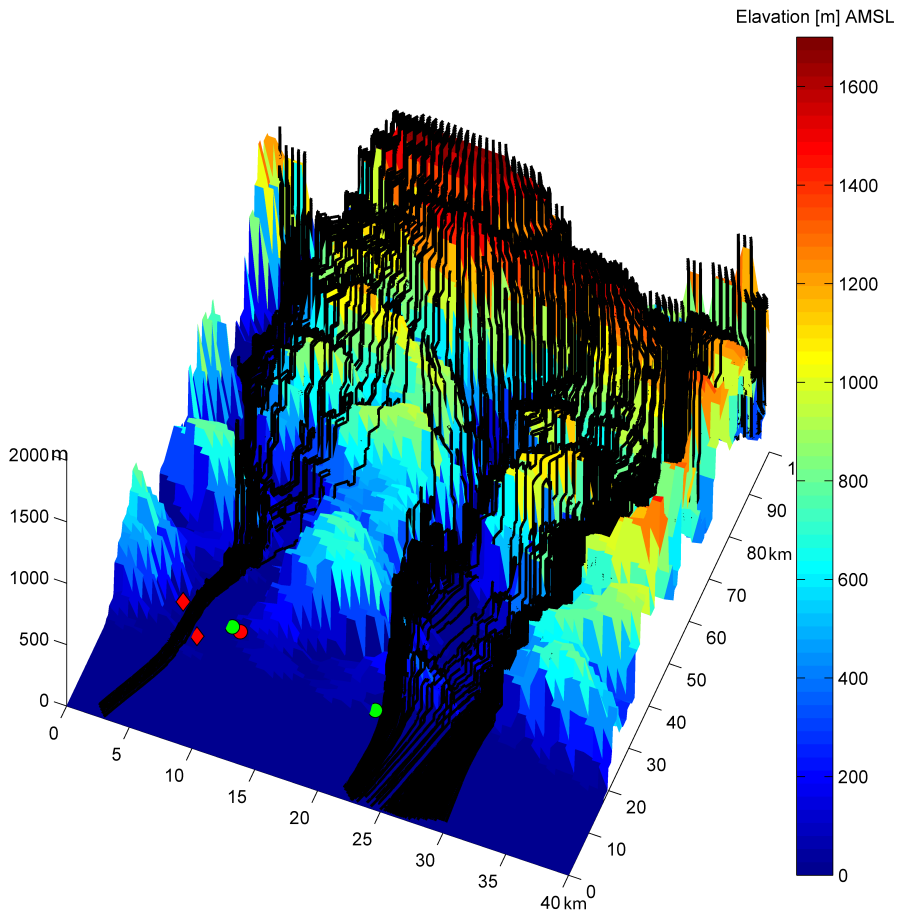

Figure 4.22. *Streamlines for particles injected at the subdomain edge distributed 500 m horizontally and from 20 MAG to 100 MAG for each 20 m. Green marks are official climate stations and red are DTU wind monitoring stations. (Notice, that the view angle influence the elevated positions.)*

The mountain ridges in the area are up to 1600 m AMSL, and the flow is highly affect up to around this levels, but the highest mountains in the area affect the flow up to 2.5-3 km AMSL Fig. 4.24. It is clear that the highest mountain north of Sarqa bends the flow even at the 2500 MAG level at the northern edge of the domain if lines are added at the southern edge, the turn between the funneled and the free geostrophic wind becomes more clear and that the level decreases with the mountain height toward the coast. These flow patterns can be used for wind turbine siting and meteorological mast positioning.
If a site location is given, the opposite function called back trajectory, can be a good tool to study the inflow to a site. In complex terrain like south Greenland the flow patterns can be very complex and hard to identify, and just a small relocation of the site can have

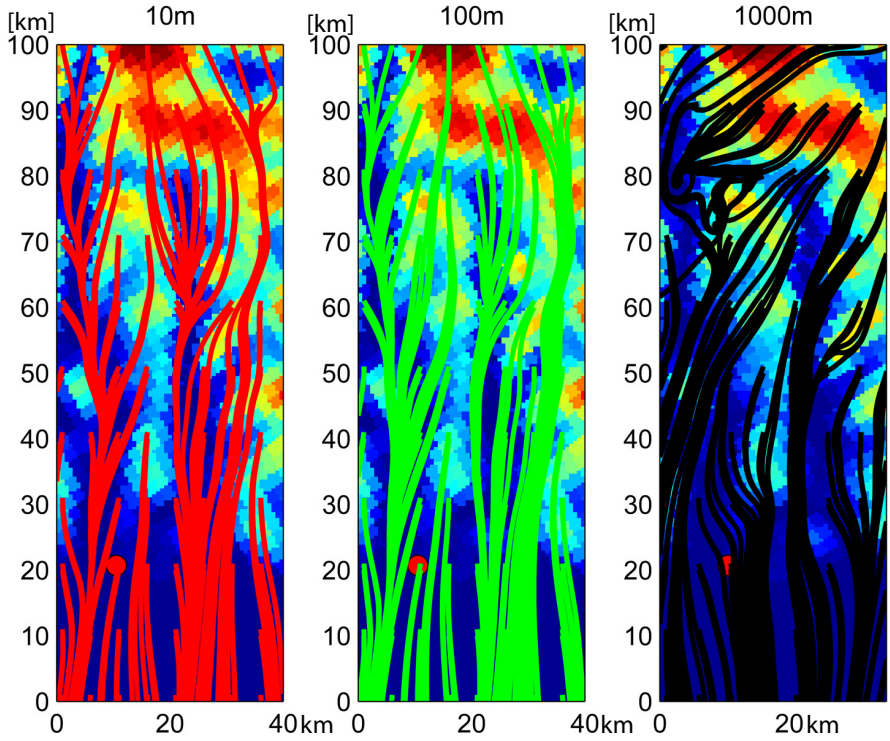

Figure 4.23. *Streamlines for particles injected from the subdomain edge and every 10 km to the end of the domain. The particles are injected with 5 km sideway spacing and at 10, 100, and 1000 MAG respectively.*

a significant effect on the wind resource. The surface conditions of the inflow path can affect the stability of the flow and a back trajectory model can in these cases be a valuable tool to study the inflow and optimize the site location. The back trajectory model is not shown this report, but it can be applied in the same way as the forward trajectory model when the historical flow fields are available.

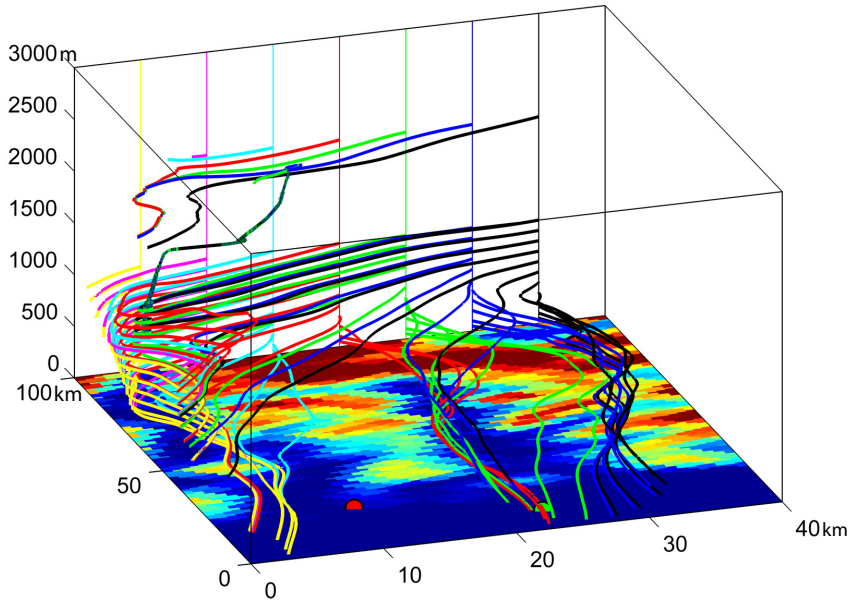

Figure 4.24. *Streamlines for particles injected at the edge of the subdomain, separated 5 km horizontally and at* $10, 50, 100 : 100 : 1000, 1500, and 2000$ *MAG*

4.7 Satellite-based wind data

One of the available sources of wind data is ocean surface wind determined based on satellite observations. The standard models calculate spatial wind variability over the scanned area based on Synthetic Aperture Radars (SAR) scan images. The fact that these are satellite scans means that data availability depends on the satellite orbit and the observation frequency. The spatial resolution of the wind field produced depends on the satellite instrument, operation mode, and data processing. One of the most popular products is the QuikSCAT ocean wind from NASA, with standard resolutions of 25 x 25 km, and 12.5 x 12.5 km (2.5 x 2.5 km can also be accessed), and the nominal temporal repeat is 12 hours.
Another popular product is the ENVISAT ASAR sensor, which provides a spatial resolution of less than 150 m and a scan of 405 km Table 4.7. The newer satellites as Radarsat 2 provide SAR images/scans with a resolution down to 10m. In the Arctic area, sea ice monitoring uses the same ASAR pictures/scan as the ocean wind, and therefore some extra pictures are available at or close to sea ice areas. The far north locations are privileged with higher visit frequency due to the satellite orbits, but not all data are available, because of prioritized use of the satellites.

Name	Resolution	Scan width	Repeat int.
	[km]	[km]	Hours
QuikSCAT	25,12.5,(5)	1800	12
ENVISAT	0.03-0.15	405	48
Radarsat 1/2	0.08-0.15	500	6
TerraSAR-X	0.08	100km	48

Table 4.7. *Example of the most popular SAR satellite products.*

4.7.1 Wind data retrieval

Over the ocean the SAR image brightness increases with the wind speed because the radar signals at these bandwidths interact with the waves at the surface. The small scale waves are reflecting the local wind conditions. The image brightness not only varies with the small scale waves, but also with the scan-angle in relation to the surface. The image processing scheme therefore need to adjust this before the data processing. After the picture calibration interpolation to the desired resolution and noise filtering is applied.
The wind field is calculated by an empirical description of the relation between the radar backscatter and the wind speed and direction 10m above sea level. Varies empirical functions for the relation is available, but for this study a model based on the CMOD5 function (4.4) [Hersbach, 2007] was used.

$$\sigma^o_{vv} = b_0 \left(b_1 + cos\phi + b_2 cos(2\phi)\right)^{1.5} \tag{4.4}$$

where:

σ^o_{vv} VV-polarized Normalized Radar Cross Section (NRCS)

ϕ Relative direction between the radar look direction and the wind direction

b_i Parameters depending on the radar incidence angle and wind speed

A comparison of the CMOD5 model with metrological mast observations on the Danish offshore site Horns rev demonstrated an accuracy in the range $\pm 1.34 m/s$ [Christiansen et al., 2006], depending on the quality of the direction data used and the BL stability etc..
To solve the function and retrieve the surface wind speed, wind direction data is needed to calculate ϕ. In most cases local gradients in the SAR images can be used to determine the wind direction, but forecast or reanalysis data are used to verify the direction, however if local buoy or offshore tower measurements are available these are incorporated. Use of global or local model direction data feed to the uncertainties both from the models and the necessary time and space interpolation. If higher level wind speeds are needed modeled Monin-Obukhov length is often used together with Monin-Obukhov similarity theory to extrapolate the 10 m wind speed to the target height.

A detailed description of the SAR-wind retrieval process is presented in [Badger, 2008] and the included references. At DTU Wind Energy there is a long tradition for utilizing the SAR data for wind resource assessment. The retrieval process is handled in the APL/NOAA SAR Wind Retrieval Software (ANSWRS) developed at the John Hopkins University, Applied Physics Laboratory (JHU/APL).

The National Oceanic and Atmospheric Administration (NOAA) publish some ocean wind pictures from the last month at:
http://www.ospo.noaa.gov/Products/ocean/sar/index.html, and the historical pictures can be accessed by contacting the staff.

4.7.2 Ocean wind model validation

The satellite-based data have multiple uses, but one of the simplest is case studies. The two pictures in Fig. 4.25a and Fig. 4.25b show the measured wind field for the ETJ on January 15-17, 2009, 11.5 hours shifted.
If the high-resolution wind field of January 16, 00:43, in Fig. 4.25b is compared with the modeled wind fields for WRF(ASR) and WRF(ERA-I) January 16, 01:00 in Fig. 4.26a and Fig. 4.26b, some major differences can be seen. The scale is not the same, but to illustrate, lines of the major patterns are applied to the model results. First, the lower bound of the low-wind area in the northwestern part of the SAR picture (solid line white in model results), is relatively well modeled in the WRF(ASR) but a bit too far north in the WRF(ERA-I). The two fjord outlets (yellow dashed lines) are not clear in the model results, but raised wind speed is noticeable in the area. This is probably a result of the coarse model resolution in relation to the terrain variations. A low-wind lee area west of Nanortalik (solid blue lines) from the coast and 40 km offshore is clearly visible in the SAR picture, but it is not well modeled by any of the models; however the WRF(ASR) shows some lee and a reduced wind speed in parts of the area. That the WRF(ASR) model this area better than the WRF(ERA-I), is equivalent with results of the point-validation, but with less deviation. In the WRF(ERA-I), the flow is able to pass the southern part of the land and flow out in this area, where, according to the measurement, it should stay farther south. In the next area (between the thin and the thick dashed white lines), the flow outlet, mainly from the fjords, raises the wind speed. The variations between the outlet from the fjords/valleys and the rest of the landscape is not visible in the model results and both models overestimate the wind speed in this area. The tip jet extends too far north, and just south of Cape Farewell, it is too wide (Thick dashed white lines). The narrow tip jet in the measured wind field might indicate a smaller and more intense jet compared to the models, but more time steps and pictures need to be studied to draw a conclusion on this. The missing fjord outlets in the models might indicate that the 2 km model resolution not is able to represent important terrain features, and the flow penetration of the south tip indicates that there might be a problem with the GTOPO2010 terrain elevation or other surface parameters. As the quality, spacial, and time resolution increases for the ocean wind data, the potential used both as validation and boundary correction tool will increase to, especially for remote islands like Greenland.

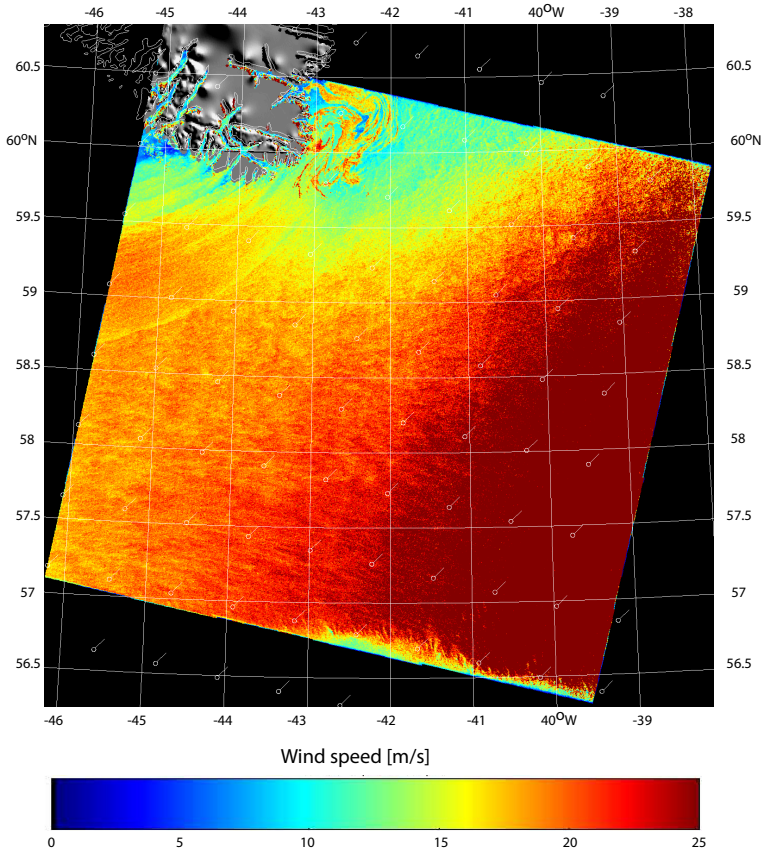

(a) *15.01.2009 13:15*

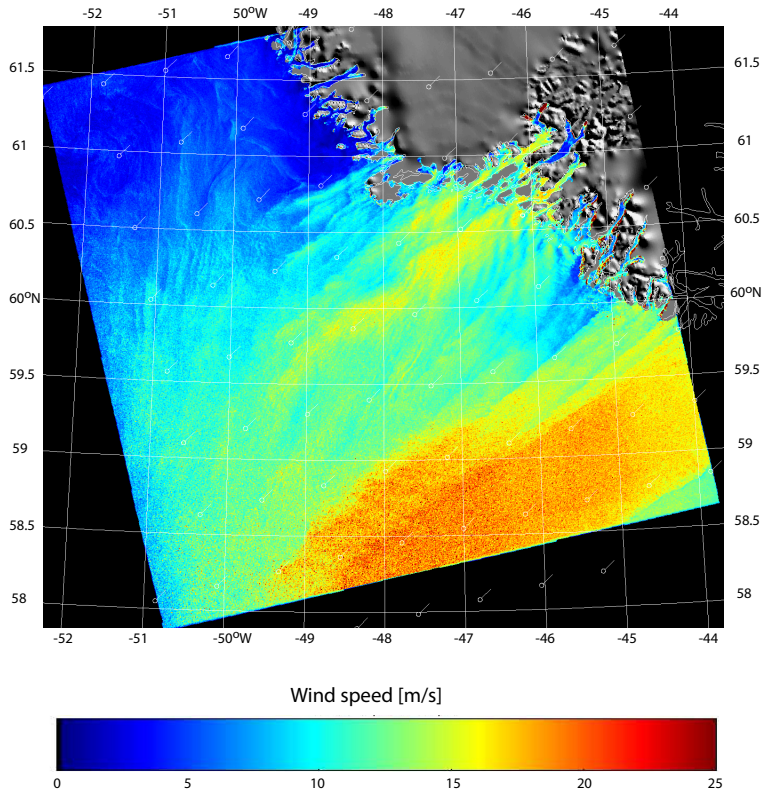

(b) *16.01.2009 00:43*

Figure 4.25. *Satellite-based wind fields for the ETJ situation on January 15-16, 2009.*

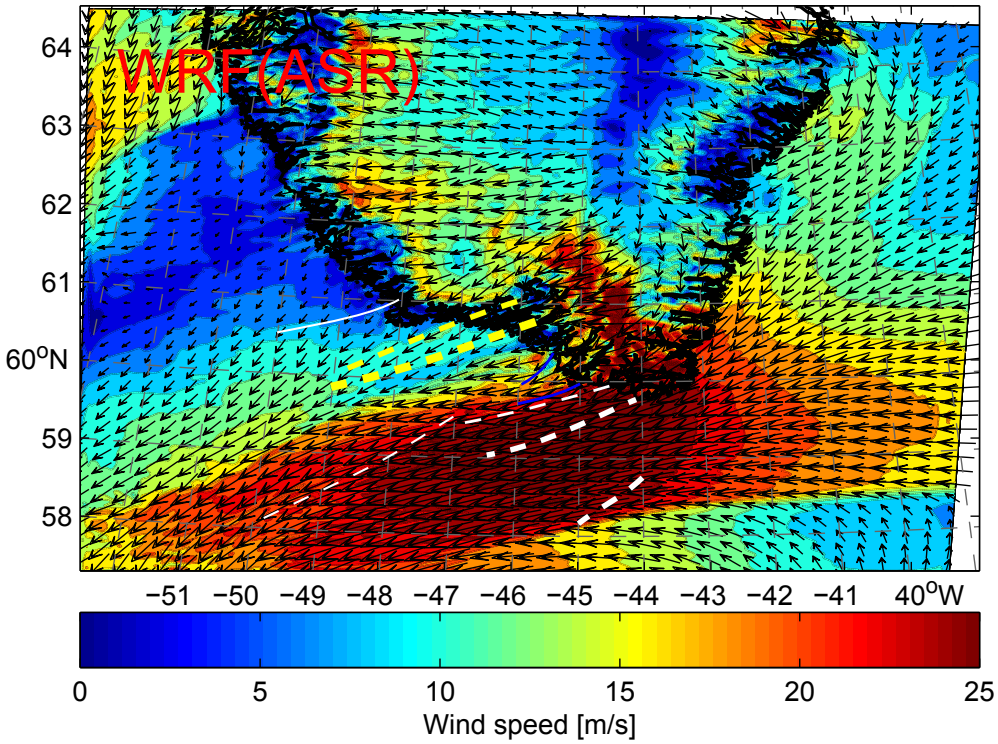

(a) *WRF(ASR) 16.01.2009 01:00*

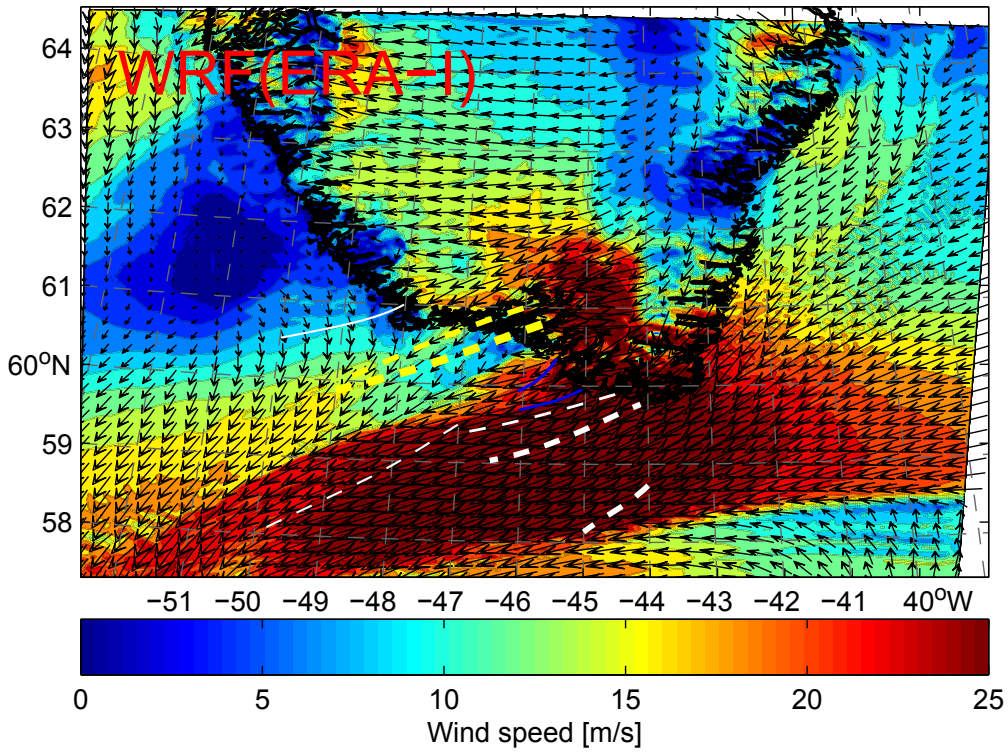

(b) *WRF(ERA-I) 16.01.2009 01:00*

Figure 4.26. *WRF-modeled wind field for January 16, 2009, 01:00, with illustration of the main line from the SAR picture Fig. 4.25a - Fig. 4.25b*

4.7.3 Wind resource assessment

Ocean wind data can also be utilized for statistical wind climates and identification of main flow patterns. One of the sources for this is the Climatology of Global Ocean Wind (COGOW) at http://cioss.coas.oregonstate.edu/cogow/index.html, where 10 years of statistics in 15 day intervals are available as both mean wind speed and direction pictures, wind roses for each 0.5 x 0.5^o and the raw data. The 10 year (2000-2009) average wind speed and direction for the first and second part of January are shown in Fig. 4.27a and Fig. 4.27b. The main difference between these two periods is a western shift of the semi-stationary Icelandic cyclone, which affects mainly the area south of Cape Farewell and the Denmark Strait.
The main flow pattern is controlled by the Icelandic cyclone; nevertheless, both the easterly and westerly extent of the Cape Farewell high-wind area show that both ETJs and WTJs are often represented. The mean wind direction does not indicate how flow direction and wind speed are related, and to study this, wind roses have to be extracted. At the green dot, south of Cape Farewell, the wind roses for the two periods were extracted Fig. 4.28a and Fig. 4.28b. The wind roses verify that the dominant wind direction is northwest, related to the WTJ, and the frequency of wind speed above 20kn is over 20% for this sector and over 40% if the two neighboring sectors are added. The ETJ on the other hand, is represented only 20% of the time in the data set. This is very different from the modeled January 2009, when the ETJ totally dominated the high-wind periods, but the number of data points used for this distribution, 160 measurements over 10 years, does not necessarily provide a good statistical representation of the real distribution. Likewise January 2009 may not be representative of general January distribution.
The general average wind speed in the area Fig. 4.27a and Fig. 4.27b is above 20kn, or 10m/s, in Cape Farewell, and in the Denmark Strait, the average wind speed for the period is above 13 m/s. For a simple check of this, coastal AWS observations for the period were extracted Table 4.8. The most southern stations show average January wind speeds in the range of 7-10 m/s, but with relatively high year-to-year variation. That the average wind speed of 10-50 km offshore should be in the range 10-13 m/s is not unrealistic if the uncertainties related to AWS observations are taken into account.

As new and more advanced satellites are put into operation and/or a better access to the existing data can be obtained, the data have the potential to be used for both reanalysis and mesoscale model validation for the Greenlandic area. This study has shown how difficult it is to find suitable sites for AWS in the complex terrain, and if the SAR-based measurements can be combined with well-located AWS on islands off the coastline, it will probably be a valuable tool for model validation, synchronization and nudging.

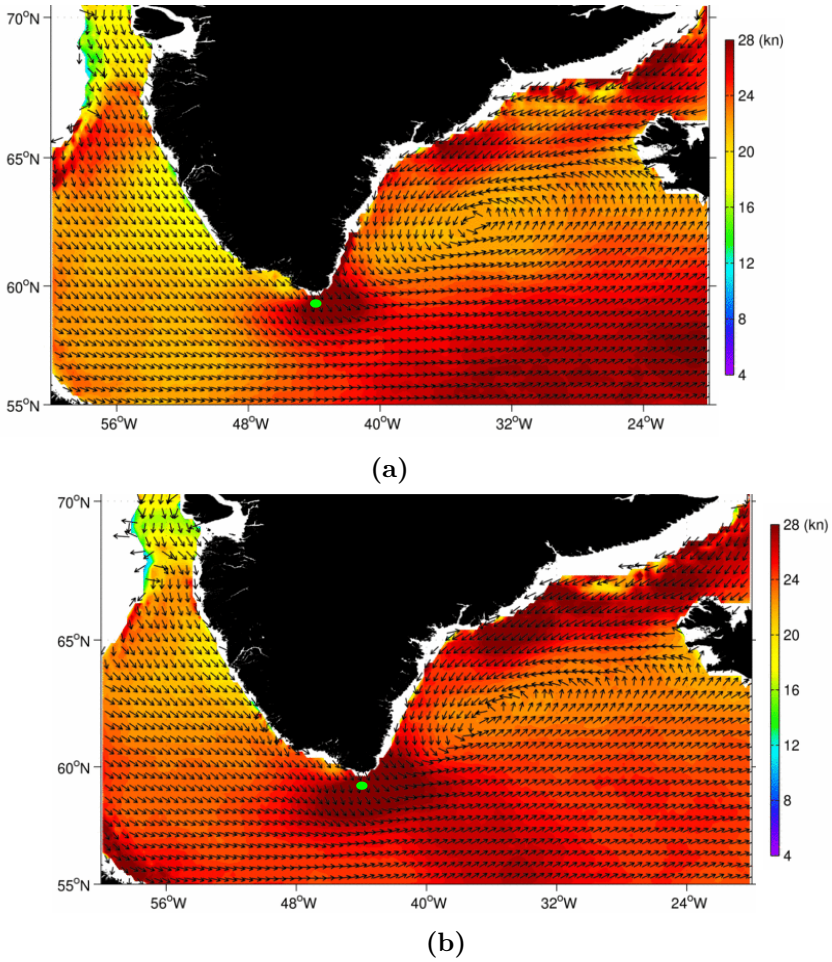

Figure 4.27. *Average wind speed and direction for the period of (a) 1-15, and (b) January 16-31, 2000-2009, both based on 25x25km observations. The green dot is the extraction point of the wind roses Fig. 4.28a [Risien and Chelton, 2006].*

Wind speed January 2000-2009

Station	Average	Min.	Max.	Latitude	Longitude
04341	5.7	3.1	7.7	70 45’	22 39’
04351	4.9	4.5	5.7	67 47’	32 18’
04360	3.1	1.9	4.9	65 36’	37 37’
04361	7.2	5.4	10.4	65 35’	37 09’
04373	9.6	6.1	13.2	64 47’	40 18’
04382	8.5	5.3	13.8	61 56’	42 04’
04390	8.9	7.0	12.2	60 03’	43 10’
04285	9.6	7.4	12.5	59 59’	45 08’

Table 4.8. *10-year January wind speed statistics for south and east coast stations. Data source [Cappelen et al., 2013].*

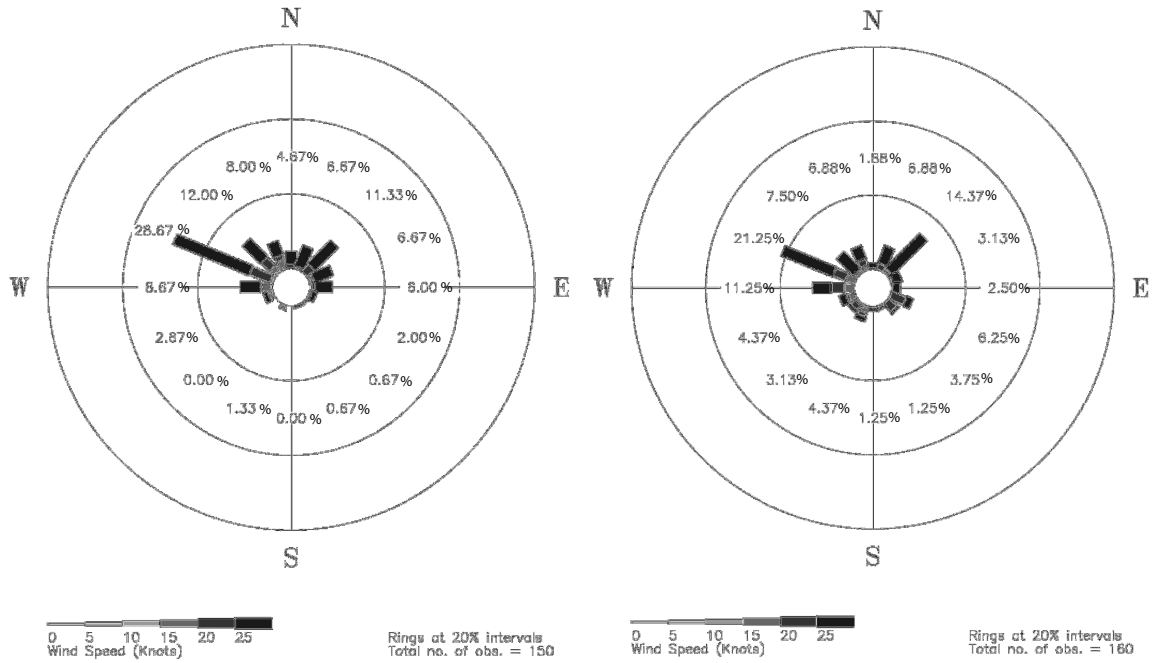

(a) *1-16.01.2000-2009* **(b)** *16-31.01.2000-2009*

Figure 4.28. *Wind roses for a point south of Cape Farewell, for the two periods of January. Extraction point is marked with a green dot in Fig. 4.27b [Risien and Chelton, 2006].*

4.8 Sea ice data

Sea ice coverage is another of the surface parameters that has been shown to have a high effect on the model results; the large difference in surface heat flux from open water and sea ice affects BL stability and lower-level flow patterns. Sea ice coverage and concentration was therefore studied to see the quality of the data. The sea ice coverage for the WRF(ASR) is shown in Fig. 4.29a, and the WRF(ERA-I) sea ice concentration is in Fig. 4.29b. As the figures illustrate, they are very different. The ASR sea ice data source is Special Sensor Microwave/Image (SSM/I) of the National Snow and Ice center http://nsidc.org, documentation: http://igloo.atmos.uiuc.edu/ASR/. The daily observations data is time interpolated to fit the model time-step. The ERA-Interim sea ice concentration data for the Greenlandic area is based on the 0.25^o data sets provided by NCEP [ECMWF, 2006]. The NCEP data is based on SSM/I (special sensor microwave/imager), processed according to the description in [Grumbine, 1996], and the raw data are available at http://polar.ncep.noaa.gov/seaice/.

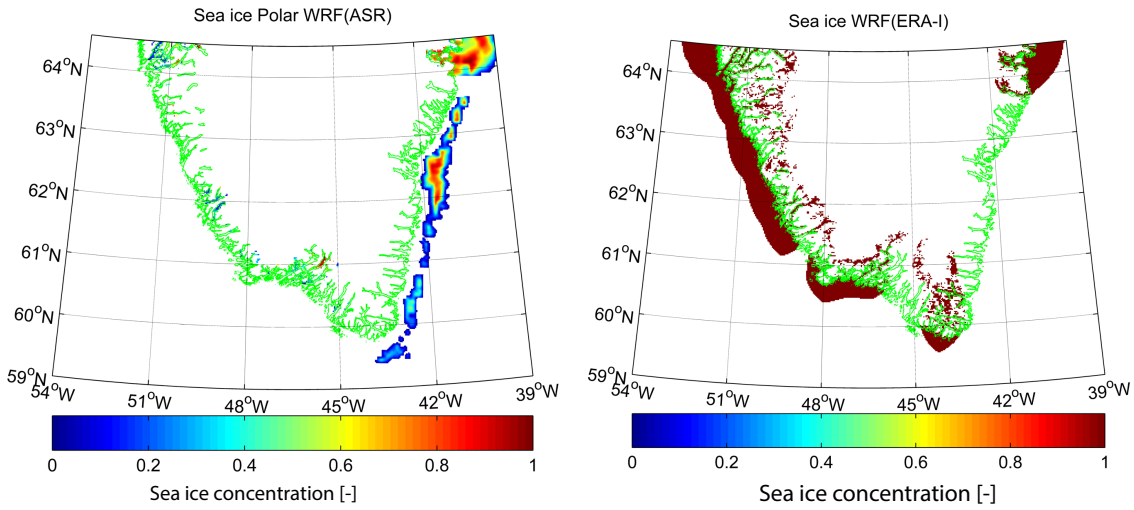

(a) *ASR 15.01.2009 21:00* **(b)** *ERA-I 15.01.2009 21:00*

Figure 4.29. *Sea ice mask/concentration for the WRF(ASR) and the WRF(ERA-I) model on January 15, 2009.*

To validate the sea ice concentration/distribution various sources were studied, both operationally dedicated products and raw satellite images, and some examples are shown in Fig. 4.30a to Fig. 4.30d. The ice concentration in Fig. 4.30a, should according to the documentation, be the base for the ERA-Interim except only ice masking is used. If the concentration is compared with Fig. 4.30b, there are similarities; both dataset missing the sea ice on the southeast coast and indicates sea ice on the southwest coast, where ice normally is very rare. Fig. 4.30b shows the concentration from the newer NOAA/NSIDC Climate Data Record of Passive Microwave Sea Ice Concentration, Version 2, for the same day. Here the sea ice is gone from the west coast, and the sea ice is now represented all the way to Cape Farewell on the east coast. The sea ice edges and concentration are derived from multiple satellite sources, but one of the most important is the ASAR, as shown in Fig. 4.30c. Note that the picture is not from the modeled period. A closer view

is shown in Fig. 4.30c, where the typical sea ice structure for the east coast is visible. The coastal part consists of stationary ice while the outer part consists of ice floes in a higher or lower concentration. If this is compared with the ASR sea ice concentration in Fig. 4.30d it is clear that the data include only a fraction of the ice floes area and not the stationary part along the coast and in the fjords. If the ASR result is compared with the official sea ice chart from the DMI Ice Service Appendix C, the outer shape of the ice is more or less the same, but the extent and the concentration are not alike.

The imperfect estimation of off-coast sea ice is one problem, but it can be solved by updating the data. Another more serious challenge is fjord sea ice. Some of the fjord sea ice is included in the ASR data, but it is only a small fraction in the widest fjords around Nuuk, Pamiut and Narsarsuaq. The resolution of the operational model for these areas is not yet so high that it can identify surface conditions in narrow fjords.
The DMI Ice Center uses low-frequent manual helicopter observations to guide ship traffic, but the observation frequency varies with ice conditions and expected traffic and includes only the official routes. The registration is simple and the information broadcasted in massage form, but some photo-based observations have been tested to minimize the cost of observations. In the future, the helicopters will most likely be replaced by high-resolution satellite observations and/or advanced drones.
A common way to solve this problem is to replace the fjord status in the model with lake status, and then use the lake model to estimate the sea ice from the surface temperature. This would probably not work very well because the relatively high tide, forces both water replacement and tidal flows, especially in the narrow parts. Another known problem with using the lake model is freezing point dependency on water salinity, which varies from fjord to fjord depending on length, depth, and fresh water supply.
Whether the lake model or a modified version can work has not been tested. The modern high-resolution satellite antennas, like the ASAR and Landsat, can be used to detect sea ice in narrow fjords, but to have enough observations (weather and orbit) and valid models to estimate all the related parameters (concentration, thinness, snow layer, albedo) on operational level is a challenge. Several institutions, including the DMI Ice Center, are working on a possible solution new products will be able in the near future.

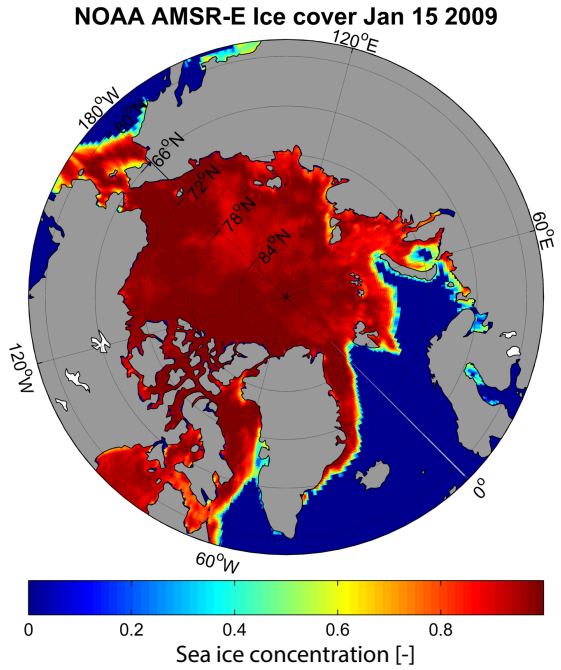

(a) *15.01.2009*

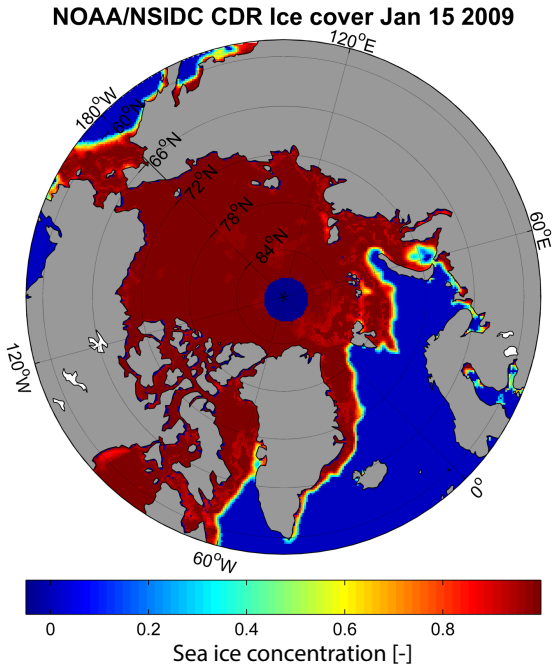

(b) *15.01.2009*

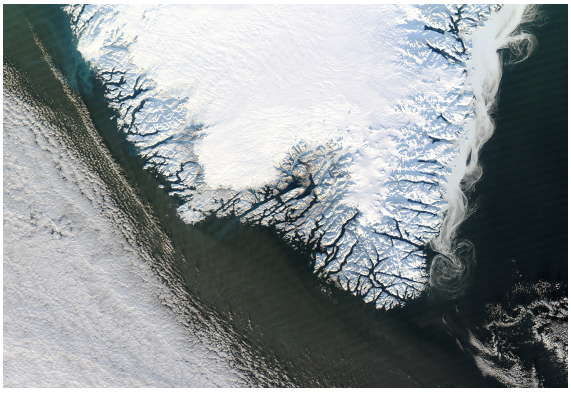

(c) *ASAR 01.03.2013*

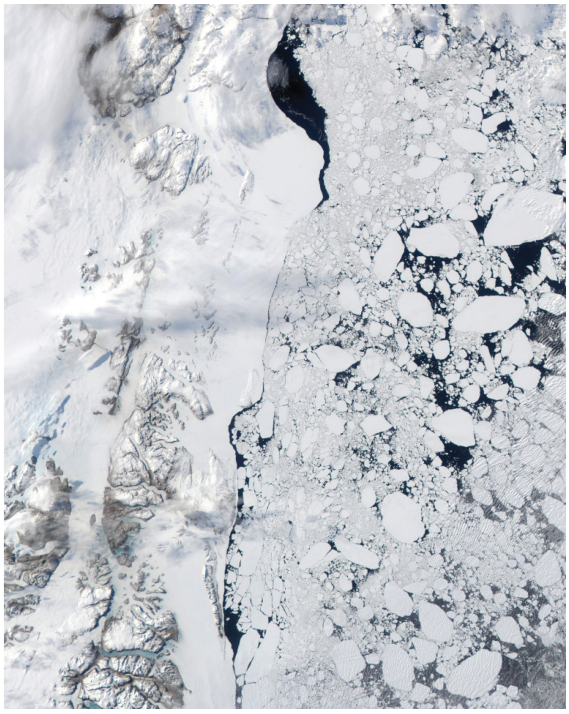

(d) *MODIS 08.06.2001*

Figure 4.30. *a) NOAA SSM/I sea ice concentration* $0.25x0.25^o$ *resolution; b) NOAA/NSIDC Version 2, in 25 x 25 km resolution; c) Example of ASAR picture of South Greenland with indication of sea ice and the drift 15m resolution (Credit: NASA image courtesy Jeff Schmaltz); d) Close-up view of typical sea ice structure on the Greenlandic east coast (Credit: Jacques Descloitres,MODIS).*

4.9 Meso-micro scale model coupling

The mesoscale models had good results for most of the validation stations in the test, but at the more complex sites, the models were not able to resolve the terrain resolution. The microscale models were able to model these small-scale features, but they were valid only in a small area due to the lack of atmospheric processes modeling and large-scale flow funneling.
The common solution to this problem is to couple the two models by nesting a high-resolution microscale model grid into the mesoscale grid, transferring the information from the mesoscale model to the microscale model grid, and solving the microscale model based on the input from the mesoscale model. There are different methods to handle this downscaling depending on the application. For wind resource mapping, statistical downscaling is often used [Duraisamy et al., 2014], and for other studies, dynamical downscaling [Wong, 2012] is preferred. A common resolution scale is to run the mesoscale model at 1-5 km resolution and the microscale at 10-50 m resolution.
The statistical downscaling principle entail mesoscale model simulation of a sufficient period to obtain a full statistical representation of the wind climate (distribution of wind speed, direction and BL stability) in each grid node, often 10-30 years, and then use the wind climate as input for the microscale model. This method minimizes the computation time due to fewer microscale runs, but it also unable time series studies. This method is known from the Wind Atlas for South Africa (WASA) project [Badger et al., 2014; Mortensen et al., 2012], among others.

Direct dynamic downscaling to more advanced CFD models with RANS, RANS2, LES, or DNS turbulence models is often used for wind resource or wind turbine load simulations in complex terrain, but the coupling and parameter adjustment in particular do not make this technique trivial. To make the transition from the coarse grid to the high-resolution grid, including high-resolution topography, a transition zone or buffer zone is needed to keep the model stable [Sørensen, 2013]. This zone is often several kilometers. The size of the domain itself often ranges from 2-30 km horizontally and 2-6 km vertically depending on the site area and the computer power available [Bechmann and Sørensen, 2011]. The mesh for these types of models often includes over $10 million$ grid points, and this makes long series or multiple directional runs very power intensive. A drawback of this setup is that the models ignore most of the atmospheric processes and often use idealized wind profiles. Combined with the often large domains, this limits performance, especially in areas with large thermal effects and very complex terrain.

A test of a coupled meso-microscale application was considered as a part of this project, but after detailed studies of the terrain, the models available and the mesoscale model results, further downscaling was skipped. The high-resolution terrain data for most of Greenland need to be validated and modified to obtain a correct description of the terrain. The models available for this purpose need a large amount of computer power, high-quality measurement data for parameter optimization, and long manual preparation time. To obtain correct mesoscale results in most of the area, the input parameters need to be further updated, especially the elevation, the land cover, the sea ice data, and before high-quality mesoscale results can be accessed, further downscaling will not make sense.

4.10 Conclusion on mesoscale modeling

In WRF simulations version 1 both model setups showed a poor performance especially on the southern part of the island. In the evaluation process the widely used GTOPO30 was found incorrect for large areas, causing flow-penetrating of a larger part of the Southern Greenlandic mountains region. An examination of the two reanalysis data set (ERA-I and ASR) showed a difference in the modeled tip jets, where the ASR showed the same penetration as found in the initial simulations and the ERA-I include a more southern positioning of the jets. An investigation of the models used to create the reanalysis data, found that the ASR used GTOPO30 based elevation data and ERA-I used updated version GMTED2010. The ASR wind field over Greenland was evaluated prior to this project, however only on the icecap part. This study illustrated that that the ASR wind field is invalid for the complex ice free part caused by e.g. incorrect elevation data. For the version 2 simulations the GMTED2010 terrain elevation was use with the same reanalysis data, relying on, that the distances to the boundaries, and the spin-up time, will minimize the effect of the incorrect ASR data. The updated simulations improved the overall performance significantly, but for some areas, the performance was still lower than expected. In the final examination, problems with both sea ice dataset were discovered and especially the ERA-I was far from reality. The modeled tip jets are still located further north, than the ocean wind observed position and penetrate the most southern part of the island. This could indicate that the updated GMTED2010 still include some of the incorrect data sources.
The 2 km resolution used in this study was found too coarse to simulate the complex flow in the widely branched fjord systems. To get a proper representation of the terrain, data with a resolution $< 500m$ must be used together with an effective meshing method. Before a proper high-resolution simulation can be setup a lot of data quality assurance need to be done.
For site selection the mesoscale modeling showed a high potential because flow-visualization can give a detail picture of the overall flow patterns in the complex terrain.

4.11 Further work mesoscale modeling of wind resources

Large improvement was achieve from the first mesoscale tests to the last version 2 model, however some improvement need to be implemented before acceptable error levels can be obtained all over the domain. To optimize the model performance some further work can be done:

- Increase the horizontal grid resolution to $\Delta x < 500$ m
- Implement valid terrain elevation data for all the domain
- Implement valid high resolution sea ice data
- Collaborate OSU on the improved version of the ASR
- Evaluate the boundary and initial conditions with SAR data
- Test different the turbulence models e.g. with LES based
- Test of 2-way nesting routines for the inner domains

- Setup a long-term simulation of multiple year
- Apply microscale coupling e.g. by WAsP CFD for prioritized areas

The initial model setup used in version 1, has been used for many wind modeling project all over the world, but this project showed the challenges involved in wind modeling in complex arctic terrain. As the list illustrate there some work before a valid model is available. More tall tower or LIDAR observation would be recommenced for further model evaluations due to less local effect as obstacle, hills snow cover etc.

Chapter 5

Wind power development in Greenland

The objectives for this chapter is; to present the historical development for Greenlandic wind power, summarize the experiences gain in this project, and setup recommendations for further development of Greenlandic wind power.

5.1 Introduction to wind power development

The Greenlandic wind turbine history started in the late 1970s when the second energy crisis raised the oil and thereby the electricity prices to the unprecedented level of up to 6 DKK/kWh in some villages. The worldwide wind energy business had an explosive expansion in this period, and inspired by the Danish solution to the crisis, the Greenlandic public forced, through the political system, the Greenlandic Technological Organization (GTO) to implement wind power in the villages. GTO was very skeptical of implementing this new technology in the small village systems.
Its skepticism was well-founded; GTO did not have the technical expertise, there was only limited experience with high wind-penetration worldwide at that time, and the atmospheric conditions in the scattered village areas were totally unknown. The compromise was to run a test in Nuuk and gain experience before a village deployment, [GTO report "Forsøgsmølle til Nuuk" 22.02.1983]. A turbine from the Danish manufacturer Windmatic was selected and the WM 14-55 turbine was delivered to pretest at Risoe, the national laboratory for renewable energy, in 1982 and shipped to Nuuk in June 1983. The turbine had a 14 m rotor diameter, an 18 m hub height, and a rated power of 55 kW. The turbine was installed in late summer 1983, and with the installation, the project appropriation of 840.000kr was used. There were several problems with the, for the time advanced technology, and the delivery time for both technical assistance and spare parts was very long. After a yaw system breakdown in a winter storm in 1986 (U10min = 36m/s), the project was abandoned, but the turbine was left at the site in the center of Nuuk. At that time, the turbine had been in operation for 3 years and had managed, in spite of the breakdowns, to keep an availability factor close to 90%. In winter 1988, during a storm, the hub was blown of the tower and scrapped. The tower was first demolished several years later. The WM 14-55 turbine used in Nuuk was only produced in 1982-1985, and only 30 were produced.
Nunatek Energy, the former GTO, submitted a final report to the government together

with a proposal for a new project in 1989. Nunatek suggested in the proposal of May 7, 1989, that another test be conducted in Nuuk, consisting of four 200 kW turbines at an estimated cost of 8 million DKK. The expected production was 2 GWh/year, or 30 million kWh/15 years. The estimated production cost was 0.26DKK/kWh based on a 15-year payback period, and it was noted that this was 0.05 DKK/kWh more than the oil energy cost of 0.21 DKK/kWh (2.10 DKK/L oil). Nunatek further suggested that these 0.05 DKK/kWh, or 100,000DKK/year, must be paid by the government [Political exposition "Redegørelse vedr. vindkraft i Grønland" 07-05-1989]. The proposal was rejected, because of both the suggested subsidy and the advanced planning stage of the Buksefjorden hydropower plant.

In the energy plan 2010, published in 1995, wind power was considered as an alternative to oil and hydro, but the easy accessible and known hydropower resources were prioritized. The latest energy plan 2020, from 2005, did not include any news compared to the 2010 plan, and the focus is still only on the known hydropower resources. Access to all reports and related political decision document, about the Nuuk wind turbine test, was provide by the Greenlandic National Archive http://www.arkiv.gl/.

After this, no large wind power project was launched in Greenland. Smaller wind turbines have traditionally been used for small remote stations, like repeater stations for telecommunication, owned by Tele Greenland A/S (Tele) and aviation related stations operated by Greenland Airports. According to the Tele veteran historical archive http://www.veteran.gl/, the first 6 micro wind turbines were installed in 1939 and 12 new in 1950. An updated communication chain was established 1978-1981 with 20 remote communication stations, all powered by two wind turbines and backup gas engines. Icing and storms at the high-altitude stations (up to 1700 AMSL) resulted in extra maintenance work, and together with a lack of high-quality turbines for replacement, only a few are left at the stations. Today PV panels and diesel generators, together with a large battery bank, form the power supply for the stations, but with oil prices of 6 DKK/L and delivery costs above $6DKK/L$, the fuel-related cost alone is very high. Tele has lately tried to implement different vertical axis turbines at some stations, but there lifetime became very short and most of them experienced a total breakdown within the first year Fig. 5.1. The motivation for using vertical axis turbines was low costs, less maintenance, and a high extreme wind resistance (according to the data sheet), initial study by [Nielsen, 2013]. This project contribute to the failure investigation, and the root cause for the tested versions was; fatigue based structural damages, and rotor overloading due to over-speeding (large centrifugal forces tore the rotor apart). The low support structures used for the installations (2-3 MAG), entailed high turbulence and added to the fatigue loads, however a higher support structure will not be able to increase the lifetime for these turbines to a satisfactorily level ($> 5years$).

Some of the tested turbines were designed with compact hybrid (not Darrieus or Savonius rotor) aluminium rotors and breakdown due to fatigue (crack growth from bolt holes and other high stress areas). The more open Darrieus type turbines, like the Ropatec at Top300, failed by rotor breakdown Fig. 5.1. The tested designs were not suitable for this climate, due to their either compact or slender design, low efficiency, and lack of aerodynamic breaks.

The test of the horizontal axis wind turbine Proven P11 6kW (2010-), is described in section 2.4 and appendix D.

To install a wind turbine, anywhere in Greenland, some basic knowledge about; the wind

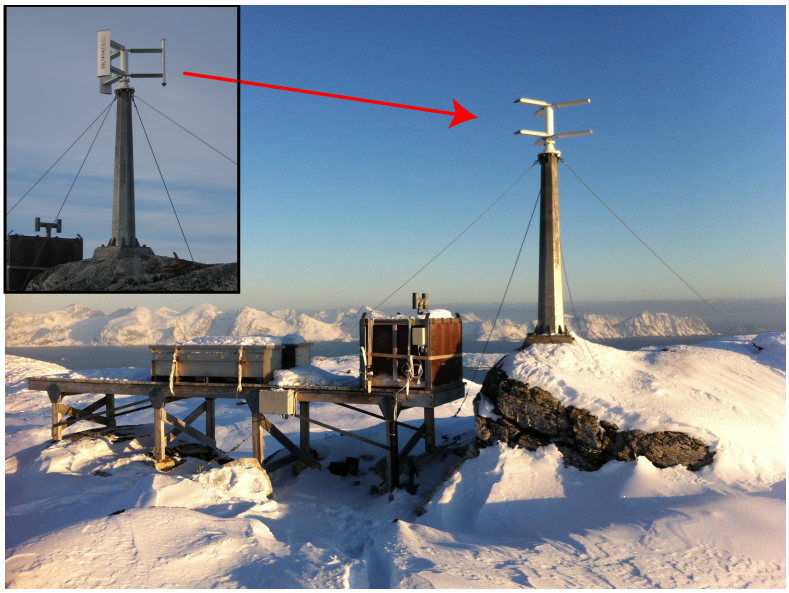

Figure 5.1. *Example of failed vertical axis turbine implementation. Ropatec turbine installed on repeater station "Top300". Lost the blades after 6 months operation in a winter storm with an maximum 10 minute average wind speed of 38 m/s.*

climate, turbine selection, icing risk, ground conditions, infrastructure, and environmental issues are needed.

5.2 Site assessment

To select turbines for complex sites, some basic parameters need to be known. The most important climate parameters are; the average wind speed (10-minute), extreme 50-year wind speed, turbulence intensity, wind shear over rotor plane, icing risk/accumulation, and inflow angle. To estimation power production, statistical wind speed distribution, estimated icing periods, and turbulence intensity are needed.

5.2.1 Initial wind resource assessment

The wind resource assessment is often split in to three levels related to the used data sources and the expected uncertainties in AEP. Level 1 ±50%, level 2 ±30% and level 3 ±10%. Level 1: screening of public available monitoring data, reanalysis data, and world wind maps etc. Level 2: modeled wind resource on microscale level, based on public data. Level 3: on-site measurements or on-site validated microscale modeled wind resource including long-term correction.
Before any wind site/area is selected, some initial studies are recommended (level 1+2), using available data, to estimate the potential and minimize the project risks. Based on the experiences from this and previous projects the following studies are recommended:

- In coastal areas the ocean wind and local climate station observation

- The katabatic outlet pattern (Infrared ASAR pictures) from the ice cap to the area combined with the main terrain shape (DEM)

- Atmospheric reanalysis data for the area, such at the 10 km ASR

- Meso- and/or microscale mapping of the wind resource in the region

For larger projects long-term high-resolution mesoscale mapping can be used to roughly estimate the wind resource and the extreme wind speeds, turbulence, and so on. For smaller projects (mini and micro turbines), the potential area is smaller, the budget does probably not allow for advanced modeling, and therefore potential sites must be selected based on other sources, as climate station and terrain.

5.2.2 Site selection

Based on the initial wind climate study, potential wind turbine sites can be selected, however not only the wind resource affecting the project feasibility. Parameters as; grid connection point, access roads, ground condition and for isolated power systems the local consumption is vital for these projects.
High-voltage cables are traditional protected by steel shells and attached to the ground and/or buried in the ground. The cost of this type of cable connection is very high due to the high labor and material consumption. For the open land two alternatives are available; traditional overhead line elevated by masts or poles, and ground-based heavy armor shielded cables, loosely attached to the ground. Both type has been used at the American bases in Greenland for decades and allow easy inspection, cheap and flexible installation and maintenance. For all types, the cost scale with the distance from site to connection point.
Greenland has a very limited transport infrastructure based on roads. Outside the cities only a limited number of low class gravel roads are available. The existing harbor and harbor connection roads are not necessarily able to handle the heavy transports related to wind turbine installations, [Sæbø et al., 2012]. Upgrade and/or new construction of harbor and access roads need to be assessed in the site selection. Road and harbor, construction and maintenance costs, are highly dependent on local material resources and available machinery, however these costs will be above average for Greenlandic turbine projects. To reach the best wind resource at elevated sites a considerable road length is need, cause of the climbing ability of the transports are limited to 7% (15 m road per m climb). For straight roads chain pulling, with multiple bulldozers and trucks the climbing ability can be doubled.
The ground conditions are another limitation for the sites. Greenlandic wind turbine foundations must, due to construction regulation, be located on bedrock, however access roads can pass more challenging soil types. The mechanical properties of the Greenlandic bedrock vary a lot from very strong to porous and this affect the foundation costs. Most wind turbine foundations are based on on-site casted steel reinforced concrete. This design will challenge the available concrete supply chain and short construction period available, 4-5 months. For other cold climate sites pre-casted foundation segments has been used and if the bedrock quality allows it a combination of traditional gravity and rock anchor foundation.
The site selection/evaluation can be grouped in some main tasks:

- Wind climate
- Potential grid connection points, access roads, ground conditions, etc.
- Terrain slopes, both close to the site (5 x total height) and further out (20 x total height)
- Obstacles in the area through GIS-maps, orthophoto, and site inspection
- Site restrictions such as drinking water catchment areas, birds and aviation restriction zones, and distances to neighbors, (Data available in NunaGIS)

Some cost-based site optimization/selection tools is available and could be useful for large-scale studies, however the models has to be modify, to account for the special conditions, and will therefore only be an advantage for larger projects.

5.3 Site wind resource assessment

When one or some sites are selected the wind resource have to be verified with a bankable certainty, level 3, ±10% on AEP or maximum ±3% on the horizontal wind speed. To fulfill this limit some kind of on-site monitoring are required to validate modelled wind resource. The on-site monitoring must fulfill the IEC 61400-1 and include; wind speed, icing conditions, inflow angle, wind shear over rotor, turbulence intensity, extreme wind speed etc., [Jakobsen and Hansen, 2016a].
Based on the experiences gathered in this project some general guidelines for measurement installation are developed. For installations at high-altitude sites or on the east coast, the measurement installation must be designed to withstand at least 70 m/s 10 minute average wind speeds, turbulence IEC class A and moderate to high icing (ISO 12494 class G3-4, R5-8). For sea level sites 60 m/s, turbulence IEC class A and low to moderate structural icing.
In general, most Greenlandic sites fit into the IEC 61400-1 class IIIA with U50 10-minute average winds less than 37.5 m/s, but for high-altitude sites, Cap Farewell area and in the steepest runoff areas of the ice cap, winds can reach class 1 or even S. For high-altitude and coastal sites the icing risk is highest, because high humidity and low temperatures often are present.

5.4 Wind turbine selection

Turbine and equipment selection for Cold Climate Complex Terrain (CCCT) sites is a complicated task, which involves a lot of project critical choices. An incorrect design parameter, risk assessment or modification can be very expensive and affect the feasibility of the whole project. Large component replacements, in these remote areas, are very expensive because it involves long transport time, low site accessibility, no heavy-lift equipment in the area, and long periods with challenging climate conditions.

5.4.1 Turbine size

For isolated energy systems the implementable wind power capacity is highly dependent on the system design and consumption patterns see chapter 2. When the maximum wind power capacity is determined the number and size of turbines can be set. The infrastructure and local equipment, harbor, roads and crane capacity must be considered when the turbine size and number are evaluated. Generally large turbines are cheaper capacity compared to small, however the new generation multi MW wind turbines (at the moment $>$ 5 MW) is not field tested to a stage where if it recommenced for these conditions. Robust turbines with a long track record are currently available from around 500kW up to 3MW. Smaller turbines are available from small manufacturers, however there fleet will be small and thereby the track record of their turbines.

5.4.2 Turbine type

While far the most modern wind turbines are upwind, three bladed, active pitch controlled machines there are differences. The most obvious difference is between the classical gear-box based drive train design and the direct drive versions. The classical design has a more

than 30 year track record and has some known weaknesses.
The direct drive (DD) can be split in to two versions, inner or outer ring stator. Some direct drive turbines basically maintained the classical design with a hub and main shaft and connected a permanent generator in the end, were the gearbox use to be. Some redesigned all the drive train and basically integrated the generator in the rotor section. The low rotational speed requires a large generator diameter. The DD has in most cases less critical components and thereby less potential failures, however the technology need to mature in the turbine business before the full potential is gained.
For the generator part two main types are available; Permanent Magnet Generator (PMG) and doubly-fed induction generator (DFIG), both with full power converter (FPC).

The main focus for the remote Cold Climate Complex Terrain (CCCT) sites must be reliability and thereby a long track record. The DD-DFIG design has a long track record and a good reputation; however it is a heavy and expensive design. The DD classic main shaft design with PMG is also heavy and expensive, but also very robust. The DD-PMG rotor design is lighter and cheaper, but still in the evolution process. The classical geared design has a long track record and the gearboxes are generally very reliable, but it involves many extra parts and need power for oil tempering in low wind periods.
For CCCT sites the preferred turbine types is DD-DFIG or classical main shaft PMG design, however the main focus is a strong design.

5.4.3 Control and diagnostics

Modern turbines are equipped with advanced supervisory control and data acquisition (SCADA), constantly monitoring the performance of all main components. The standard setup includes a long range of accelerometers, thermometers, cameras etc. Selected turbines or sites are further equipped with Turbine Load Control systems, monitoring the deformations of the blades, tower sections etc. for safe and optimal operation in abnormal conditions.
The SCADA system sends our alarms if abnormal behavior of components or conditions occur. The alarms are handled by a central diagnostic with turbine specific experts. In most cases the cause is identified and solved remotely, however in some cases technicians need to visit the turbine. The diagnostic systems are in most cases able to detect defects long time before they become critical and thereby plan for a replacement in the best possible season.

The turbine SCADA system is linked to a site server or for isolated system to the power system master controller.

5.4.4 Cold climate & complex terrain modification

Standard turbines are not default applicable for cold climate complex terrain sites, however most turbine manufactures has cold climate packages and some risk mitigation setups for complex sites. The cold climate packages often include:

- Blade de-icing system
- Heated yaw bearing and lubrication system
- Heated gearbox and oil systems
- Heated main bearings and lubrication system
- Low temperature coolants
- Nacelle heating system

Some manufactures has sold standard turbines for cold climate areas or turbines only with blade de-icing. In many cases this will only lead to minor problems in the first years of operation, however increased wear on bearings, pumps, yaw gears, yaw ring etc. will increase the maintenance costs on the long range.

Complex terrain often involve periods on increased turbulence, large variations of the wind direction, abnormal wind shear etc. To minimize the loads these turbines are often equipped with; turbine load control systems, the main shaft is strengthened, larger main bearings, increased number of yaw gears, strengthened tower sections etc. These turbines are IEC 61400-1 class S turbines and will be significantly more expensive than the standard version, depending on the amount of modifications. On average the additional costs for S class turbines are 25% more.

5.4.5 Operation & Maintenance

Operation and Maintenance (O&M) of wind turbines on very remote locations with challenging climate condition require detailed planning from the beginning of the project. All turbines need a yearly service by highly skilled technicians and multiple visits for error correction of less skilled technicians. The visit frequency is very individual from turbine to turbine and depends for example on; model, wind conditions, service quality, and O&M planning. For turbines in larger parks the mean time between visits are 12-15 days and some days longer for turbines our side parks.
For remote areas like this some extra planning is required. Two local technicians can with advantage be trained (GWO level 3) to handle the unplanned visits. Travel routes for high level technicians, and spare parts etc. For some sites helipads, snowmobile routes, emergency shelters, local tooling storage etc. must be established.
The nacelle of modern MW-size DD turbines are designed width focus on serviceability and most tasks can be handled indoor. There are access to all parts/rooms of the from the tower/nacelle and limit the outdoor work.
The turbines are designed for 10% main component replacement over the lifetime. The risk of main component failure and a replacement plan is therefore recommended. The blades also need service and the surface need surface dressing to neutralize erosion. Both

main component replacements and large-scale blade service requires longer periods of outdoor work and thereby carefully planning to minimize the entailed down time.

The turbine manufactures provide a wide range of service and warranty packages. Most turbines are delivered with a 5 year warranty, including component and availability warranty, remote diagnostics and schedule service. The warranty can be extended to year 20.

5.5 Icing assessment

Most parts of Greenland have periods of cold weather and thereby a risk of structural icing. The icing can affect wind monitoring and turbine operation, and need to be addressed on an early stage of a wind power project.
For icing to occur, the temperature must be at or below the freezing point, and high humidity is often involved. An exception is freezing rain where super-cooled rain freezes on a surface or rain freezes on cold structures. Icing reports from Greenland are often related to fog/clouds or wet snow hitting cold structures and forming the classical rime ice. Most icing is reported in the coastal mountain regions, where humid air from the sea passes cold elevated structures.
Most Greenlandic communication stations are installed in these areas. The stations are regularly inspected, all year around, and most icing reports come from these inspections. Two examples of structural icing of communications stations are shown in Fig. 5.2. The first example is from the station Tref, close to Nanortalik, South Greenland, and shows light rime icing where the structures are covered with a few centimeter of ice. In the next figures Fig. 5.2c and Fig. 5.2d, an example of heavy icing from Qingaaq station, east of Nuuk, 2009, is shown. The station is located on a small island 1600 m AMSL in the large Godthaabsfjord, exposed to humid air from all directions.

Heavy icing events, such as Qingaaq 2009, are very rare even in these exposed areas. At lower elevations and inland, this type of heavy icing is not reported at all. Several of the communication stations are equipped with small wind turbines and/or solar panels to minimize fuel consumption, and for these installations, ice combined with high wind can be a challenge. Another location where icing has caused problems is at the Summit station on top of the ice cap. In the period 2007-2013, a 6 kW Proven P11 turbine was in operation at the station and one of the lessons learned from this is that even light blade icing, as shown in Fig. 5.5a, has a large impact on turbine performance.
Modern medium and large size turbines can be fitted with cold climate packages, including blade deicing. The cold climate package, of course consumes some power, but in the case of short icing events, this will be a limited part of the production. The icing risk was described by [Hudecz, 2013], who conducted a detailed study of potential icing periods at the Nanortalik Dump site. Icing was identified in 27 hours of the first year, or 0.3% of the time, but some methods indicated longer periods of light icing, though these could not be verified. A two year study was conducted in this project, based on the new instrumentation (heated ultrasonic vs. cup relation). 18 hours of potential icing was identified, and based on this, icing is not considered as a big problem at the Nanortalik dump site Fig. 5.3.

Different filter was used to identify the icing affected periods. The effect of the filters on

the collected data for 2013 is demonstrated Fig. 5.3. The raw 10 minutes average wind speeds is plotted Fig. 5.3a and it is clear that some deviations a present. The heated sonic anemometer, "Usa-1 Usonic", is not as stable in operation as the cup anemometer, and therefore a number of the 10 minutes values is lower for the cup. Ideal two identical instruments should be used (one heat and one unheated), but this was not available for this study. The difference between the used instruments is primarily affecting; the wind speed variation-response (sample vs. continues and inertia), and flow inclination (tilt) response.
The first filter applied is a temperature filter removing all measurements with temperatures above 3 degree C. The relatively high 3 degree level is used to account for freezing rain and other high temperature phenomenons. The temperature filter did not affect the potential icing effected data ($Usonic > Cup$) Fig. 5.3b.
The next filter level is a wind speed filter that extract all data were ($Usonic > Cup + 1m/s$). The used high quality instruments should be able to measure the horizontal wind speed within a few percent; however the drag on the cups will change when the ice is building up on their surface and slow down the spinner. The 1 m/s offset is chosen because only significant icing, that will effect resource monitoring and later on the turbine is of interest Fig. 5.3c. Measurements corresponding to 18 hours per year exceed this limit and these 18 hours covers tree events; December 13.(14 hours), January 8. (8 hours), and April 11. (5 hours) or 27 hours in total.
The icing events are often related to high humidity levels and a humidity filter is a good tool to spot the events. Both the December and January event is easily spotted by the combined filtering, while the April event is not that significant Fig. 5.3d.

The December 13 icing event is a classical Greenlandic icing event, where a rapidly change in the weather, wind direction change from Northwest to East, change the weather situation Fig. 5.4. The humidity is high, and when the temperature drops to subzero the icing risk is high. In the morning there is a period with positive temperatures where the cup de-ices, but when the temperature drops the ice is building up again. The maximum wind speed deviation is observed around noon and decreases in the afternoon. The temperature stay below zero, however the icing effect on the cup drops with the relative humidity level. This indicate that the cup anemometer is able to de-ice in subzero temperatures when no more humidity/ice is added. The same behavior is observed for January, 8. 2014, while the April event ends with positive temperatures.

5.5.1 Handling of icing

In most wind resource assessment processes, icing is handled, simply by excluding the periods where icing is detected. If the icing frequency is low, this is not a problem for the resource estimation (Statistical distribution of the basic parameters). If longer periods of is observed this method can affect the relation between the observed and actual wind variability. In these cases heated instruments must be used for the wind resource assessment.
Icing will affect the turbine performance, but a relation between the instrument icing and potential blade icing is difficult to predict. How the ice buildup on the blade surfaces is a difficult process that depends of a lot of parameters [Hudecz, 2013] and to predict the

on rotor performance is even more complex.
To minimize the blade icing, cold climate turbines will often be equipped with a deicing system. The turbine controller detects icing either by vibrations or by decreasing rotor performance. When ice is detected the process is; to pitch out of the wind to stop the rotor, activate the blade heating for a predefined period, and then go back to operation. The interval between these cycles depends among others on the actual ice rate.
In this way, icing affects the AEP by lost production in the stop and buildup period, and for powering the deicing system. The effect on the AEP depends both on turbine and climate, and can be significant. The icing effects have to be assessed in all cold climate projects and mainly in the wind resource and site assessments.

(a) *Tref (N60°12.956, W045°22.10, 900 m AMSL)*

(b) *Tref with light rime icing.*

(c) *Qingaaq (N64°23.63817′, W051°05.96817′, 1600 m AMSL)*

(d) *Qingaaq with heavy icing.*

Figure 5.2. *Examples of structural icing at Greenlandic communication stations, all pictures provided by Steen Grossmann at Tele.*

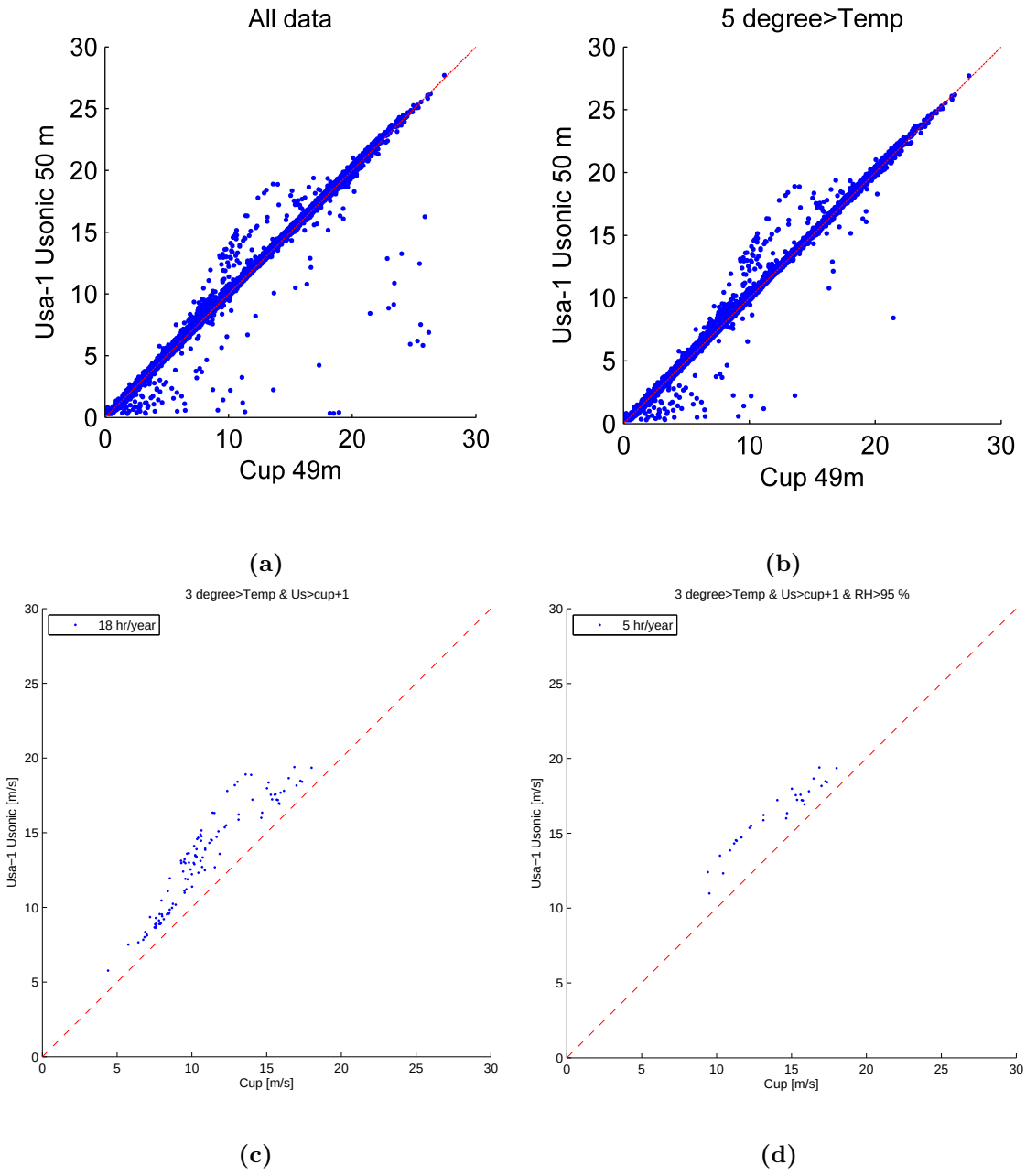

Figure 5.3. *Ice detection example for 2013-14 by filtering heated ultrasonic and cup data, based on 12-month data sets.*

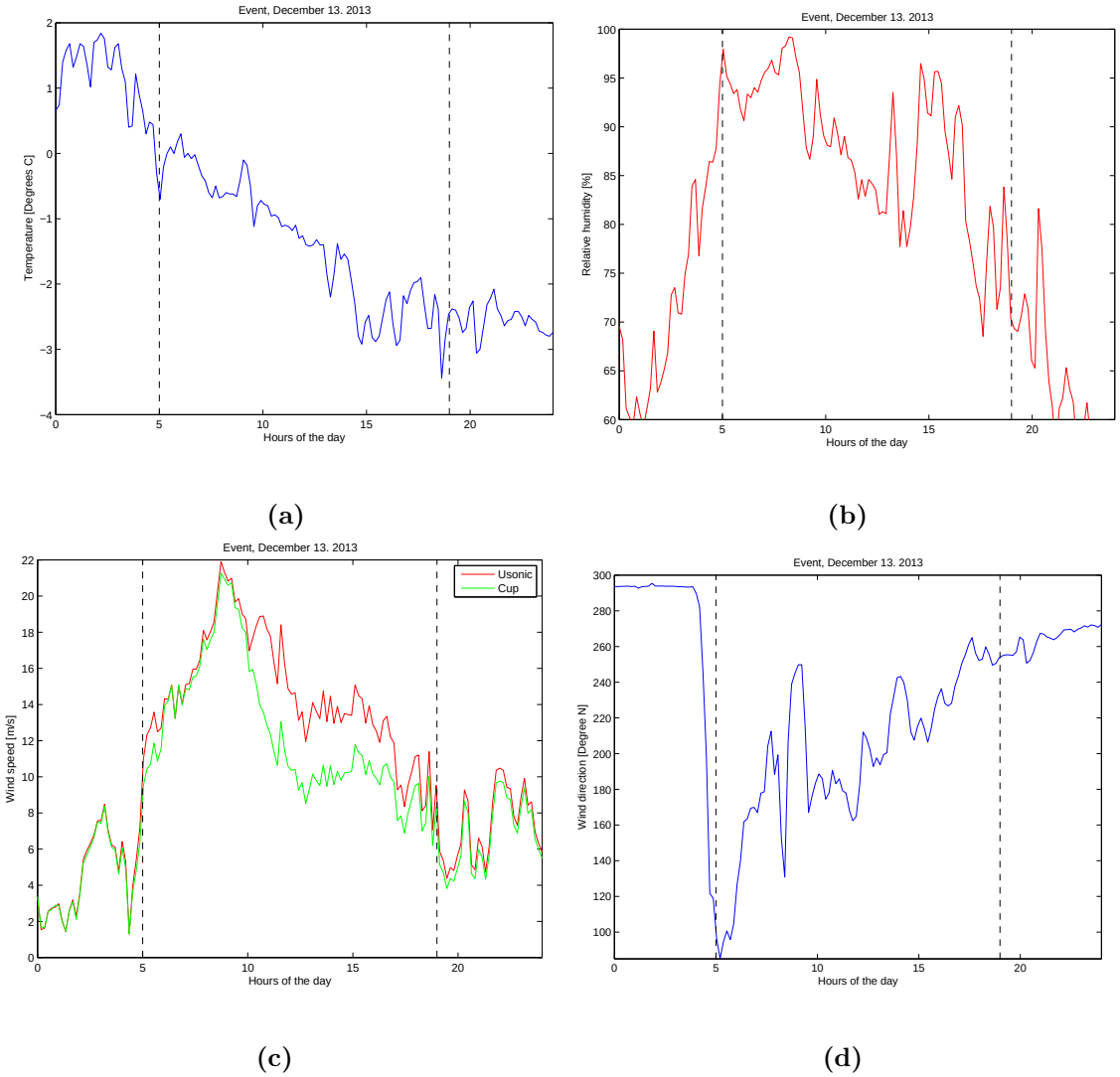

Figure 5.4. *Potential icing event December, 13. 2013, selected by data filtering on Nanortalik dump site.*

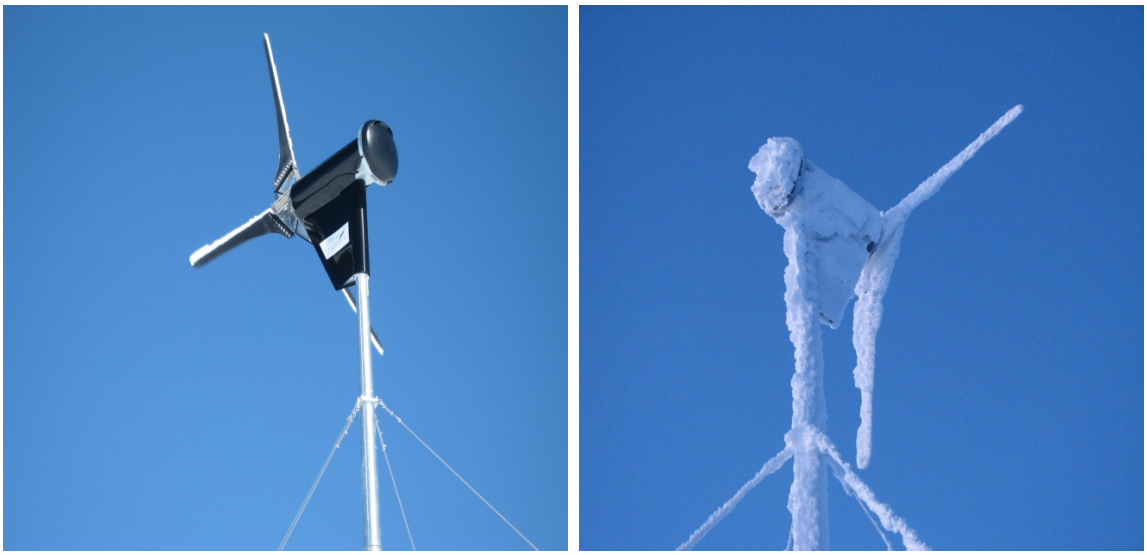

(a) *Summit wind turbine, light icing (N72°34.62′W38°27.08′ 3200 m AMSL)*

(b) *Summit wind turbine, fully iced*

Figure 5.5. *Icing of wind turbine at Summit station, (Figure credit; Tracy Dahl, CH2M Hill Polar Services).*

5.6 Wind turbine installation

To select an optimal site in very complex terrain is a challenging task and requires a lot of data. Extremely high local material and labor costs can make a small mistake or omission very expensive. Cable connection and road construction are often crucial for the site selection, but in some situations, existing roads or planned roads can be used reduce the costs [Sæbø et al., 2012].
For turbines above $\approx 60kW$, service and supply roads are normally needed. The road requirements depend on the turbine size and the terrain, but a normal width is 4.5m and more in the curves. For areas with very steep slopes, the installation crane can be used to bring the largest parts from road level to road level and eliminate turning radius problems. The prescribed maximum slope for turbine transport on gravel roads is 6-7% , but for straight roads, bulldozers are often used to pull the trucks up, and then slopes up to 15% can be used. The cost of road construction in Greenland is very dependent on the soil, the local access to construction materials, and the necessary blasting work. If the material is available and no blasting is necessary, longer Greenlandic service roads cost in the range 1.1-1.3 mill.DKK/km (250 DKK/m^2) plus crane-pad and storage area. When service roads are in place the foundation work take 4-8 weeks depending on size, design, ground conditions and supply. A traditional gravity foundation (6-700 m^3 concrete) will be very expensive due to the high Greenlandic concrete costs (2.5 times normal prices + extra transport costs). Alternative foundation types were pre-casted concrete or steel structures are used in combination with rock anchors. An example of combined foundations is the McMurdo Wind Farm at Antarctica, where pre-casted concrete footer-blocks is set in to the ground and firmly attached to the bedrock by long anchors. The upper part of the foundation consist in this case of a bolted steel structure, however other sites has successfully used pre-casted concrete structures for this to.

Turbine installation require heavy lift equipment and normally crawler cranes of +300

Figure 5.6. *Combination foundation consisting of pre-casted concrete, rock anchors and a steel structure (Figure credit: Phil Roberts, Meridian Energy)*

tons with extender boom are used. The largest crane available in Greenland is a 120 tons and the installation crane therefore need to be shipped for the installation. A standard

crawler crane is shipped in sections of around 40 tons and can be offloaded by standard cargo ships. The heavy turbine parts as tower sections and nacelle cannot be unload by standard onboard ship cranes and therefore the installation crane need to handle this too. For a project this cause a double crane assembly, extra time and costs. Crane assembly, turbine installation and crane disassembly is a 4-5 day operation depending on the weather conditions etc. The total crane operation is a two week job plus two weeks of transport. In the four week rental period, for a single turbine installation, the crane will only operate 4 days and the crane costs will be high. Multiple turbine installation will of cause reduce the crane cost per turbine. The 120 tons crane available in Greenland can, with small adjustments, be used for support and service jobs, and for turbine erections up to around 500 kW.
For smaller turbines under $60kW$, helicopter installation can be a good alternative to roads and cranes, Fig. 5.7a. The lift capacity of rentable helicopters sets the limit for turbines at around the 60 kW, depending on turbine design. The 6 kW, Proven P11, test turbine installed in relation to this project was installed by helicopter, in one piece, but larger turbines need to be installed in sections. A detailed description of the project is available in Appendix D. Other important factors in the process selection are; service and decommissioning.

Service will require some lifting capacity; however for $<$ 60 kW turbines this can be

(a) *Test turbine installation at Sarfannguit site 1, heli-lift from the harbor to the site, August 2009.*

(b) *Test turbine installation at Sarfannguit site 1, cabling and adjustments, August 2009.*

Figure 5.7. *Sarfannguit wind turbine installation, personal pictures*

handled by local helicopters.

5.7 Conclusion drawn from the WP development

The isolated grids, the terrain, and the harsh climate, challenge the Greenlandic wind power development, but high energy costs and the year-around heat demand is an advan-

tage for wind power. The experiences gained in the early experiments with wind power, was not followed up, as the technology evolved. The one-sided focus on hydro power utilization, has stopped the exploration of other resources and technologies. For areas without hydro power resources, this narrow political focus, has been very expensive and affected the local development.
The Greenlandic power system has in this project been grouped into three system types; village, city diesel, and hydro/industry systems. In the village systems, small turbines ($<$ 100 kW), in combination with PV, energy storage, and modern system design, has a large potential. Most of these systems will be able to cut at least 50% of their diesel consumption by savings, system optimization and RE implementation and in areas with high wind resources a 50% RE penetration is possible.

The city diesel system can in the same way include both wind and PV, but the district heating systems in these cities can absorb excess energy and thereby increase the optimal and acceptable RE capacity. Some of these systems can implements small commercial size turbines (1-2 MW) and thereby lower the costs and minimize the risks. A verified high wind resource and good infrastructure is the key to success for wind projects in the cities.

The hydro cities and larger industrial system can handle large commercial turbines and thereby get wind power at the lowest costs. The infrastructure (harbor, roads and over-headlines) around the larger cities and industrial installations are often more developed and can be utilized for large RE projects. The lowest production costs can most likely be obtained in these systems, but the energy prices is also lowest in these systems. The most sustainable wind and PV projects will probably be found in the largest city diesel systems.

In the cost distribution of future Greenlandic wind projects, the wind turbine cost will only be a small fraction of the total budget, and if the site condition requires an S-class turbine owing to high extreme winds or turbulence, this will only have a minor effect on the total budget. If the wind resource is good at a particular site, but for example the extreme wind speed exceeds class 1, (50m/s), the 20-30% extra cost for an S-class turbine might be a good choice, compared to other sites with poorer wind resources. Usable wind resources are available in the fjord systems, in the mountains, off the coast, and especially in the Cape Farewell area.
A wide range of data sources and modeling tools can be used to get an idea of the wind climate in an area, even before any measurements are done. The studies done in this project, has shown how important a proper pre-studies is for wind power projects. Mesoscale models are a good tool, especially for large-scale planning, but there is still some work to be done before full accuracy can be achieved in Greenland.
Construction work in these remote areas, with harsh climate, require detailed planning and this will challenge potential wind power projects. The experiences from the Nuuk test, this project and other larger project show that long-term planning, flexible budgets, time for bad weather periods and skilled technicians is crucial for success in this environment. Experiences from Canada, Northern Norway, the Faroe Islands and Antarctica show that wind power are applicable in cold climate complex terrain areas.

Chapter 6

Conclusion

In this project, Greenlandic power systems were sorted into three categories; village diesel, city diesel and city hydropower. Each category was studied generally, and one system in each group was studied in more detail. Overall, it was found that smart meters, together with power plant SCADA data, were a good basis for system analysis, but better access to data (central database rather than local storages) would have made the job much easier. It is recommended that Nukissiorfiit establish a system where high- and low-resolution SCADA data and smart meter data are easy accessible for system updates, regular analysis of system performance, and identification of potential problems. The AMR can together with the SCADA data make the base for RE implementation studies in Greenland

Some ineffective design and control of systems was identified, and the easily accessible savings potential was estimated to be 20% of consumption. On top of this, a considerable amount of oil can be saved by using low-load optimized modern diesel units. The increased low-load efficiency of modern engines not only saves fuel from the time of installation, but also minimizes the efficiency reduction in case of decreasing demand and implementation of RE co-production. The RE potential the small Greenlandic systems is high, but to earn the full potential the control and production units need to be up to date. For most diesel based energy systems, modern energy storage systems was found feasible and further more increases the potential renewable energy penetration.
The waste heat from the diesel generator unit is not utilized very efficiently; often the district heating grid is too small to absorb full production, and in most cases, the heat recovery system is poorly designed and controlled. In general, the waste from the jacket water has to be used, and for the city diesel plants, a full CHP package must be used to utilize at least 80% of the energy. For all diesel systems, PV, wind, and hydro are implementable, and in most cases, the RE sources are profitable.

Wind monitoring in the complex terrain and harsh climate has challenged the measurement systems to their limits and in some cases beyond. Various instruments and towers were tested during the project, and there was not always a strong connection between quality and price. For example, for cup anemometers, the medium-cost version was often better than the cheapest versions, but the high-cost versions were not significant better. The wind conditions were studied for several areas and sites. For the Nanortalik site, a high turbulence level was found in the lower 20 MAG and the same for Sarfannguit 1, while Sarfannguit 2 had very low turbulence intensity all the way down. Monitoring

of surface wind is in general difficult in this terrain, but if the WMO guidelines or similar are applied, it is possible. This often involves tall tower installations and/or data cleaning and multiple masts for validation purpose. The historical metrological data sets are generally inhomogeneous, often with changes in observation site, instruments, and observation intervals. The oldest historical data also have a tendency to include higher extreme winds and lower mean wind speeds than the new automatically collected data.

Satellite observations of ocean wind, and infrared flow patterns on the ice cap and sea ice proved higher potential to validate models and to derive knowledge about the basic flow patterns in the area. Fjord winds are very difficult to model correctly, but the outlet can be observed in the ASAR-based ocean wind. These, in combination with mesoscale modeling, were found to give a good indication of the wind resource distribution and the main wind directions in most areas.

Two mesoscale models, WRF and Polar WRF were validated against 14-point measurements for an 800 x 800 km domain, and the flow patterns were compared to satellite observations. Some errors were found and tracked back to erroneous elevation data (version 1) and sea ice (version 2), but how large an effect the incorrect data had on the performance in the different parts of the domain is unknown, though some areas were found highly affected. The comparison between the models and the ocean wind data showed a shift in space of the high-wind areas related to the Greenlandic tip jet, and again the WRF was not able to model outlet from the fjords. The potential used of mesoscale models for wind resources estimation is high, at least for larger planning. To achieve the full accuracy in further runs, the input-data need to be validated and the model resolution to be on a level that reflect the local terrain of the fjord system areas.

To model the atmosphere correctly, high quality and resolution surface data is needed. Multiple elevation model dataset was studied for both micro- and mesoscale modelling resolution. Many incorrect data was found, but the general outcome of these studies is the combined models are best, and the elevation data need to be validated before use. Other surface data problems were discovered in the commercial sea ice data. These also need to be validated and often corrected before implementation. Surface data correction in this terrain is not trivial, but modern high-resolution satellite data is useful in these processes.

The wind application model WAsP was tested and used for site selection and estimation of power production. The model performed well within 500 m of the Sarfannguit test site and will be usable for local studies. Other tests in, e.g., Sisimiut and Uummannaq showed that above 500 m, the accuracy decreased, typically due to meteorological features or flow separation. The selected test-site, Sarfannguit 2, showed a great improvement from the site 1 resource, from 5.5 to 6.1 m/s at 10MAG which was very close to what was estimated by the model.
A larger test with tall towers and distances up to 10 km was launched, in the Nanortalik area, but the data collection has not been launch yet. The towers was placed at strategic locations with different flow conditions; one mountain top site at Qaqqarsuasik (525m AMSL) with free inflow from most directions, a fjord outlet site at the Maligissat Qaqqaa tongue (185m AMSL) and the current flat terrain Nanortalik site 1601 (19m AMSL). The locations make the sites ideal for cross-prediction test of local microscale models and

mesoscale test of different flow types (fjord outlet, high altitude and sea-level mountain wave affected). Tall tower observations were used to minimize the surface and object effect on the observations and get up in a turbine relevant height.

General mesoscale models was found used full for resource mapping and flow studies of larger areas, while the microscale model is good for very local planning. Combined models were not tested due to lag of resources.

Chapter 7

Further work

Although during the years of PhD study, several topics related to arctic wind power were investigated, the findings have raised a number of questions and have given ideas for further improvements, studies and researches. In this chapter some of these suggestions are listed.

Wind monitoring

On the measurement part, the next step is to start the validation campaign at the two sites in the Nanortalik area.

There is a need of high-altitude measurements to verify models and resources and the new Nanortalik campaign is the first in this direction. Generally the tall tower/LIDAR monitoring sites (40-150m above ground) should be concentrated close to cities that can handle large scale wind integration to utilize the collected data.

The existing monitoring stations must be concentrated at fewer sites, but with higher masts. More specific it is possible to collect the 4 10m tubular tower in the Uummannaq area and build one 40m tower for better observations.

Mesoscale modeling

For the modeling part, the first step is to combine the different data sets to obtain better sea ice and elevation data. In the sea ice case, different high-resolution satellite data as ASAR can be used to optimize the existing data series. For elevation, the GIMP data can be used at the ice cap, but in the mountain regions and in the north, it needs to be corrected for both vertical and horizontal errors.

When new surface data is validated, a new model validation can be worked-out in all inhabited areas, and if it gives reasonable results, a high-resolution (0.1-1 km) long term ($> 10 years$) run can be used to map the overall wind resource distribution in the areas of interest.

Microscale modeling

Performance test of the more advanced CFD based models would be interesting for the future development. Coupled meso-microscale models have high potential if a sufficient performance can be achieve.

System optimization

Optimal use of collected smart meter and SCADA data for system design, grid optimization, and monitoring of the water and power system has a large potential for Greenland. The data is only used for billing today, and the systems are designed and controlled on a very limited basis. The data are collected, but to utilize their full potential, a better

structure and data flow is needed.

Based on this study, solar power has a great potential, at least for the diesel cities/villages, and mapping of the resources to prioritize investments is recommended. The current PV expansion are mainly driven by small private initiatives in the lager diesel based cities. This is an national economic unfavorable solution because of high investment costs, high energy costs and ineffective system control due to many autonomous production units. Larger central systems maybe based on co-operative societies could be a interesting to study.

Battery based energy storage has a large potential for the Greenland energy system. With the latest developments and the expected technological and cost developments, this need to be incorporated in future studies of the Greenlandic systems. Battery storage was not within the scope of this project and was not a part of the system analysis model used in this project; however part of the future work is to incorporate storage strategies in the Greenlandic system models.

References

Aakervik, E., Ydersbond, Y., and Tallhaug, L. (2011). Analysis of wind measurements from Nanortalik, Nanortalik municipality, Greenland. Technical report, Kjeller, Vindteknikk, Kjeller.

Algren, L. (2012). *Feasibility of Photovoltaics in Greenlandic Power Systems*. PhD thesis.

Artz, R. U. S., Ball, G. A., Behrens, K. G., Bonnin, G. U. S., Bower, C. U. S., Canterford, R. A., Childs, B. U. S., Claude, H. G., Crum, T. U. S., Dombrowsky, R. U. S., Edwards, M. S. A., Evans, R. U. S., Feister, E. G., Forgan, B. A., Hilger, D. U. S., Holleman, I. N., Hoogendijk, K. N., Johnson, M. U. S., Klapheck, K.-H. G., Klausen, J. S., Koehler, U. G., Ledent, T. B., Luke, R. U. S., Nash, J. U. K., Oke, T. C., Painting, D. U. K., Pannett, R. N. Z., (China), Q. Q., Rudel, E. A., Saffle, R. U. S., Schmidlin, F. U. S., Sevruk, B. S., Srivastava, S. I., Steinbrecht, W. G., Stickland, J. A., Stringer, R. A., Sturgeon, M. U. S., Thomas, R. U. S., Van der Meulen, J. N., Vanicek, K. C. R., Wieringa, J. N., Winkler, P. G., Zahumensky, I. S., and (China), Z. W. (2010). Guide to Meteorological Instruments and Methods of Observation. Technical report, Meteorological, Wold Organization, Geneva.

Atlason, G. F. and Holm, F. M. (2006). Forundersøgelser for vandkraft i Sarfannguaq. Technical report, Technical University of Denmark.

AWS Scientific, I. (1997). Wind Resource Assessment Handbook. Technical report, National Renewable Energy Laboratory, Golden.

Badger, J., Frank, H., Hahmann, A. N., and Giebel, G. (2014). Wind-Climate Estimation Based on Mesoscale and Microscale Modeling: Statistical–Dynamical Downscaling for Wind Energy Applications. *J. Appl. Meteorol. Climatol.*, 53(8):1901–1919.

Badger, M. (2008). Ocean winds from synthetic aperture radar. *Ocean Remote Sens. Recent Tech. Appl.*, pages 31 – 54.

Bakalian, F., Hameed, S., and Pickart, R. (2007). Influence of the Icelandic Low latitude on the frequency of Greenland tip jet events: Implications for Irminger Sea convection. *J. Geophys. Res.*, 112(C4):C04020.

Ball, F. (1956). The Theory of Strong Katabatic Winds. *Aust. J. Phys.*, 9(3):373.

Bamber, J. L., Ekholm, S., and Krabill, W. B. (2001). A new , high-resolution digital elevation model of Greenland fully data. *J. Geophys. Res. B Solid Earth*, 106(B4):6733–6745.

Baunbaek, L. (2013). Grønlands energiforbrug 2012. Technical report, Grønlands Statistik.

Bechmann, A. and Sørensen, N. N. (2011). Hybrid RANS/LES applied to complex terrain. *Wind Energy*, 14(2):225–237.

Bjerknes, J. and Solberg, H. (1922). Life cycles of cyclones and polar front theory of atmospheric circulation. *Geofys*, 3:3–18.

Box, J. E. (2004). Greenland ice sheet surface mass balance 1991–2000: Application of Polar MM5 mesoscale model and in situ data. *J. Geophys. Res.*, 109(D16):D16105.

Bromwich, D. H., Cassano, J. J., Klein, T., Heinemann, G., Hines, K. M., Steffen, K., and Box, J. E. (2001). Mesoscale Modeling of Katabatic Winds over Greenland with the Polar MM5.

Cappelen, J. (2004). Klimaobservationer i Groenland 1958-99. Technical report, DMI, Copenhagen.

Cappelen, J., Jørgensen, B. V., and Laursen, E. V. (2001). DANISH METEOROLOGICAL INSTITUTE The Observed Climate of Greenland , 1958-99 - with Climatological Standard Normals , 1961-90 Klimaobservationer i Grønland , 1958-99. Technical report, DMI.

Cappelen, J., Kern-hansen, C., Vaarby, E., and Viskum, P. (2013). Technical Report 13-04 Greenland - DMI Historical Climate Data Collection -with Danish Abstracts John Cappelen (ed) Colophon Other contributors :. Technical report, DMI.

Cassano, J. J. (2001). Evaluation of Polar MM5 simulations of Greenland's atmospheric circulation. *J. Geophys. Res. Atmos.*, 106(24).

Cassou, C. (2004). North Atlantic winter climate regimes: Spatial asymmetry, stationarity with time, and oceanic forcing. *J. Clim.*, 17(5):1055 – 1068.

Christiansen, M. B., Koch, W., Horstmann, J., Hasager, C. B., and Nielsen, M. (2006). Wind resource assessment from C-band SAR.

Danielson, J. J., Gesch, D. B., and Geological, U. S. (2011). Global Multi-resolution Terrain Elevation Data 2010 (GMTED2010). Technical report, U.S. Geological Survey.

Davies, T. (2002). Adiabatic formulation of models. Technical report, The European Centre for Medium-Range Weather Forecasts.

Dee, D. P., Uppala, S. M., Simmons, a. J., Berrisford, P., Poli, P., Kobayashi, S., Andrae, U., Balmaseda, M. a., Balsamo, G., Bauer, P., Bechtold, P., Beljaars, a. C. M., van de Berg, L., Bidlot, J., Bormann, N., Delsol, C., Dragani, R., Fuentes, M., Geer, a. J., Haimberger, L., Healy, S. B., Hersbach, H., Hólm, E. V., Isaksen, L., Kållberg, P., Köhler, M., Matricardi, M., McNally, a. P., Monge-Sanz, B. M., Morcrette, J.-J., Park, B.-K., Peubey, C., de Rosnay, P., Tavolato, C., Thépaut, J.-N., and Vitart, F. (2011). The ERA-Interim reanalysis: configuration and performance of the data assimilation system. *Q. J. R. Meteorol. Soc.*, 137(656):553–597.

Dragsted, J. (2011). Solar heating in Greenland. Technical report, DTU Civil Engineering Report R-240 (UK).

REFERENCES

Dragsted, J., Jakobsen, K. R., Larsen, E., and Hudecz, A. (2012). Fyrtaarnsprojekt VI - afsluttende 2012. Technical report, DTU, 2012 BYG Danmarks Tekniske universitet.

Dragsted, J., Villumsen, A., Larsen, E., Jakobsen, K. R., Hudecz, A., Kotol, M., and Villumsen, O. (2011). Fyrtaarnsprojekt V - afsluttende report 2011. Technical report, BYG DTU, WEB.

Dudhia, J. (1989). Numerical study of convection observed during the winter monsoon experiment using a mesoscale two-dimensional model.pdf. *J. Atmos. Sci.*, 46(20):3077–3107.

Duraisamy, V. J., Dupont, E., and Carissimo, B. (2014). Downscaling wind energy resource from mesoscale to microscale model and data assimilating field measurements. *J. Phys. Conf. Ser.*, 555(1):012031.

DuVivier, A. K. and Cassano, J. J. (2013). Evaluation of WRF Model Resolution on Simulated Mesoscale Winds and Surface Fluxes near Greenland. *Mon. Weather Rev.*, 141(3):941–963.

ECMWF (2006). IFS DOCUMENTATION Cy31r1. Technical report, European Centre for Medium-Range Weather Forecasts, Shinfield Park.

Ekholm, S. (1996). A full coverage, high-resolution, topographic model of Greenland computed from a variety of digital elevation data. *J. Geophys. Res. B Solid Earth*, 101(10):21961 – 21972.

Finnby, A., Paal, B., and Lem, B. M. (2011). Wind resource analysis and implementation in Nanortalik system. Technical report, DTU, Nanortalik.

Gesch, D. B., Verdin, K. L., and Greenlee, S. K. (1999). New Land Surface Digital Elevation Model Covers the Earth. *Eos, Trans. Am. Geophys. Union*, 80(6):69–70.

Gesch, D. B. U. and Greenlee, S. U. (2004). Global Digital Elevation Model (GTOPO30). Technical report, U.S. Geological Survey, EROS, Redlands, California, USA.

Golder, D. (1972). Relations among stability parameters in the surface layer. *Boundary-Layer Meteorol.*, 3(1):47–58.

Grabow, V. R. (2013). Potentialer for udnyttelse af PV i Groenland. Technical report.

Greatbatch, R. J. (2000). The North Atlantic Oscillation. *Stoch. Environ. Res. Risk Assess.*, 14(4):0213–0242.

Grégoire, L. I. (2013). Rural Electrification with PV Hybrid Systems. Technical report, INTERNATIONAL ENERGY AGENCY.

Grumbine, R. W. (1996). Automated Passive Microwave Sea Ice Concentration Analysis At NCEP. Technical Report March, National Ocean and Atmospheric Administration.

Hall, C. M., Hansen, G., Sigernes, F., and Kuyeng Ruiz, K. M. (2011). Tropopause height at 78° N 16° E: average seasonal variation 2007 2010. *Atmos. Chem. Phys.*, 11(11):5485–5490.

Hansen, K. S. and Hansen, K. S. (2007). Vindenergi i Grønland. In Villumsen, A., editor, *Vindenergi i Grønl.*, page 7, Sisimiut, Groenland. Arctic technology center, DTU.

Hansen, K. S., Villumsen, A., and Hansen, M. (2006). Fyrtårnsbygd - 083 Sarfannguaq. Technical report, DTU.

Harden, B. (2012). *BARRIER WINDS OFF SOUTHEAST GREENLAND AND THEIR IMPACT ON THE OCEAN*. PhD thesis.

Harden, B. E., Renfrew, I. a., and Petersen, G. N. (2011). A Climatology of Wintertime Barrier Winds off Southeast Greenland. *J. Clim.*, 24(17):4701–4717.

Hasager, C. B., Pena, A., Christiansen, M. B., Astrup, P., Nielsen, M., Monaldo, F., Thompson, D., and Nielsen, P. (2008). Remote Sensing Observation Used in Offshore Wind Energy.

Heinemann, G. (1999). The KABEG'97 field experiment: An aircraft-based study of katabatic wind dynamics over the Greenland ice sheet. *BOUNDARY-LAYER Meteorol.*, 93(1):75 – 116.

Heinemann, G. and Klein, T. (2002). Modelling and observations of the katabatic flow dynamics over Greenland.

Hersbach, H. (2007). An improved C-band scatterometer ocean geophysical model function: CMOD5. *J. Geophsical Res. C-Oceans*, 112(C3).

Hines, K. M. and Bromwich, D. H. (2008a). Development and testing of Polar Weather Research and Forecasting (WRF) Model. Part I: Greenland ice sheet meteorology.

Hines, K. M. and Bromwich, D. H. (2008b). Development and Testing of Polar Weather Research and Forecasting (WRF) Model. Part I: Greenland Ice Sheet Meteorology*. *Mon. Weather Rev.*, 136(6):1971–1989.

Hines, K. M., Bromwich, D. H., Bai, L.-S., Barlage, M., and Slater, A. G. (2011). Development and Testing of Polar WRF. Part III: Arctic Land*. *J. Clim.*, 24(1):26–48.

Holm, F. M. (2008). Videregående analyser af vandkraftpotentialet for Sarfannguaq. Technical report.

Hong, S.-y., Noh, Y., and Dudhia, J. (2006). A New Vertical Diffusion Package with an Explicit Treatment of. *Mon. Weather Rev. USA*, 134:2318–2341.

Howat, I., Negrete, A., and Smith, B. (2014). The Greenland Ice Mapping Project (GIMP) land classification and surface elevation datasets. *Cryosph. Discuss*, 8(1):1–26.

Hudecz, A. (2013). Icing Problems of Wind Turbine Blades in Cold Climates. Technical Report November, Department of Wind Energy, Technical University of Denmark, Kgs.Lyngby.

Hurrell, J. W. (1995). Decadal trends in the north atlantic oscillation: regional temperatures and precipitation. *Science*, 269(5224):676–9.

REFERENCES

Hurrell, J. W. and Deser, C. (2009). North Atlantic climate variability: The role of the North Atlantic Oscillation. *J. Mar. Syst.*, 78(1):28–41.

Hvidegaard, S. M., Sandberg Sørensen, L., and Forsberg, R. (2012). ASTER GDEM validation using LiDAR data over coastal regions of Greenland. *Remote Sens. Lett.*, 3(1):85–91.

Iversen, H. S. and Kristensen, J. S. (2003). Vindresurser i Groenland. Master's thesis, Danmarks Tekninske Universitet, Kgs.Lyngby.

Jakobsen, K. R. (2009). *Simulering af energiforsyningen i Sarfannguaq*. PhD thesis, Danmarks Tekniske Universitet.

Jakobsen, K. R. and Hansen, K. S. (2016a). Experience of exploring wind resources in west Greenland. *Manuscr. under preperation*.

Jakobsen, K. R. and Hansen, K. S. (2016b). Experience of exploring wind resources in west Greenland.

Jakobsen, K. R., Villumsen, A., Hudecz, A., Andersen, P. H. D., and Grønvold, H. (2011). *Fyrtaarnsprojekt IV 2010*. DTU Byg, Danmarks Tekniske Universitet.

Jakobsen, K. R. and Vincent, C. L. (2016). Evaluation of WRF Mesoscale Model performance for south Greenland. page 13.

James, W. and Agency, U. D. M. (1990). *Digitizing the future*. Washington, D.C, 3rd ed edition.

Janjić, Z. I. (1994). The Step-Mountain Eta Coordinate Model: Further Developments of the Convection, Viscous Sublayer, and Turbulence Closure Schemes.

Jung, T. and Rhines, P. B. (2007). Greenland's Pressure Drag and the Atlantic Storm Track. *J. Atmos. Sci.*, 64(11):4004–4030.

Kellogg, W. (1951). A PROPOSED MODEL OF THE CIRCULATION IN THE UPPER STRATOSPHERE. *J. Meteorol.*, 8(4):222 – 230.

Klein, T. (2002). Modelling and observations of the katabatic flow dynamics over Greenland. *tellus*, pages 542–554.

Konzelmann, T. (1994). PARAMETERIZATION OF GLOBAL AND LONGWAVE INCOMING RADIATION FOR THE GREENLAND ICE-SHEET. *Glob. Planet. Change*, 9(1-2):143 – 164.

Krag, J., Nielsen, T. R., and Svendsen, S. (2002a). Grønlandsk vejrdata Nuuk Uummannaq. Technical report.

Krag, J., Nielsen, T. R., and Svendsen, S. (2002b). Grønlandsk vejrdata Nuuk Uummannaq. Technical report, Department of Civil Engineering at the Technical University of Denmark.

Lerche, M. and Holt, M. (2008). Mikrovandkraft i Groenland Case study for Sarfannguaq. Technical report.

Lundin, E. (2010). Hydropower in Sarfannguaq. Technical report.

Marchesiello, P., Capet, X., Menkes, C., and Kennan, S. C. (2011). Submesoscale dynamics in tropical instability waves. *Ocean Model.*, 39(1-2):31–46.

Moore, G. W. K. (2003). Gale force winds over the Irminger Sea to the east of Cape Farewell, Greenland. *Geophys. Res. Lett.*, 30(17):1894.

Moore, G. W. K. (2005). Tip jets and barrier winds: A QuikSCAT climatology of high wind speed events around Greenland. *J. Clim.*, 18(22).

Moore, G. W. K., Renfrew, I. A., and Cassano, J. J. (2013). Greenland plateau jets. *Tellus a*, 65.

Mortensen, N. G. and Antoniou, I. (2006). IMPROVING WAsP PREDICTIONS IN (TOO) COMPLEX TERRAIN. Technical report, DTU Wind Energy, Roskilde.

Mortensen, N. G. and Bowen, A. J. (2004). WAsP prediction errors due to site orography. Technical report, Risoe DTU).

Mortensen, N. G., Hansen, J. C., and Kelly, M. C. (2012). Wind Atlas for South Africa (WASA) Observational wind atlas for 10 met. stations in Northern, Western and Eastern Cape provinces.

NCAR (2012). Advanced Research WRF (ARW) Modeling System Version 3.

Nielsen, J. E. and Kartic, I. (1993). Solenergipotentiale i Grønland. Technical report.

Nielsen, K. B. (2013). *Design and verification of VAWT*. PhD thesis, Technical University of Denmark.

Nukissiorfiit (2014). Enhedsomkostninger 2013. Technical report, Nukissiorfiit, Nuuk.

Nukissiorfiit, H. (2005). Hydropower resources in Greenlnad. Technical report, Nuuk.

Obukhov, A. M. (1971). Turbulence in an atmosphere with a non-uniform temperature. *Boundary-Layer Meteorol.*, 2(1):7–29.

Orr, A., Hanna, E., Hunt, J. C., Cappelen, J., Steffen, K., and Stephens, A. (2005). Characteristics of Stable Flows over Southern Greenland. *Pure Appl. Geophys.*, 162(10):1747–1778.

Outten, S. D., Renfrew, I. A., and Petersen, G. N. (2009). An easterly tip jet off Cape Farewell, Greenland. II: Simulations and dynamics.

Palmer, C. (1959). Stratospheric polar vortex in winter. *J. Geophys. Res.*, 64(7):749 – 764.

Panofsky, H. (1963). DETERMINATION OF STRESS FROM WIND AND TEMPERATURE MEASUREMENTS. *Q. J. R. Meteorol. Soc.*, 89(379):85 – 94.

Petersen, L. (2014). Grønlandsbefolkning 2014. Technical report, Grønlands statistik.

REFERENCES

Petter Lindelöw-Marsden, Troels F. Pedersen, J., Gottschall, Allan Vesth, R. W. U. P., Michael, and Courtney, S. (2010). *Flow distortion on boom mounted cup anemometers.* Wind Energy Division, DTU, Roskilde.

Pleim, J. E. (2007). A Combined Local and Nonlocal Closure Model for the Atmospheric Boundary Layer. Part II: Application and Evaluation in a Mesoscale Meteorological Model. *J. Appl. Meteorol. Climatol.*, 46(9):1396–1409.

Putnins, P. (1970). The climate of Greenland. *Elsevier*, 7:128.

Rasmussen, L. (1989). Katabatic winds in Greenland.pdf. *Vejret english Ed.. Danish Meteorol. Soc.*, pages 3–33.

Reid, S. (2001). Correlation of real and model wind speeds in different terrains. *Weather Forecast.*, 16(5):620 – 627.

Renfrew, I. a., Outten, S. D., and Moore, G. W. K. (2009). An easterly tip jet off Cape Farewell, Greenland. I: Aircraft observations. *Q. J. R. Meteorol. Soc.*, 135(645):1919–1933.

Risberg, T. (2009). Nanortalik A preliminary analysis of the wind measurements, rev 1. Technical report, Kjeller vindteknikk.

Risien, C. M. and Chelton, D. B. (2006). A satellite-derived climatology of global ocean winds. *Remote Sens. Environ.*, 105(3):221–236.

Rögnvaldsson, Ó., Bao, J.-W., Ágústsson, H., and Ólafsson, H. (2011). Downslope windstorm in Iceland WRF/MM5 model comparison. *Atmos. Chem. Phys.*, 11(1):103–120.

Rotach, M. W. (1999). On the influence of the urban roughness sublayer on turbulence and dispersion. *Atmos. Environ.*, 33(24-25):4001–4008.

Rzeszotko, J. (1997). METAR format. *Approach Nav. Saf. Center's Aviat. Mag.*, 42(2).

Sæbø, K., Manger, S. R., Løland, T. D., and Laukhamar, A. G. (2012). The Nanortalik Energy System. Technical report, DTU, Nanortalik.

Santoso, E. and Stull, R. (1998). Wind and temperature profiles in the radix layer: The bottom fifth of the convective boundary layer. *J. Appl. Meteorol.*, 37(6):545 – 558.

Skamarock, W. C. (2004). Evaluating Mesoscale NWP Models Using Kinetic Energy Spectra. *Mon. Weather Rev.*, 132(12):3019–3032.

Sørensen, N. N. (2013). CFD applications in wind energy using RANS. *Cfd Atmos. Flows Wind Eng.*

Statistik, G. (1999). Tal om Grønlands bygder 1998. Technical report.

Stearns, C. (1970). Determining surface roughness and displacement height. *Boundary-Layer Meteorol.*, 1(1):102 – 111.

Stull, R. (1988). *An introduction to boundary layer meteorology.* Kluwer Academic Publishers.

Tufte, E. D. N. (2014). *Impacts of Low Load Operation of Modern Four-Stroke Diesel Engines in Generator Configuration.* PhD thesis, Norwegian University of Science and Technology.

Villumsen, A., Jakobsen, K. R., Nielsen, M. H., Dragsted, J., Larsen, E., Hansen, K. S., and Jakobsen, K. R. (2010a). Fyrtaarnsprojekt III - afsluttende rapport 2009.

Villumsen, A., Jakobsen, K. R., and Villumsen, O. (2010b). Baeredygtig energiforsyning - hvad vaelger Groenland.

Walker, G. T. (1924). Correlation in seasonal variations in weather IX: A further study of world weather. *Mem. Indian Meteor*, (24):275–332.

Walker, G. T. and Bliss, E. W. (1932). World Weather V. *Mem. R. Meteorol. Soc.*, 4:53–84.

Walraven, R. (1978). Calculating the position of the Sun. *Sol. Energy*, 20(5):393 – 397.

Wilson, A. B., Bromwich, D. H., and Hines, K. M. (2011). Evaluation of Polar WRF forecasts on the Arctic System Reanalysis domain: Surface and upper air analysis. *J. Geophys. Res.*, 116(D11):D11112.

Wong, R. Y. T. (2012). High-resolution dynamical downscaling techniques for wind resource assessment. *Eur. Wind Energy Conf. Exhib. 2012, Ewec 2012*, 2:1324 – 1329.

Appendix A

Appendix A

A.1 Introduction to collected wind data

In this appendix the wind data collected and processed in this project is presented. The equipment used for the campaigns was sponsored by the Greenlandic VEK funds (Vedvarende energi, Energieffektiviseringer og Klima), the travel expenses was covered by Arctic Technology Centre (ARTEK), and the manpower was mainly delivered by this project.
The Sisimiut dump site and the Sattut site was not serviced in this project, but the raw data has been quality checked, processed, and published in this project. The collected raw data can be accessed at the web-page: http://www.winddata.com/Greenland [Hansen and Hansen, 2007]. All data, used in this project, is by default processed according to the standard procedure in [AWS Scientific, 1997]. If other processes is these will be described in the relevant section.

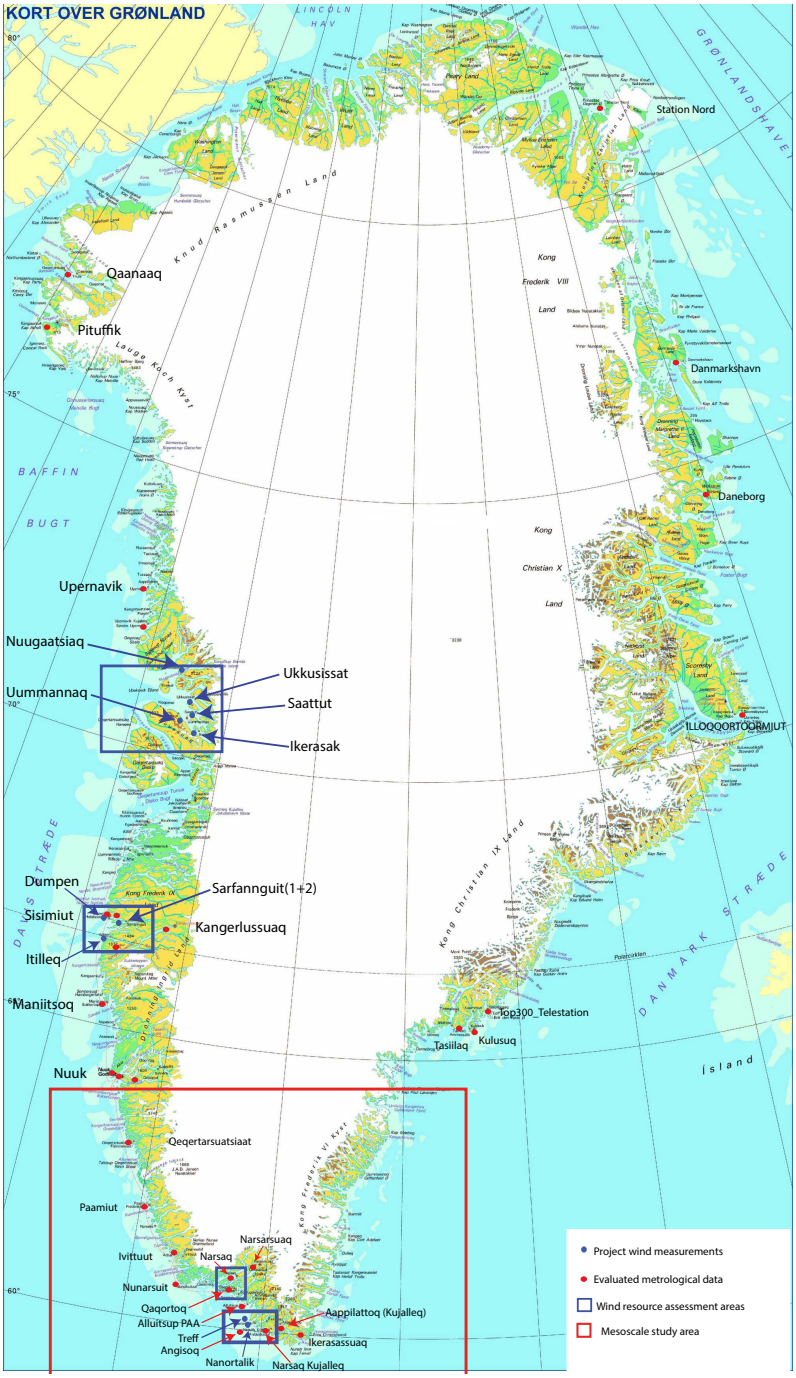

Figure A.1. *Geographically overview of project activities. Data source: KMS(G250)*

A.2 Dumpen, Sisimiut

The site Dumpen is located south of Sisimiut at a 78m hilltop, approximately 1 km from town. The inflow from SW to NW is almost undisturbed from the seaside, while the flow from Eeastern direction is highly influenced by the mountain "Kaellingehaetten" 778m with in a distance of 2km. Inflow from the Northern direction is influenced by Sisimiut town and some minor mountains.

Station	Coordinate	Elevation	Start date	End date
Dumpen	$N66^o55.609$ $W53^o40.057$	m AMSL	05.08.2004	12.08.2008
ID:1098	X 383365 Y 7425721	78		

Table A.1. *Basic data for Dumpen site, Sisimiut Greenland*

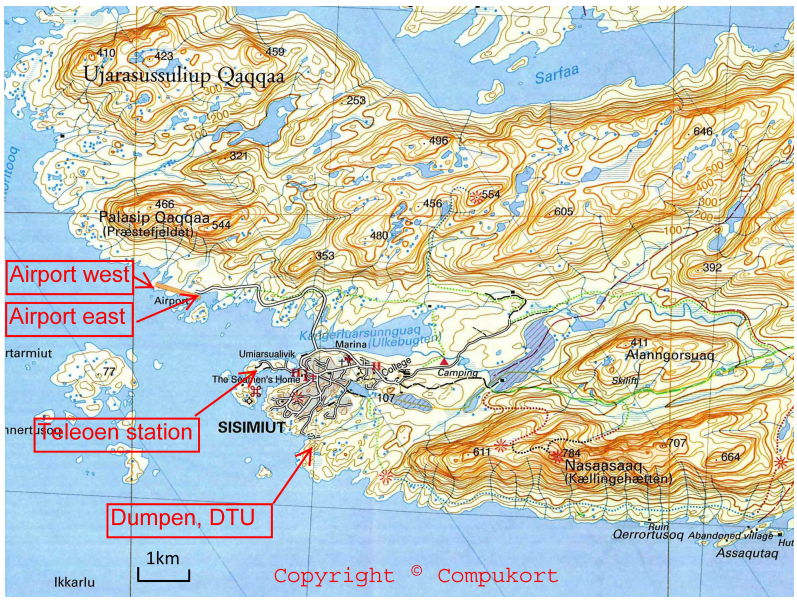

Figure A.2. *Geographically overview Sisimiut stations. Data source: Compukort*

Time series	Parameter	Frequency	Height [MAG]
ws10	Wind speed	10 min.	10
wd10	Wind direction	10 min.	10
t10	Air temperature	10 min.	3

Table A.2. *Monitoring parameter Dumpen, Sisimiut Greenalnd*

Figure A.3. *Dumpen site Sisimiut, seen from west (Photo provided by Kurt S. Hansen, DTU)*

Period	Data	DRR	U mean	Weibull A	Weibull K	U 50
Full campaign	174057	0.823	4.87	5.35	1.37	35.4
Reference year 1	50752	0.966	5.49	6.04	1.38	-
Reference year 2	51542	0.981	4.75	5.24	1.42	-
Reference year 3	52458	0.998	4.58	5.01	1.34	-
Ref. year average			4.94	5.43	1.38	-

Table A.3. *Basic statistic for Dumpen, Sisimiut Greenalnd*

The low data recovery rate (DRR) for the full data serie was caused by two down periods, see . The deceasing mean wind speed (U mean) could indicate instrument drifting caused by abrasion, but it need further investigation to verify this theory. The 50 year extreme wind speed (U 50) is based on the standard Gumbel-based maximum extrapolation.

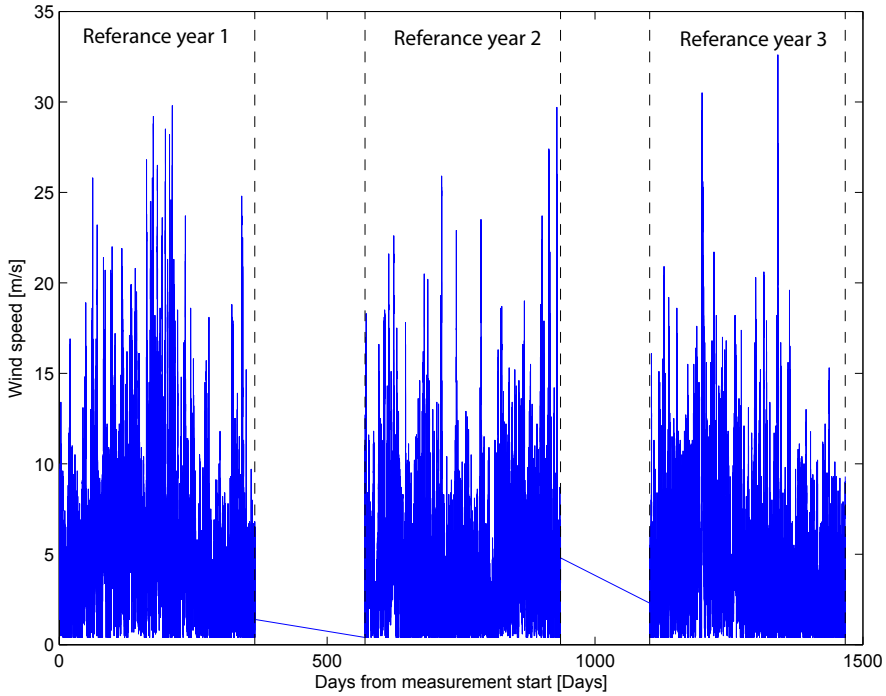

(a) *Wind speed data for Dumpen, full campaign*

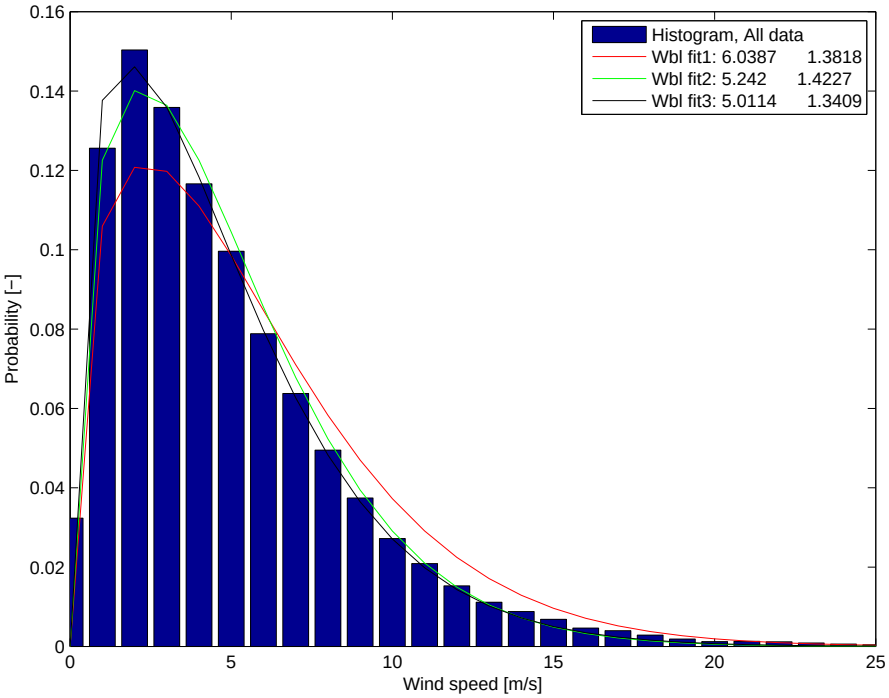

(b) *Wind speed probability distribution and weibull fit*

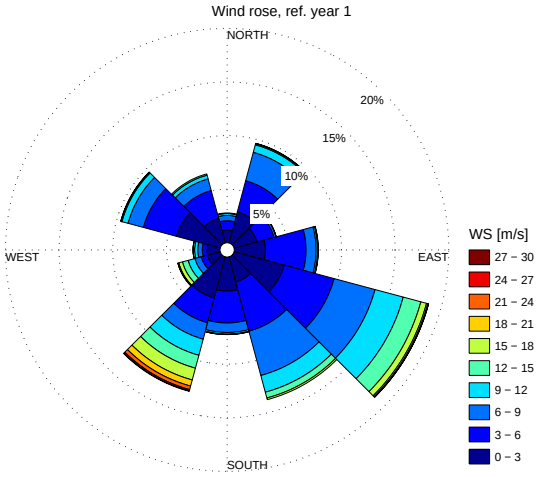

(a) *Wind rose Dumpen, year 1*

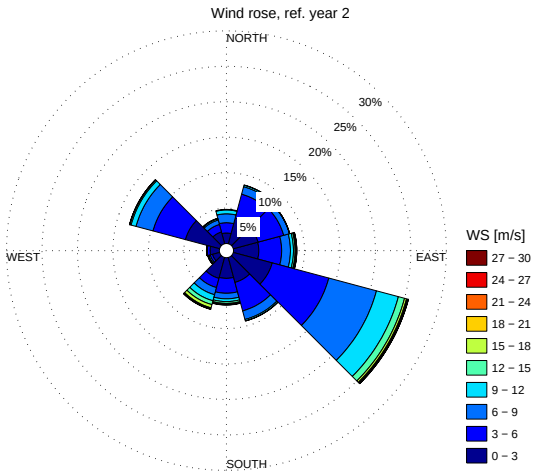

(b) *Wind rose Dumpenn, year 2*

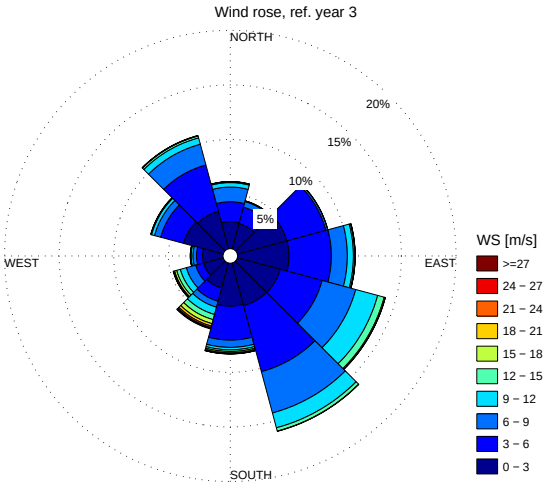

(c) *Wind rose Dumpen, year 3*

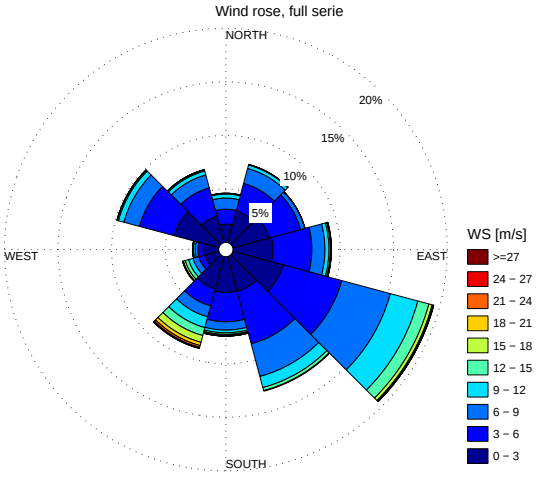

(d) *Wind rose Dumpen, full campaign*

A.3 Sarfannguit

Site 1 in Safannguaq is located on a hill top south of the village. Site 2 is located 500m southeast of site 1. The installation at site 1 was updated with external power supply and doublet instruments in August 2010. Near site 1 a small 6kW Proven P11 wind turbine is installed for test purpose.

Station	Coordinate	Elevation [MAG]	Start date	End date
Safannguaq site 1	$N66^o53.716$ $W052^o51.977$	82	01.08.2003	Still active
Safannguaq site2	$N66^o53.617$ $W052^o52.580$	109	01.09.2010	Still active

Table A.4. *Basic data for Sarfannguit sites, Sarfannguit Greenland*

Figure A.6. *Sarfannguit area, (Data source: Topo-kort, KMS)*

Figure A.7. *Sarfannguit ortophoto, Red star site 1 and Blue star site 2 (Data source: Google Earth)*

A.3.1 Sarfannguit, site 1

Sarfannguaq site 1 has had some technical problems during the measuring campaign. During the 6 years of operation the site has had many problems e.g. instrument problems,

defect logger, and stolen memory cards. This entailed several interrupted series with a length of less than a year. A statistic of the collected data can be seen in Table A.6.

Time series	Parameter	Logging interval	Height [MAG]	Measuring period
wsEast	Wind speed	10 min.	10	01.08.2003-
wdEast	Wind direction	10 min.	9.5	01.08.2003-
wsWest	Wind speed	10 min.	10	01.09.2010-
wdWest	Wind speed	10 min.	9.5	01.09.2010-
t10	Air temperature	10 min.	2.1	01.08.2003-
Pres	Air pressure	10 min.	2.1	01.08.2003-
rhum	Relative humidity	10 min.	1.9	01.08.2003-

Table A.5. *Instrumentation for Sarfannguit 1*

Period	Data	DRR	U mean	Weibull A	Weibull K	U 50
Full campaign	315610	0.600	5.63	6.32	1.80	30.8
Reference year 1	50504	0.972	6.27	7.05	1.86	-
Reference year 2	49076	0.934	5.50	6.17	1.77	-
Reference year 3	51347	0.977	5.68	6.37	1.79	-
Reference year 4	50969	0.967	5.26	5.89	1.777	-
Reference year 5	51172	0.974	5.60	6.30	1.84	-
Ref. year average			5.66	6.35	1.81	-

Table A.6. *Basic statistic for Sarfannguit site 1*

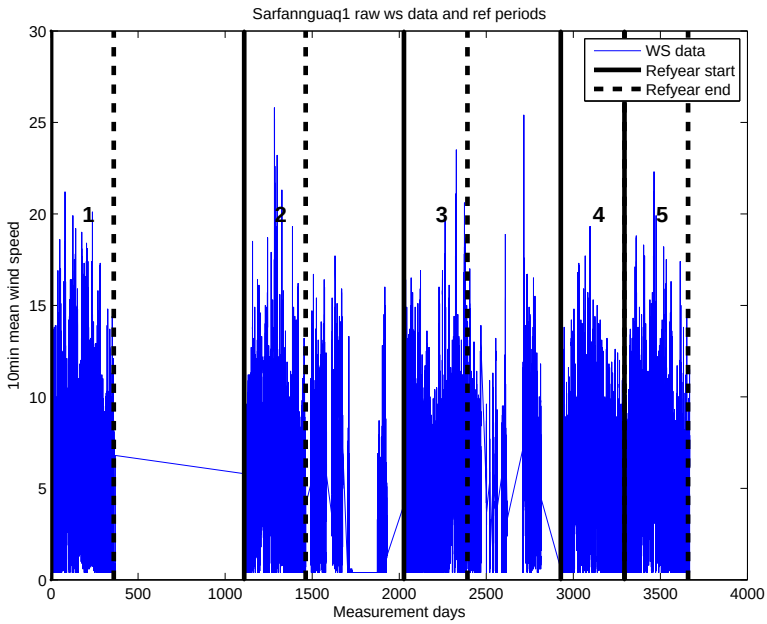

Figure A.8. *Wind speed data for Sarfannguit 1 and reference year bounds, full campaign*

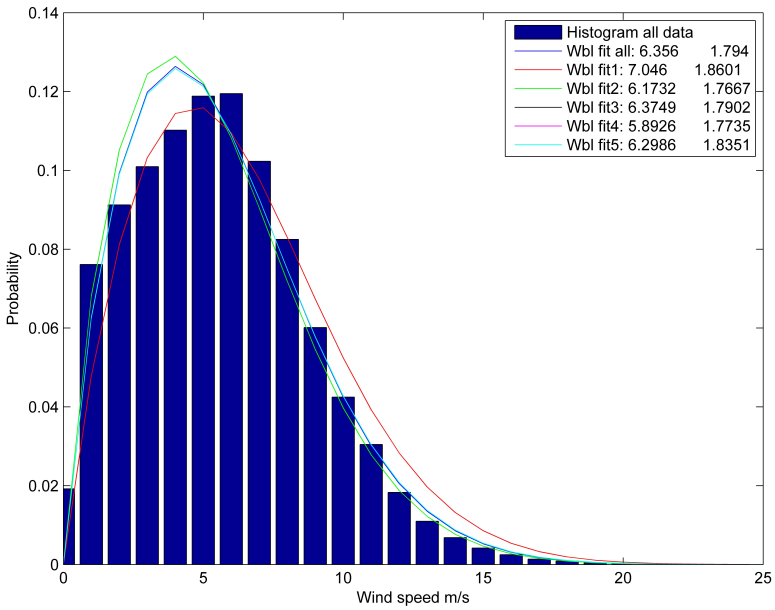

(a) *Wind speed probability distribution and weibull fit*

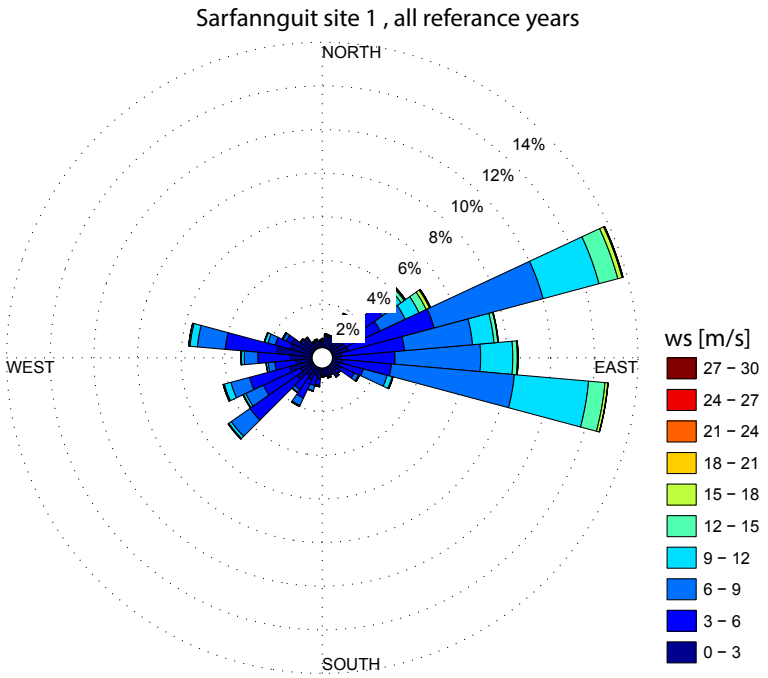

(b) *Sarfannguit 1 wind rose for all reference years*

A.3.2 Sarfannguit, Site 2

Sarfannguit 2 has only expired one large (37 days) down period due to vandalism. According to the standard process for data validation, this will trigger a scrapping of the first measuring period of 327 days (328 days< 1 year), because of the limited amount of data and the short breakdown an exception was made. This affect the data recovery rate (DRR) for the first reference year Table A.7.

Time series	Parameter	Type	Logging interval	Height [MAG]	Measuring period
ws11	Wind speed	10 min.	11.65	01.09.2010-	
wd11	Wind direction	10 min.	11.30	01.09.2010-	
Ws8	Wind speed	10 min.	8.00	01.09.2010-	
Ws4	Wind speed	10 min.	4.00	01.09.2010-	
t10	Air temperature	10 min.	2.3	01.08.2011-	
Pres	Air pressure	10 min.	2.7	01.08.2011-	
pyr	Solar radiation	10 min.	3.0	01.08.2011-	
rhum	Relative humidity	10 min.	2.1	01.08.2011-	

Table A.7. *Instrumentation for Sarfannguit 2*

Period	Data	DRR	U mean	Weibull A	Weibull K	U 50
Full campaign	136651	0.963	6.19	6.91	1.71	37
Reference year 1	47454	0.903	6.09	6.79	1.71	-
Reference year2	52566	0.997	5.91	6.58	1.64	-
Reference per 3	36144	1.00	6.73	7.56	1.86	-
Ref. year average			6.00	6.69	1.68	-

Table A.8. *Basic statistic for Sarfannguit site 2*

A.3.3 Wind speed relation for Sarfannguit sites

The overlapping period used for this study includes 106.013 measurements or round two years of measurements. As expected, there is a good correlation between the measured wind speeds. A simple linear fitting show that the average relation is $WS_{site2} = 1.1WS_{site1} + 0.1m/s$. This agree width the relation found in the WAsP model used for selecting site 2, based on site 1 data.

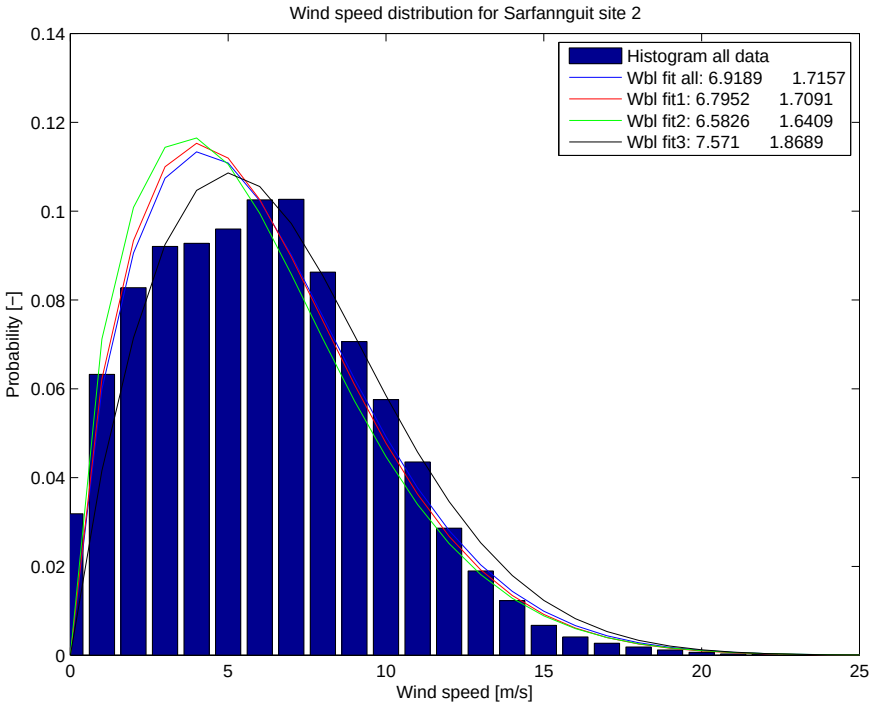

(a) *Wind speed probability distribution and weibull fit, site 2*

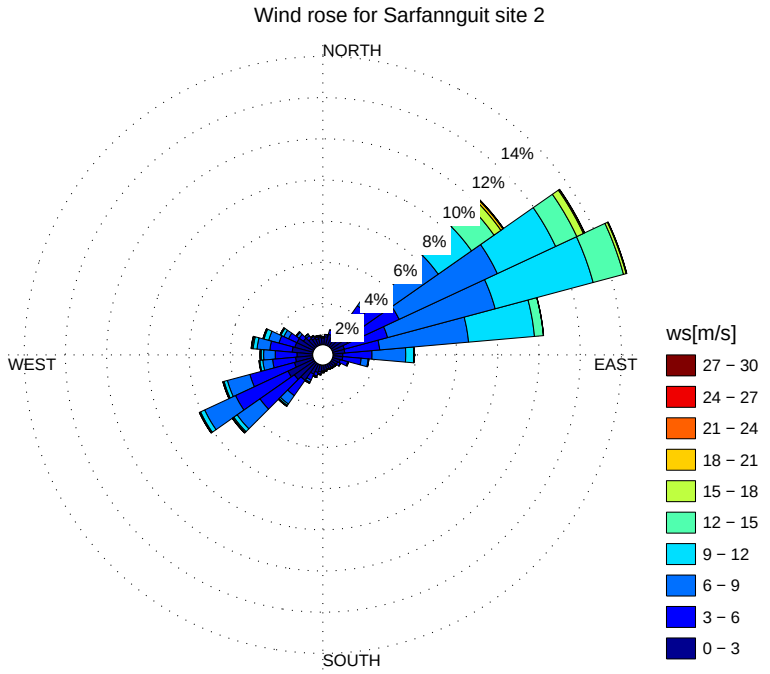

(b) *Sarfannguit 2 wind rose for all reference years*

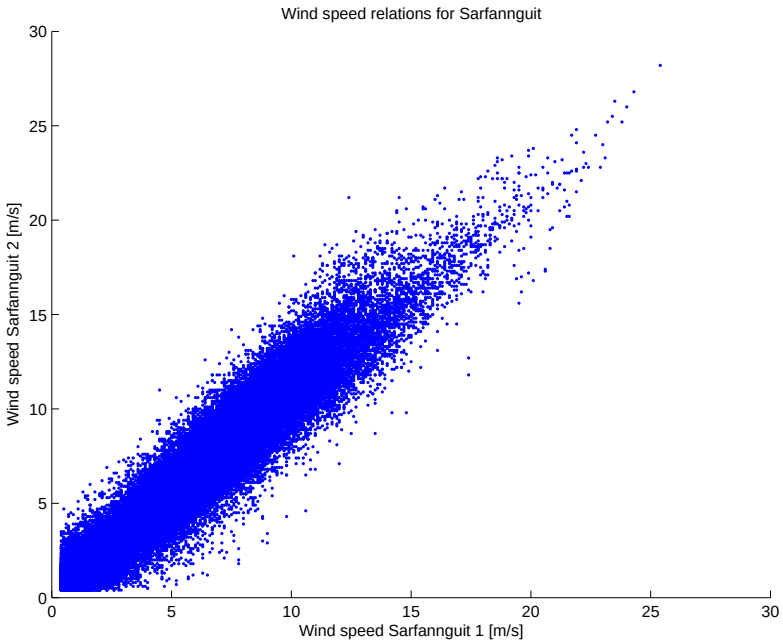

Figure A.11. *Wind speed relation for the two Sarfannguit sites, based on 2 years measurements*

A.4 1601, Nanortalik

The Nanortalik wind monitoring site was adapted from a Nordic research project in 2009. The site is located in the northeastern part of the town close to the dump site. In 2012 the system was upgraded with new instrumentation and logger system. The system was connected to the Risoe-based veaonline system http://veaonline.risoe.dk/, data from the first period is available on the wind data server: http://www.winddata.com/Greenland.

Station	Coordinate	Elevation [MAG]	Start data	End data
Nanortalik Dump	$N60^o8.602$ $W045^o13.555$	19	25.06.2007	Still active
ID: 1601	X 487453 Y 6667400	-	-	-

Table A.9. *Basic site data, Nanortalik dump*

Figure A.12. *Nanortalik dump site, 1601. Author private photo, November 2012*

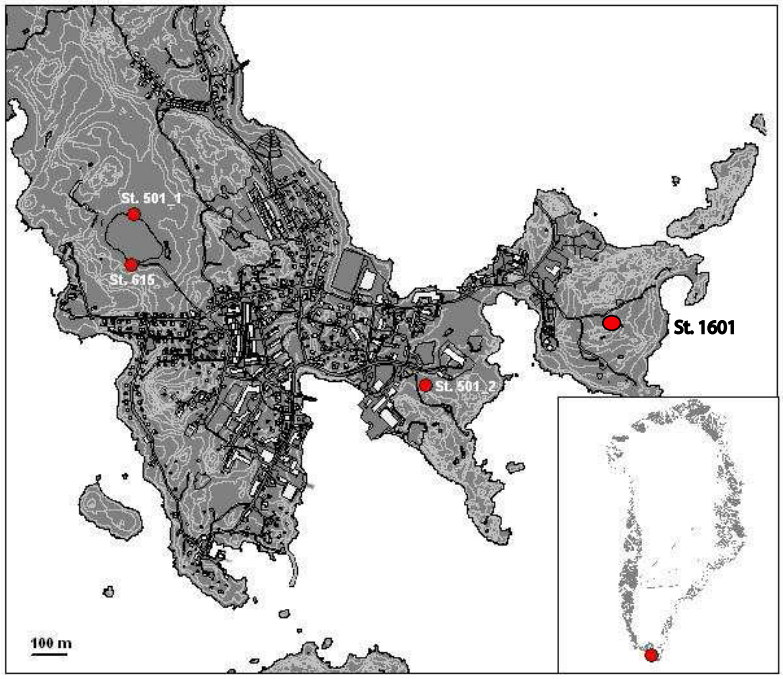

Figure A.13. *Meteorological stations in Nanortalik including the wind monitoring station, 1601. Data Source: ASIAQ*

Type	Instrument type	Logging interval	Height [MAG]	Measuring period
WS	NRG 40	10min	48.8	25.06.2007-01.07.2009
WS	NRG 40	10min	30	25.06.2007-01.07.2009
WS	NRG 40	10min	10	25.06.2007-01.07.2009
WS	RISØ P2546A	10min	48.8	25.06.2007-
WS	NRG IceFree 3	10min	43.8	25.06.2007-01.08.2012
WD	NRG IceFree 3	10min	40.8	25.06.2007-01.03.2010
WD	NRG 200P	10min	41.4	25.06.2007-
AT	NRG110S	10min	3	25.06.2007-
		2012 setup		
WS+AT	Metek Usonic 3D Heated	20Hz	50m	01.10.2012-
WS	RISØ P2546A	10min	48.9	25.06.2007-
WS	RISØ P2546A	10min	30	01.09.2012-
WS	RISØ P2546A	10min	10	01.09.2012-
PT	Potential temperature	10min	48.5-5	01.12.2012-
WD	NRG 200P	10min	48.8	01.09.2012-
WD	NRG 200P	10min	10	01.09.2012-
AT	NRG110S	10min	3	25.06.2007-
RH	NRG RH-X5	10min	3	01.09.2012-
IR	HoloOptics T44	60min	5	01.12.2012-
GR	Hekseflux LP02-05	10min	6	01.10.2012-
RH2	Vaisala HMP155	10min	3	01.12.2012-
AT2	Vaisala HMP155	10min	3	01.12.2012-

Table A.10. *Monitoring parameters, Nanortalik dump*

Period	Data	DRR	U mean	Weibull A	Weibull K	U 50
Full campaign	308283	0.978	6.06	6.74	1.49	30.8
Reference year 1	51443	0.979	6.5	7.84	1.52	-
Reference year 2	51873	0.987	6.1	6.84	1.53	-
Reference year 3	51493	0.978	5.1	5.64	1.52	-
Reference year 4	52097	0.991	6.3	7.00	1.46	-
Reference year 5	51259	0.975	6.4	7.16	1.50	-
Reference year 6	50118	0.954	5.9	6.60	1.49	-
Ref. year average			5.9	6.66	1.50	-

Table A.11. *Basic statistic for Nanortalik dump site*

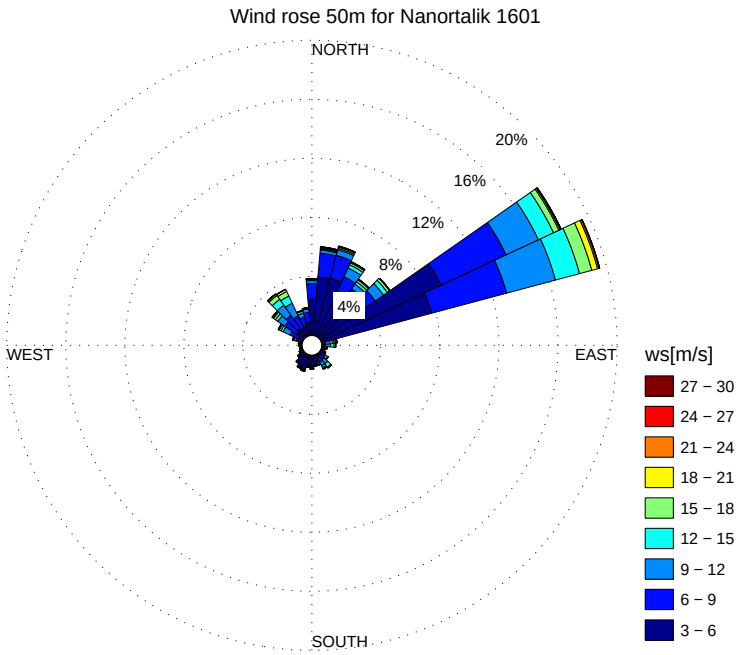

Figure A.14. *Wind rose 1601 Nanortalik Dump*

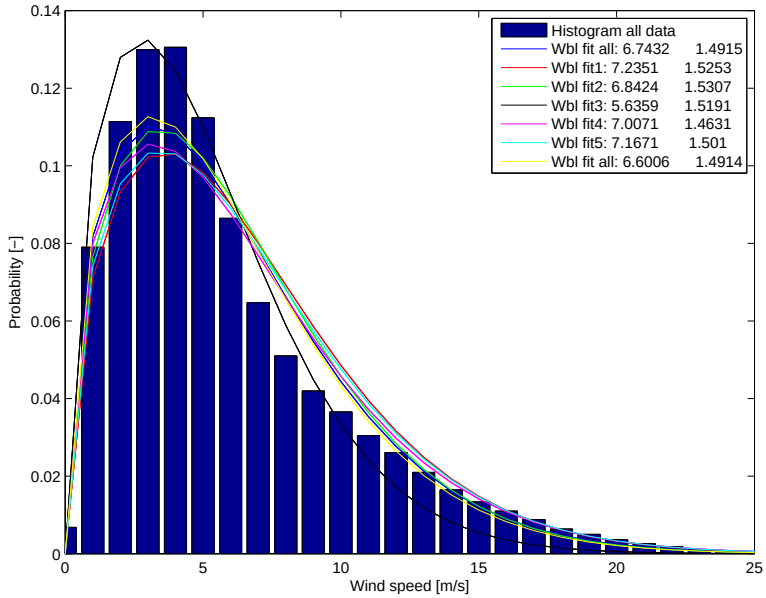

Figure A.15. *Wind distribution 1601 Nanortalik Dump (2013)*

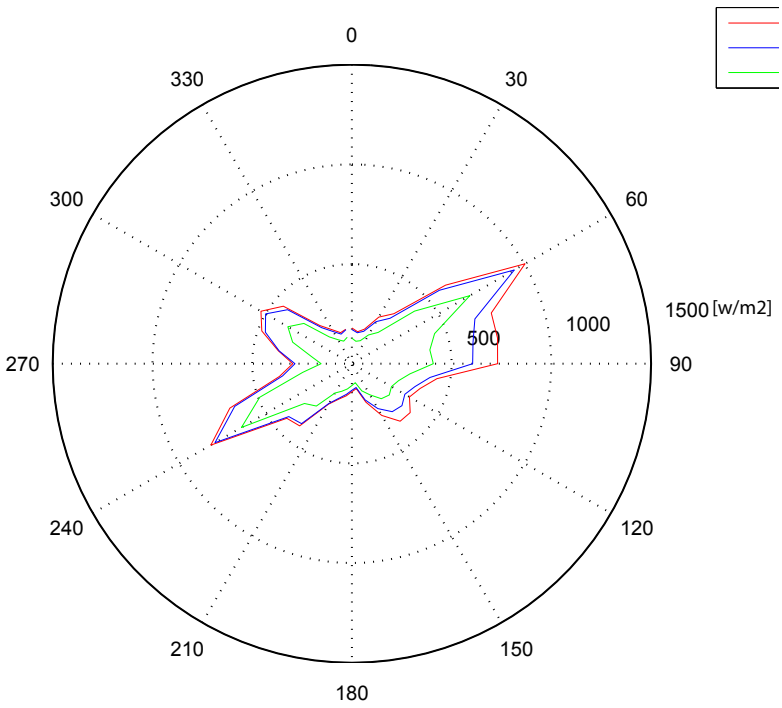

Figure A.16. *Wind power distribution 1601 Nanortalik Dump (2013)*

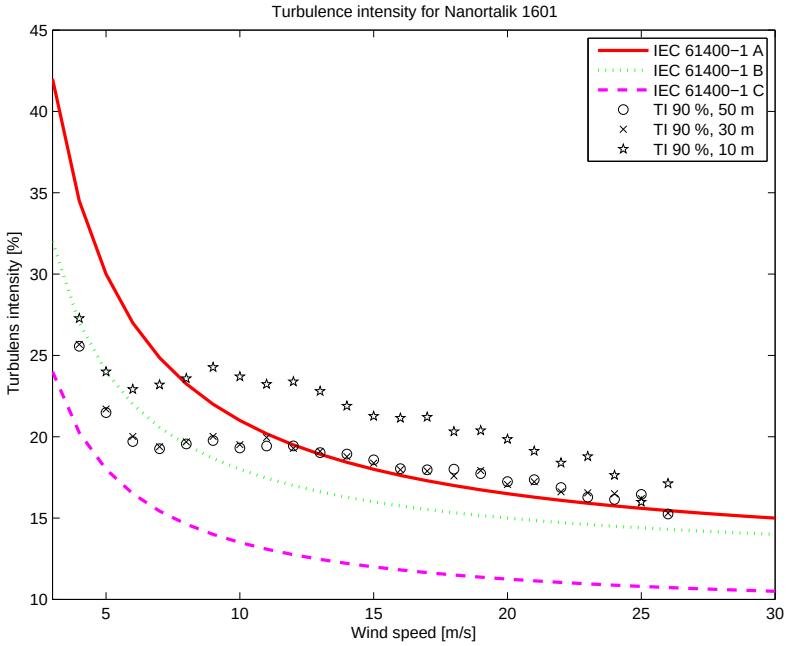

Figure A.17. *Turbulence intensity 1601 Nanortalik Dump (2013)*

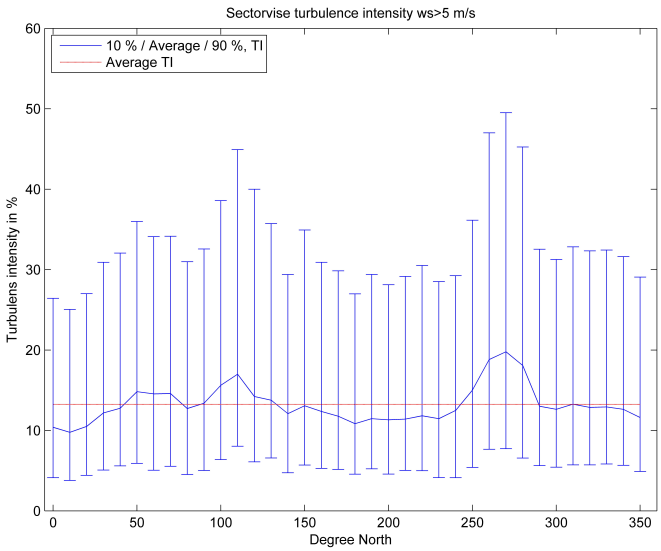

Figure A.18. *Turbulence intensity in sectors,1601 Nanortalik Dump*

A.5 Nanortalik validation sites

The Nanortalik validation sites was mainly designed for model validation. The two stations forms together with the Nanortalik dump site 1601 a triangle, for optimal cross prediction test. The sites is exposed for different wind conditions and will also be optimal for large scale modeling validation like Mesoscale.

Station	Coordinate	Elevation [MAG]	Start date	End date
Nanortalik North	$N60^o10.684$ $W045^o16.875$	168	Not activated	-
Nanortalik South	$N60^o07.765$ $W045^o18.594$	528	Not activated	-
Nanortalik 1601	$N60^o8.602$ $W045^o13.555$	19	25.06.2007	Still active

Table A.12. *Basic data for Nanortalik sites, Nanortalik Greenland*

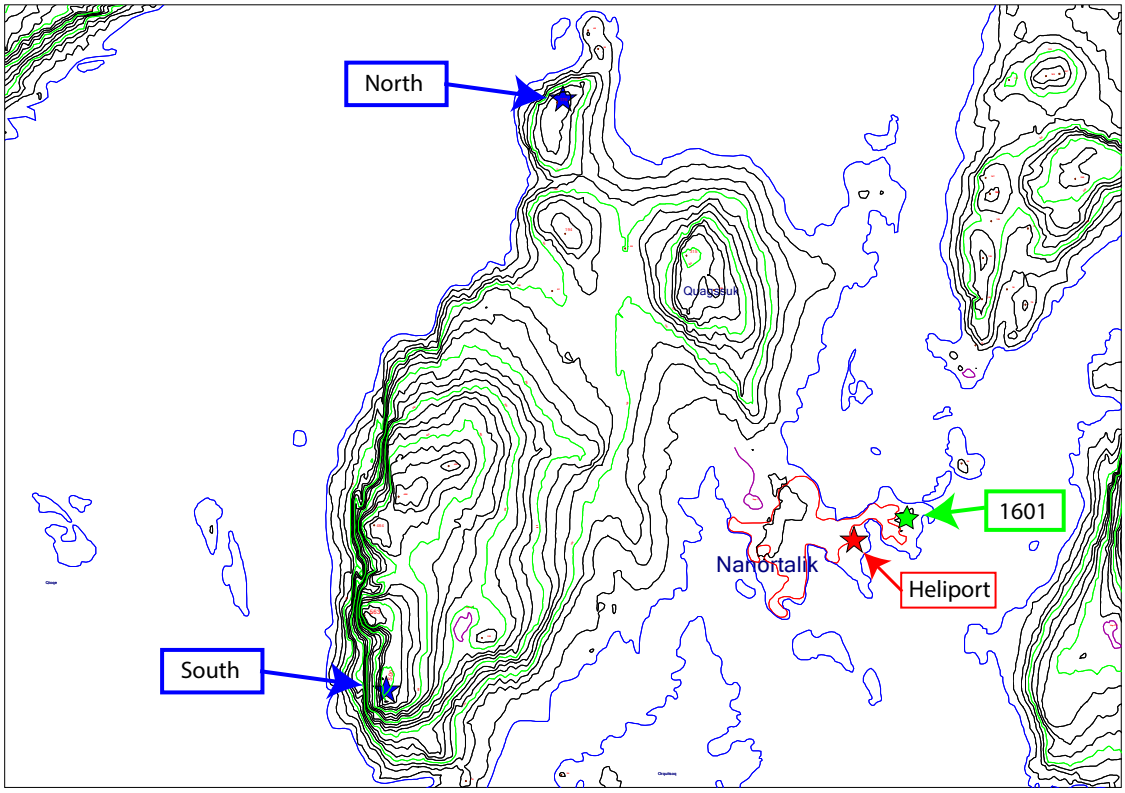

Figure A.19. *Nanortalik validation sites. Data source: ASIAQ k1 DEM*

The measurement system was based on NRG Symphonie loggers adjust this setup. Design of cabinets, power and signal system was done in the project, based on the experiences gain from other campaigns. The power supply is based on 20 Wp PV with a backup battery bank.

Place	Instrument	Instrument type	Logging interval	Height [MAG]
Top	Thies first anemometer	4.3351.10.00	10min	41
Top boom	Thies first vane	4.3150.10.110	10min	39
Top boom	Risø cup	P2546A	10min	39
Boom	Thies first anemometer	4.3351.10.00	10min	25
Boom	Thies compact vane	4.3129.10.712	10min	25
Boom	Thies first anemometer	4.3351.10.00	10min	10
Boom	Thies compact vane	4.3129.10.712	10min	10
Mast	Galltec Mela	KPC 1/5 ME	10min	3
Mast	Barometric pressure sensor	P-GE 6/11	10min	3
Mast	battery voltage		10min	3

Table A.13. *Instrumentation for Nanortalik site, North*

The stations is designed in corporation with GE:Net that also delivered the mechanical components. The tower is designed to withstand a maximum wind speed of 60 m/s and structural icing, class G4/R6, according to ISO 12494:2012. The tower support anchors is specially designed glue-in rock anchors, tailor made for the soil conditions at the sites.

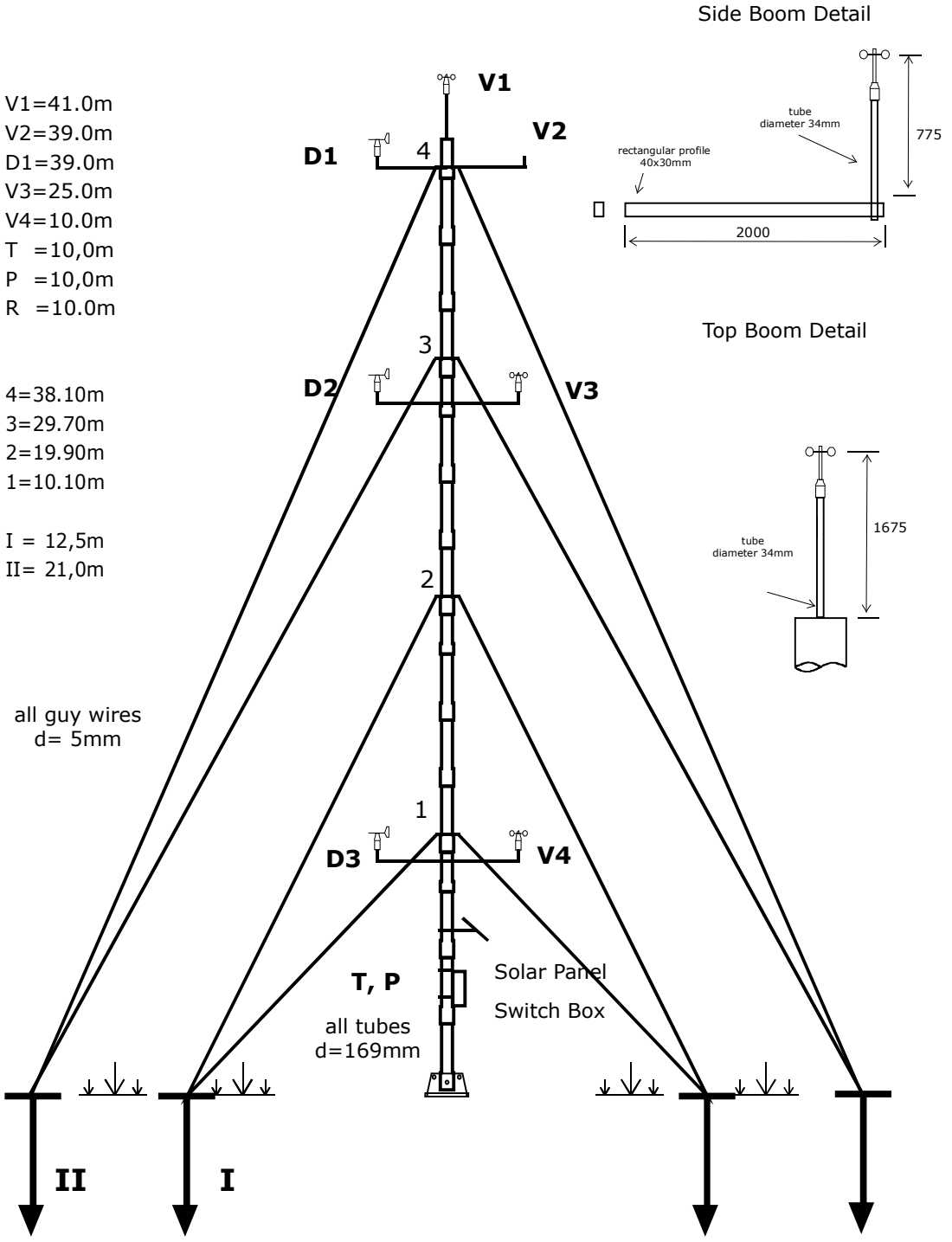

Figure A.20. *Mast design for Nanortalik site North*

All equipment was collected, tasted and packed, for helicopter hoisting at our work shop in Nanortalik. From the Heliport the packages were hoisted to the sites. All tools and temporary equipment were transported to site South, by helicopter and later on manually transported to site North.

Figure A.21. *Equipment package delivered, by helicopter, to Nanortalik site North*

During the installation the weather changed from cold and sunny to windy with snow. The high wind and above half a meter snow put the installation behind schedule. After the weather changed site South was not reachable by foot due to snow and ice covered slopes.

Figure A.22. *Tower base installation site North*

When the bases and anchor points was established it was decided that the towers could not be erected in a safe way under these weather conditions (high wind, snow and fog) and the final installation was postponed to the spring 2013. After securing the equipment the crew left the area.

Figure A.23. *Tower installation site South*

In the meantime (November 2012 - April 2013) large changes was made in the management structure, weakening the decisiveness. The decision process became so slow, that the final permission, could not be ready for the 2013 field season. All activities were schedule, crew, boats and equipment was booked leaving all partners very frustrated.

A.6 Tref site

The site is located 10km northwest of Nanortalik on a hill top 910 m AMSL, next to a Tele repeater station. The site was mainly used for high altitude instrument tests, but wind turbine test was considered for the site. Tele has operated horizontal axis wind turbines at the site, but was replaced with diesel in the 80ties.

Station	Coordinate	Elevation [MAG]	Start date	End date
TREF	$N60^o12.955$ $W045^o22.101$	886	14.08.2012	10.2014
	X 479468,7 Y 6675411,0	-	-	-

Table A.14. *Basic data for Tref site, Nanortalik Greenland*

Figure A.24. *Tower installation at the Tref site*

Time series	Parameter	Logging interval	Height [MAG]	Measuring period
Ws8	Wind speed heated	10 min.	8.1	14.08.2012-10.2014
Wd8	Wind direction	10 min.	8.1	14.08.2012-10.2014
t10	Air temperature	10 min.	3	14.08.2012-10.2014
Ws8.4	Wind speed	10 min.	8.4	14.08.2012-10.2014
Wd8.4	Wind direction heated	10 min.	8.4	14.08.2012-10.2014

Table A.15. *Instrumentation for Tref site, Nanortalik Greenland*

A.7 Remaining DTU sites

For informations about the other DTU sites used in this project (Assargutag, Itelleq, Uummannaq, Ikerasak, Saattut, Ukkusissat, Nuugatsiaq), consult the home page: http://www.winddata.com/Greenland [Hansen and Hansen, 2007] or contact the author.

Appendix B

Terrain data

Terrain data for Greenland has been collected for many years and with varies methods. The complex terrain with a surface mix of rock, open water, ice and vegetation gives the traditional methods a hard time and it means big representation error. Before the satellites, Aerial photography and marked control points was used to compute the terrain elevation. This method is very expensive if high resolution and quality need to be obtained in bigger areas. In the past several campaigns with different focus has been lanced to collect terrain data. The best released elevation data based on this method has a horizontal resolution for the open land of 100x100m and cities and settlements 5x5m. An

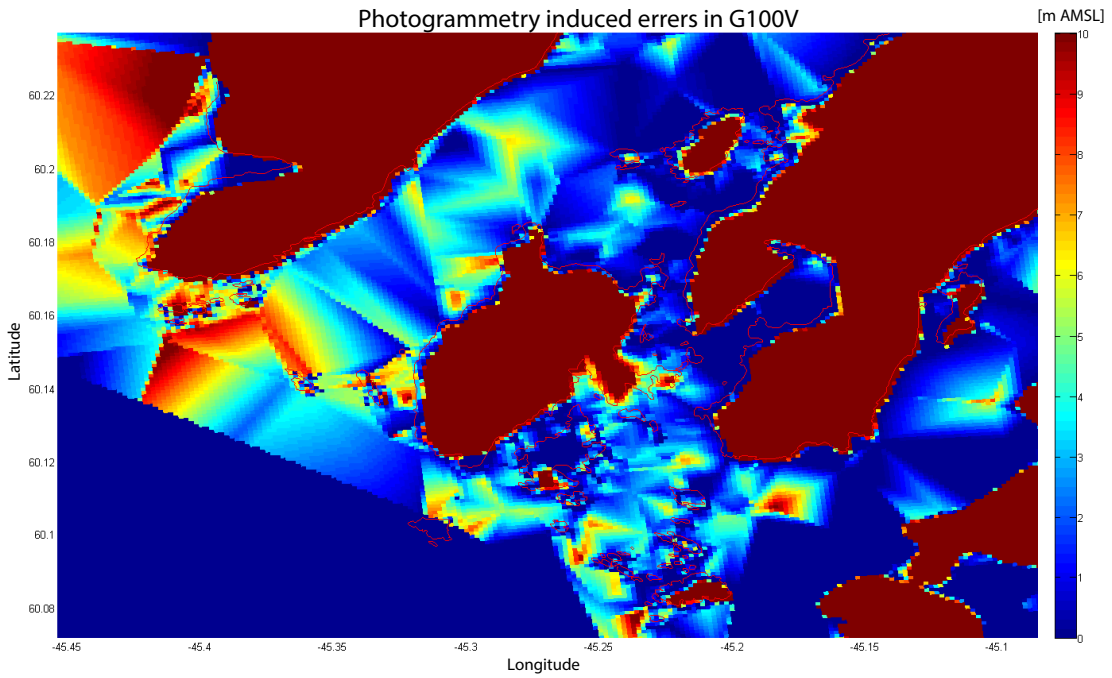

Figure B.1. *Example of how photogrammetry data include large amounts of errors, here show in the offshore area of Nanortalik. The map data used is from G100V(6650+100 and 150)*

example of the errors in Aerial photography based DEM data is showed Fig. B.1 The high resolution shore lines (red) indicate the shore and open water limits. The errors induced by the triangulation methods are very clear in the fjord regions. The expected surface height is round 0, but in this case heights of up to $\pm 30m$ are observed. The offshore

errors can relatively easy be corrected if shoreline data are available, but the same type of errors can be represented in the onshore data.

There ar different kinds of maps available for Greenland , most of them based on aerial photogrammetry in different resolutions and of different quality. Informations about most of the available maps can be provided by Asiaq, KMS or DTU space and the map cover of different area can be explored at nunagis.gl Fig. B. A list of the standard maps used in this project is listed Table B.1. The GTK maps is old maps covering most of the ice-free land, but not always in the best quality and this product is replaced by the G250 maps for all Greenland in both raster and vector format. The higher resolution maps includes the class 1 area map and the base map of settled areas and the G50 city map is a GIS map including informations on installations and constructions.

Name	Type	Curves	DEM	Format	Updated	Ownership	Supplier
GTK-xxxx	10	100m	1:250.000	Raster	1975-85	GST	GST
G250	9	100m	1:250.000	Vector		GST	GST
G250	9	100m	1:2.5000.00	Vector		GST	GST
G250	9	100m	1:5.000.000	Vector		GST	GST
GL. Class 1	3	25m	100x100m	Vector	continuously	Asiaq	Asiaq
GL. Base	2	0.5	10x10m	Vector	continuously	Asiaq	Asiaq
G50.City	1	0.5	5x5m	Vector	continuously	Asiaq	Asiaq

Table B.1. *Standard maps available for Greenland*

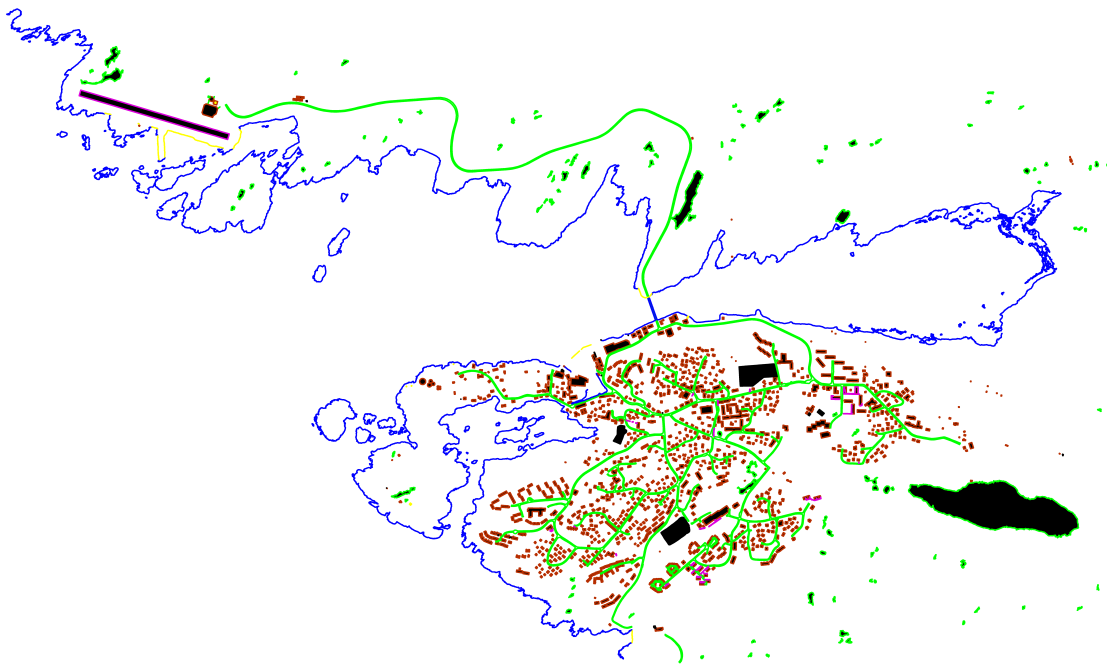

Figure B.2. *Example of basic layers of a G50. city map. Sisimiut G50 selected layers*

Digital hiking maps in raster formats 1:100.000, 1:75.0000 and 1:20.000 is available in the populated areas and raw Aerial photography based DEM can normally be bought from

the owner, however the quality of these data is often very poor and is not preferable.
In the last 15 year satellites and airborne laser scanners (ALS) has introduced new data sources and possibilities. Higher resolutions and better data processing has in the last years made the satellite based DEM data much better, but there are still relatively big representation errors in very complex terrain as the ice-free part of Greenland. To minimize the errors and use the available data a combination of the different technics are used to create DEM data e.g. [Ekholm, 1996]. Satellite DEM data based on e.g. the Advanced Space borne Thermal Emission and Reflection Radiometer (ASTER) covers all Greenland with a resolution of around 30m. ALS data is only available for a very limited area of Greenland, but the resolution and the quality of the data is often better than what the satellite delivers. For very steep slopes the accuracy of this method, as for the others, drops dramatically. ASL is mainly use to calibrate other data or to get higher resolutions in a limited area of interest, but with the development of drone based ALS it gets more widely used. For wind resource purpose people has been limited by the lag of high quality DEM data outside the city and settlement areas, but with the new data sources and especially in combination a usable resolution can be obtained. An upgraded version of the Ekholm model was published in 2010 [Bamber et al., 2001](1km) and was later incorporated in the global GMTED2010 (1km)[Danielson et al., 2011]. This model has been used to the mesoscale modeling in this project, nevertheless this model has also areas with very low quality especially in South and North, but the central ice Cap is well represented. This model was late refined, but the quality of the complex rock and ice cap margin areas remaind relatively low.
As part of the Greenland Ice-sheet Mapping Project (GIMP) a complete Greenlandic DEM was published in 2013, with a resolution of 30m, based on Landsat-7 ETM+ and RADARSAT-1(1999-2002), ICESAT GLAS (2003-2009),SPOT-5/SPIRIT(2007-2008) and Global Digital Elevation Model V2 (GDEM,ASTER) [Howat et al., 2014],
http://bprc.osu.edu/GDG/gimpdem.php. For the ice-free part a combination of the GDEMv2 and SPIRIT data is used and mainly the GDEMv2. The RMSE of the GDEM was fount to be in the range of 10-65m and the 95% confidence level 26-70m [Hvidegaard et al., 2012]. The accuracy of the SPIRIT data is unknown, but the GIMP group claim that the RMSE of the GIMP version 1 is 8.5 for the iced part, 18.3 for the ice-free part and 9.1m on average. With a RMSE of the GDEMv2 of 20-70m [Hvidegaard et al., 2012] this is a large improvement.
The GIMP v1 DEM has been tested for some of the sites in this project and larger errors is found both in horizontal and vertical plane. Large errors is discovered at glacier fronts and in the medium to high complex areas. The land mask data delivered with the GIMP v1 has a very poor quality, se example from Sisimiut area Fig. B.3 but it has in this project been replaced with the G250V or the Noaa (Global Self-consistent, Hierarchical, High-resolution Geography shorelines)

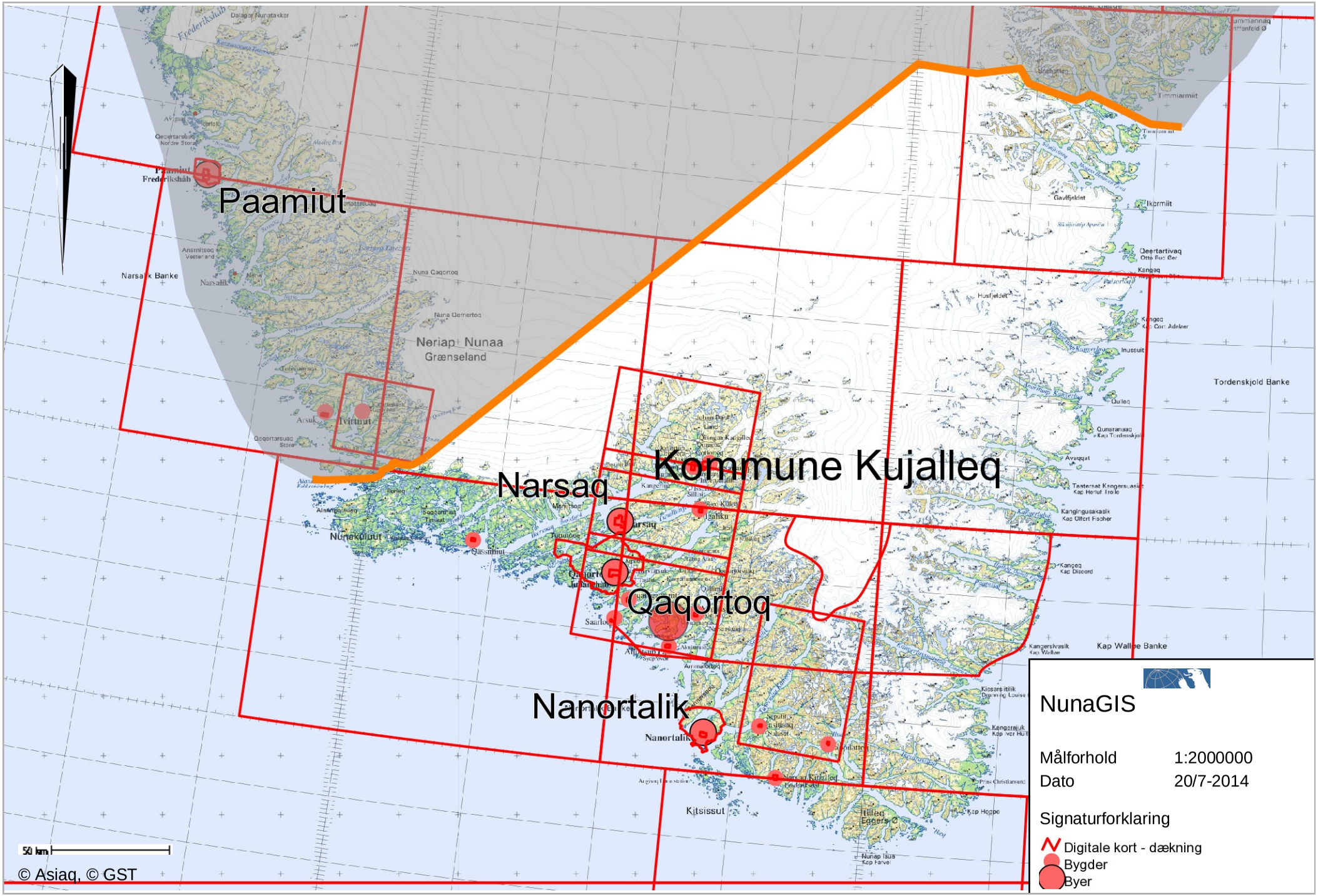
Paamiut
Narsaq
Kommune Kujalleq
Qaqortoq
Nanortalik
Neriap Nunaa
Grænseland
Narsaq Banke
Tordenskjold Banke
Kap Wallbe Banke
Kitsissut
50 km
© Asiaq, © GST
NunaGIS
Målforhold 1:2000000
Dato 20/7-2014
Signaturforklaring
Digitale kort - dækning
Bygder
Byer

For the microscale modeling the G50. city maps is combined with the class 1 maps for area extension. The terrain slope is then compared with the GMTED 30m data in the class 1 area to obtain a better representation. In some areas ALS data is available with resolution down to 0.1m and accuracies down to a few centimeter, however this is only in areas of interest to larger construction project or research.
For obstacle modelling the G50. city maps layer including all structures is combined with manual laser measurements of the structure heights or for the Greenlandic standard houses the shape can be looked up. Most Greenlandic cities has a reference station for Differential GPS (DGPS) use and thereby relative accurate (0.01-0.1m) manual point measurements can be done by reference corrected DGPS measurements. In some area point database exists and can be used to extract surface points and minimize the validation work. Outside the G50 maps the class 1 maps is used for coastlines, lakes, peaks, major and DTM. To obtain a better accuracy the terrain variation is compared to the GDEM v2. Finally it is adjusted to local fix point as can be collected from the KMS database, Asiaq and the local authorities.

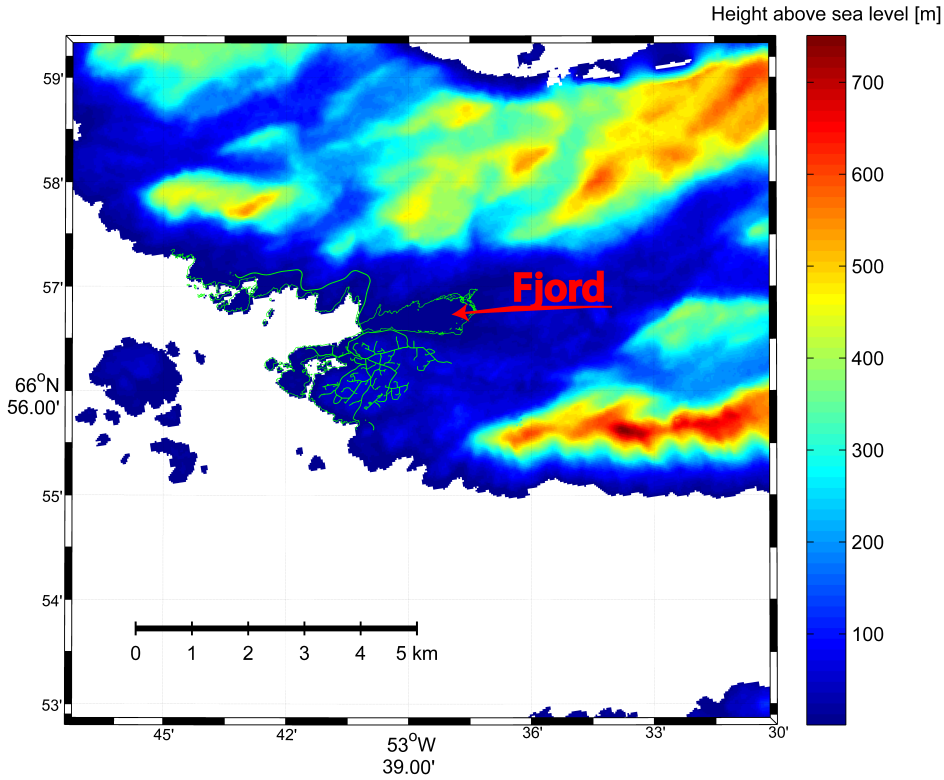

Figure B.3. *Example of GIMP DEM using the GIMP land mask data*

Appendix C

Sea ice chart

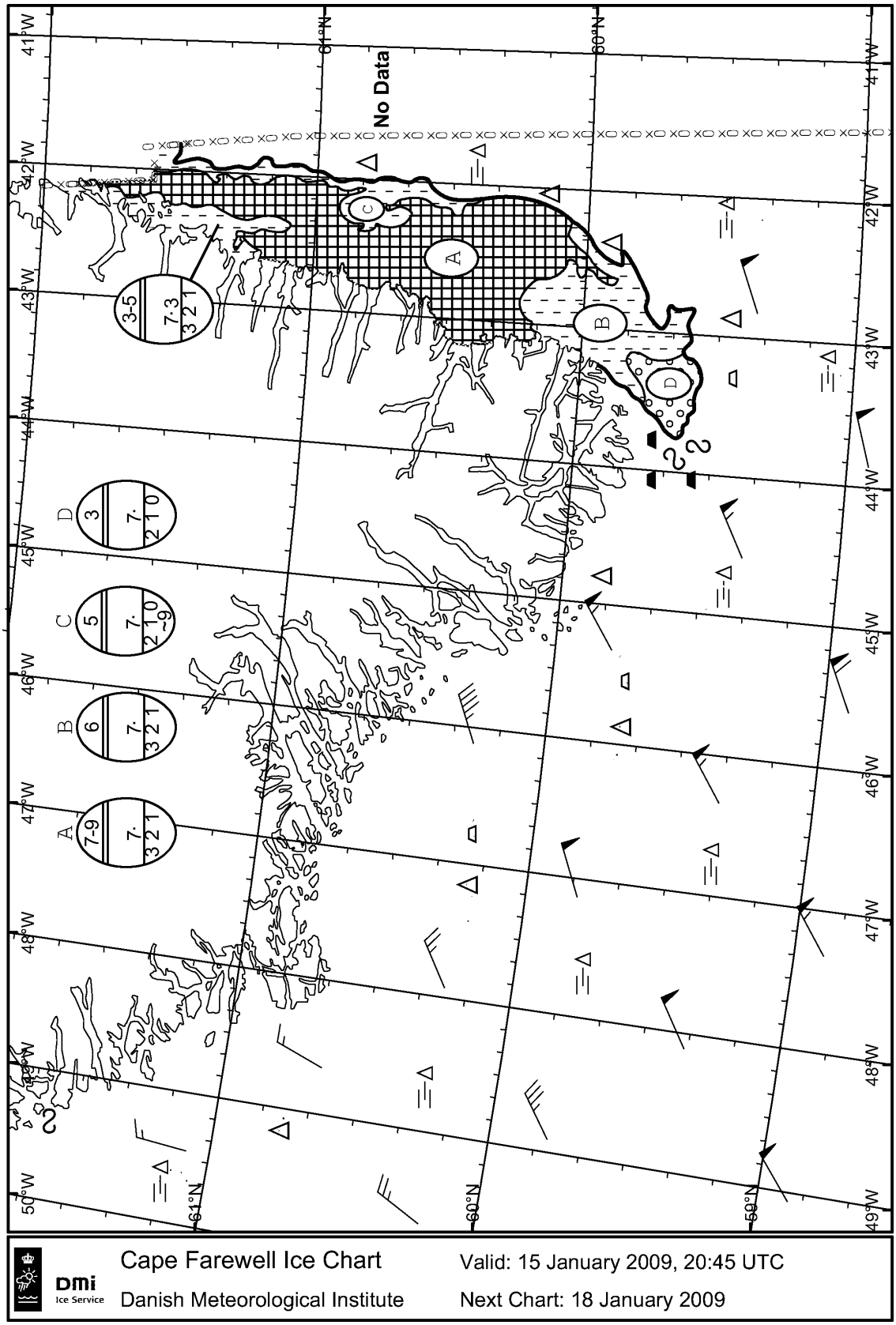
No Data
A
B
C
D
3-5
7·3
3 2 1
D
3
7·
2 1 0
C
5
7·
2 1 ~9 0
B
6
7·
3 2 1
A
7-9
7·
3 2 1
41°W
42°W
43°W
44°W
45°W
46°W
47°W
48°W
49°W
50°W
61°N
60°N
59°N
Cape Farewell Ice Chart
Valid: 15 January 2009, 20:45 UTC
DMI
Ice Service
Danish Meteorological Institute
Next Chart: 18 January 2009

Appendix D

Test turbine installation

Article about the test turbine in Sarfannguit developed as apart of this project and partly published in the light house project III report December, 2009 [Villumsen et al., 2010a]. All operation and maintenance, reporting and testing was done in the frame of this project.

TEST OF SMALL 6 KW WIND TURBINE IN ISOLATED GREENLANDIC GRID

INSTALLATION OF TEST TURBINE FOR TEST OF PERFORMANCE IN ARCTIC ENVIRONMENT AND THE INFLUENCE ON THE POWER QUALITY IN THE GRID

Author: Kasper Rønnow Jakobsen, M.S.c.Eng. & PhD student

Arctic Technology center has as a part of the Light house project installed a small 6 kW Proven wind turbine on a mountain top near the village Sarfannguaq in the western Greenland. The purpose of this installation is to investigate how wind turbines perform in the rough Arctic climate. Another purpose is to investigate the action on the relatively weak grid.

SELECTION OF TURBINE

The Arctic center has measured the wind potential in the area since 2003 and we have a relatively good knowledge about the wind resources and the extreme wind speeds in the area. The mean wind at the location is 5.9 m/s and the 50 years, 10 minutes extreme wind is estimated to 37 m/s. The turbulence intensity, at 15m/s, is calculated to 0.12 and the temperature range is -40 to 25°C.

According to the IEC classification of wind turbines this site is a class IIIB site cause of the 50 year wind. If we take, the temperature in to consideration the air density can be up to 18 % higher than standard conditions. It means that the loads on the turbine in case of a 50-year extreme wind will correspond to the load at 44m/s or what corresponds to a class I site.

We have to be very carefully in our choice of turbine and other component both the low temperatures, snow and ice is a challenge for the components. In relation to the turbine the glaze and rime icing was basis for major concerns.

FIGURE 1: PICTURE BY OLE B. SKIPPER

FIGURE 2 PICTURE BY TRACY DAHL

Under the right weather conditions a big layer of glaze will cover all in the area. If the turbine is parked there are no other problems in this, but if the turbine is rotating the ice can be thrown off and cause rotor unbalance

and damage the turbine. Thrown off ice can also cause a risk for people in the area depending of the size of the pieces.

Another important is to get electrical components and lubricating system that can with stand the -40°C without any heating.

Turbine size

The turbine size, for the test, must be selected so that it not, at any time, will damage the existing control system or influence the safety of supply. By investigate the power consumption and the production of the village for several years we found that the minimum consumption was 24 kW. Steering committee decided from this that the turbine must be smaller the 10 kW.

At a market, survey we found that more or less only one turbine product for filled the requirements and it was the Proven turbines. We chose the 6 kW version because that the next is a 15 kW turbine and the electrical group was concerned of how this size will affects the gird.

The 6 kW Proven P11 turbine

The 6 kW Proven turbine is a three bladed down wind turbine. The rotor diameter is 5.5 m and the hub height is 9 m.

The turbine is mounted on a 9 m tilt-up tower that can be erected by winch. In this case the tower is equipped with four specially designed guy wires.

The turbine control system is complete mechanically. The blades I mounted on a hinge and the angle is controlled by springs. When the load on the blades increases the springs will allow the blades to bend backwards in direction of the wind. The way the hinge is angled cause that the blades not only bend backwards but also pitch.

Figure 3, turbine installation in Sarfannguaq

The generator is a 12 pole direct drive permanent magnet generator that is connected to the ground cable through a slip ring. The rated rotational speed is 200 RPM.

The turbine can either be grid connected, battery connected or used for direct heating. The weight of the turbine is around 600 kg and the 9 m tower weighs 400 kg.

Wind turbine generator and inverter test

The wind turbine generator, inverter and communication unit was tested in the high voltage lab at DTU. When the turbine was unpacked, and the generator cover was removed, the technician discovered that the generator front flywheel disk was unbalanced with an offset of up to 5mm. Measurements and a video of the disk unbal-

ance was send to Proven by the dealer Getek A/S to find a solution. Proven answer was within there tolerances and it should not give any problems.

During the test, the generator key parameter was determined Tabel 1[1]

Resistance [Ω]	Magnetization Inductance [mH]	Leakage Inductance [mH]	Synchronous Inductance [mH]
1.566	15.55	3.533	19.083

TABEL 1, GENERATOR KEY PARAMETER

INSTALLATION IN SARFANNGUAQ

The installation started d. 9 of July with marking of the foundation and rock anchor at the site. The company Polar Entreprise was chosen to do the foundation work. For the foundation we use a special designed rock foundation instead of the normal gravity foundation. The design was based on a cast base to level the surface and some rock anchor drilled and glued in to mountain with "Sikadur" epoxy mortar. For guy wire anchor we used standard rock anchor and thread bars with diameters of 25-40 mm and a length of 1-1.3 m was used for the base. D. 22 of July, the turbine parts arrived to the harbor in Sarfannguaq. The preassembly was carried out in the harbor, where heavy lift equipment was available, and the turbine was prepared for the heli-lift. We decided to assemble the turbine and the tower at the harbor to minimize the work on site. Only the light parts as cover plates and blades was mounted on site.

D. 26 of July the helicopter crew from Air transport Europe inspect the site. They selected a landing spot for the chopper and we planned the last details about the job. We rented the helicopter together with municipality, Qeqqata because they also had a job for it in the area. D. 29 of July the Mi-8 helicopter from Air transport Europe arrived. The weather conditions were not optimal as the wind speed was about 8 m/s, but the crew decided to carry out the lift.

The foundation pin bolt was mounted when the helicopter carried the weight of the turbine. When the pin bolt was in position the helicopter lowered the turbine to vertical position and released it and the crew continued with the lift for Qeqqata kommunia.

[1] A. MAHMOUD WIND TURBINE (PROVEN6-300) TESTING & INSTALLATION, http://find.artek.byg.dtu.dk/pubs/search/?topic=Energi

FIGURE 4, HELI LIFT OF WIND TURBINE

FIGURE 5, TURBINE IN LOWERED POSITION

We continued with the final assembling and afterwards raised the turbine and released the brake. Nothing happened but the wind speed was low so we decided to continue with the power line. The next days while we worked on the power line we observed the turbine, but nothing happened even when the wind speed was above 8 m/s. We lowered the turbine again and checked the rotation resistance when we released the brake. The resistance was so high that we had to use a lot of force just to turn the rotor. We found that the brake was so tight, even under released condition, that it was impossible for the wind driven power to turn the rotor. The brake system was disassembled and adjusted. It was now possible to turn the rotor when the turbine was lowered, FIGURE 5. We raised the turbine again and mounted the guy-wires, but the turbine still did not rotate. We collect a long bar with a rope loop in the end and it was used to pull the blades down and turn the rotor. We discover that there was a non constant resistance when we tried to turn the rotor. We lowered it again and discovered that, when the rotor was pointing down watch, the weight of it pulled the main shaft and moved all the rotating parts so much that the generator rotor periodic got in contact with stator. Luckily it was possible to adjust the stator position so much that this problem could be solved. The group was however concerned about this because we still do not knows how much it will move when the rotor is fully loaded. At this time the turbine was parked, to waiting for a production license.

FIGURE 6, TURBINE FINALLY INSTALLED AND THE GUY WIRES PRESTRESSED

GRID CONNECTION

The turbine output is with varying voltage and frequency of up to 300 V and 20 Hz. To connect this to a grid with constant voltage and frequency we have to use a converter. To protect these electrical devices from the rough Arctic environment they were located in the power plant. It means in this case that a 500m long cable, powered directly from the generator and to the power plant. A standard 4x 10mm^2 cable is used and to secure the cable and the generator a 10A circuit breaker was applied in the bottom of the tower. In the power plant the cable is connected to a control box also with manual and circuit breaker. The cable is, all the way from the bottom of the tower to the power plant, protected by a steel pipe, to avoid damaged from traffic, animal etc.

The control box, ECM6004ME/300, which is deliver with the turbine contains a 3-phase rectifier. The output power for the box is then 3-phaase DC current at up to 300 Volt in normal operation.

The DC power output is connected to three converter sin this case “Windy boy 3000”, one on each phase. The converter converts the DC power to 230 V 50 Hz power. The converter constantly monitors the voltage, frequency and the grid impedance and if one of the parameters exceeds the predefined limit in more than the predefined time, the converter will disconnect the turbine. On the grid side of the converter there is an electricity meter and a manual switch.

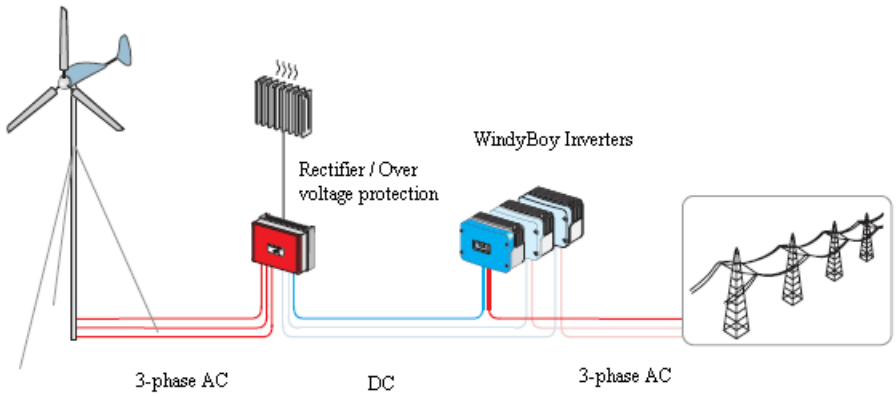

START-UP AND CONTROL

The production permission were given in 2010 and the turbine was started august 2010, but during the first years of operation several problems were discovered.

OPERATION AND MAINTENANCE

The biggest problem is the windy boy inverters, they was not able to stay connected to the grid more than a few seconds at the time and therefore the system has only delivered a fraction of the potential production to the grid. The inverters disconnect at the moments when grid frequency disturbances exceed ±0.1Hz. The technicians have to solve this problem because frequency disturbances are very common in the weak village grid.

There has been one major breakdown of the monitoring system and some offline situations[2]. The technicians has tried to solve the problem by adding an UPS power backup unit august 2011, but the system is still not totally stable and has to be restarted with monthly intervals.

The wind turbine has had some mechanical problems caused by the unstable flywheel disk. Sometime during the first year of operation the stator and one or more of the permanent magnets has been in contact and parts of the magnets has been knocked off. Several magnet pieces were removed from the generator enclosure but unfortunately one piece has escaped and hit the leading edge one of the blades. The magnet made a hole in the blade surface, but the effect on the blade strength estimated to be limited. The hole was covered by some styrene filler to minimize the flow disturbance.

It is not only the flywheel that was damaged the entire main shaft seems to be displaced. It means that the break disk is shifted in relation to the breaking mechanism and is has caused some problems with break slip and the break function. We made a temporary solution by reduce the pad thickness, but it is not an optimal solution.

The maintenance work on the turbine is very limited due to the simple design. Lower the turbine, lubricate the bearings, check the break and the slip ring close the nacelle and raise the turbine.

[2] K.L.Olsen 2010, Fast data acquisition from wind turbine, http://find.artek.byg.dtu.dk/pubs/search/?topic=Energi/10-19.pdf

ECONOMY

This turbine is a test turbine and it is equipped with a lot of extra part, therefore the economy for this turbine is not that interesting. The interesting thing is what the economy for a standard setup in these areas. To estimate this we strip our installation costs to only the necessary parts.

Expense	Cost [DKK]
Foundation	35.000
Guy wire	3600
Wind turbine 6kW	159.800
Invertere 3xWindy boy 3000	9200
Connection cable 500m,4x10mm2	12.000
Cabling work 27Hr	5670
Helicopter lift	22.000
Installation 84Hr	17.640
Inland transport	17.500
Transport to Greenland	15.900
Total installation cost	298.310
Yearly maintenance cost	4500

The expected production for a good Greenlandic site (5.5m/s) 12MWh/year and the expected lifetime is 20years that gives a potential production at 240.000kWh and a electricity price of 1.62kr/kWh. The value of the produced electricity is very dependent of the marketing conditions and if you are allowed and able to use it yourself. If you are forced to sell it to the grid the price will, in a village, be around the oil electricity price. If you as private investor are allowed to use the electricity yourself in a net meter system, the value is at the moment 3,24kr/kWh.

Electricity value		
Energy 1L oil	9,96	kWh/L
Oil price	6,11	DKK/L
Energy price	0,61	DKK/kWh
Generator efficiency	0,3	
Oil electricity price	2,04	DKK/kWh

If we make a simple calculation of the payback time for the two scenarios it show that the project with selling the electricity for the oil electricity price only pay's the costs, but if the grid owner will allow a net meter setup then it is a good investment.

Simple Payback time, selling	Grid	Net meter
Yearly income (12.000kWh)	24538	38880
Yearly maintenance cost	4500	4500
Yearly remaining	20038	34380
Simple payback time (Years)	14,8	8,7

CONCLUSION

The turbine was damage, somewhere on its way from Proven to DTU's testlab. The flywheel were hit or pushed very hardly and it caused that it bended and displaced the entire main shaft. The consequence of this damage should have been discovered in the lab before it was shipped to Greenland. The damage resulted in a lot of problems during the installation process and it can be a challenge to fix it onsite. Artek must in co-operation with Getek A/S find a permanent solution so the turbine can work properly.

The simple rock anchor foundation together with the guy wire seems to work properly and was a good alternative to the standard cast concrete foundation.

The helicopter installation process went well due to an experienced crew from Air transport Europe. We chose to install the turbine vertically directly on the foundation and push the pin bolt in position while the helicopter was caring the turbine. Another time some kind of fixture could be an advantage because the tolerance in the pin bolt connection is very tight and difficult to connect when the tower constantly moves.

The inverter settings are not sufficient adjusted jet and it means that the grid connection is unstable. In long periods of the first years, the system has been offline and it means that the staff at DTU not is able to adjust parameters in the inverter controller. The parameter will as soon as possible be adjusted and hopefully that will stabilize the connection.

The turbine construction is simple and seems to work well in the arctic environment. We had some concerns about blade icing and snow build up in the generator, based on the experiences from the similar turbine installed at Summit camp, but it seems to be unfounded. The staff or the locals have not experienced any icing or snow buildup on the turbine yet. By using the alternative site, 5300kWh/year extra could be produced, but the extra cabling cost will add round 100.000kr to the costs. For new and bigger installation site 2 will be preferable.

The maintenance work can be minimized by extending the lubrication connections so they are assemble close to the nacelle cover. An inspection camera can be used to inspect the break and the slip ring and you do not have to open a close the cover. The turbine is now lowered and raised by a manual operated Tirfor winch, but a hydraulic can be used if site access allows it.

Appendix E

Populærvidenskabelig artikel

Mandatory popular scientific article published together with this report.

Fremtidens grønlandske energiforsyning

Hvilke muligheder har Grønland for at nedbringe afhængigheden af importeret olie

Den grønlandske energiforsyning er primært baseret på importerede olie produkter, som har en negativ effekt på samfundsøkonomien og miljøet. For at nedbringe afhængigheden af importeret olie har Grønland opbygget en væsentlig vankraftkapacitet, som i 2013 leverede 14% af forbruget. Grønland har stadig et betydelig uudnyttet vandkraftpotentiale, men dets geografiske placering i forhold til forbrugerne medføre for høje omkostninger. Derfor søger Grønland alternative løsninger, som effektivisering og alternative energikilder.

Dette projekt har undersøgt mulighederne for at effektiviserer de grønlandske energisystemer, og hvilke energikilder der vil være rentable at inkludere i de enkelte system typer. Det primære fokus har været på vindkraft, men solenergi i form af solceller til el-produktion, har vist sig at være et godt supplement/alternativ, specielt for de mindre systemer.

Vedvarende energiresurser

Undersøgelserne af de grønlandske vindresurser og metoderne til at kortlægge dem har vist at der findes anvendelige vindkraftområder i både de syd- og vestlige dele af landet. Men det vil kræve yderligere studier at kortlægge vindresurserne for hele landet.

Solresurserne afhænger af den geografiske placering, men i høj grad også af fugtigheden i atmosfæren. I de kystnære og lavtliggende områder begrænser skyer og tåge solindstrålingen, og derfor findes de højeste resurser inde i landet og oppe i fjeldene. Områder med hyppige vinde fra indlandsisen vil opleve mere klart vejr og har dermed en højere indstråling. For nogle områder vil placeringen af de bedste sol- og vindresurser derfor være sammenfaldende, hvilket minimere installationsomkostningerne.

Vedvarende energiintegration

For diesel byer og bygder viser undersøgelserne at et energimix af sol, vind og diesel, kombineret med et mindre energilager og kontrollerede storforbrugere vil være en rentabel løsning. Det vil kræve en opdatering af de eksisterende energisystemer, der ofte bygger på forældet teknologi.

I vandkraftbyerne er vandkraftresurserne så begrænsede, at de kun kan dække elforbruget og en del af fjernvarmeforbruget. En total fortrængning af den oliebaserede opvarmning i byerne vil kræve udbygning med vand, vind og/eller sol i MW skala og generelt er store centrale anlæg den billigst løsning. Sol kan kun bidrage med del af varmeproduktion, da resursen er størst om sommeren, hvor behovet er mindst. Vindresurserne er derimod i fase med varmeforbruget og ved installationer i multi-MW klassen vil produktionsprisen være attraktiv. For varmeproduktionen i byerne kan udviklingen inden for havvandsbaserede varmepumper have afgørende betydning. Virkningsgraderne i dag er 3-3,5 men forventes over 4 i fremtiden.

Effektivisering af energiforbruget

Der findes et stort uudnyttet effektiviseringspotentiale i Grønland og det gælder alle sektorer. Ved intelligent styring og opdatering af bygninger og anlæg kan en stor del sparres. I dette projekt har fokus været på de private husholdninger, handel og service, og forsyningssektoren, men industrien har også et stort potentiale. Den offentlige el og varmeforsyning anvender 720 GWh/år og 27% af dette går tabt inden det når forbrugerene og der til kommer et ukendt tab på de offentlige forbrændingsanlæg. Tabet i forsyningssektoren svare til en regning på over 117 millioner/år, som fordeles blandt de grønlandske forbrugere. De 27% dækkerover meget store variationer fra nogle få procent i vandkraftbyerne til 80% i de

mindste diesel bygder. Det største effektiviseringspotentiale er fundet i de diesel forsynede byerne, hvor varmeproduktionen ofte kun udnyttes i ringe grad.

For at udnytte restvarmeproduktion og sikre en fleksibel forsyning er det vigtigt at hovedparten af bygningsmassen i byerne gradvist kobles på fjernvarmenettene, hvilket også åbner for en sikker integration af nye energikilder. Med store offentligkontrollerede bygningsmasser vil den nødvendig opdatering og udvidelse af fjernvarmenettene kunne gennemføres, og sikre en effektivudnyttelse af overskudsvarme fra industri, forbrænding, og elproduktion.

Grønlandsenergiforbrug 2013

Grønlands Indlandske energiforbrug	**2500GWh**	
– *Importerede olieprodukter*		84%
– *Vandkraftproduktion*		14%
– *Affaldsforbrænding*		2%
Forbrug el og fjernvarme sektoren	**721GWh**	
- *Elforbrug*		44%
- *Fjernvarmeforbrug*		29%
- *Konverteringstab*		27%

Kilde: Grønlandsstatistik for energi, december 2014

Analyse af fjernaflæste forbrugsdata og andre tilgængelige data om klima, bygninger og installationer har vist sig som et effektivt redskab til at identificere effektiviseringspotentialer. Disse data kan blive et stort aktiv for Grønland, hvis man forstår at udnytte potentialet.

I de grønlandske husholdninger viste analysen at udskiftning af ældre cirkulation pumper er den bedst energiinvestering, men utidssvarende hårde hvidevare og fejl-indstillede varmekabler er også blandt store strømslugere. På varmesiden er gamle og dårlig styrede centralvarmeanlæg, dårligt isolerede huse og forkert udluftning de store syndere.

Besparelser ved udskiftning af husholdningsmaskiner

Enhed (Per vask eller år)	Ældre	Ny	Ældre	Ny	Sparret	Tilbagebetalingstid
	kWh	kWh	Liter	Liter	Kr./enhed	År
Opvaskemaskine (per vask)	2.0	0.7	35	6.5	4.25	5.0 (280 vaske/år)
Vaskemaskine (per vask)	1.5	0.77	100	37.5	4.02	4.2 (220 vaske/år)
Tørretumbler (per vask)	4.25	1.08	0	0	10.42	3.8 (160 vaske/år)
Cirkulationspumpe (per år)	569	65	0	0	1658	0.8
Køleskab (per år)	292	97	0	0	642	3.3
Kummefryser (per år)	547	215	0	0	1092	2.2

Beregningerne er udført efter den gældende EU standard for husholdningsmaskiner og med en elpris på 3,29kr./kWh og en vandpris på 0,035kr/L (Bygdepriser 1/1-2014).)

Appendix F

Equations used for statistical evaluation

Equations used for statistical evaluation of model performance, Table 4.6.

$$Mean = \frac{1}{N}\sum_{t=1}^{N} W_t \tag{F.1}$$

$$MAE = \frac{1}{N}\sum_{t=1}^{N} |S_t - M_t| \tag{F.2}$$

$$Bias = \frac{1}{N}\sum_{t=1}^{N} S_t - M_t \tag{F.3}$$

$$Correlation = \frac{\sum_{t=1}^{N}(S_t - \overline{S})(M_t - \overline{M})}{\sqrt{\sum_{t=1}^{N}(S_t - \overline{S})^2 \sum_{t=1}^{N}(M_t - \overline{M})^2}} \tag{F.4}$$

$$RMSE = \sqrt{\frac{\sum_{t=1}^{N}(S_t - M_t)^2}{N}} \tag{F.5}$$

$$Total = \frac{1}{n}\sum_{i=1}^{N} Station_i \tag{F.6}$$

where:

W_t Wind speed/direction at time t[m/s]

S_t Station wind speed/direction at time t[m/s]

M_t Simulated wind speed/direction at time t [m/s]

N Number of time step to evaluate [-]

$Station_i$ Station value for total statistic [m/s or -]

Appendix G

WRF(ASR) V2 input file

```
 &time_control
 start_year                          = 2009, 2009, 2009, 2009,
 start_month                         = 01, 01, 01, 01,
 start_day                           = 01, 01, 01, 01,
 start_hour                          = 18, 18, 18, 18,
 start_minute                        = 00,  00,  00,  00,
 start_second                        = 00,  00,  00,  00,
 end_year                            = 2009, 2009, 2009, 2009,
 end_month                           = 01, 01, 01, 01,
 end_day                             = 03, 03, 03, 03,
 end_hour                            = 00, 00, 00, 00,
 end_minute                          = 00,  00,  00,  00,
 end_second                          = 00,  00,  00,  00,
 interval_seconds                    = 10800,
 input_from_file                     = .T., .T., .T., .T.,
 history_interval                    =  60, 60, 60, 60,
 frames_per_outfile                  =   37,  37,  37,  37,
 iofields_filename                   = "out_d01.txt", "out_d02.txt",
"out_d03.txt",
 restart                             = .false.,
 restart_interval                    = 21600,
 io_form_history                     = 2
 io_form_restart                     = 2
 io_form_input                       = 2
 io_form_boundary                    = 2
 auxhist8_outname                    = "ten_min_winds_d<domain>",
 auxhist8_interval                   = 10,   10,   10,  10,
 io_form_auxhist8                    = 2,
 frames_per_auxhist8                  = 500, 500, 500,   500,
 auxinput4_inname                    = "wrflowinp_d<domain>"
 auxinput4_interval                  = 180,180,180,
 io_form_auxinput4                   = 2
 debug_level                         = 0
 /

 &domains
 time_step                 = 108,
 time_step_fract_num       = 0,
 time_step_fract_den       = 1,
 max_dom                   = 3,
s_we                      = 1,        1,        1,
e_we                      = 86,      160,      262,
s_sn                      = 1,        1,        1,
e_sn                      = 83,      169,      220,
s_vert                    = 1,        1,        1,
e_vert                    = 41,       41,       41,
num_metgrid_levels                   = 35,
 p_top_requested                     = 5000,
 eta_levels   = 1.0000, 0.9965, 0.9930, 0.9895, 0.9860,
                0.9825, 0.9714, 0.9539, 0.9308, 0.9034,
                0.8724, 0.8388, 0.8034, 0.7669, 0.7298,
                0.6926, 0.6558, 0.6196, 0.5842, 0.5499,
                0.5168, 0.4848, 0.4540, 0.4244, 0.3958,
                0.3683, 0.3417, 0.3158, 0.2906, 0.2659,
                0.2415, 0.2174, 0.1934, 0.1694, 0.1453,
                0.1212, 0.0969, 0.0698, 0.0454, 0.0215,
```

```
                0.000
 dx                         = 18000,     6000,     2000,
 dy                         = 18000,     6000,     2000,
 grid_id                    = 1,         2,         3,
 parent_id                  = 1,         1,         2,
 i_parent_start             = 1,        18,        34,
 j_parent_start             = 1,        15,        67,
 parent_grid_ratio          = 1,         3,         3,
 parent_time_step_ratio     = 1,         3,         3,
 feedback                   = 1,
 smooth_option              = 0,
/

 &physics
 mp_physics                          = 10,    10,    10,    10,
 ra_lw_physics                       = 4,     4,     4,     4,
 ra_sw_physics                       = 4,     4,     4,     4,
 radt                                = 30,    30,    30,    30,
 sf_sfclay_physics                   = 2,     2,     2,     2,
 sf_surface_physics                  = 2,     2,     2,     2,
 bl_pbl_physics                      = 2,     2,     2,     2,
 bldt                                = 0,     0,     0,     0,
 cu_physics                          = 3,     3,     0,     0,
 cudt                                = 5,     5,     5,     5,
 isfflx                              = 1,
 ifsnow                              = 0,
 icloud                              = 1,
 surface_input_source                = 1,
 num_land_cat                        = 20,
 num_soil_layers                     = 4,
 sst_update                          = 1,
 maxiens                             = 1,
 maxens                              = 3,
 maxens2                             = 3,
 maxens3                             = 16,
 ensdim                              = 144,
 fractional_seaice                   = 1,
 seaice_thickness                    = 1,
 /

 &fdda
 /

 &dynamics
 w_damping                           = 0,
 diff_opt                            = 1,
 km_opt                              = 4,
 diff_6th_opt                        = 2,         2,       2,
 diff_6th_factor                     = 0.06,    0.08,    0.08,    0.08,
 base_temp                           = 290.
 damp_opt                            = 0,
 zdamp                               = 5000.,   5000.,   5000.,   5000.,
 dampcoef                            = 0.15,    0.15,    0.15,    0.15,
 khdif                               = 0,       0,       0,
 kvdif                               = 0,       0,       0,
 non_hydrostatic                     = .true.,.true.,.true.,.true.,
```

```
moist_adv_opt                       = 1,     1,
scalar_adv_opt                      = 1,     1,
/

&bdy_control
spec_bdy_width                      = 5,
spec_zone                           = 1,
relax_zone                          = 4,
specified                           = .true., .false.,.false.,.false.,
nested                              = .false., .true., .true., .true.,
/

&grib2
/

&namelist_quilt
nio_tasks_per_group = 0,
nio_groups = 1,
/
```

DTU Wind Energy is a department of the Technical University of Denmark with a unique integration of research, education, innovation and public/private sector consulting in the field of wind energy. Our activities develop new opportunities and technology for the global and Danish exploitation of wind energy. Research focuses on key technical-scientific fields, which are central for the development, innovation and use of wind energy and provides the basis for advanced education at the education.

We have more than 230 staff members of which approximately 60 are PhD students. Research is conducted within 9 research programmes organized into three main topics: Wind energy systems, Wind turbine technology and Basics for wind energy.

Technical University of Denmark
Department of Wind Energy
Frederiksborgvej 399
Building 118
4000 Roskilde
Denmark
Phone 46 77 50 85
info@vindenergi.dtu.dk
www.vindenergi.dtu.dk